The Dissertation Committee for Shagufta Hasnain Shabbir Certifies that this is the approved version of the following dissertation:

THE USES OF SUPRAMOLECULAR CHEMISTRY IN SYNTHETIC METHODOLOGY DEVELOPMENT

Committee:

Eric V. Anslyn, Supervisor

Brent L. Iverson

C. Grant Willson

John T. McDevitt

Sean M. Kerwin

THE USES OF SUPRAMOLECULAR CHEMISTRY IN SYNTHETIC METHODOLOGY DEVELOPMENT

by

Shagufta Hasnain Shabbir, B.S, M.S.

Dissertation

Presented to the Faculty of the Graduate School of

The University of Texas at Austin

in Partial Fulfillment

of the Requirements

for the Degree of

Doctor of Philosophy

The University of Texas at Austin

May, 2009

Dedication

This dissertation is dedicated to Ahad, the *noor* of my eyes

Acknowledgements

First, I want to thank my advisor Eric V. Anslyn, for his continuous support in the Ph.D program. He was always there to listen and to give advice. He taught me how to set goals in life and work hard to achieve those goals. He is responsible for helping me complete the writing of this dissertation as well as the challenging research that lies behind it. He had confidence in me when I doubted myself, and brought out the best in me. He also made Anslyn Lab a wonderful workplace and home for the past five years. A special thanks goes to my mentor and dear friend Dr. Lei Zhu. He was always there for me. He taught me everything I needed to know about Indicator Displacement Assays. Without him I would be lost. Thank's for listening and caring. Also thanks to my coworkers at the Anslyn Lab and my friends for guiding me and being fun to be with. I am greatly indebted to my organic chemistry professor Dr. Micheal Blanda for inspiring my love for organic chemistry and encouraging me to join the Ph.D program. Lastly, I want to thank my family: my husband Hasnain Shabbir for his unconditional support of all my endeavours. My son who smiles at me when I come home, reminding me that all is not lost.

The Uses of Supramolecular Chemistry in Synthetic Methodology Development

Publication No._____

Shagufta Hasnain Shabbir, Ph.D.

The University of Texas at Austin, 2009

Supervisor: Eric V. Anslyn

Enantioselective indicator displacement assays (eIDAs), was transitioned to a high-throughput screening protocols, for the rapid determination of concentration and enantioselectivity (*ee*) of chiral diols and α-hydroxycarboxylic acid. To improve the design of our previously established receptor based on *o*-(*N,N*-dialkylaminomethyl)arylboronate scaffolds for eIDAs. The rigidity of the receptor, which pertinent from the formation of an intramolecular N-B dative bond was investigated. *o*-(Pyrrolidinylmethyl)phenylboronic acid its complexes with bifunctional substrates such as catechol, α-hydroxyisobutyric acid, and hydrobenzoin was studied in detail by x-ray crystallography and ^{11}B NMR. Our structural study predicts that the formation of an N-B dative bond, and/or solvolysis to afford a tetrahedral boronate anion, depends on the solvent and the complexing substrate present. To simplify the operation of eIDAs, we introduced an analytical method, which utilize a dual-chamber quartz cuvette, which reduces the number of spectroscopic measurements from two to one and introduced artificial neural networks (ANNs) which simplifies data analysis. In a second example a

high-throughtput screening protocol for hydrobenzoin was developed. The method involves the sequential utilization of what we define herein as screening, training, and analysis plates. Several enantioselective boronic-acid based receptors were screened using 96-well plates, both for their ability to discriminate the enantiomers of hydrobenzoin and to find their optimal pairing with indicators resulting in the largest optical responses. The best receptor/indicator combination was then used to train an ANN to determine concentration and *ee*. To prove the practicality of the developed protocol, analysis plates were created containing true unknown samples of hydrobenzoin generated by established Sharpless asymmetric dihydroxylation reactions, and the best ligand was correctly identified. The system was extended to pattern recognition for the rapid determination of identity, concentration, and *ee* of chiral vicinal diols. A diverse enantioselective sensor array was generated with three chiral boronic acid receptors and pH indicators. The optical response produced by the sensor array, was analyzed by two pattern recognition algorithms: principal component analysis (PCA) and ANNs. The PCA plot demonstrated good chemoselective and enantioselective separation of the analytes, and ANNs was used to accurately determine the concentration and *ee* of five unknown samples.

Table of Content

List of Schemes xi

List of Figures xiii

List of Table viii

Chapter 1: The Uses of Supramolecular Chemistry in Synthetic Methodology Development 1

1.1 Enzymes and Catalysis 1

1.2 Evolution of Enzyme Like Catalysis in Organic Synthesis 3

1.3 Supramolecular Interaction Aiding in Asymmetric Catalyst Discovery . 9

1.3.1 Combinatorial Chemistry 11

1.3.1 Fluorescents Screening Approaches 15

1.2.3 UV-visible Screening Approaches 20

1.4 Summary and Outlook 33

1.5 References for Chapter 1 34

Chapter 2: A Structural Investigation of the N-B Interaction in an o-(*N,N*-Dialkylaminomethyl)arylboronate System 39

2.1 Saccharide Sensing with Molecular Receptors Based on Boronic Acid 39

2.1.1 X-ray Crystallographic Analysis of Boronic Acid Receptors ... 46

2.2 Results and Discussion 51

2.2.1 X-ray Crystallographic Analysis 51

2.2.1 ^{11}B NMR Analysis 52

Structural characterization in solution 52

^{11}B NMR titrations in aprotic and protic media 55

^{11}B NMR - pH profiles 60

2.3 Conclusion 65

2.4 Experimental 66

2.4.1 Synthesis 66

2.4.2 X-ray Crystal Structure Determination 67

2.4.3 General Procedure for ^{11}B NMR Titrations 68

2.4.4 General Procedure for ^{11}B NMR – pH Profiles 69
2.5 References for Chapter 2..... 69

Chapter 3: Two Methods for the Determination of Enantiomeric Excess (*ee*) and Concentration of a Chiral Sample with a Single Spectroscopic Measurement76
3.1 Enantioselective Indicator Displacement Assays (eIDAs) 76
3.1:1 Binding Isotherm..... 78
3.1.2 Competitive Spectrophotometry 80
3.1.3 *Ee* Measurement by Indicator-Displacement Assay 83
3.1.4 Isosbestic Point Analysis 87
3.2 Results and Discussion: 93
3.2.1 Artificial Neural Network Analysis 93
3.3 Conclusion..... 99
3.4 Experimental..... 99
3.4.1 Typical Procedure for Double-Chamber Cuvette *ee* Titration... 99
3.4.2 ANN Training Procedure.....100
3.5 References for Chapter 3.....100

Chapter 4: A General Protocol for Creating High-throughput Screening Methods for Reaction Yield and Enantiomeric Excess Applied to Hydrobenzoin.....103
4.1 High-Throughput Screening Protocol.....103
4.2 Results and Discussion.....107
4.2.1 Synthesis 107
4.2.2 Design Criteria 108
4.2.3 Indicator Displacement Assay Optimization (Step 1).....111
4.2.4 Screening for Enantioselectivity (In Preparation of Step 2).....136
4.2.5 Screening Plate (Step 2) 142
4.2.6 Brief Description of ANN 145
4.2.7 Training the ANN (Step3) 147
4.2.8 Analysis of a Catalytic Asymmetric Dihydroxylation (Application of Steps 4 and 5).....152
4.3 Summary 157
4.4 Experimental.....158

4.4.1 Determination of K_{HI} Between Boronic Acid Hosts and Selected Indicators 158
4.4.2 Determination of K_{HG} Between Boronic Acid Hosts and (*R*,*R*) & (*S*,*S*)-Hydrobenzoin 159
4.4.3 96-well Plate Analysis 160
Screening Plate 160
Training/ Analysis Plate 161
4.4.4 NMR Analysis of the Enantiomeric Purity of Hydrobenzoin 162
4.4.5 Synthesis of the Boronic Acid Hosts 162
4.5 References for Chapter 4 165
Chapter 5: Pattern-Based Recognition for the Rapid Determination of Identity, Concentration, and Enantiomeric Excess of Subtly Different Diols 170
5.1 Pattern Recognition Sensor Array 170
5.2 Result and Discussion 173
5.2.1 Synthesis 173
5.2.2 X-ray Crystallographic Analysis: 174
5.2.3 Structural Characterization in Solution by ^{11}B NMR 177
5.2.4 Generating a Chemo and Enantioselective Array 178
5.2.5 Principal Component Analysis (PCA) 188
5.2.6 Artificial Neural Networks (ANN's) Analysis 191
5.3 Conclusion 193
5.4 Experimental Section 193
5.4.1 Synthesis 193
5.4.2 NMR Analysis of the Enantiomeric Purity of 5.4: 195
5.4.3 Standard UV-vis Titrations: 195
5.4.4 96-well Plate Analysis: 195
5.4.5 X-ray Crystal Structure Determination 196
5.5 References for Chapter 5 197
Bibilography 201
Vita 220

List of Schemes

Scheme 1.1: The chemoselective acylation of alcohols in the presence of amines catalyzed by zinc cluster **1.1** 4

Scheme 1.2: The Monsanto process for the synthesis of L-DOPA[12] 5

Scheme 1.3: Hydroxylation of the steroid derivative catalyzed by manganese porphyrin carrying four beta-cyclodextrins[18] 6

Scheme 1.4: Regiocontrolled cyclization of epoxide **1.8** to the five-membered ring ether **1.9** by the Cavitand catalyst **1.7** 8

Scheme 1.5: Synthetic pathway to D-*myo*-Inositol-Phosphate (**1.14**) from *myo*-Inositol (**1.11**)[21] 9

Scheme 1.6: Rh-catalyzed hydrogenation of the acetamidoacrylate 12

Scheme 1.7: **A**) Hetero-Diels-Alder reaction of aldehydes with Danishefsky's Diene. **B**) A combinatorial library of chiral metal complexes by combining diol ligand Lm and Ln in a parallel fashion. **C**) The diol ligands used for catalyst preparation 14

Scheme 1.8: Fluorescence screening assay of the peptide library for acylation reaction [32] 17

Scheme 1.9: Enantioselective fluorescent recognition of mandelic acid 19

Scheme 1.10: Asymmetric α-alkylation reaction of *N*-(diphenylmethylene)glycine methyl ester (**1.22**) with bromomethyl-*trans*-stilbene (**1.23**) for the synthesize of chiral ligands (*S*)- **1.24** and (*R*)- **1.24** for monoclonal antibody 19G2 sensor array by using Cinchona-derived catalyst. 20

Scheme 1.11: Enantioselective hydrolysis of racemic *p*-nitrophenyl 2-methyldecanoate 21

Scheme 1.12: An enzymatic method screening method to determine the enantiomeric excess of the addition reaction of diethylzinc to benzaldehyde 23

Scheme 1.13: Double cuvette in situ enzymatic screening (ISES) 24

Scheme 1.14: A) Dual Lewis acid–Lewis base catalyzed addition of acetyl cyanide to benzaldehyde. B) Enzymatic method for enantiomeric excess determination of O-acetylated cyanohydrins. 26

Scheme 1.15: Use of a simple spot test to screen catalyst for the hydroamination of cyclohexadiene with aniline. A red color indicates remaining aniline reactant. The reaction was made enantioselective by using Trost chiral ligand (*R,R*)-**1.38** [44] 27

Scheme 1.16: Copper catalyzed asymmetric conjugate addition of diethylzinc to *para*-*n*-heptyloxyphenyl-substituted chalcone. Tf = trifluoromethanesulfonyl 28

Scheme 1.17:**A**) Enantioselective indicator displacement assays for valine based on displacement of Chrom Azurol S (CAS) from complex $[Cu^{II}$(*R,R*-**1.42**)-(CAS)$]^{2-}$ **B**) The asymmetric reaction analyzed by the assay 31

Scheme 1.18: (**A**) 1,2 diphenylethylenediamine (**PD**), 1,2-diaminocyclohexane (**DC**), 1,2-diaminopropane (**DP**), bis-(4-methoxyphenyl)-1,2-diaminoethane (**MD**) (**B**) $[Cu^{I}$(*R*)-**1.43**] chiral complex (**C**) CD spectrum for (*R*)-**1.43** [0.4mM] and 2 equiv of the enantiomers of PD [0.8mM].....33

Scheme 3.1: Two-step enantioselective indicator-displacement assays (eIDAs). **A**) Achiral host–(**3.1**); indicators–4-methylesculetin (ML); guest – α-hydroxycarboxylate phenylactate (PL). **B**) Chiral host – (*S,S*)-**3.2**; indicators – alizarin complexone (AC); guest – (*R*)α-hydroxycarboxylate phenylactate (D-PL) and (*S*)α-hydroxycarboxylate phenylactate (L-PL). ΔAbs – absorbance change; $[G]_t$ – guest concentration; *ee* – enantiomeric excess Eq. 3.1 is an empirical polynomial fit for an *A* vs. $[G]_t$ displacement curve. Eq. 3.2 is a theoretical function derived from solution multi-equilibria and Beer's Law analysis 77

Scheme 4.1: **A**) Indicator displacement assay (IDA) **B**) Enantioselective indicator displacement assay (eIDA) using a chiral host for chiral diols with bromopyrogallol red (BPG) as the indicator, H: host, I: indicator, G: guest/analyte, Δ Abs: absorbance change, $[G]_t$: total guest concentration, *ee*: enantiomeric excess, *: indicates chiral center.....105

Scheme 4.2: **A**) Structures of the library of boronic acid hosts **B**) General reductive amination to synthesize chiral boronic acids **C**) Synthesis of host (*S,S*)-**4.5**.....108

Scheme 5.1. Structures of hosts, guests/analyte and indicators used in this study.....172

List of Figures

Figure 1.1: Schematic picture of the transition-state stabilized in lysozyme. The oxocarbenium ion is stabilized by interaction with Asp[52] and Glu[35] [7] 2

Figure 1.2: Photoinduced electron transfer mechanism 16

Figure 2.1: (**a**) Reversible association between an arylboronic acid and a vicinal diol. (**b**) Arylboronic acid and vicinal diol association under alkaline conditions. (**c**) Arylboronic acid and vicinal diol association in the presence of piperidine [29].....40

Figure 2.2: Shinkia's and Wang's boronic acid sensor **2.2**, and suggestive species involved in fluorescence change 43

Figure 2.3: Enantioselective indicator displacement assay using host-**2.4**(*S,S*) for (*S,S*)-hydrobenzoin and (*R,R*)-hydrobenzoin with pyrocatechol violet (PV) as indicator. 45

Figure 2.4: Left: Chemdraw presentation of the cyclic anhydride of **2.5**. Right: ORTEP diagrams (50% probability ellipsoids) of the cyclic anhydride of **2.5**. Hydrogen atoms are removed for clarity.....47

Figure 2.5: Left: Chemdraw presentations of the complexes between **2.5** and catechol. Right: OREP diagrams (50% probability ellipsoids) of arbitrary conformers of **2.6** and **2.6**·CH_3OH. Most hydrogen atoms are removed for clarity.....48

Figure 2.6: The formation of zwitterionic amino boronate **2.8** reported by Reetz, *et al.*.49

Figure 2.7: Chewdraw presentation and crystal structure (ORTEP, 50% probability ellipsoids) of dimethyl *o*-(*N*-benzylaminomethyl)phenylboronate (**2.9**).....50

Figure 2.8: View of complex **2.6** showing the atom-labeling scheme. Displacement ellipsoids are scaled to the 50% probability level. The dashed line is indicative of a H-bonding interaction with geometry.....51

Figure 2.9: (**A**) The ^{11}B NMR assignments for different species in the equilibrium between **2.5** and **2.6** (blue: trigonal planar boron, orange: tetrahedral boron with an N-B dative bond, red: tetrahedral boronate anion). (**B**) The reversible association between **2.5** and catechol in $CDCl_3$ to create **2.6**. (**C**) The reversible association between **2.5** and catechol in CD_3OD to create **2.6**•CD_3OD.....54

Figure 2.10: ^{11}B NMR spectra of compound **2.5** (10 mM) in the presence of 0 – 80 mM hydrobenzoin in $CDCl_3$ (**A**) and CD_3OD (**B**), respectively. The tiny signal at 19 ppm in B is from the non-interfering impurity boric acid. In (**A**), the free boronic acid **2.5** in $CDCl_3$ exists as a mixture of different aggregates, e.g. cyclic trianhydride in **Figure 2.5**. 56

Figure 2.11: ^{11}B NMR spectra of compound **2.5** (10 mM) in the presence of 0 – 80 mM catechol to create complex **2.6** in $CDCl_3$ (A) and CD_3OD (B), respectively. 58

Figure 2.12: ^{11}B NMR spectra of compound **2.5** (10 mM) in the presence of 0 – 80 mMα-hydroxyisobutyric acid to afford complex **2.11** in $CDCl_3$ (**A**) and CD_3OD (**B**), respectively. The tiny signal at 19 ppm in B is from the non-interfering impurity boric acid. However, a signal at 12-13 ppm appears to grow in during the upper spectra of part B, possibly indicative of an N-B species at an exceedingly small fraction. 60

Figure 2.13: Deprotonation of a boronic ester in aqueous media (or acid when R = H). Different colors represent different ^{11}B NMR chemical shifts for respective species. The zwitterionic and fully deprotonated species have similar ^{11}B NMR resonances (red) due to similar chemical environments..... 61

Figure 2.14: ^{11}B NMR spectra of compound **2.5** (20 mM, **A**) and **2.6** (20 mM, **B**) in 75% methanolic solution with HEPES (25 mM) with pH ranging from 3 to 12. The signals at 19 ppm are from the non-interfering impurity boric acid..... 62

Figure 2.15: ^{11}B NMR spectra of compound **2.7 (**20 mM) **A**) and **2.12 (**20 mM) **B**) in 75% methanolic solution with HEPES (25 mM) with pH ranging from 3 to 12. The signals at 19 ppm are from impurity boric acid. 64

Figure 2.16: ^{11}B NMR spectra of compound **2.7 (**20 mM), **A**) and **2.13 (**20 mM), **B**) in 75% methanolic with pH ranging from 3 to 11. The signals at 19 ppm are from impurity boric acid..... 65

Figure 3.1: (**A**) A dual-chamber quartz cuvette containing indicators ML (left) and AC (right). (**B**) Overlay of two indicator-host isotherms. Blue: absorption spectra of ML (92.0 μM) in 75% methanolic aqueous solution buffered with 10 mM HEPES at pH 7.4 (default buffer) in the presence of 0 – 0.44 mM of 1; Red: absorption spectra of

AC (115 μM) in the default buffer in the presence of 0 – 0.26 mM of (*S,S*)-**3.2**. (**C**) Absorption spectra of ML (198 μM), 1 (0.559 mM), AC (285 μM), and (*S,S*)-**3.2** (0.765 mM) in their designated chambers in the default buffer in the presence of PL (6.0 mM) with *ee* of D-PL varying from -1 to 1. (**D**) Two independent equations that correlate the absorbance (A) to $[G]_t$ and *ee* at wavelengths λ_1 (387 nm) and λ_2 (536 nm).....89

Figure 3.2: (**A**) Absorbance change at 387 nm of ML (202 μM), 1 (307 μM), AC (284.5 μM), and (*S,S*)-**2** (400 μM), in their designated chambers in the default buffer, upon increasing *ee* of D-PL. Diamonds: $[G]_t$ = 0.98 mM. Squares: $[G]_t$ = 1.47 mM. Triangles: $[G]_t$ = 1.96 mM. (**B**) Open diamonds: the absorbance change at 387 nm of the dual-chamber ensemble in **Figure 3.2A** upon increasing concentration of L-PL (D-PL produced an identical curve, not shown). The average absorbance from the *ee* titrations (coding scheme as in **Figure 3.2A** at three different $[G]_t$ values are overlaid on the calibration curve.....92

Figure 3.3: Filled squares: absorbance changes at 536 nm of the dual-chamber ensemble upon increasing *ee* of D-PL. (**A**) $[G]_t$ = 0.98 mM; (**B**) $[G]_t$ = 1.47 mM; (C) $[G]_t$ =1.96 mM. Empty triangles: data calculated from Eq. 3.2 by the computer program Mathematica 5.1 93

Figure 3.4: Structures of two MLP networks in this study. Both have three layers: (**A**) the input layer at left has 2 variables – A_{387} and A_{536}. The input layer is connected to, and processed by a hidden layer in the middle with 6 nodes. Two variables, $[G]_t$ and %*R*, are generated to the output layer at right; (**B**) the input layer has 43 variables from A_{392} to A_{602} with 5 nm intervals. The hidden layer has 11 nodes.....95

Figure 4.1: Structures of the selected catechol based indicators.....112

Figure 4.2: **A**) UV-visible titration of host-**4.1** with PV (150 μM) **B**) 1:1 binding isotherm (plot of the difference in absorbance at 520 nm with the addition of the host). All titrations were carried out in 100% MeOH, 10 mM *para*-toluenesulfonic acid and Hunig's base buffer, pH: 7.4, association constant K_{HI} (10^3 M^{-1}). All measurements were taken at 25°C. The solid line is the calculated curve resulting from iterative data fitting to a 1:1 binding isotherm.....114

Figure 4.3: **A**) UV-visible titration of host (*S*,*S*)-**4.2** with PV (150 μM) **B**) 1:1 binding isotherm (plot of the difference in absorbance at 520 nm with the addition of the host). All titrations were carried out in 100% MeOH, 10 mM *para*-toluenesulfonic acid and Hunig's base buffer, pH: 7.4, association constant K_{HI} (10^3 M^{-1}). All measurements were taken at 25°C. The solid line is the calculated curve resulting from iterative data fitting to a 1:1 binding isotherm..... 114

Figure 4.4: **A**) UV-visible titration of host (*R*)-**4.3** with PV (150 μM) **B**) 1:1 binding isotherm (plot of the difference in absorbance at 520 nm with the addition of the host). All titrations were carried out in 100% MeOH, 10 mM *para*-toluenesulfonic acid and Hunig's base buffer, pH: 7.4, association constant K_{HI} (10^3 M^{-1}). All measurements were taken at 25°C. The solid line is the calculated curve resulting from iterative data fitting to a 1:1 binding isotherm..... 115

Figure 4.5: **A**) UV-visible titration of host (*R*,*R*,*R*,*S*)-**4.4** with PV (150 μM) **B**) 1:1 bindingisotherm (plot of the difference in absorbance at 520 nm with the addition of the host). All titrations were carried out in 100% MeOH, 10 mM *para*-toluenesulfonic acid and Hunig's base buffer, pH: 7.4, association constant K_{HI} (10^3 M^{-1}). All measurements were taken at 25°C. The solid line is the calculated curve resulting from iterative data fitting to a 1:1 binding isotherm. 115

Figure 4.6: **A**) UV-visible titration of host (*S,S*)-**4.5** with PV (150 μM) **B**) 1:1 binding isotherm (plot of the difference in absorbance at 520 nm with the addition of the host). All titrations were carried out in 100% MeOH, 10 mM *para*-toluenesulfonic acid and Hunig's base buffer, pH: 7.4, association constant K_{HI} (10^3 M^{-1}). All measurements were taken at 25°C. The solid line is the calculated curve resulting from iterative data fitting to a 1:1 binding isotherm..... 116

Figure 4.7: **A**) UV-visible titration of host (*R*)-**4.6** with PV (150 μM) **B**) 1:1 binding isotherm (plot of the difference in absorbance at 520 nm with the addition of the host). All titrations were carried out in 100% MeOH, 10 mM *para*-toluenesulfonic acid and Hunig's base buffer, pH: 7.4, association constant K_{HI} (10^3 M^{-1}). All measurements were taken at 25°C. The solid line is the calculated curve resulting from iterative data fitting to a 1:1 binding isotherm..... 116

Figure 4.8: **A**) UV-visible titration of host (*R*)-**4.7** with PV (150 μM) **B**) 1:1 binding isotherm (plot of the difference in absorbance at 520 nm with the addition of the host). All titrations were carried out in 100% MeOH, 10 mM *para*-toluenesulfonic acid and Hunig's base buffer, pH: 7.4, association constant K_{HI} (10^3 M^{-1}). All measurements were taken at 25°C. The solid line is the calculated curve resulting from iterative data fitting to a 1:1 binding isotherm..... 117

Figure 4.9: **A**) UV-visible titration of host (*R*)-**4.8** with PV (150 μM) **B**) 1:1 binding isotherm (plot of the difference in absorbance at 520 nm with the addition of the host). All titrations were carried out in 100% MeOH, 10 mM *para*-toluenesulfonic acid and Hunig's base buffer, pH: 7.4, association constant K_{HI} (10^3 M^{-1}). All measurements were taken at 25°C. The solid line is the calculated curve resulting from iterative data fitting to a 1:1 binding isotherm..... 117

Figure 4.10: **A**) UV-visible titration of host (*S*)-**4.8** with PV (150 μM) **B**) 1:1 binding isotherm (plot of the difference in absorbance at 520 nm with the addition of the host). All titrations were carried out in 100% MeOH, 10 mM *para*-toluenesulfonic acid and Hunig's base buffer, pH: 7.4, association constant K_{HI} (10^3 M^{-1}). All measurements were taken at 25°C. The solid line is the calculated curve resulting from iterative data fitting to a 1:1 binding isotherm..... 118

Figure 4.11: **A**) UV-visible titration of host-**4.1** with AC (200 μM) **B**) 1:1 binding isotherm (plot of the difference in absorbance at 540 nm with the addition of the host). All titrations were carried out in 100% MeOH, 10 mM *para*-toluenesulfonic acid and Hunig's base buffer, pH: 7.4, association constant K_{HI} (10^3 M^{-1}). All measurements were taken at 25°C. The solid line is the calculated curve resulting from iterative data fitting to a 1:1 binding isotherm..... 118

Figure 4.12: **A**) UV-visible titration of host (*S,S*)-**4.2** with AC (200 μM) **B**) 1:1 binding isotherm (plot of the difference in absorbance at 540 nm with the addition of the host). All titrations were carried out in 100% MeOH, 10 mM *para*-toluenesulfonic acid and Hunig's base buffer, pH: 7.4, association constant K_{HI} (10^3 M^{-1}). All measurements were taken at 25°C. The solid line is the calculated curve resulting from iterative data fitting to a 1:1 binding isotherm..... 119

Figure 4.13: **A**) UV-visible titration of host (*R*,*R*,*R*,*S*)-**4.4** with AC (200 μM) **B**) 1:1 binding isotherm (plot of the difference in absorbance at 540 nm with the addition of the host). All titrations were carried out in 100% MeOH, 10 mM *para*-toluenesulfonic acid and Hunig's base buffer, pH: 7.4, association constant K_{HI} (10^3 M^{-1}). All measurements were taken at 25°C. The solid line is the calculated curve resulting from iterative data fitting to a 1:1 binding isotherm. 119

Figure 4.14: **A**) UV-visible titration of host (*R*)-**4.6** with AC (200 μM) **B**) 1:1 binding isotherm (plot of the difference in absorbance at 540 nm with the addition of the host). All titrations were carried out in 100% MeOH, 10 mM *para*-toluenesulfonic acid and Hunig's base buffer, pH: 7.4, association constant K_{HI} (10^3 M^{-1}). All measurements were taken at 25°C. The solid line is the calculated curve resulting from iterative data fitting to a 1:1 binding isotherm..... 120

Figure 4.15: **A**) UV-visible titration of host (*S*)-**4.6** with AC (200 μM) **B**) 1:1 binding isotherm (plot of the difference in absorbance at 540 nm with the addition of the host). All titrations were carried out in 100% MeOH, 10 mM *para*-toluenesulfonic acid and Hunig's base buffer, pH: 7.4, association constant K_{HI} (10^3 M^{-1}). All measurements were taken at 25°C. The solid line is the calculated curve resulting from iterative data fitting to a 1:1 binding isotherm..... 120

Figure 4.16: **A**) UV-visible titration of host (*S*)-**4.8** with AC (200 μM) **B**) 1:1 binding isotherm (plot of the difference in absorbance at 540 nm with the addition of the host). All titrations were carried out in 100% MeOH, 10 mM *para*-toluenesulfonic acid and Hunig's base buffer, pH: 7.4, association constant K_{HI} (10^3 M^{-1}). All measurements were taken at 25°C. The solid line is the calculated curve resulting from iterative data fitting to a 1:1 binding isotherm..... 121

Figure 4.17: **A**) UV-visible titration of host (*R*)-**4.8** with AC (200 μM) **B**) 1:1 binding isotherm (plot of the difference in absorbance at 540 nm with the addition of the host). All titrations were carried out in 100% MeOH, 10 mM *para*-toluenesulfonic acid and Hunig's base buffer, pH: 7.4, association constant K_{HI} (10^3 M^{-1}). All measurements were taken at 25°C. The solid line is the calculated curve resulting from iterative data fitting to a 1:1 binding isotherm..... 121

Figure 4.18: **A**) UV-visible titration of host-**4.1** with A (200 μM) **B**) 1:1 binding isotherm (plot of the difference in absorbance at 483 nm with the addition of the host). All titrations were carried out in 100% MeOH, 10 mM *para*-toluenesulfonic acid and Hunig's base buffer, pH: 7.4, association constant K_{HI} (10^3 M^{-1}). All measurements were taken at 25°C. The solid line is the calculated curve resulting from iterative data fitting to a 1:1 binding isotherm..... 122

Figure 4.19: **A**) UV-visible titration of host (*S,S*)-**4.2** with A (200 μM) **B**) 1:1 binding isotherm (plot of the difference in absorbance at 483 nm with the addition of the host). All titrations were carried out in 100% MeOH, 10 mM *para*-toluenesulfonic acid and Hunig's base buffer, pH: 7.4, association constant K_{HI} (10^3 M^{-1}). All measurements were taken at 25°C. The solid line is the calculated curve resulting from iterative data fitting to a 1:1 binding isotherm..... 122

Figure 4.20: **A**) UV-visible titration of host (*R*,*R*,*R*,*S*)-**4.4** with A (200 μM) **B**) 1:1 binding isotherm (plot of the difference in absorbance at 483 nm with the addition of the host). All titrations were carried out in 100% MeOH, 10 mM *para*-toluenesulfonic acid and Hunig's base buffer, pH: 7.4, association constant K_{HI} (10^3 M^{-1}). All measurements were taken at 25°C. The solid line is the calculated curve resulting from iterative data fitting to a 1:1 binding isotherm. 123

Figure 4.21: **A**) UV-visible titration of host (*R*)-**4.6** with A (200 μM) **B**) 1:1 binding isotherm (plot of the difference in absorbance at 483 nm with the addition of the host). All titrations were carried out in 100% MeOH, 10 mM *para*-toluenesulfonic acid and Hunig's base buffer, pH: 7.4, association constant K_{HI} (10^3 M^{-1}). All measurements were taken at 25°C. The solid line is the calculated curve resulting from iterative data fitting to a 1:1 binding isotherm..... 123

Figure 4.22: **A**) UV-visible titration of host (*S*)-**4.6** with A (200 μM) **B**) 1:1 binding isotherm (plot of the difference in absorbance at 483 nm with the addition of the host). All titrations were carried out in 100% MeOH, 10 mM *para*-toluenesulfonic acid and Hunig's base buffer, pH: 7.4, association constant K_{HI} (10^3 M^{-1}). All measurements were taken at 25°C. The solid line is the calculated curve resulting from iterative data fitting to a 1:1 binding isotherm..... 124

Figure 4.23: **A**) UV-visible titration of host (*R*)-**4.8** with A (200 μM) **B**) 1:1 binding isotherm (plot of the difference in absorbance at 483 nm with the addition of the host). All titrations were carried out in 100% MeOH, 10 mM *para*-toluenesulfonic acid and Hunig's base buffer, pH: 7.4, association constant K_{HI} (10^3 M^{-1}). All measurements were taken at 25°C. The solid line is the calculated curve resulting from iterative data fitting to a 1:1 binding isotherm..... 124

Figure 4.24: **A**) UV-visible titration of host (*S*)-**4.8** with A (200 μM) **B**) 1:1 binding isotherm (plot of the difference in absorbance at 483 nm with the addition of the host). All titrations were carried out in 100% MeOH, 10 mM *para*-toluenesulfonic acid and Hunig's base buffer, pH: 7.4, association constant K_{HI} (10^3 M^{-1}). All measurements were taken at 25°C. The solid line is the calculated curve resulting from iterative data fitting to a 1:1 binding isotherm..... 125

Figure 4.25: **A**) UV-visible titration of host-**4.1** with PG (75 μM) **B**) 1:1 binding isotherm (plot of the difference in absorbance at 420 nm with the addition of the host). All titrations were carried out in 100% MeOH, 10 mM *para*-toluenesulfonic acid and Hunig's base buffer, pH: 7.4, association constant K_{HI} (10^3 M^{-1}). All measurements were taken at 25°C. The solid line is the calculated curve resulting from iterative data fitting to a 1:1 binding isotherm..... 125

Figure 4.26: **A**) UV-visible titration of host (*S,S*)-**4.2** with PG (75 μM) **B**) 1:1 binding isotherm (plot of the difference in absorbance at 380 nm with the addition of the host). All titrations were carried out in 100% MeOH, 10 mM *para*-toluenesulfonic acid and Hunig's base buffer, pH: 7.4, association constant K_{HI} (10^3 M^{-1}). All measurements were taken at 25°C. The solid line is the calculated curve resulting from iterative data fitting to a 1:1 binding isotherm..... 126

Figure 4.27: **A**) UV-visible titration of host (*R,R,R,S*)-**4.4** with PG (75 μM) **B**) 1:1 binding isotherm (plot of the difference in absorbance at 380 nm with the addition of the host). All titrations were carried out in 100% MeOH, 10 mM *para*-toluenesulfonic acid and Hunig's base buffer, pH: 7.4, association constant K_{HI} (10^3 M^{-1}). All measurements were taken at 25°C. The solid line is the calculated curve resulting from iterative data fitting to a 1:1 binding isotherm. 126

Figure 4.28: **A**) UV-visible titration of host (*R*)-**4.6** with PG (75 μM) **B**) 1:1 binding isotherm (plot of the difference in absorbance at 420 nm with the addition of the host). All titrations were carried out in 100% MeOH, 10 mM *para*-toluenesulfonic acid and Hunig's base buffer, pH: 7.4, association constant K_{HI} (10^3 M^{-1}). All measurements were taken at 25°C. The solid line is the calculated curve resulting from iterative data fitting to a 1:1 binding isotherm..... 127

Figure 4.29: **A**) UV-visible titration of host (*S*)-**4.6** with PG (75 μM) **B**) 1:1 binding isotherm (plot of the difference in absorbance at 420 nm with the addition of the host). All titrations were carried out in 100% MeOH, 10 mM *para*-toluenesulfonic acid and Hunig's base buffer, pH: 7.4, association constant K_{HI} (10^3 M^{-1}). All measurements were taken at 25°C. The solid line is the calculated curve resulting from iterative data fitting to a 1:1 binding isotherm..... 127

Figure 4.30: **A**) UV-visible titration of host (*R*)-**4.8** with PG (75 μM) **B**) 1:1 binding isotherm (plot of the difference in absorbance at 420 nm with the addition of the host). All titrations were carried out in 100% MeOH, 10 mM *para*-toluenesulfonic acid and Hunig's base buffer, pH: 7.4, association constant K_{HI} (10^3 M^{-1}). All measurements were taken at 25°C. The solid line is the calculated curve resulting from iterative data fitting to a 1:1 binding isotherm..... 128

Figure 4.31: **A**) UV-visible titration of host (*S*)-**4.8** with PG (75 μM) **B**) 1:1 binding isotherm (plot of the difference in absorbance at 420 nm with the addition of the host). All titrations were carried out in 100% MeOH, 10 mM *para*-toluenesulfonic acid and Hunig's base buffer, pH: 7.4, association constant K_{HI} (10^3 M^{-1}). All measurements were taken at 25°C. The solid line is the calculated curve resulting from iterative data fitting to a 1:1 binding isotherm..... 128

Figure 4.32: **A**) UV-visible titration of host-**4.1** with ML (75 μM) **B**) 1:1 binding isotherm (plot of the difference in absorbance at 380 nm with the addition of the host). All titrations were carried out in 100% MeOH, 10 mM *para*-toluenesulfonic acid and Hunig's base buffer, pH: 7.4, association constant K_{HI} (10^3 M^{-1}). All measurements were taken at 25°C. The solid line is the calculated curve resulting from iterative data fitting to a 1:1 binding isotherm..... 129

Figure 4.33: **A**) UV-visible titration of host (*S,S*)-**4.2** with ML (75 μM) **B**) 1:1 binding isotherm (plot of the difference in absorbance at 380 nm with the addition of the host). All titrations were carried out in 100% MeOH, 10 mM *para*-toluenesulfonic acid and Hunig's base buffer, pH: 7.4, association constant K_{HI} (10^3 M^{-1}). All measurements were taken at 25°C. The solid line is the calculated curve resulting from iterative data fitting to a 1:1 binding isotherm..... 129

Figure 4.34: **A**) UV-visible titration of host (*R,R,R,S*)-**4.4** with ML (75 μM) **B**) 1:1 binding isotherm (plot of the difference in absorbance at 380 nm with the addition of the host). All titrations were carried out in 100% MeOH, 10 mM *para*-toluenesulfonic acid and Hunig's base buffer, pH: 7.4, association constant K_{HI} (10^3 M^{-1}). All measurements were taken at 25°C. The solid line is the calculated curve resulting from iterative data fitting to a 1:1 binding isotherm. 130

Figure 4.35: **A**) UV-visible titration of host (*R*)-**4.6** with ML (75 μM) **B**) 1:1 binding isotherm (plot of the difference in absorbance at 380 nm with the addition of the host). All titrations were carried out in 100% MeOH, 10 mM *para*-toluenesulfonic acid and Hunig's base buffer, pH: 7.4, association constant K_{HI} (10^3 M^{-1}). All measurements were taken at 25°C. The solid line is the calculated curve resulting from iterative data fitting to a 1:1 binding isotherm..... 130

Figure 4.36: **A**) UV-visible titration of host (*S*)-**4.6** with ML (75 μM) **B**) 1:1 binding isotherm (plot of the difference in absorbance at 380 nm with the addition of the host). All titrations were carried out in 100% MeOH, 10 mM *para*-toluenesulfonic acid and Hunig's base buffer, pH: 7.4, association constant K_{HI} (10^3 M^{-1}). All measurements were taken at 25°C. The solid line is the calculated curve resulting from iterative data fitting to a 1:1 binding isotherm..... 131

Figure 4.37: **A**) UV-visible titration of host (*R*)- **4.8** with ML (75 μM) **B**) 1:1 binding isotherm (plot of the difference in absorbance at 520 nm with the addition of the host). All titrations were carried out in 100% MeOH, 10 mM *para*-toluenesulfonic acid and Hunig's base buffer, pH: 7.4, association constant K_{HI} (10^3 M^{-1}). All measurements were taken at 25°C. The solid line is the calculated curve resulting from iterative data fitting to a 1:1 binding isotherm..... 131

Figure 4.38: **A**) UV-visible titration of host (*S*)- **4.8** with ML (75 μM) **B**) 1:1 binding isotherm (plot of the difference in absorbance at 380 nm with the addition of the host). All titrations were carried out in 100% MeOH, 10 mM *para*-toluenesulfonic acid and Hunig's base buffer, pH: 7.4, association constant K_{HI} (10^3 M^{-1}). All measurements were taken at 25°C. The solid line is the calculated curve resulting from iterative data fitting to a 1:1 binding isotherm..... 132

Figure 4.39: **A**) UV-visible titration of host-**4.1** with BPG (30 μM) **B**) 1:1 binding isotherm (plot of the difference in absorbance at 570 nm with the addition of the host). All titrations were carried out in 100% MeOH, 10 mM *para*-toluenesulfonic acid and Hunig's base buffer, pH: 7.4, association constant K_{HI} (10^3 M^{-1}). All measurements were taken at 25°C. The solid line is the calculated curve resulting from iterative data fitting to a 1:1 binding isotherm..... 132

Figure 4.40: **A**) UV-visible titration of host (*S,S*)- **4.2** with BPG (30 μM) **B**) 1:1 binding isotherm (plot of the difference in absorbance at 570 nm with the addition of the host). All titrations were carried out in 100% MeOH, 10 mM *para*-toluenesulfonic acid and Hunig's base buffer, pH: 7.4, association constant K_{HI} (10^3 M^{-1}). All measurements were taken at 25°C. The solid line is the calculated curve resulting from iterative data fitting to a 1:1 binding isotherm..... 133

Figure 4.41: **A**) UV-visible titration of host (*R,R,R,S,S*)- **4.4** with BPG (30 μM) **B**) 1:1 binding isotherm (plot of the difference in absorbance at 570 nm with the addition of the host). All titrations were carried out in 100% MeOH, 10 mM *para*-toluenesulfonic acid and Hunig's base buffer, pH: 7.4, association constant K_{HI} (10^3 M^{-1}). All measurements were taken at 25°C. The solid line is the calculated curve resulting from iterative data fitting to a 1:1 binding isotherm. 133

Figure 4.42: **A**) UV-visible titration of host (*R*)- **4.6** with BPG (30 μM) **B**) 1:1 binding isotherm (plot of the difference in absorbance at 520 nm with the addition of the host). All titrations were carried out in 100% MeOH, 10 mM *para*-toluenesulfonic acid and Hunig's base buffer, pH: 7.4, association constant K_{HI} (10^3 M^{-1}). All measurements were taken at 25°C. The solid line is the calculated curve resulting from iterative data fitting to a 1:1 binding isotherm..... 134

Figure 4.43: **A**) UV-visible titration of host (*S*)- **4.6** with BPG (30 μM) **B**) 1:1 binding isotherm (plot of the difference in absorbance at 570 nm with the addition of the host). All titrations were carried out in 100% MeOH, 10 mM *para*-toluenesulfonic acid and Hunig's base buffer, pH: 7.4, association constant K_{HI} (10^3 M^{-1}). All measurements were taken at 25°C. The solid line is the calculated curve resulting from iterative data fitting to a 1:1 binding isotherm..... 134

Figure 4.44: **A**) UV-visible titration of host (*R*)- **4.8** with BPG (30 μM) **B**) 1:1 binding isotherm (plot of the difference in absorbance at 570 nm with the addition of the host). All titrations were carried out in 100% MeOH, 10 mM *para*-toluenesulfonic acid and Hunig's base buffer, pH: 7.4, association constant K_{HI} (10^3 M^{-1}). All measurements were taken at 25°C. The solid line is the calculated curve resulting from iterative data fitting to a 1:1 binding isotherm..... 135

Figure 4.45: **A**) UV-visible titration of host (*S*)- **4.8** with BPG (30 μM) **B**) 1:1 binding isotherm (plot of the difference in absorbance at 570 nm with the addition of the host). All titrations were carried out in 100% MeOH, 10 mM *para*-toluenesulfonic acid and Hunig's base buffer, pH: 7.4, association constant K_{HI} (10^3 M^{-1}). All measurements were taken at 25°C. The solid line is the calculated curve resulting from iterative data fitting to a 1:1 binding isotherm..... 135

Figure 4.46: Enantioselective indicator displacement assay (eIDA) of host-**4.1** (700 μM) /PV (150 μM) with (*R*,*R*)-hydrobenzoin and (*S*,*S*)-hydrobenzoin. All titrations were carried out in 100% MeOH, 10 mM *para*-toluenesulfonic acid and Hunig's base buffer, pH =7.4, association constant K_{HI} (10^3 M^{-1}). All measurements were taken at 25°C. The solid lines are calculated curves resulting from iterative data fitting for displacement assay.[51] 138

Figure 4.47: Enantioselective indicator displacement assay (eIDA) of host (*S*,*S*)-**4.2** (300 μM) /PV (150 μM) with (*R*,*R*)-hydrobenzoin and (*S*,*S*)-hydrobenzoin. All titrations were carried out in 100% MeOH, 10 mM *para*-toluenesulfonic acid and Hunig's base buffer, pH =7.4, association constant K_{HI} (10^3 M^{-1}). All measurements were taken at 25°C. The solid lines are calculated curves resulting from iterative data fitting for displacement assay.[51] 138

Figure 4.48: Enantioselective indicator displacement assay (eIDA) of host (*R*)-**4.3** (960 μM) /PV (150 μM) with (*R*,*R*)-hydrobenzoin and (*S*,*S*)-hydrobenzoin. All titrations were carried out in 100% MeOH, 10 mM *para*-toluenesulfonic acid and Hunig's base buffer, pH =7.4, association constant K_{HI} (10^3 M^{-1}). All measurements were taken at 25°C. The solid lines are calculated curves resulting from iterative data fitting for displacement assay.[51] 139

Figure 4.49: Enantioselective indicator displacement assay (eIDA) of host (*R,R,R,S*)-**4.4** (500 μM) /PV (150 μM) with (*R*,*R*)-hydrobenzoin and (*S*,*S*)-hydrobenzoin. All titrations were carried out in 100% MeOH, 10 mM *para*-toluenesulfonic acid and Hunig's base buffer, pH =7.4, association constant K_{HI} (10^3 M^{-1}). All measurements were taken at 25°C. The solid lines are calculated curves resulting from iterative data fitting for displacement assay.[51] 139

Figure 4.50: Enantioselective indicator displacement assay (eIDA) of host (*S,S*)-**4.5** (2010 μM) /PV (220 μM) with (*R*,*R*)-hydrobenzoin and (*S*,*S*)-hydrobenzoin. All titrations were carried out in 100% MeOH, 10 mM *para*-toluenesulfonic acid and Hunig's base buffer, pH =7.4, association constant K_{HI} (10^3 M^{-1}). All measurements were taken at 25°C. The solid lines are calculated curves resulting from iterative data fitting for displacement assay.[51] 140

Figure 4.51: Enantioselective indicator displacement assay (eIDA) of host (*S*)-**4.6** and host (*R*)-**4.6** (400 μM) /PV (150 μM) with (*R*,*R*)-hydrobenzoin and (*S*,*S*)-hydrobenzoin. All titrations were carried out in 100% MeOH, 10 mM *para*-toluenesulfonic acid and Hunig's base buffer, pH =7.4, association constant K_{HI} (10^3 M^{-1}). All measurements were taken at 25°C. The solid lines are calculated curves resulting from iterative data fitting for displacement assay.[51] 140

Figure 4.52: Enantioselective indicator displacement assay (eIDA) of host (*R*)-**4.7** (420 μM) /PV (75 μM) with (*R*,*R*)-hydrobenzoin and (*S*,*S*)-hydrobenzoin. All titrations were carried out in 100% MeOH, 10 mM *para*-toluenesulfonic acid and Hunig's base buffer, pH =7.4, association constant K_{HI} (10^3 M^{-1}). All measurements were taken at 25°C. The solid lines are calculated curves resulting from iterative data fitting for displacement assay.[51] 141

Figure 4.53: Enantioselective indicator displacement assay (eIDA) of host (*R*)-**4.8** and host (*S*)-**4.8** (400 μM)/PV (150 μM) with (*R*,*R*)-hydrobenzoin and (*S*,*S*)-hydrobenzoin. All titrations were carried out in 100% MeOH, 10 mM *para*-toluenesulfonic acid and Hunig's base buffer, pH =7.4, association constant K_{HI} (10^3 M^{-1}). All measurements were taken at 25°C. The solid lines are calculated curves resulting from iterative data fitting for displacement assay. [51] 141

Figure 4.54. **A**) Screening plate with indicators, A: Alizarin (200 μM), AC: Alizarin complexone dihydrate (200 μM), BPG: Bromopyrogallol red (60 μM), ML: 4-Methylesculetin (125 μM), PG: Pyrogallol red (75 μM) PV: Pyrocatechol violet (150 μM) and host (*S,S*)-**4.2**, host (*R,R,R,S*)-**4.4**, host (*S*)-**4.6**, host (*S*)-**4.8** (See Table S1) and 5 mM hydrobenzoin **B**) Displacement of indicator BPG (60 μM) from host (*S,S*)-**4.2** (200 μM) with (*R*,*R*)-hydrobenzoin (5 mM), Racemic mixture (5 mM) and (*S*,*S*)-hydrobenzoin (5 mM). All solution were made in 100% MeOH, 10 mM *para*-toluenesulfonic acid and Hunig's base buffer, pH = 7.4. All measurements were taken at 25°C. 143

Figure 4.55. Three layered Multilayered Perceptron Artificial Neural Network, analyte concentration ($[G]_t$), percentage of (*R,R*)-hydrobenzoin (% *RR*)..... 145

Figure 4.56. ANN training set, *ee* titration at 570 nm of (**A**) host-**1** (1200 μM) and BPG (60 μM), (**B**) host (*S,S*)-**4.2** (200 μM) with BPG (60 μM), and (**C**) host (*R,R*)-**4.2** (200 μM) with BPG (60 μM) at four different concentrations of hydrobenzoin (2 mM, 4 mM, 6 mM, 10 mM). All solution were made in 100% MeOH, 10 mM *para*-toluenesulfonic acid, and Hunig's base buffer, pH = 7.4. All measurements were taken at 25°C. 148

Figure 4.57: Layout of the training/ analysis plate, solvent 100% methanol, pH 7.4, 10 mM buffer (*para*-toluenesulfonic acid and Hunig's base), analyte (*R,R*)-hydrobenzoin and (*S,S*)-hydrobenzoin, host (*S,S*)-**2** (200 μM), BPG (60 μM). 150

Figure 4.58. Asymmetric dihydroxylation of *trans*-stilbene with two cinchona alkaloids **A**) $(DHQD)_2PHAL$, **B**) (DHAD)CLB 152

Figure 4.59. ^1H NMR 300 MHz on a Varian Mercury 300 spectrometer in $CDCl_3$ of the racemic mixture of hydrobenzoin after derivatization..... 154

Figure 4.60. ANN training set, *ee* titration at 570 nm of (**A**) host-**4.1** (1200 μM) with BPG (60 μM), (**B**) host (*S,S*)-**4.2** (200 μM) with BPG (60 μM), (**C**) host (*R,R*)-**4.2** (200 μM) with BPG (60 μM) at six different concentrations of hydrobenzoin (2 mM, 3 mM, 4 mM, 6 mM, 8 mM, 10 mM). All solution were made in 100% MeOH, 10 mM *para*-toluenesulfonic acid and Hunig's base buffer, pH = 7.4. All measurements were taken at 25°C..... 156

Figure 5.1: ^{1}H NMR 300 MHz on a Varian Mercury 300 spectrometer in $CDCl_3$ of the racemic mixture of **4.4** after derivatization..... 174

Figure 5.2: Left: Crystal structure of host (*R*,*R*)-**5.2** complex with (*S*,*S*)-hydrobenzoin (**5.3b**). Right: ChemDraw representation of the crystal structure. 176

Figure 5.3: Enantioselective indicator displacement assay (eIDA) of host (*S,S*)-**5.2** and (0.48 mM) /PV (150 μM) with (*R*,*R*)-hydrobenzoin and (*S*,*S*)-hydrobenzoin. All titrations were carried out in 100% MeOH, 10 mM *para*-toluenesulfonic acid and Hunig's base buffer, pH =7.4, association constant K_{HI} (10^3 M^{-1}). All measurements were taken at 25°C. The solid lines are calculated curves resulting from iterative data fitting for displacement assay. 176

Figure 5.4: ^{11}B NMR spectra of compound **5.5** host (*R*,*R*)-**5.2** complex with (*S*,*S*)-hydrobenzoin in $CDCl_3$ (**A**) and CD_3OD (**B**). The signal at 18.6 ppm is the external standard trimethyl borate. 178

Figure 5.5: A) UV-visible titration of host (*S*,*S*)-**5.2** with A (200 μM), Host:Indicator complex (H:I), free indicator (I) **B)** 1:1 binding isotherm (plot of the difference in absorbance at 470 nm with the addition of the host). Stock solutions were prepared in 100% degassed spectral grade MeOH, using 10 mM *para*-toluenesulfonic acid and Hunig's base buffer, pH 7.4. Association constant: *K*, difference in molar absorptivity between the H:I complex and free I: de, total indicator concentration: It. The solid line is the calculated curve resulting from iterative data fitting to a 1:1 binding isotherm. All measurements were taken at 25ºC. 179

Figure 5.6: A) UV-visible titration of host (*S*,*S*)-**5.2** with AC (200 μM), Host:Indicator complex (H:I), free indicator (I) **B)** 1:1 binding isotherm (plot of the difference in absorbance at 550 nm with the addition of the host). Stock solutions were prepared

in 100% degassed spectral grade MeOH, using 10 mM *para*-toluenesulfonic acid and Hunig's base buffer, pH 7.4. Association constant: *K*, difference in molar absorptivity between the H:I complex and free I: de, total indicator concentration: It. The solid line is the calculated curve resulting from iterative data fitting to a 1:1 binding isotherm. All measurements were taken at 25ºC. 180

Figure 5.7: A) UV-visible titration of host (*S*,*S*)-**5.2** with BPG (29.59 μM), Host/Indicator complex (H:I), free indicator (I) **B)** 1:1 binding isotherm (plot of the difference in absorbance at 570 nm with the addition of the host). Stock solutions were prepared in 100% degassed spectral grade MeOH, using 10 mM *para*-toluenesulfonic acid and Hunig's base buffer, pH 7.4. Association constant: *K*, difference in molar absorptivity between the H:I complex and free I: de, total indicator concentration: It. The solid line is the calculated curve resulting from iterative data fitting to a 1:1 binding isotherm. All measurements were taken at 25ºC. 181

Figure 5.8: A) UV-visible titration of host (*S*,*S*)-**5.2** with ML (75 μM), Host:Indicator complex (H:I), free indicator (I) **B)** 1:1 binding isotherm (plot of the difference in absorbance at 380 nm with the addition of the host). Stock solutions were prepared in 100% degassed spectral grade MeOH, using 10 mM *para*-toluenesulfonic acid and Hunig's base buffer, pH 7.4. Association constant: *K*, difference in molar absorptivity between the H:I complex and free I: de, total indicator concentration: It. The solid line is the calculated curve resulting from iterative data fitting to a 1:1 binding isotherm. All measurements were taken at 25ºC. 182

Figure 5.9: A) UV-visible titration of host (*S,S*)-**5.2** with PG (74 μM), Host:Indicator complex (H:I), free indicator (I) **B)** 1:1 binding isotherm (plot of the difference in absorbance at 520 nm with the addition of the host). Stock solutions were prepared in 100% degassed spectral grade MeOH, using 10 mM *para*-toluenesulfonic acid and Hunig's base buffer, pH 7.4. Association constant: *K*, difference in molar absorptivity between the H:I complex and free I: de, total indicator concentration: It. The solid line is the calculated curve resulting from iterative data fitting to a 1:1 binding isotherm. All measurements were taken at 25ºC. 183

Figure 5.10: A) UV-visible titration of host (*S,S*)-**5.2** with PV (150 μM), Host:Indicator complex (H:I), free indicator (I) **B)** 1:1 binding isotherm (plot of the difference in absorbance at 520 nm with the addition of the host). Stock solutions were prepared in 100% degassed spectral grade MeOH, using 10 mM *para*-toluenesulfonic acid and Hunig's base buffer, pH 7.4. Association constant: *K*, difference in molar absorptivity between the H:I complex and free I: de, total indicator concentration: It. The solid line is the calculated curve resulting from iterative data fitting to a 1:1 binding isotherm. All measurements were taken at 25ºC. 184

Figure 5.11 A) Method used to screen for host (*R*,*R*)-**5.2** with indicators: pyrogallol red (**PG**), alizarin (**A**), 4-methylesculetin (**ML**), alizarin complexone dihydrate (**AC**), bromopygallol red (**BPG**), and pyrocatechol violet (**PV**). The concentration of the indicators and the host are listed in **Table 5.5**. (*R*,*R*)-hydrobenzoin (**5.3a**), (*S*,*S*)-hydrobenzoin (**5.3b**), (3*S*,4*R*)-2,3-dihydroxy-4-phenyl-butane-2-one (**5.4a**), (3*R*,4*S*)-2,3-dihydroxy-4-phenyl-butane-2-one (**5.4b**), methyl(2*S*,3*R*)-2,3-dihydroxy-3-phenyl-propionate (**5.5a**), methyl(2*R*,3*S*)-2,3-dihydroxy-3-phenyl-propionate (**5.5b**), diethyl D- tartrate (**5.6a**), diethyl L-tartrate (**5.6b**) B) Absorption spectrum of host (*R*,*R*)- **5.2**:ML with diol **5.5a**:Racemic mixture (**5.5a:5.5b**): **5.5b**. C) Absorption spectrum of host (*R*,*R*)- **5.2**:PV with diol **5.5a**:Racemic mixture (**5.5a: 5.5b**):**5.5b**. All studies were carried out in 100% MeOH, 10 mM buffered solution of Hunig's base and *para*-toluenesulfonic acid to pH 7.4 at 25°C. 186

Figure 5.12. PCA of the enantiomers of the four diols analyzed with host (*S*,*S*)-**5.1**:PV host (*R*,*R*)-**5.2**:ML, and host (*S*,*S*)-**5.2**:PV. The diols are labeled on the PCA plot. All studies were carried out in 100% MeOH, 10 mM buffered solution of Hunig's base and *para*-toluenesulfonic acid to pH 7.4 at 25 °C. 189

Figure 5.13. **A**) PCA of diol **5.5** *ee* titration at three different concentrations △: 2 mM, ◇: 4 mM, ○: 5 mM. *ee*, yellow: -1, pink: -0.6, green: -0.2, blue: 0, red: 0.2, orange: 0.4, brown: 0.6, purple: 1, where 1 is 100% methyl(2*S*,3*R*)-(-)-2,3- dihydroxy-3-phenylpropionate (**5.5a**) and -1 is 100% methyl(2*R*,3*S*)-(-)-2,3- dihydroxy-3-phenylpropinate (**5.5b**) **B**) Multilayer perceptron (MLP) artificial neural network generated for the determination of *ee* and analyte total concentration ($[G]_t$). All

studies were carried out in 100% MeOH, 10mM buffered solution of Hunig's base and *para*-toluenesulfonic acid to pH 7.4 at 25 °C. 191

List of Table

Table 2.1: ^{11}B NMR chemical shifts (δ/ppm) of selected boronic acids and esters in $CDCl_3$ and CD_3OD, respectively.[a] N. D.: not determined. 53

Table 3.1: Determination of concentration and *ee* of PL samples. IA: determined by isosbestic point analysis 91

Table 3.2: Determination of concentration and %*R* of PL samples with a trained MLP network (**Figure 3.4B**)..... 96

Table 3.3: Determination of concentration and %*R* of PL samples with a trained MLP network (**Figure 3.4B**). $[G]_t$ (actual) = 1.47 mM. 98

Table 4.1: Binding constant K_{HI} ($10^3 M^{-1}$) of boronic acid hosts with indicators. All titrations were carried out in 100% MeOH, 10 mM *para*-toluenesulfonic acid and Hunig's base buffer, pH =7.4. All measurements were taken at 25°C. 113

Table 4.2: Binding constant K_{HG} (10^3 M^{-1}) of boronic acid hosts, $K_{HG(S,S)}$with (*S*,*S*)-hydrobenzoin and $K_{HG(R,R)}$ with (*R*,*R*)-hydrobenzoin. All titrations were carried out in 100% MeOH, 10 mM *para*-toluenesulfonic acid and Hunig's base buffer, pH =7.4. All measurements were taken at 25°C. The error reported here results from the computer fit to the experimental isotherm. In our pervious experience, there is approximately 10% error at most in the reproducibility in the K_{HG} value..... 137

Table 4.3: Screening plate Δ Abs between (*R,R*)-hydrobenzoin & (*S,S*)-hydrobenzoin (5 mM) calculated for A at 480 nm, AC at 540 nm, ML at 380 nm, BPG at 570 nm, PG at 420 nm PV at 520 nm. 144

Table 4.4: Screening plate Δ Abs between (*R,R*)-hydrobenzoin & (*S,S*)-hydrobenzoin (10 mM) calculated for A at 480 nm, AC at 540 nm, ML at 380 nm, BPG at 570 nm, PG at 420 nm, PV at 520 nm..... 144

Table 4.5. Determination of *ee* and $[G]_t$ of 16 unknown samples of hydrobenzoin. Average Absolute Error = (|Actual value|- |Experimental value|)..... 151

Table 4.4. Determination of *ee* and $[G]_t$ of Sharpless asymmetric dihydroxylation reaction, * as determined by ^1H NMR..... 157

Table 4.7: The concentration of the indicators and the boronic acid host in the 96-well plate analysis. 162
Table 5.1: Binding constant K (10^4 M^{-1}) of the host (*S*,*S*)-**5.2** with the indicators. 179
Table 5.2: Screening plate Δ Abs between the enantiomeric guests (5 mM) with host (*S,S*)- **5.1** and the indicators calculated for, A at 450 nm, AC at 550 nm, ML at 380 nm, BPG at 570 nm, PG at 520 nm and PV at 520 nm. 187
Table 5.3: Screening plate Δ Abs between the two enantiomeric guests (5 mM) with host (*R*,*R*)-**5.2** and the indicators calculated for, A at 450 nm, AC at 550 nm, ML at 380 nm, BPG at 570 nm, PG at 520 nm and PV at 520 nm. 187
Table 5.4: Artificial Neural Network Analysis of unknown solutions 192
Table 5.5: Concentration of the hosts and the indicators used in the 96-well plate. 196

Chapter 1: The Uses of Supramolecular Chemistry in Synthetic Methodology Development

1.1 Enzymes and Catalysis

Enzyme catalysis involves molecular recognition at the most sophisticated level. These catalysts can accelerate the rate of a chemical reaction up to 10^{20} times the rate of the uncatalyzed reaction in water.[1] After urease was first crystallized by James Summer in 1926,[2] the lock and key model of enzyme action was generally adopted by the scientific community,[3] where the binding of the substrate molecule to the enzyme active site results in activation of the substrate. This model was later modified to the induce fit model where the enzyme folds around a specific substrate to induce binding interactions that lead to catalysis.[4] In 1946, Linus Pauling proposed that enzymes accelerate reactions because they bind to the transition state better then the substrate, and thereby lower the activation energy.[5] This postulate was supported by crystal structure of lysozyme, with the polysaccharide (N-acetylglucosamine)$_3$ bound at its active site. The structure showed the transition state for glycoside cleavage to be stabilized by the electrostatic field of carboxylates contributed by Asp^{52} and Glu^{35} on either side of the active-site cleft, positioned to interact with the developing positive charge on the oxocarbenium ion (**Figure 1.1**).[6] In the years since, thousands of enzymes have been purified and characterized, and the pace of this endeavor is rapidly accelerating.

What are the lessons learned from enzymes? First the proximity and orientation are crucial. The enzymes primary bring the two reactive species close to each other in a specific orientation. Second, enzymes have the ability to fold around a specific substrate to permit binding (induce-fit model). Third, enzymes provide extra stability to the

transition state by binding the transition state better then the ground state. Conclusively, the key feature of enzymes reactivity is their ability to bind, and thus selectively stabilize, the transition state and intermediate for a particular reaction. Thus catalysis can be defined in terms of molecular recognition of the transition state.

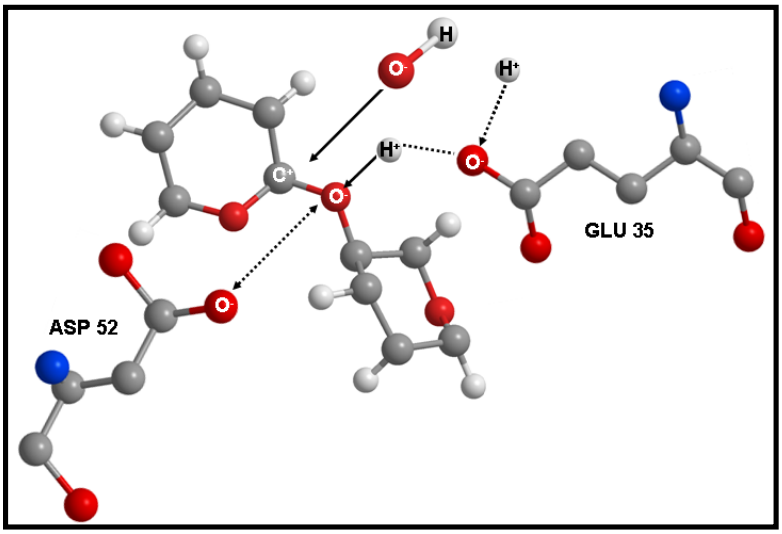

Figure 1.1: Schematic picture of the transition-state stabilized in lysozyme. The oxocarbenium ion is stabilized by interaction with Asp^{52} and Glu^{35}.[7]

The non-covalent forces through which substrates and other molecules bind to enzymes involve electrostatic, hydrogen bonding, and hydrophobic interactions. These are supramolecular interactions (beyond the molecule). They are fairly weak interactions, i.e ten kcal/mol or less. However, we have come to realize that a large number of these interactions can lead to big effects, such as catalysis. In general, the spatial arrangement of functionalized groups in the enzyme substrate complex can enhance, or override the substrates natural reactivity. Enzymes literally hold their substrate in place to control

chemo, regio and enantioselectivity. In a global sense, enzyme catalysis arises from supramolecular interactions.

As enzymes are highly substrate specific molecules, their scope is limited. Synthetic catalysts are of interest because of their potential to catalyze a reaction on a broad range of substrates. The construction of bio inspired catalytic systems by conventional covalent chemistry is a complex and time-consuming endeavor, as enzymes contain a great variety of components. One goal of supramolecular chemistry is to design complex catalytic systems by exploiting non-covalent interacts. To this end, chemist, have utilized supramolecular chemistry for the development of highly efficient catalysis for organic transformations. Herein we are highlighting a few of these discoveries.

1.2 Evolution of Enzyme Like Catalysis in Organic Synthesis

There is intense interest in the use of laboratory mimics of enzymes to catalyze organic reaction. A truly remarkable advance by Ohshima *et. al* [8] is zinc catalyst **1.1**. This enzyme mimic reverses the intrinsic reactivity of alcohols and amines to efficiently catalyze the acylation of alcohols in a manner similar to lipase.[9] When a molecule containing both the OH group and an NH_2 group reacts with methyl benzoate in the presence of the catalyst, the OH group reacts preferentially (**Scheme 1.1**). They suggested that μ-oxo-tetranuclear zinc cluster **1.1** acts as the active catalyst. The presence of the Zn-O-Zn structure, and the higher activity of the cluster than of the monomer, suggested a corporative mechanism of the zinc ions similar to the aminopeptidase. The two zinc ions within the cluster coordinate to the oxygen atoms of the substrates and brings them in close proximately to each other, thereby inducing catalysis.

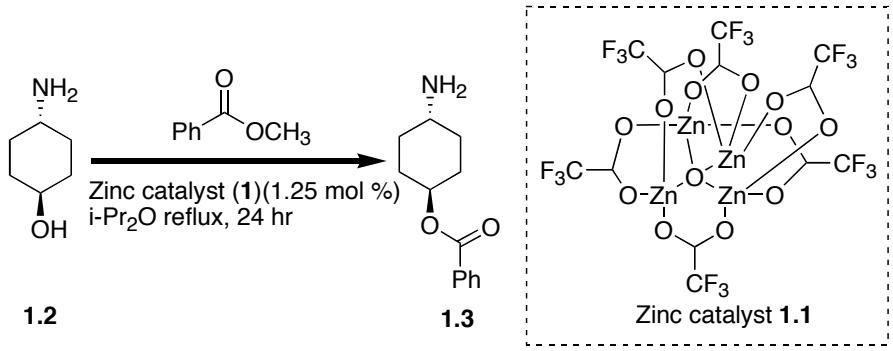

Scheme 1.1: The chemoselective acylation of alcohols in the presence of amines catalyzed by zinc cluster **1.1**.

One feature of enzyme selectivity is asymmetric catalysis, because enzymes are chiral molecules they selectively catalyze the reaction of one enantiomer over another, and can induce asymmetry from enantiotopic groups. This is clearly demonstrated by Frank Westheimer and Birgi Vennesland in the case of yeast alcohol dehydrogenase (YADH).[10] The investigators carried out several isotopic scrambling experiments and proved that YADH can distinguish between the *pro-S* and the *pro-R* hydrogens of ethanol as well as the *si* and the *re* faces of the nicotinamide ring of NAD^+. The stereospecificity of YADH is by no mean unusual. As we consider biochemical reactions we shall find that nearly all enzymes that participate in chiral reactions are absolutely stereospecific.

The unique handedness of the essential molecules of life, and the key role of chirality in the development of new drugs,[11] are a sources of inspiration and practical considerations for efforts to design efficient catalytic procedures that prepare single enantiomers of biologically active compounds. For years chemist believed that natural enzymes are the only ones that can efficiently catalyzed a highly selective enantioselective asymmetric reaction. The discovery of "Monsanto process"[12](**Scheme 1.2**), where a chiral rhodium catalyst was used to synthesize the drug L-DOPA use to

treat Parkinson disease was a break through. As stated by Knowles in 1983 "*This was the first time ever when anyone has achieved enzyme like selectivity with a man-made catalyst*".[13] These supramolecular systems employ chiral ligands to control seteroselectivity of a catalyzed reaction. The reaction mechanism of the Rh-phosphine complex catalyzed hydrogenation has been elucidated by Halpern.[14] Initially an enamide coordination complex is produced in which the olefin bond and the carbonyl oxygen interact with the Rh(I) center. The hydrogens is oxidatively added to the metal center to form Rh(III) dihydride intermediate. The hydrogens are then successively transferred to the carbons of the olefinic bond by way of a five membered chelate alkyl-Rh(III) intermediate. In this reaction the Rh-phosphine complex facilitates one of the transition states to be lower in energy than the other; reminiscence of an enzyme catalyzed biological reaction. The coordination of the reactive intermediates to the metal center is the hallmark of organometallic reactions. This binding leads to activation of the reactive species that leads to catalysis. In the past 35 years, metal catalyzed enantioselective transformations have enjoyed significant growth as it was recognized that these are among the most efficient ways to produce enantiomerically pure compounds. This effort was rewarded by 2001 Nobel Prize in Chemistry, which was shared by Knowles, Noyori, Sharpless.[15-17]

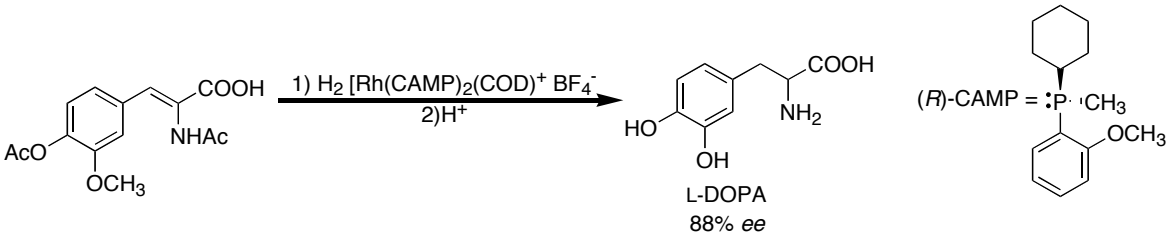

Scheme 1.2: The Monsanto process for the synthesis of L-DOPA.[12]

Early example of bio mimetic chemistry came from Breslow and coworkers, who developed a laboratory mimic of the enzyme cytochrome P450 (**Scheme 1.3**).[18] A metalloprophyrin with four cyclodextrin rings was used to catalyze regio and stereoselective hydroxylation of a steroid derivative. The position hydroxylated is not the most reactive, but is the one selected by the geometry of the catalyst-substrate complex. Molecular models indicate that the two *tert*-butylphenyl groups can bind into the cyclodextrins on the opposite sides of catalyst **1.4** so as to put ring B of the steroid directly over the metalloporphyrin unit. With 10 mol% catalyst **1.4** and an excess of iodosobenzene, the substrate **1.5** was selectively converted to **1.6**.[19] This example elegantly demonstrated the importance of binding in catalysis. The reaction is completely selective for hydroxylation of a single steroid position with regio- and stereoselectivity. With other substrates that fit the catalyst less well, more than one hydroxylation product is formed and no hydroxylation occurs under the conditions used with substrates that do not bind to the catalyst.

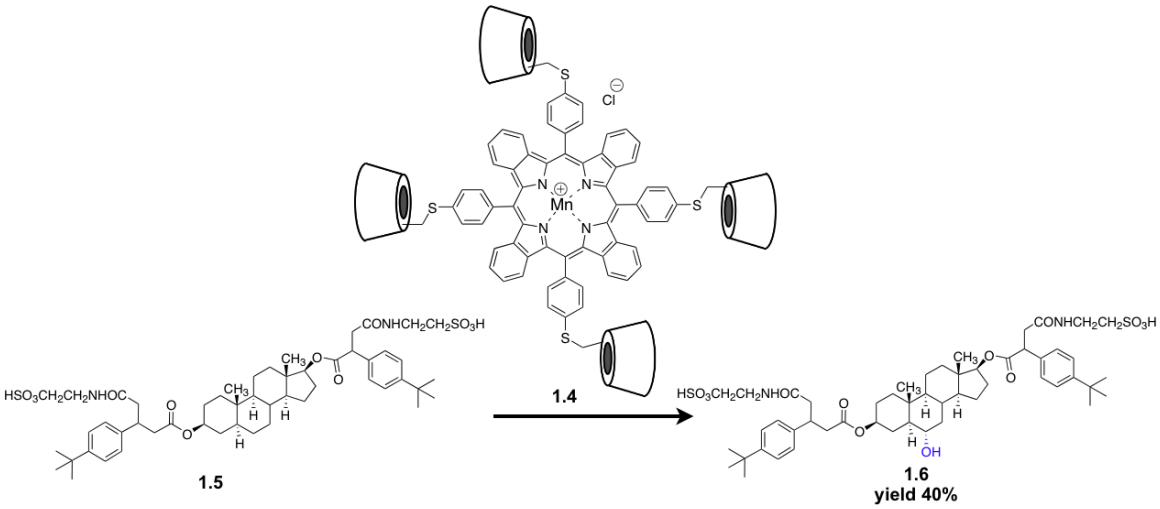

Scheme 1.3: Hydroxylation of the steroid derivative catalyzed by manganese porphyrin carrying four beta-cyclodextrins.[18]

The advancement in supramolecular catalysis is not limited to transition metal catalyzed reaction, organocatalysis is also a rapidly developing field. Organocatalysis often employs chiral compounds as catalyst to carry out a variety of organic transformation. Recent examples of this type of methodology can be found, for example in the work of Rebek *et. al*.[20] The investigators goal was to study the factors effecting the ring opening reactions of epoxides to afford either the five or six-membered ring products. The catalyst used was a cavitand (**1.7)** functionalized with a Kemp's triacid derivative (**Scheme 1.4**). The cavitand adopts a vase like structure that is stabilized by hydrogen bonds provided by the secondary amides around the rim of the receptor. These amides together, with the inward directing carboxylic acid group and the electron-rich π-surface of the receptor, provide the bound guest with organic functionality that are otherwise unavailable in solution. Cavitand **1.7** catalyzes a regiocontrolled cyclization of alcohol **1.8** to afford the five-membered ring product **1.9**. Moreover, the presence of the cavitands provides >100 fold rate enhancement of the cyclization reaction of **1.8** over the control reaction. The factors that the investigators suggested based on NMR spectroscopy that are responsible for this regiocontrolled cyclization reaction are: 1) Molecular recognition is involved as the substrate is surrounded by the catalyst of finite capacity. 2) Complexation exposes the epoxyalcohol to a high local concentration of the Brønsted acid. 3) CH-π contacts between the concave π-surface of the host and the alkyl backbone of the guest induces coiling of the substrate into conformations resembling the transition-state structures of the cyclization reaction. This system incorporates the arrangement of functionality and the unique solvation provided within the structured interior of natural enzymes.

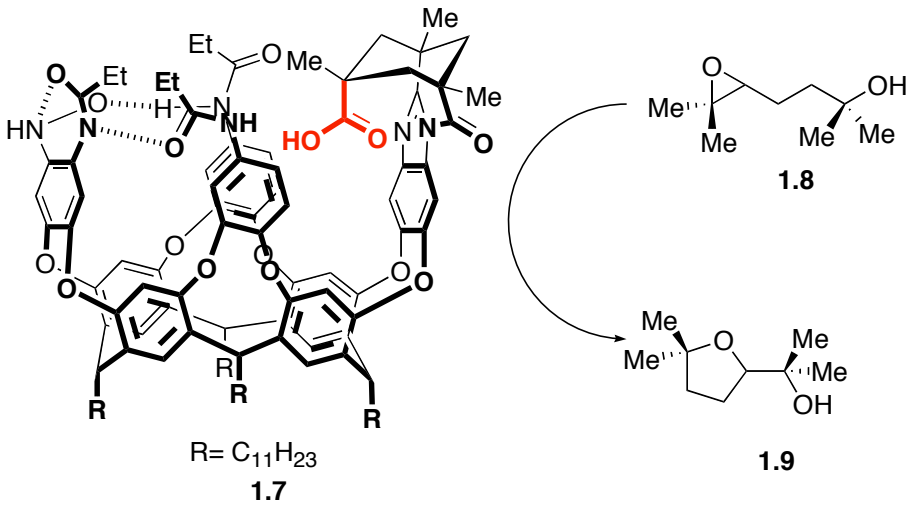

Scheme 1.4: Regiocontrolled cyclization of epoxide **1.8** to the five-membered ring ether **1.9** by the Cavitand catalyst **1.7**.

Miller and coworkers[21] have developed a kinase mimic that enables a catalytic, asymmetric synthesis of D-*myo*-inositol-1-phosphate (**1.14**) from *myo*-inositol (**1.11**) by using small peptide based catalysts (**1.10**) **Scheme 1.5**. Traditional known routes to this molecule involves numerous steps and the use of chiral auxiliaries.[22] The peptide based catalysts developed leads to the target molecule in a more efficient and direct manner. The investigators attached a small peptide sequence on modified His residue which forms intermediates such as the phosphorylated catalyst (phospho-imidazolium ion). Because the catalyst is attached to a small peptide sequence, the high-energy phospho-imidazolium ion is generated in a chiral environment, with functionality that interacts with multifunctional substrate in a site-specific fashion. As a result, phosphate transfer (to substrates such as **1.12**) occurs with both regio and enantioselectivity to produce regio and enantiopure products such as **1.14**. The reaction yields D-*myo*-inositol-1-phosphate in a 96% yield with a 98% *ee*.

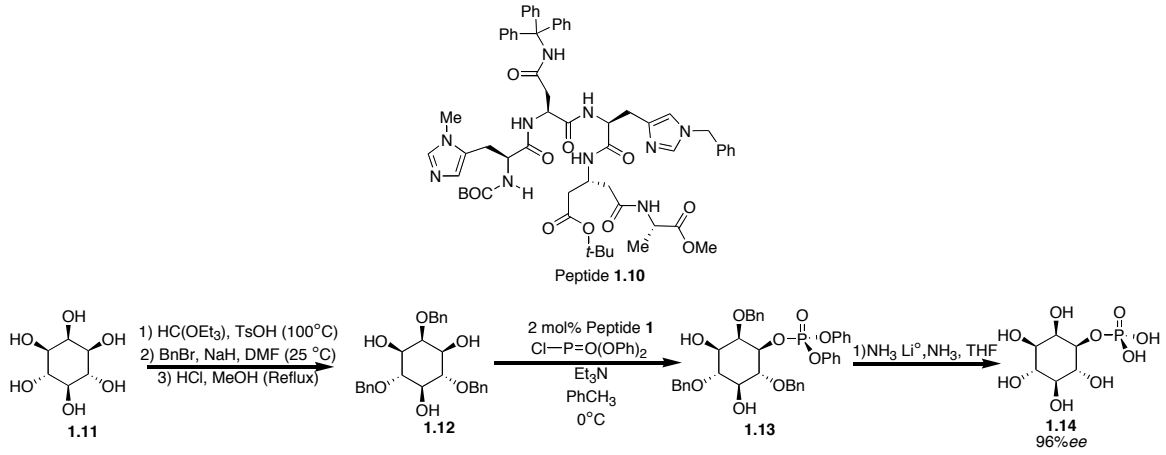

Scheme 1.5: Synthetic pathway to D-*myo*-Inositol-Phosphate (**1.14**) from *myo*-Inositol (**1.11**).[21]

1.3 SUPRAMOLECULAR INTERACTION AIDING IN ASYMMETRIC CATALYST DISCOVERY

The above discussion highlights a few seminal discoveries in the field of catalysis. It nicely explains how chemists have used supramolecular chemistry to design catalysts, which are used in synthetic methodology. We should realize that designing catalysis that mimics enzyme reactivity is not a trivial task. The molecular recognition interaction involved in binding are weak interactions which can be very difficult to analyze. Whenever chemists try to quantify weak interactions we find ourselves at the edge of detectability, as these interaction are very sensitive to environment. For example, an interaction which is potent in chloroform can be non-existent in water. To this end, understanding supramolecular interactions is the arsenal needed to develop efficient synthetic methodologies.

Today, the preparation of enantiomerically pure compounds is one of the most actively pursued fields in synthetic chemistry. Despite significant progress in the field of

theoretical and computational chemistry, there are still limited approaches to predict via a model the best catalyst for a given reaction. This long standing problem has a simple physiochemical origin as noted by Knowles in 1983[23] "*Since achieving 95% ee only involves energy differences of about 2 kcal, which is no more than the barrier encountered in a simple rotation of ethane, it is unlikely that before the fact one can predict what kind of ligand structures will be effective*". Note that 2 kcal/mol is also around the strength of one hydrogen bond, therefore one hydrogen bond difference between the substrate and the catalysis could make a huge difference in enantioselectivity. Therefore the search for active and enantioselective catalysts for synthetically important reactions stands as a major challenge for chemists. Further despite the introduction of combinatorial chemistry and miniaturization,[24] the determination of enantioselectivity in the screening of asymmetric catalytic reactions is often the rate determining step. Techniques that allow for the simultaneous screening of numerous catalysts hold promise for the field since they allow for accelerated catalyst discovery.[25,26]

Currently, chiral HPLC is the most commonly used technique to determine *ee*'s of asymmetric organic reactions. However, with the advent of combinatorial chemistry, which allows one to generate a large library of potential candidates (catalyst) for an asymmetric reaction, the need for faster techniques to determine enantioselectivity has been manifested. Therefore, many groups around the world are designing high-throughput screening methods based on enantioselective receptors. By introducing chirality into the binding sites, such receptors could carry out enantioselective recognition of chiral organic molecules. These sensors would be used for the rapid determination of enantiomeric excess to screen catalysts, for desired enantioselectivity in a particular reaction.

1.3.1 Combinatorial Chemistry

Before presenting and evaluating the screening systems that have developed, a few recent reports of the developments in the combinatorial preparation of enantioselective transition metal catalysts is appropriate. It will become apparent that these seminal contributions constitute the beginning of a fascinating new research area within supramolecular chemistry.

Combinatorial chemistry is the applied use of technologies and automation for the rapid chemical synthesis of relatively large number of compounds[24] The application of combinatorial chemistry to catalysis enables chemists to generate and evaluate a large number of catalyst simultaneously. Therefore, more simply stated, chemists use combinatorial chemistry to search for serendipitous supramolecular interactions in a catalyst that induces enantioselectivity in an asymmetric reaction.

Reetz and coworkers[27] recently described a new concept in the area of combinatorial enantioselective transition metal catalysis. They demonstrated that a mixture of two different monodentate phosphate ligands (L) coordinated to rhodium (Rh) leads to enhanced enantioselectivity in reduction of enamines (**Scheme 1.6**). The preparation of RhL^aL^b in pure form in solution was not expected. However, the mixture of all three catalyst may lead to enhanced enantioselectivity provided RhL^aL^b is more active and more selective than either of the traditional catalysts. The Rh-catalyzed hydrogenation of the acetamidoacrylate in dichloromethane was chosen as the test reaction (**Scheme 1.6**). The hydrogenation experiments were carried out in parallel manner using 20 or more flasks and *ee* values were determined by GC or HPLC. It was apparent that certain L^a/L^b combinations leads to high enantioselectivities, approaching 98% *ee*, compared to the use of homocombination, which leads to *ee* values of 92-94%. Rh-catalyzed hydrogenation of *N*-acyl enamine and dimethyl itoconate was also studied.

In each case heterocombination of ML^aL^b gave the best result. Ultimately the goal of all chiral ligand designs is to create a chiral environment around the metal to direct stereochemistry and impart the appropriate electronic characteristic at the metal center for efficient catalysis. The challenge is to find the right ligating groups that optimally fit the scaffold and makes the catalytic system more efficient. Small changes in the ligand structure can have profound effects. Therefore, efficient combinatorial approaches to catalyst optimization allows one to generate data sets of much greater complexity; perhaps of sufficient complexity to uncover trends that may be missed in a one variable at a time optimization algorithium.

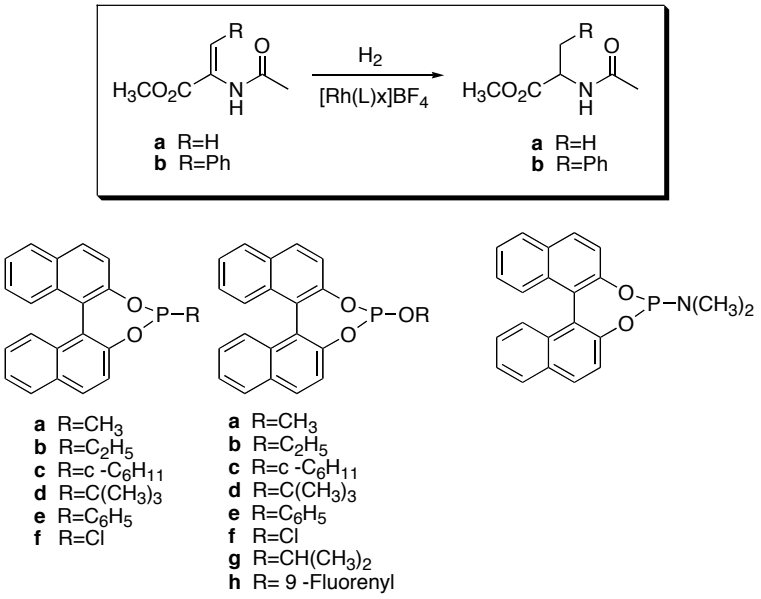

Scheme 1.6: Rh-catalyzed hydrogenation of the acetamidoacrylate.

Ding and coworkers[28] developed a highly efficient enantioselective catalyst for the hetero-Diels-Alder reaction by high-throughput screening of a combinatorial library of chiral titanium complexes. A combinatorial library of chiral metallic complexes was

generated by combining a diol ligand Lm with $Ti(OiPr)_4$ and an alternative diol Ln in a parallel fashion as shown in **Scheme 1.7**. They explained that these molecular assemblies form spontaneously and the composition of the mixture depends on thermodynamic factors. The substrate dictates assembly of the various metallic complexes which leads to the highly enantioselective asymmetric catalyst. A catalyst library of 104 members was generated from a 13 chiral ligands, which were then evaluated for the reaction of Danishesky's diene with benzaldehyde by using a high-throughput chiral HPLC technique. The investigators identified catalyst **L5/Ti/L5** and **L5/Ti/L6** as both efficient catalyst, and then optimized the reaction by using different solvents and catalyst loading. Under solvent free conditions, highly efficient ligand-metal loading as low as 0.005 mol % of **L5/Ti/L6** was identified for the cycloaddition of furfural to Danishefsy's diene to give the corresponding cycloadduct in 63% yield with 96.3% *ee*. Each derivative used in this example has identical hydroxyl ligating groups and a rather subtle variation in the biaryl scaffold. These variations cause a significant change in enantioselectivity. As the energy difference as small as 2 kcal/mol, which is right in the range of a hydrogen bond, can cause a huge change in enantioselectivity the prediction of the kind of interaction that causes that change is hard to predict. This example highlights the relevance of combinatorial approach in the search of efficient catalyst in organometallic reactions.

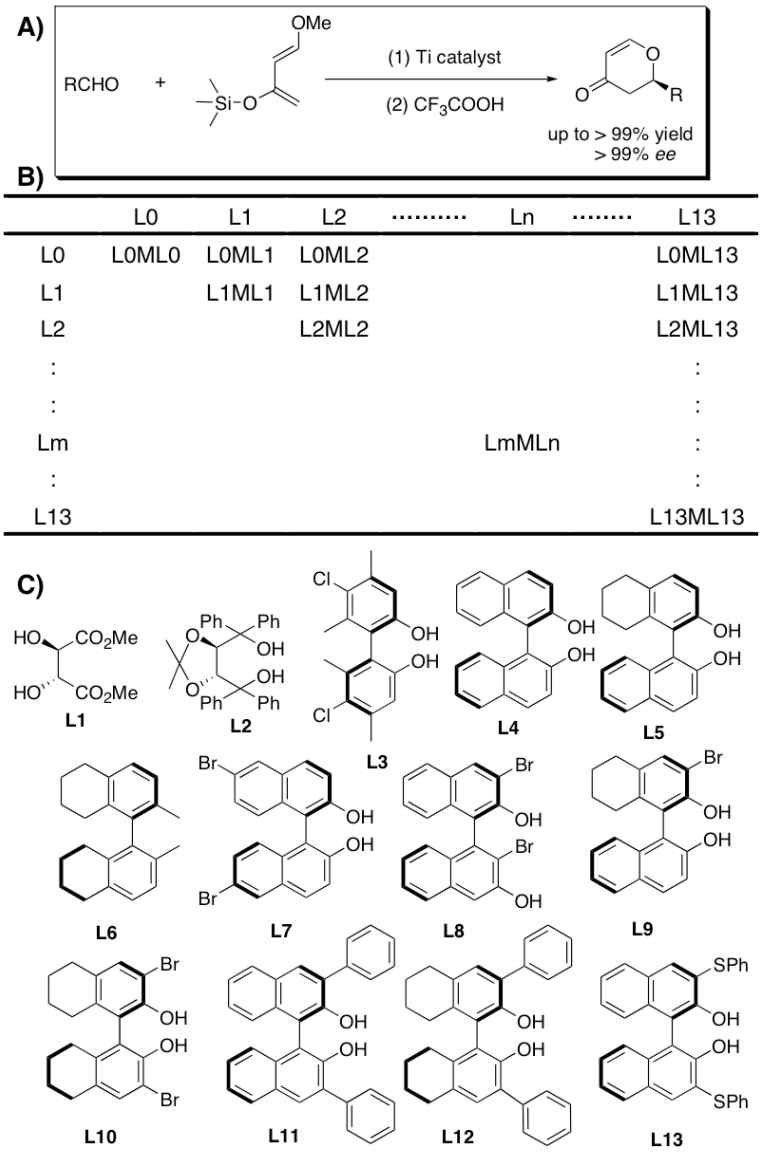

Scheme 1.7: **A**) Hetero-Diels-Alder reaction of aldehydes with Danishefsky's Diene. **B**) A combinatorial library of chiral metal complexes by combining diol ligand Lm and Ln in a parallel fashion. **C**) The diol ligands used for catalyst preparation.

1.3.1 Fluorescents Screening Approaches

Although the use of chiral HPLC and GC has been well established they are limited in the number of reactions that can be screened per day. A fairly rapid chiral HPLC run requires 10 minutes and often longer, which translates to only 144 reactions screened per day.[25] To circumvent the limitation of serial chromatography, several groups have created optical techniques using fluorescence or absorbance based on supramolecular chemistry interactions to screen asymmetric reactions.

Among the high-throughput screening methods for the discovery of chiral catalysts for asymmetric reactions, the use of fluorescence sensors is particularly interesting because fluorescence can provide both high sensitivity and real-time measurement.[29] In this section we describe some of the seminal work where fluorescence sensors are used directly or indirectly to screen for asymmetric catalysis.

Photoinduced electron transfer has been widely used as the preferred tool in fluorescent sensor design, its use eminates from supramolecular chemistry.[30, 31] In a general sense, PET sensors generally consist of a fluorophore and a receptor linked by a short spacer. When the electrons of the fluorophore are excited, electron transfer occurs from the donors high lying filled orbital, which results in quenching of the fluorescence (**Figure 1.2**). Upon binding of the analyte, the energy level of the donor orbital is lowered, thereby diminishing the ability to transfer an electron to the excited-state acceptor, and fluorescence is restored. The advantage of this method is that it results in an off-to-on signal.

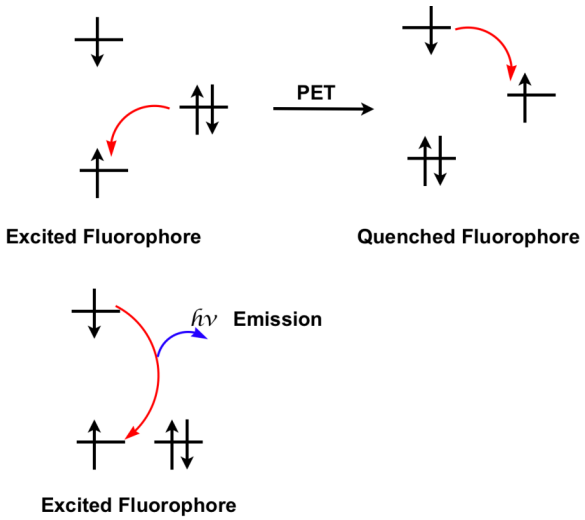

Figure 1.2: Photoinduced electron transfer mechanism.

The assay described by Copeland and Miller[32] relies upon a fluorescently labeled split and pool peptide library synthesized on solid-phase beads. The sensing mechanism is based on photoinduced electron transfer (PET). The library is screened for activity of an acylation reaction. As the acylation reaction between alcohol **1.15** and acetic anhydride proceeds, acetic acid and ester **1.16** (**Scheme 1.8**) are generated. The acetic acid is signaled by the increase in the fluorescence intensity of the fluorophore, which is linked to the peptide catalyst on solid support. A sample of the library was selected at random and screened for the reaction of racemic **1.15**. Approximately about 1000 catalysts were screened conveniently over the course of a 60 min period. From the assay the brightest beads were manually selected, washed, and subjected to a single bead kinetic resolution. The beads with the highest selectivity were then deconvoluted by Edman degradation, resynthesized and subjected to the reaction condition. A key feature of this assay is that the fluorescence signal is coupled to catalyst activity, but not to the degree of enantioselectivity. The investigators showed that the most active catalyst also

exhibits a good degree of enantioselectivity This arises from selective binding, the result of secondary effects like hydrogen bonding, ion pairing and π-π interactions, present in the transition-state between the substrate and the catalyst. These are supramolecular interactions, and the technique described beautifully identifies the lead catalyst that encompasses interactions that result in high enantioselectivity.

A lead peptide was identified that provides a selectivity factor (k_{rel}) of 8.2. A directed second generation split and pool peptide was synthesized such that the new peptide sequences in the library were biased toward the lead structure. These second-generation catalysts were screened again, and revealed an active and enantioselective peptide catalyst for a range of different alcohols. In this particular approach, thousands of peptide based catalysts were screened, and thus the high-throughput screening approach devised by this group was crucial for rapid analysis in an efficient manner. This study nicely highlights the potential of possessing high-throughput screening methods for the development of new catalytic asymmetric transformations.

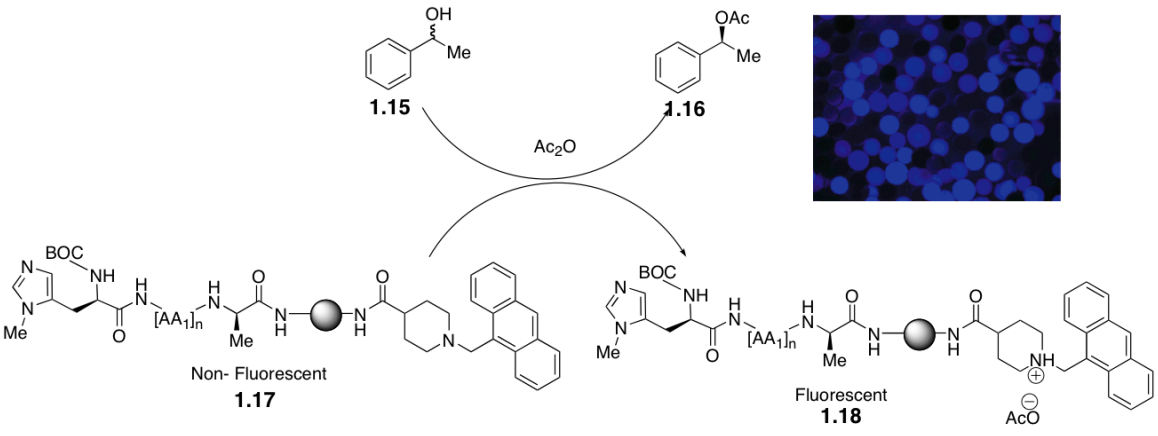

Scheme 1.8: Fluorescence screening assay of the peptide library for acylation reaction.[32]

Lin Pu and coworkers[33] have used their highly enantioselective fluorescent sensor bisbinaphthyl macrocycle (*S*)- and (*R*)-**1.21** to determine *ee'*s of substituted mandelic acids (**1.20**) (**Scheme 1.9**). To utilize the enantioselective fluorescent sensor in chiral catalyst screening they prepared an alkylated derivative of mandelic acid that precipitated out of the catalyst screening reaction mixture, thereby allowing simple product separation. This strategy allowed the investigators to screen the asymmetric reaction of **1.19** with trimethylsilyl cyanide (TMSCN) in the presence of $Ti(O^iPr)_4$ and chiral ligand (+)/(-)-diisopropyltartrate (DIPT) under various reaction conditions. Due to the insolubility of the product in the reaction mixture it was isolated by centrifugation and filtration. The products were then treated with the fluorescent sensors (*S*) and (*R*)- **1.21** in THF and the *ee'*s were predicted through *ee* calibration curves. The sensor (*S*)- **1.21** has a high enantioselectivity and sensitivity to (*S*)-mandelic acid over (*R*)-mandelic acid and visa versa. The investigators concluded by NMR spectroscopy[34] that in the macrocycle-mandelic acid complex, (*S*)-mandelic acid is probably located much deeper inside the chiral cavity of the (*S*)- **1.22** than (*R*)-mandelic acid which, significantly shields the alpha proton of the (*S*)-mandelic acid by the aromatic rings of the macrocyle. This supramolecular interaction could be the origin of the dramatic difference in the fluorescence responses of the (*S*)- **1.21** towards the two enantiomers of mandelic acid. The ^1H NMR spectroscopic study also indicates that (*S*)- **1.21** probably binds more than one equivalent of (*S*)-mandelic acid. This screening method also utilizes PET. Upon binding of the analyte to the chiral receptor the fluorescence signal turns on.

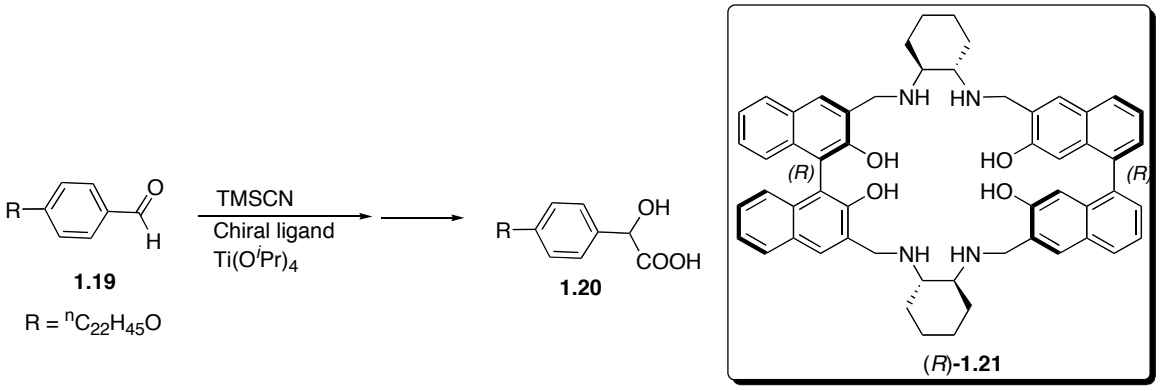

Scheme 1.9: Enantioselective fluorescent recognition of mandelic acid.

Janda and coworkers[35] employed monoclonal antibody 19G2 to screen asymmetric α-alkylation reactions. This monoclonal antibody was found to bind to both (*R*)-**1.24** and (*S*)- **1.24**, but only the 19G2-(*S*)- **1.24** complex afforded a blue fluorescence. The investigator screened asymmetric α-alkylation reaction of **1.22** with **1.23** using Cinchono alkaloids phase transfer catalysis. A catalyst library consisting of 35 catalysts derived from Cinchona alkaloid was synthesized. *Ee* calibration curves of (*S*)- **1.24** and (*R*)-**1.24** were developed by mixing each *ee* solution with 19G2 at a constant concentration. The fluorescence intensities were measured (λ_{ex}= 327 nm, λ_{em}= 416 nm) by using a 96-well plate reader, and a calibration curve relating fluorescence intensity to *ee* was plotted. The fluorescence values of each of the 35 product mixtures were then obtained the same way and the *ee* values were calculated from the calibrated graph. The blue fluorescent monoclonal antibody sensor was able to identify high-performance catalysts for the asymmetric α-alkylation reaction of *N*-(diphenylmethylene)glycine methyl ester with bromomethyl-*trans*-stilbene (**Scheme 1.10**). The investigators suggested that the emission of the blue-fluorescent is due to the formation of an exciplex between the antibody and the (*S*)-**1.24**. An exciplex is a cooperative interaction of two

molecules in the excited-state. There initial study with 19G2 and stilbene hapten complex suggested that there is a π-stacking interaction between the aromatic ring of the substrate and the tryptophane unit of the antibody. At > 250 K twisting or spring-like vibrations between the excited-state stilbene hapten molecules and the antibody causes a changes in the π-overlap. This electronic perturbations results in emission.[36]

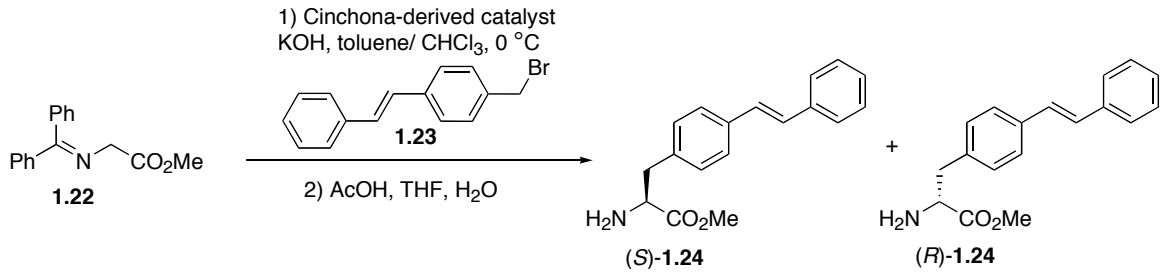

Scheme 1.10: Asymmetric α-alkylation reaction of *N*-(diphenylmethylene)glycine methyl ester (**1.22**) with bromomethyl-*trans*-stilbene (**1.23**) for the synthesize of chiral ligands (*S*)- **1.24** and (*R*)- **1.24** for monoclonal antibody 19G2 sensor array by using Cinchona-derived catalyst.

1.2.3 UV-visible Screening Approaches

Visible detection of color for the determination of enantiomeric excess values is an important step forward in the development high-throughput screening method for asymmetric catalyst discovery. In this section we highlight some techniques based on UV-visible spectroscopy towards screening for enantioselectivity.

Reetz *et al*. reported the first high-throughput screening strategy based on UV-vis spectroscopy in 1997. He used in vitro evolution of an enzyme to increase the enantioselectivity of a given biocatalytic reaction.[37] The enantioselective hydrolysis of racemic *p*-nitrophenyl 2-methyldecanoate (**1.25**) was chosen as the test reaction. The enzyme chosen was the lipase from the bacterium Pseudomonas aeruginosa. This enzyme

catalyzes the hydrolysis of **1.25** in favor of the (*S*)-configuration acid **1.26** with a selectivity of only a 2% *ee.* Using "error-prone" polymerase chain reaction (epPCR), the lipase gene consisting of 933 base pair was subjected to random mutagenesis resulting in 1000 mutants that were screened for enantioselectivity in the test reaction. Conventional product separation based on liquid or gas chromatography was unsuitable due to the large number of samples, therefore 96-well plate microtiter plates were used. The rate of enzyme hydrolysis of the enantiomerically pure (*R*)-**1.25** and (*S*)-**1.25** was measured by monitoring the change in absorbance of the *p*-nitrophenol anion at 410 nm as a function of time. Of the 1000 mutants of the first generation tested, 12 showed an increase in enantioselectivity. The improved mutants were then mutated again and rescreened. After four generations the investigators were able to increase the enantioselectivity of the test reaction from 2% *ee* to 81% *ee*. The point specific interaction between the catalyst (lipase) and the substrate leads to a high enantioselectivity. The molecular basis of the enatioselectivity is difficult to predict, as the energies involved are small. The evolutive optimization of enzyme structure described does not require any knowledge of enzyme structure or catalytic activity and allows the investigators to rapidly identify the enzyme that gives high enantioselectivity.

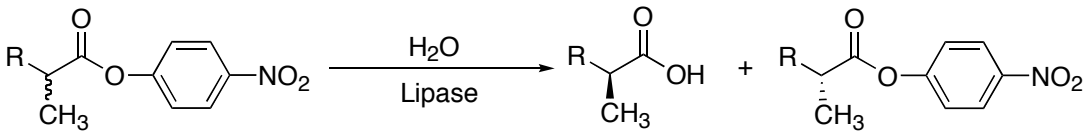

1.25
R = *n*-C_8H_{17}

(*S*)-**1.26**

(*R*)-**1.27**

Scheme 1.11: Enantioselective hydrolysis of racemic *p*-nitrophenyl 2-methyldecanoate.

Paul Abato and Christopher T. Seto[38]developed an enzymatic method for the determination of enantiomeric excess (EMD*ee*). They chose the addition of diethylzinc to benzaldehyde as a test-bed for their EMD*ee* technique. The reaction yields 1-phenylpropanol (**1.30**). Subsequently, the (*S*)-**1.30** enantiomer of the product is oxidized to the ketone (**1.31**) using the (*S*)-aromatic alcohol dehydrogenase from *Thermoanaerobium sp*. The rate of the enzymatic reaction was monitored by observing the formation of NADPH by UV spectroscopy at 340 nm. The (*S*)-**1.30** enantiomer is a good substrate for the enzyme with a K_M value of 6.4 ± 1.1 mM, while (*R*)-**1.30** is an inhibitor with the K_i value of 6.0 ± 1.5 mM. The Michaelis-Menten equation provides a direct relationship between the rate of this enzymatic oxidation and the concentrations of (*S*)-**1.30** and (*R*)-**1.30**. Therefore, the rate of this oxidation is used as a direct measurement of the enantiomeric excess of the samples and 1-phenylpropanol. They were able to analyze 100 unknown samples in 30 min by using a 384-well plate. The important feature of EMD*ee* is its high stereoselectivity. The alcohol dehydrogenase used in these studies has a high selectivity for the (*S*)-aromatic alcohol and does not process the (*R*) enantiomer to any significant extent under the assay conditions. Herein, the investigators are utilizing natural seteroselectivity of enzymes to identify the chiral catalyst needed for this reaction.

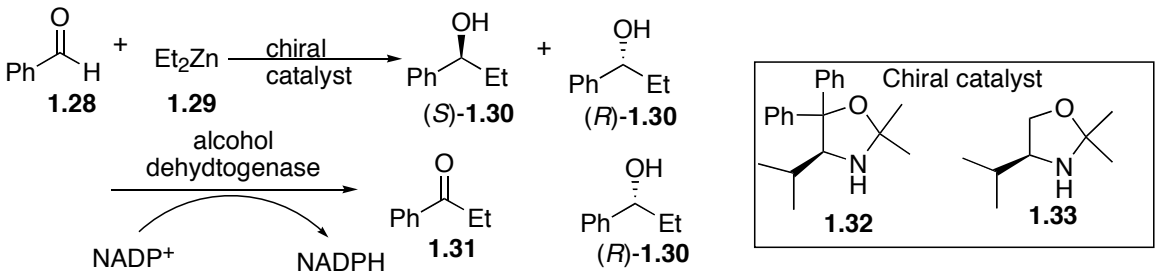

Scheme 1.12: An enzymatic method screening method to determine the enantiomeric excess of the addition reaction of diethylzinc to benzaldehyde.

David B. Berkowitz *et.al* [39] have also reported an enzymatic screening method. They employed two reporting enzymes in parallel cuvettes, for which they coined the term in situ enzymatic screening (ISES). The reporting enzymes provide information on both relative rates and enantioselectivity. To demonstrate proof of principle, the investigators chose the hydrolytic kinetic resolution of (±)-propylene oxide, a reaction known to be catalyzed efficiently by chiral Co(III)-salen complexes.[40] The alcohol dehydrogenases from *horse liver* (HLADH) and *Thermoanaerobium brockii* (TBADH) were used. The former enzyme prefers (*S*)-1,2 propanediol, whereas the latter favors the (*R*)-1,2 propanediol. A library of chiral salen ligands was created, and the experiment was set up such that the Co(III)-salen catalysts were placed in the lower organic layer ($CHCl_3$ and epoxide) in the two parallel cuvettes (**Scheme 1.13**). The aqueous reporting layers contained TBADH/$NADP^+$ (cuvette 1) and HLADH/NAD^+ (cuvette 2). The increase in absorbance at 340 nm was followed in parallel by UV-vis spectroscopy. The kinetic data from the two enzymes was then used to measure *ee* of the unknown samples and identify the active Co(III)salen catalyst. Herein the investigators used the inherent stereospecificity of the enzymes as an analytical tool to determine the ideal ligating groups for this particular organometallic reaction.

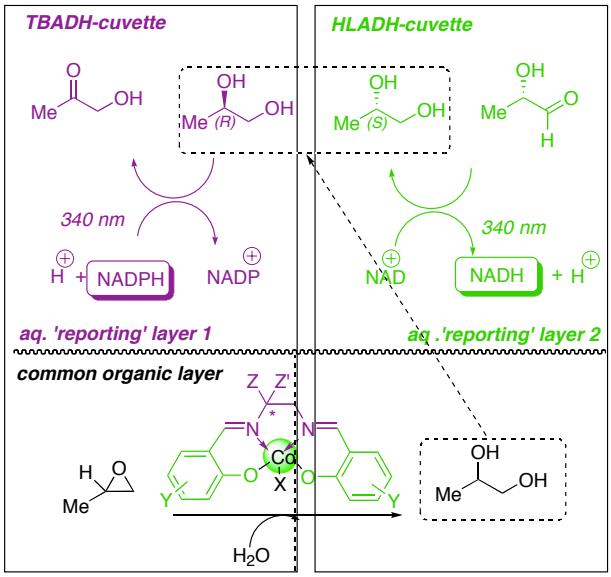

Scheme 1.13: Double cuvette in situ enzymatic screening (ISES).

Enantiomerically pure cyanohydrins are versatile synthetic building blocks. Moberg and co-workers[41] have developed an efficient catalytic system employing dual Lewis acid-Lewis base activation for the preparation of highly enantioenriched O-acetyled cyanohydrins from aldehydes and acetyl cyanide. The reaction produces a high yield of the desired compounds without the formation of the byproduct. By varying the reaction conditions, in particular the nature of the Lewis acid and the Lewis base, yields and enantioselectivity of the reaction can be optimized. In collaboration with Hult and Hamberg,[42] they developed a high-throughput enzymatic method for the simultaneous determination of enantioselectivity and yield by using a combination of a non-selective and a selective enzyme. In the catalyzed reaction (**Scheme 1.14A**) various *ee* values for the chiral O-acetylated cyanohydrin are obtained. The analysis of the yield was based on

the quantification of unreacted benzaldehyde by using UV-vis spectroscopy (**Scheme 1.14B**). Benzaldehyde was reduced by NADH in the presence of horse liver alcohol dehydrogenase (HLADH). Upon reduction of benzaldehyde NADH (which absorbs at 340 nm) was converted to NAD^+ (which does not absorbs), allowing the amount of unreacted benzaldehyde to be determined. This analysis was followed by enzymatic hydrolysis of (*S*)-acetylated cyanohydrin using Candida Antarctica lipase B (CALB), which has a high (*S*)-enantioselectivity. The cyanohydrin of the *S*-product is in equilibrium with benzaldehyde and can, therefore, be analyzed in the same way as unreacted aldehyde by NADH oxidation. Unselective hydrolysis using pig liver esterase (PLE) finally affords the free cyanohydrin of the second enantiomer, which is also in equilibrium with benzaldehyde, and is analyzed by NADH. Since all analytes are quantified by using the same aliquot and only ratios between the different signals are used to calculate the enantiomeric excess and conversion, a precise knowledge of concentration and volume is not required. The principle is to convert a mixture of enantiomers to a mixture of chemically different species by selective enzymatic transformations, which enables a measurement of enantiomeric excess by simple chemical analysis. For this analysis the investigators developed a method based on quantification of benzaldehyde, which allows them to quantify yield and *ee* of the asymmetric reaction.

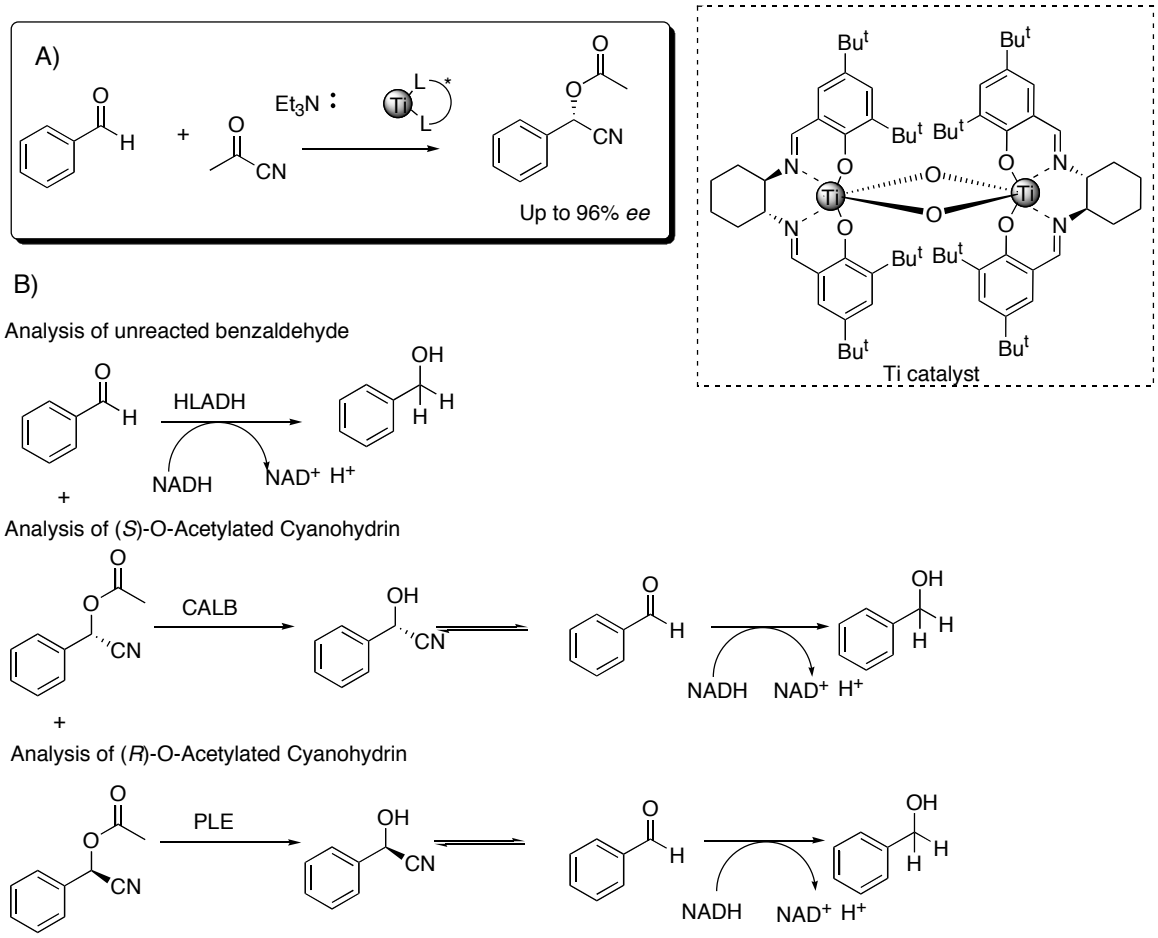

Scheme 1.14: A) Dual Lewis acid–Lewis base catalyzed addition of acetyl cyanide to benzaldehyde. B) Enzymatic method for enantiomeric excess determination of O-acetylated cyanohydrins.

Hartwig and coworkers[43] have developed a colorimetric assay to simultaneous evaluate a large number of potential catalyst for the hydroamination of 1,3 dienes. The colorimetric response indicates the presence or absence of aniline. The colorimetric assay was based on furfural, which undergoes a condensation and ring opening with 2 equiv of aniline in the presence of acid to create a red product, but not with an alkylated aniline. Thus, after the addition of furfural and trifluoroacetic acid (TFA), the reactions that

consume the largest amount of aniline shows an absent of the red color. These experiments were carried out in a 96-well plate and identified [Pd(π-allyl)Cl_2] and PPh_3 as the most active catalyst. After the identification of the active catalyst they developed an enantioselective version of this process by using Trost ligand **1.38**[44]and [Pd(π-allyl)Cl_2] in the absence of acid **Scheme 1.15**. This technique allowed the investigators to screen several ligands that would create an ideal scaffold around the metal center and allow the reaction to take place. The screening process allowed them to optimize the achiral reaction and extend its application to an enantioselective transformation.

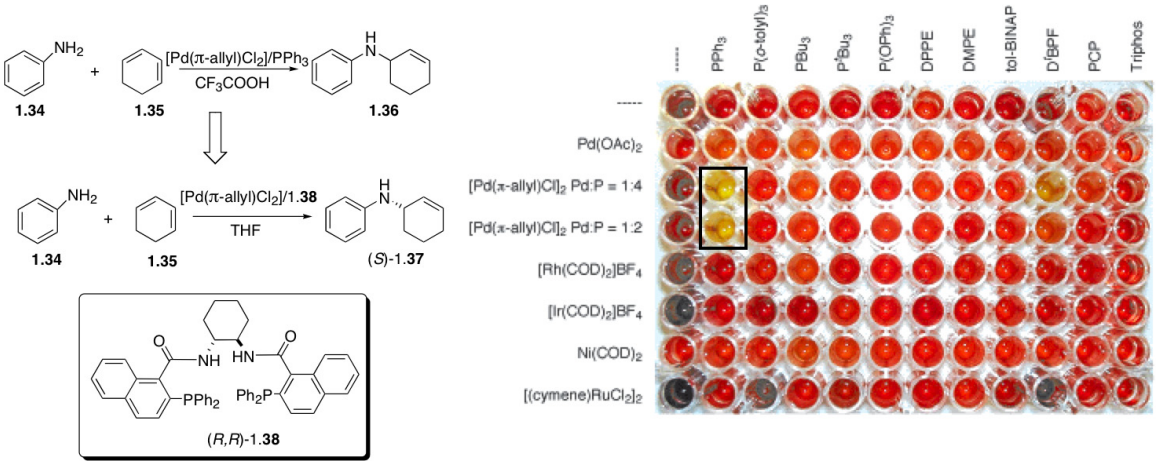

Scheme 1.15: Use of a simple spot test to screen catalyst for the hydroamination of cyclohexadiene with aniline. A red color indicates remaining aniline reactant. The reaction was made enantioselective by using Trost chiral ligand (*R,R*)-**1.38**.[44]

Feringa and co-workers designed a colorimetric assay based on cholesteric liquid-crystalline (LC) films.[45] Cholesteric, or twisted nematic liquid-crystalline phases, can be induced by doping achiral nematic liquid crystals host compound with a suitable chiral dopant. The helical twisting of the LC is caused by supramolecular interactions of the

chiral substrate with the liquid-crystalline film. The magnitude of the helical twisting power of any chiral dopant is too small to obtain colored liquid-crystalline phases, since there is a limit to the amount of dopant that can be added to the liquid crystal. Thus, in order to obtain a significant color change the chiral analyte has to be derivatized prior to use in the analysis. For example, *para*-n-heptyloxyphenyl-substituted chalcone **1.40** is used as the starting material instead of chalcone. Samples of the LC doped with **1.41** with 100, 90, 80, 70, 60, 50% *ee* gave LC with color ranging from violet-blue 100% *ee* to deep red 50% *ee* (**Scheme 1.16**). To demonstrate the screening process, the investigators chose to study the copper-catalyzed asymmetric conjugate addition of diethylzinc to chalcone **1.40** with six chiral phosphoramidite ligands. The enantiomeric excess values of these reactions were accurately determined by the color of the LC and **1.39** was identified as the most active and selective ligand for this reaction. The drawback of this method is the necessity for derivatization of the starting material. However, this methodology allows fast and accurate screening of enantioselectivities in asymmetric catalysis.

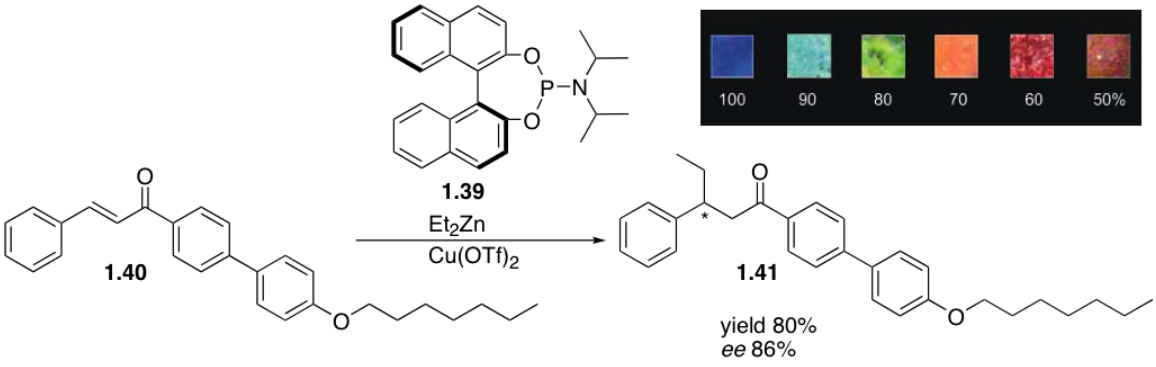

Scheme 1.16: Copper catalyzed asymmetric conjugate addition of diethylzinc to *para-n*-heptyloxyphenyl-substituted chalcone. Tf = trifluoromethanesulfonyl.

High-throughput screening methods are also being developed in our lab for asymmetric catalyst discovery. The method is based on an Indicator Displacement Assay (IDA).[46] An indicator displacement assay relies upon a colorimetric or fluorescent indicator that changes optical or electrochemical properties when bound to a host relative to being free in the bulk medium. The advantage of this method is it eliminates the need of attaching the fluorophore to the receptor, subsequently simplifying the synthesis of the receptors. The most commonly used indicators are pH indicators.[47] The competition between an indicator and the guest of interest for the binding site of the host allows the determination of total guest (or analyte) concentration $[G]_t$. We have expanded the scope of IDA to enantioselective indicator displacement assays (eIDA's) by incorporating chirality into the host,[48-51] which allows us to quantify *ee* in addition to the concentration of a chiral analyte. This approach relies on the energetic difference between the two diastereomeric complexes that are formed when a chiral host interacts with the two enantiomers of the guest molecule. Artificial Neural Networks (ANNs) has been used by the investigators as the data analysis tool. ANN-based approaches have advantages that include a capacity to self-learn and to model complex data without the need for a detailed understanding of the underlying phenomena.[52, 53] There are many types of neural networks for various applications available in the literature. Multilayered perceptron (MLP) is the simplest, and therefore most commonly used neural network with a feed-forward topology. In many of our studies a simple three layered MLP network is utilized.

The Anslyn group has shown that chiral boronic acid based receptors can enantiodiscriminate chiral diols and chiral alpha-hydroxycarboxylic acids using eIDA[50] (discussed in chapter 3). They have also reported that eIDA with chiral Cu^{II} complexes and indicator chrom azurol S (CAS) was used to discriminate 13 of the 20 natural α-amino acids (**Scheme 1.17A**). The assay was first developed using a UV-vis

spectrophotometer where the *ee* calibration curves were generated to determine the *ee* of the unknown amino acid solution.[54] To transition into a high-throughput screening method, a 96-well plate format was used to create *ee* calibration curves. The *ee* of unknown solution were then analyzed and the results were compared to those previously obtained with a conventional UV-vis spectrophotometer. The two techniques show little or no difference in accuracy.[55]

To examine the practicality of the assay a sample of valine was synthesized using the asymmetric reaction shown in **Scheme 1.17B**.[56] The *ee* value of the unknown valine solutions was first analyzed by eIDA using $[Cu^{II}(R,R\text{-}\mathbf{1.42})\text{-}(CAS)]^{2-}$ method. The *ee* results of the eIDA method were show to differ from chiral HPLC and chiral shift reagent by 4.7% and 12.0%. The same data used to generate *ee* calibration curves for valine was then used to train an ANN, and the *ee* value for the unknown valine solutions predicted by ANN were compared to those obtained with chiral HPLC and chiral shift reagent. The errors between % L-valine values were 5.9% and 2.2% respectively. The two examples using eIDAs just described are truly high-throughput as samples can be analyzed very rapidly using 96-well (or more) plate format, and no derivitization is required.

The Anslyn's group has extended the definition of supramolecular chemistry within the context of analytical chemistry; noncovalent or reversible covalent interaction are considered supramolecular. The term Supramolecular Analytical Chemistry was defined by Anslyn,[57] "*the dynamic exchange of synthetic chemical structures that create assemblies which result in signal modulation upon addition of analytes*." The metal-coordinated assembly and the reversible covalent bond formation of boronic receptors are example of such dynamic assemblies.

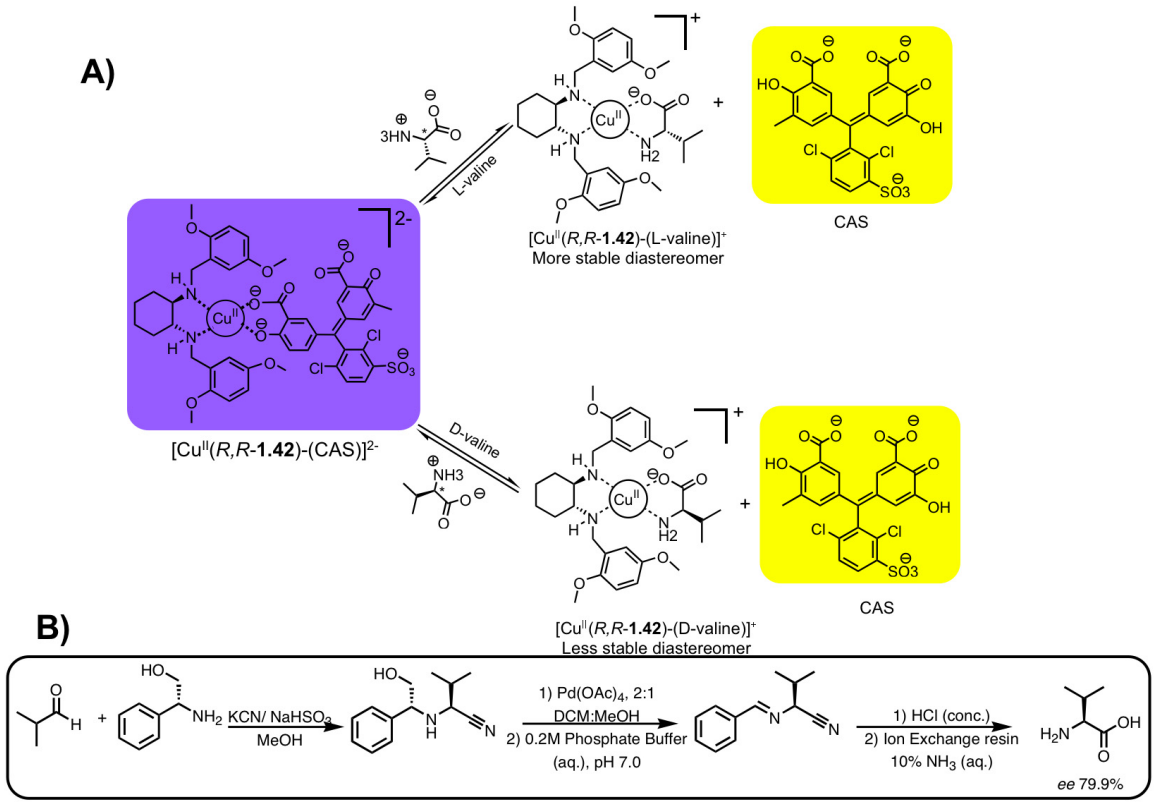

Scheme 1.17:**A**) Enantioselective indicator displacement assays for valine based on displacement of Chrom Azurol S (CAS) from complex [Cu^{II}(*R,R*-**1.42**)-(CAS)]$^{2-}$ **B**) The asymmetric reaction analyzed by the assay.

Most recently in Anslyn's group circular dichroism spectroscopy (CD) was used to determine the *ee* and concentration of unknown diamines samples.[58] To adapt CD techniques to HTS we exploited the chiral metal [Cu(I)(BINAP)$(MeCN)_2$]PF_6 (**1.43**) complex that has a CD active metal to ligand charge transfer (MLCD) band. Both *R* and *S* complexes show MLCT bands around 340 nm, and the enantiomers give opposite cotton effects. To demonstrate the ability to distinguish enantiomers as well as chemical identity we studied the interaction of the analytes shown in **Scheme 1.18** with (*R*)-**1.43**. Each diamine, as well as the enantiomers thereof, leads to different CD active MLCT bands.

As a representative example, the CD spectra produced by the addition of 2 equiv of either (1*R*,2*R*)-PD or (1*S*,2*S*)-PD to a solution of (*R*)-**1.43** in acetonitrile are shown in **Scheme 1.18**. Discrimination of all the analytes involved recording the CD spectra of each at 0.8 mM concentration, and to ensure reproducibility each experiment was performed five times. The data was analyzed at four wavelengths and subjected to linear discrimination analysis (LDA).[59] The LDA plot shows excellent discrimination of all the diamines and their enantiomers. To determine concentration and enantiomeric excess of unknown analyte solutions, *ee* titrations were performed at three different concentrations of PD. Five replicates were done for each *ee* titration. The data was analyzed using principal component analysis (PCA) showing orthogonal concentration and *ee* axes.[59] To transition into a high-throughput screening method and to obtain quantitative values of *ee* and concentration ANN was used and the assay was transitioned to a 96-well plate format. Four test PD solutions were analyzed and the values of concentration and (%*R,R*) had an average error of only 7.7% and 2.6% respectively. Metal coordination combined with CD spectroscopy was used to create a pattern recognition protocol for several diamines. Due to the intrinsic chirality of the host, the substrates are classified enantioselectively on the PCA plot.

Currently molecular recognition is driven by the goal of synthesizing receptors for various guest as a means of mimicking Mother Nature. However, because of the simplicity of the synthetic receptors, they cannot compete with enzymes because of their lack of specificity of binding. However in our group, we have used this lack of selectivity of synthetic receptors as a virtue in the context of array sensing. As described above, we have are able to design simple receptor to create arrays that can quantify *ee* and concentration.

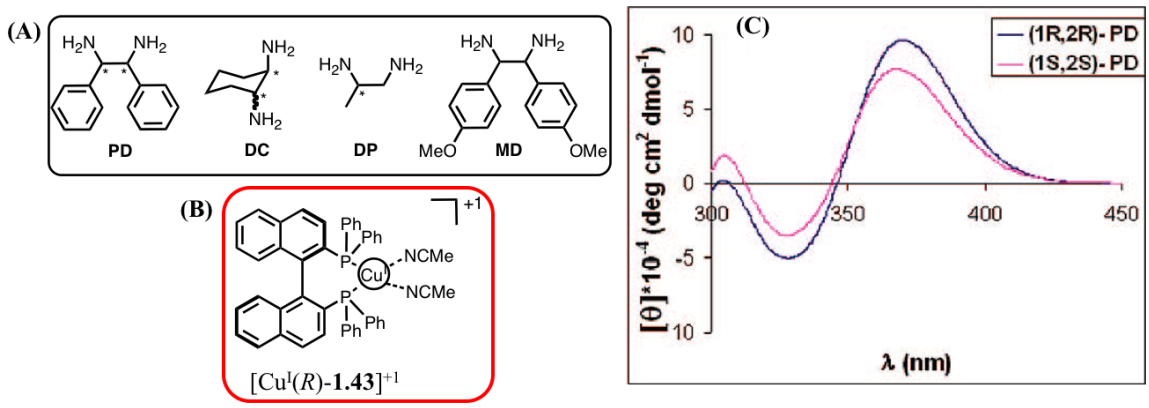

Scheme 1.18: (**A**) 1,2 diphenylethylenediamine (**PD**), 1,2-diaminocyclohexane (**DC**), 1,2-diaminopropane (**DP**), bis-(4-methoxyphenyl)-1,2-diaminoethane (**MD**) (**B**) [Cu^{I}(*R*)-**1.43**] chiral complex (**C**) CD spectrum for (*R*)-**1.43** [0.4mM] and 2 equiv of the enantiomers of PD [0.8mM].

1.4 Summary and Outlook

The examples illustrated in this chapter demonstrate how chemists are able to rapidly create a library of chiral catalyst that can potentially serve as mimics of natural enzyme systems. The screening of these catalysts for their efficiency and selectivity is often the rate-determining step. Over the last five years molecular sensors have been developed by supramolecular chemist to determine enantioselectivity, now the true potential of these molecular sensors for asymmetric catalyst discovery is being explored. Each reaction is unique thus new strategies have been developed by chemist to indicate enantioselectivity. This opens up a new chapter in the field of molecular recognition, simply because now large libraries of catalyst can actually be screened rapidly by these high-throughput screening methods. The proceeding chapter describes the journey towards the development of a high-throughput screening method for the determination of concentration and enantioselectivity of chiral 1,2 diols and alpha-hydroxycarboxylic

acids, using boronic acid receptors. To design efficient enantioselective receptors, the structural aspect of these receptors was investigated by x-ray crystallography and ^{11}B NMR.

1.5 REFERENCES FOR CHAPTER 1

1. Lad, C.; Willaims, N. H.; Wolfenden, R., The Rate of Hydrolysis of Phosphomonoester Dianions and the Exceptional Catalytic Proficiencies of Protein and Inositol Phosphatases. *Proc. Natl. Acad. Sci. U. S. A.* **2003,** 100, 5607.

2. Summer, J. B., The Isolation and Crystallization of The Enzyme Urease. Prelimanry Paper. *J. Biol. Chem* **1926,** 69, 435.

3. Fisher, E.; Dtsch, B., **1894,** 27, 3189.

4. Koshland, D. E., How a non-conformist theory beat scepticism and got into the textbooks. *Nature* **2004,** 432, 447.

5. Pauling, L., *Eng. News* **1946,** 24, 1375.

6. Warshel, A.; Levitt, M., Theoretical studies of enzymic reactions: Dielectric, electrostatic and steric stabilization of the carbonium ion in the reaction of lysozyme. *J. Mol. Biol* **1976,** 103, 227.

7. Benkovic, S. J.; Hammes-Schiffer, S., A perspective on enzyme catalysis. *Science (Washington, DC, U. S.)* **2003,** 301, (5637), 1196-1202.

8. Ohshima, T.; Iwasaki, T.; Maegawa, Y.; Yoshiyama, A.; Mashima, K., Enzyme-Like Chemoselective Acylation of Alcohols in the Presence of Amines Catalyzed by a Tetranuclear Zinc Cluster. *J. Am. Chem. Soc.* **2008,** 130, 2944-2945.

9. Gardossi, L.; Bianchi, D.; Klibanov, A. M., Selective Acylation of Peptide Catalyzed by Lipases in Organic Solvent. *J. Am. Chem. Soc.* **1991,** 113, 6328-6329.

10. Voet, D.; Voet, J. G., *Biochemistry*. 3rd ed.; John Wiley & Sons, inc: 2004.

11. Breuer, M.; Ditrich, K.; Habicher, T.; Hauer, B.; Kefleler, M.; StÜrmer, R.; Zelinski, T., Industrial Methods for the Production of Optically Active Intermediates. *Angew. Chem., Int. Ed.* **2004,** 43, (7), 788-824.

12. Knowles, W. S., Asymmetric Hydrogenation (Nobel Lecture 2001). *Adv. Synth. Catal* **2001,** 345, (1-2), 3-13.

13. Knowles, W. S., Asymmetric Hydrogenation (Nobel Lecture 2001). *Adv. Synth. Catal* **2001,** 345, (1-2), page 7, 2nd paragraph.

14. Halpern, J., Mechanism and seteroselectivity of asymmetric Hydrogenation. *Science* **1982,** 217, (4558), 401-407.

15. Knowles, W. S., Asymmetric Hydrogenations (Nobel Lecture) *Angew. Chem., Int. Ed.* **2002,** 41, 1998-2007.

16. Sharpless, K. B., Searching for New Reactivity (Nobel Lecture). *Angew. Chem., Int. Ed.* **2002,** 41, 2024-2032.

17. Noyori, R., Asymmetric Catalysis: Science and Opportunities (Nobel Lecture). *Angew. Chem., Int. Ed.* **2002,** 41, 2008-2022.

18. Breslow, R.; Huang, Y.; Zhang, X.; Yang, J., An artificial cytochrome P450 that hydroxylates unactivated carbon with regio- and stereoselectivity and useful catalytic turnovers. *Proc. Natl. Acad. Sci. U. S. A.* **1997,** 94, 11156-11158.

19. Fang, Z.; Breslow, R., Metal Coordination-Directed Hydroxylation of Steroids with a Novel Artificial P-450 Catalyst. *Org. Lett.* **2006,** 8, 251-254.

20. Shenoy, S. R.; Crisóstomo, F. R. P.; Iwasawa, T.; Rebek, J., Organocatalysis in a synthetic receptor with an inward directed carboxylic acid. *J. Am. Chem. Soc.* **2009,** 130, (17), 5658-5659.

21. Sculimbrene, B. R.; Miller, S. J., Discovery of a Catalytic Asymmetric Phosphorylation through Selection of a Minimal Kinase Mimic: A Concise Total Synthesis of D-myo-Inositol-1-Phosphate. *J. Am. Chem. Soc.* **2001,** 123, (41), 10125-10126.

22. Billington, D. C., *The Inosital Phosphate. Chemical Synthesis and Biological Significance*. Wiley VCH: Germany, 1992.

23. Knowles, W. S., Asymmetric hydrogenation. *Acc. Chem. Res.* **1983,** 16, (3), 106-112.

24. Reetz, M. T., Combinatorial and Evolution-Based Method in the Creation of Enantioselective Catalyst. *Angew. Chem., Int. Ed.* **2001,** 40, 284-310.

25. Traverse, J. F.; Snapper, M. L., High-throughput method for the development of new catalytic asymmetric reaction. *Drug Discovery Today* 2002, pp 1002-1012.

26. Shimizu, K. D.; Snapper, M. L.; Hoveyda, A. L., High-Throughput Strategies for the Discovery of Catalysis. *Chem. Eur. J* **1998,** 4, (10), 1885-1889.

27. Reetz, M. T.; Sell, T.; Meiswinkel, A.; Mehler, G., A New Principle in Combinatorial Asymmetric Transition-Metal Catalysis: Mixture of Chiral Monodentate P Ligands. *Angew. Chem., Int. Ed.* **2003,** 42, (7), 790-793.

28. Long, J.; Hu, J.; Shen, X.; Ji, B.; Ding, K., Discovery of Exceptionally Efiicient Catalysts for Solvent Free Enantioselectivity Hetero-Diel-Alder Reaction. *J. Am. Chem. Soc.* **2002,** 124, (1), 10-11.

29. Pu, L., Fluorescence of Organic Molecules in Chiral Recognition. *Chemical Reviews* **2004,** 104, (3), 1687-1716.

30. Kubo, K., PET sensors. *Top. Fluoresc. Spectrosc.* **2005,** 9, (Advanced Concepts in Fluorescence Sensing, Part A), 219-247.

31. Kavarnos, G. J., Fundamentals of photoinduced electron transfer. In VCH Publishers: New York, 1993.

32. Copeland, G. T.; Miller, S. J., Selection of Enantioselective Acyl Transfer Catalysts from a Pooled Peptide Library through a Fluorescence-Based Activity Assay: An Approach to Kinetic Resolution of Secondary Alcohols of Broad Structural Scope. *J. Am. Chem. Soc.* **2001,** 123, 6496-6502.

33. Li, Z.-B.; Lin, J.; Qin, Y.-C.; Pu, L., Enantioselective Fluorescent Recognition of a soluble "Supported" Chiral Acid: Towards a New Method for Chiral Catalyst Screening. *Org. Lett.* **2005,** 7, (16), 3441-3444.

34. Li, Z.-B.; Lin, J.; Pu, L., A Cyclohexyl-1,2-diamines-Derived Bis(binaphthyl) Macrocycle: Enhanced Sensitivity and Enantioselectivity in The Fluorescent Recognition of Mandelic Acid. *Angew. Chem., Int. Ed.* **2005,** 44, 1690-1693.

35. Masayuki Matsushita; Yamamoto, K. Y. N.; Wirsching, P.; Lerner, R. A.; Janda, K. D., High-Throughput Screening by Using a Blue-Fluorescent Antibody Sensor13. *Angew. Chem., Int. Ed.* **2003,** 42, (48), 5984-5987.

36. Simeonov, A.; Masayuki Matsushita; Juban, E. A.; Thompson, E. H. Z.; Hoffman, T. Z.; IV, A. E. B.; Taylor, M. J.; Wirsching, P.; Rettig, W.; McCusker, J. K.; Stevens, R. C.; Millar, D. P.; Schultz, P. G.; Lerner, R. A.; Janda, K. D., Blue-Fluorescent Antibodies. *Science* **2000,** 290, 307.

37. Reetz, M. T.; Zonta, A.; Schimossek, K.; Leibeton, K.; Jaeger, K.-E., Creation of Enantioselective Biocatalysts for Organic Chemistry by In Vitro Evolution. *Angew. Chem., Int. Ed.* **1997,** 36, 2830-2832.

38. Abato, P.; Seto, C. T., EMDee: An Enzyme Method for Determination Enantiomeric Excess. *J. Am. Chem. Soc.* **2001,** 123, 9206-9207.

39. Dey, S.; Karukurichi, K. R.; Shen, W.; Berkowitz, D. B., Double-Cuvette ISES: In-Situ Estimation of Enantioselectivity and Relative Rate for Catalyst Screening. *J. Am. Chem. Soc.* **2005,** 127, 8610-8611.

40. Schaus, S. E.; Brandes, B. D.; Larrow, J. F.; Tokunaga, M.; Hansen, K. B.; Gould, A. E.; Furrow, M. E.; Jacobsen, E. N., Highly Selective Hydrolytic Kinetic Resolution of Terminal Epoxides Catalyzed by Chiral (salen)CoIII Complexes. Practical Synthesis of Enantioenriched Terminal Epoxides and 1,2-Diols. *J. Am. Chem. Soc.* **2002,** 124, (7), 1307-1315.

41. Lundgren, S.; Wingstrand, E.; Penhoat, M.; Moberg, C., Dual Lewis Acid & Lewis Base Activation in Enantioselective Cyanation of Aldehydes Using Acetyl Cyanide and Cyanoformate as Cyanide Sources. *J. Am. Chem. Soc.* **2005,** 127, (33), 11592-11593.

42. Hamberg, A.; Lundgren, S.; Penhoat, M.; Moberg, C.; Hult, K., High-Throughput Enzymatic Method for Enantiomeric Excess Determination of O-Acetylated Cyanohydrins. *J. Am. Chem. Soc.* **2006,** 128, (7), 2234-2235.

43. Lober, O.; Kawatsura, M.; Hartwig, J. F., Palladium-Catalyzed Hydroamination of 1,3-Dienes: A Colorimetric Assay and Enantioselective Addition. *J. Am. Chem. Soc.* **2001,** 123, 4366-4367.

44. Barry M. Trost, R. C. B., On Ligand Design for Catalytic Outer Sphere Reactions: A Simple Asymmetric Synthesis of Vinylglycinol. *Angew. Chem., Int. Ed.* **1996,** 35, (1), 99-102.

45. Eelkema, R.; van Delden, R. A.; Feringa, B. L., Direct visual detection of the stereoselectivity of a catalytic reaction. *Angew. Chem., Int. Ed.* **2004,** 43, (38), 5013-5016.

46. Nguyen, B. T.; Anslyn, E. V., Indicator-displacement assays. *Coord. Chem. Rev.* **2006,** 250, (23+24), 3118-3127.

47. Rancke-Madsen, E., *Indicators*. 1st ed.; Pergamon Press: New York, 1972.

48. Folmer-Andersen, J. F.; Lynch, V. M.; Anslyn, E. V., Colorimetric enantiodiscrimination of alpha -amino acids in protic media. *J. Am. Chem. Soc.* **2005,** 127, (22), 7986-7987.

49. Zhu, L.; Zhong, Z.; Anslyn, E. V., Guidelines in implementing enantioselective indicator-displacement assays for alpha -hydroxycarboxylates and diols. *J. Am. Chem. Soc.* **2005,** 127, (12), 4260-4269.

50. Zhu, L.; Anslyn, E. V., Facile quantification of enantiomeric excess and concentration with indicator-displacement assays: An example in the analyses of alpha -hydroxyacids. *J. Am. Chem. Soc.* **2004,** 126, (12), 3676-3677.

51. Zhu, L.; Shabbir, S. H.; Anslyn, E. V., Two methods for the determination of enantiomeric excess and concentration of a chiral sample with a single spectroscopic measurement. *Chem. Eur. J.* **2007,** 13, (1), 99-104.

52. Jansson, P. A., Neural networks an overview. *Anal. Chem.* **1991,** 63, (6), 357A-362A.

53. Burns, J. A.; Whitesides, G. M., Feed-forward neural network in chemistry: mathmatical system for classification and pattern recognition. *Chem. Rev.* **1993,** 93, (8), 2583-2601.

54. Leung, D.; Folmer-Andersen, J. F.; Lynch, V. M.; Anslyn, E. V., Using Enantioselective Indicator Displacement Assays To Determine the Enantiomeric Excess of alpha -Amino Acids. *J. Am. Chem. Soc.* **2008,** 130, (37), 12318-12327.

55. Leung, D.; Anslyn, E. V., Transitioning Enantioselective Indicator Displacement Assays for alpha -Amino Acids to Protocols Amenable to High-Throughput Screening. *J. Am. Chem. Soc.* **2008,** 130, (37), 12328-12333.

56. Chakraborty, T. K.; Azhar Hussain, K.; Venkat Reddy, G., [alpha]-phenylglycinol as chiral auxiliary in diastereoselective strecker synthesis of [alpha]-amino acids. *Tetrahedron* **1995,** 51, (33), 9179-9190.

57. Anslyn, E. V., Supramolecular analytical chemistry. *J. Org. Chem.* **2007,** 72, (3), 687-699.

58. Nieto, S.; Lynch, V. M.; Anslyn, E. V.; Kim, H.; Chin, J., High-throughput screening of identity, enantiomeric excess, and concentration using MLCT transitions in CD spectroscopy. *J. Am. Chem. Soc.* **2008,** 130, (29), 9232-9233.

59. Jurs, P. C.; Bakken, G. A.; McClelland, H. E., Computational Methods for the Analysis of Chemical Sensor Array Data from Volatile Analytes. *Chem. Rev.* **2000**, 2649-2678.

Chapter 2: A Structural Investigation of the N-B Interaction in an o-(*N*,*N*-Dialkylaminomethyl)arylboronate System

2.1 Saccharide Sensing with Molecular Receptors Based on Boronic Acid

Saccharides and related molecular species are involved in the metabolic pathways of living organisms, therefore the detection of biologically important sugars (D-glucose, D-fructose, D-galactose, etc.), is vital in various medicinal and industrial contexts. The recognition of D-glucose is of particular interest, since the breakdown of D-glucose transport in humans has been correlated with several diseases: renal glycosuria[1, 2], cystic fibrosis[3], diabetes[4, 5], and also human cancer[6]. Clear evidence exists that tight control of blood sugar levels in diabetics sharply reduces the risk of the debilitating long-term complications associated with this autoimmune diseases[7]. Industrial application of saccharide detection range from the monitoring of fermenting processes to establishing the enantiomeric purity of synthetic drugs.[8]

Since the discovery that phenylboronic acid condenses with mannitol and other polyols to form phenylboronates,[9] arylboronic acid functional groups have been incorporated into receptors for the detection of polyols and their derivatives.[10-15] Over the past fifty years, sensing applications[16-34] and chromatographic protocols[35-42] that target these molecules based on their reversible covalent associations with boronic acid receptors have been created, including a few near-clinical applications.[43, 44] Furthermore, some structural and mechanistic understanding of this important reversible covalent association has been gained.[45-58] Early studies of arylboronic acid/diol association and arylboronic ester exchange reactions showed that the equilibrium (**Figure 2.1a**) becomes

rapid when the reactions proceed in aqueous alkaline solutions (**Figure 2.1b**), or in the presence of certain nitrogenous bases such as piperidine **2.1** (**Figure 2.1c**).[39, 48, 59, 60] To explain the favorable thermodynamic effect seen at high pH (**Figure 2.1a**) in comparison to neutral pH (**Figure 2.1b**) it was hypothesized that the formation of hydroxyboronate complexes of 1,2 diols is accompanied by a significant release of angle strain, resulting from the rehybridization of boron from sp^2 to sp^3.

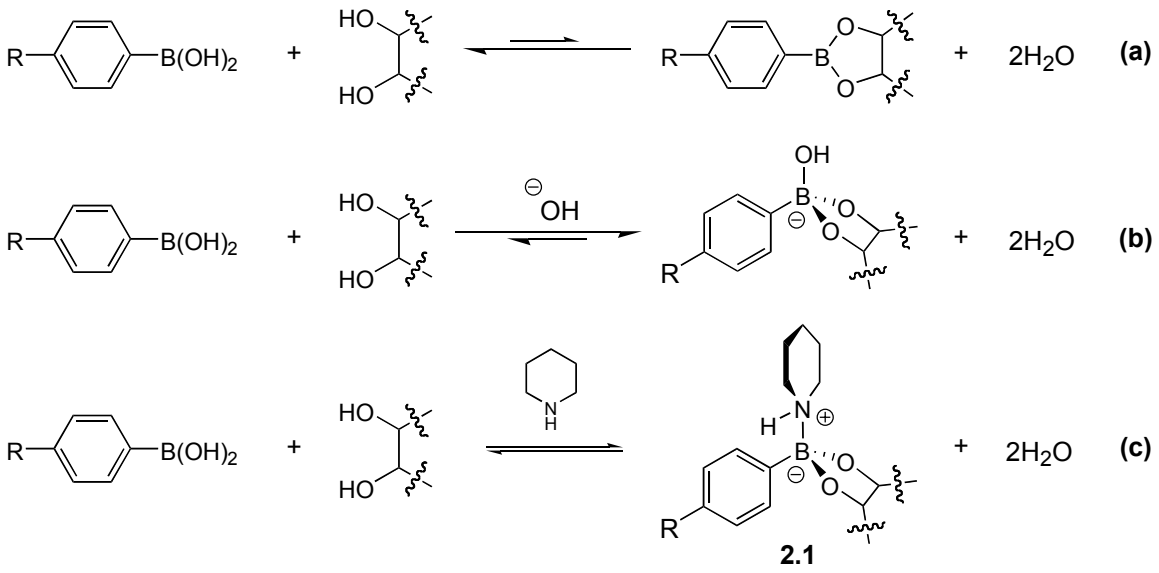

Figure 2.1: (**a**) Reversible association between an arylboronic acid and a vicinal diol. (**b**) Arylboronic acid and vicinal diol association under alkaline conditions. (**c**) Arylboronic acid and vicinal diol association in the presence of piperidine.[29]

Formation of a saccharide complex at neutral pH is essential if practical boronic acid based sensors are to be developed. Since the pK_a of the boronic acid saccharide complex is 1-2 units lower than the pK_a of the boronic acid, the boronic acid-saccharide complex will only exist in significant amounts at neutral pH if the pK_a of the boronic acid itself is $\leq$ 7. The pK_a of phenyl boronic acid has been reported as 8.8, hence phenyl

boronic acid requires basic aqueous conditions to form strong complexes. Therefore, to realize strong binding at neutral pH, the pK_a of the boronic acid must be lowered. This can be achieved by incorporating electron-withdrawing groups onto the aromatic moiety; e.g 4-carboxy-3-nitrophenylboronic acid has a pK_a of 7.0.[61] Another approach, pioneered by Wulff,[41] employs a neighboring aminomethyl substituent. The pK_a of these *o*-aminomethylarylboronic acids has been determined as 5.3 and it was observed that the formation of the boronic ester was several orders of magnitude faster in this case.

To create sensing ensembles for saccharides one must incorporate a mechanism that translates analyte binding into some kind of modulation of the reporter, thereby altering the optical or electrochemical properties. Fluorescent sensors for saccharides are of particular practical interest. This is in part due to the inherent sensitivity of the fluorescence technique. Only a small amount of sensor is required (typically 10^{-6}M), offsetting the synthetic costs of such sensors. The utilization of the photoinduced electron-transfer mechanism stands out as the most popular.[62]

Eleven years ago, Shinkai *et al*. published a landmark study on saccharide sensing using the fluorescent boronic acid receptor **2.2**.[63] It was postulated that the N-B coordination in **2.2** is enhanced upon association with saccharide substrates. This enhanced coordination arrests the photoinduced electron transfer (PET) process from the tertiary amino group to the anthracenyl fluorophore. Hence, the fluorescence of **2.2** is turned on in the presence of saccharide molecules in aqueous media.[16, 17, 64] In the following years, beautiful elaborations on the basic design embodied in **2.2** have emerged for tuning selectivity and sensitivity, and such examples are generally seen as crowning achievements in the field of chemosensing.[8-14]

Recently, data from Wang's group suggested that N-B dative bonds may not be present in the boronate esters formed between *o*-aminomethylphenyl boronic acids and

saccharide molecules in aqueous media due to the competing solvolysis process (**2.3d** in **Figure 2.2**).[57, 65] By analyzing the pH profiles of compound **2.2** and its complexes, the fluorescence intensity variations upon association with different saccharide molecules (including fructose and sorbitol that bind to boronic acids trivalently to preclude N-B bond formation), and computational analysis of the N-B bond strengths, Wang *et al*. concluded that the alternative solvolysis pathway should be operative in aqueous media, and strengthened solvolysis may be the cause of the fluorescence modulation of compound **2.2** upon association with saccharide molecules.

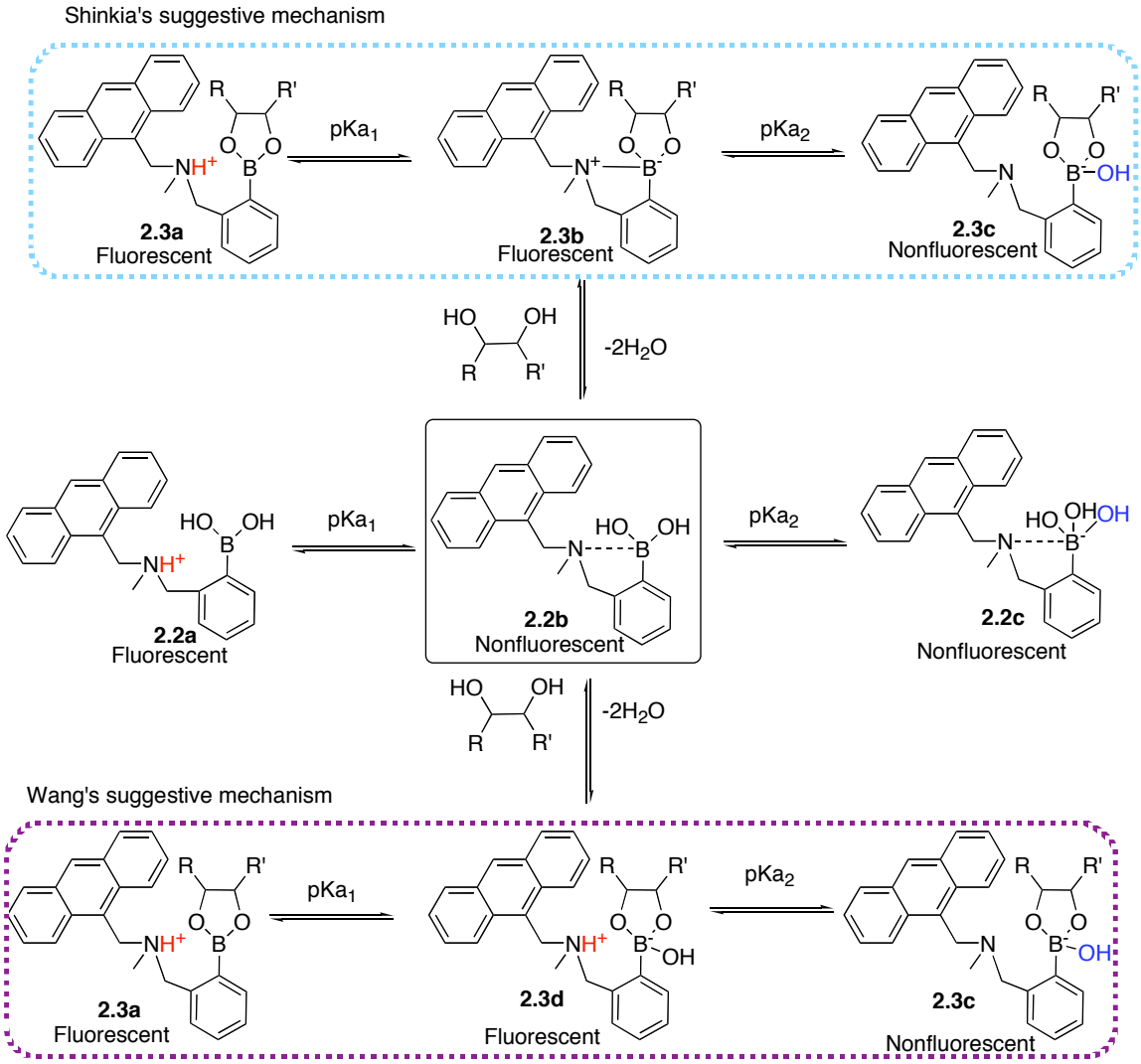

Figure 2.2: Shinkia's and Wang's boronic acid sensor **2.2**, and suggestive species involved in fluorescence change.

The question regarding N-B coordination in *o*-(*N,N*-dialkylaminomethyl)phenylboronate derivatives attracted our attention because we were exploring chiral molecules that have reasonable structural rigidity for enantioselective sensing of α-hydroxycarboxylates and chiral diols. In a structure such as **2.4** (**Figure**

2.3), the spiro arrangement around the boron atom results from formation of the N-B dative bond, and should pose a significant enantioselective bias to the association of chiral substrates such as the chiral vicinal diol (hydrobenzoin) depicted in **Figure 2.3**. Based upon this assumption, the studies on enantioselective sensing of α-hydroxycarboxylates and chiral vicinal diols were performed in aqueous media, and enantioselectivity was achieved.[24, 29] To further improve the enantioselectivity of structures such as **2.4**, we set out on a structural study to confirm or refute the presence of the N-B bond in an *o*-(*N,N*-dialkylaminomethyl)phenylboronate. With this study, we wish to provide a comprehensive picture, from a structural perspective, of the reversible association between an *o*-(*N,N*-dialkylaminomethyl)phenylboronic acid and its substrates in protic media. Further, future sensing technology development based upon boronic acid receptors should greatly benefit from the structural details revealed in this study of this particularly important association event.

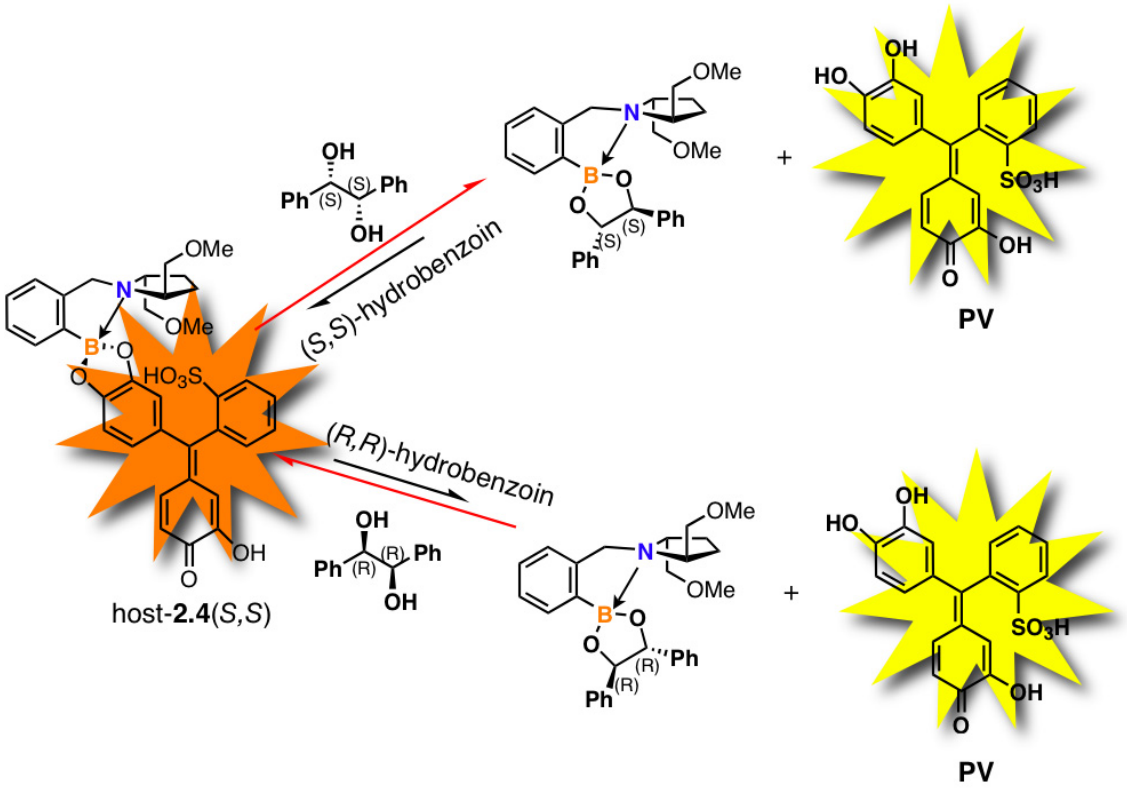

Figure 2.3: Enantioselective indicator displacement assay using host-**2.4**(*S,S*) for (*S,S*)-hydrobenzoin and (*R,R*)-hydrobenzoin with pyrocatechol violet (PV) as indicator.

A method for the direct observation of an N-B dative bond, or the lack thereof, in an *o*-(*N,N*-dialkylaminomethyl)arylboronate under various experimental conditions was desired. The study described herein was used to investigate the existence of the N-B bond, as well as the factors that modulate the characteristic of the N-B interaction. Initially free boronic acid receptors and complexes with catechol were analyzed by x-ray crystallography.[66]

2.1.1 X-ray Crystallographic Analysis of Boronic Acid Receptors

Previously in our group crystals of x-ray diffractable quality of boronic acid receptors **2.5**[29] were created by diffusing pentane or hexanes into concentrated solutions of chloroform.[66] It was postulated that the use of an aprotic solvent would facilitate N-B bond formation by excluding solvolysis. Compound **2.5** trimerizes into a cyclic anhydride to afford a 6-member-ring motif with alternating boron and oxygen atoms (**Figure 2.4**). Two out of the three boron atoms (B1, B2) adopt a tetrahedral configuration with the pyrrolidinyl nitrogen atoms (N1, N2) coordinated. The lengths of the N-B bonds[67] are 1.743 Å and 1.744 Å, respectively, comparable to the values reported for other boronic acid molecules with similar configurations.[25, 55] The other boron (B3) center adopts a trigonal planar configuration, with nitrogen atom N3 left unbound. The O1-B3-O3 angle is 121.33º, which is typical for an sp^2 hybridization. The average B3-O bond length is 1.37 Å, slightly shorter than that of B1/B2-O bonds (1.43Å). The shorter bond length is a result of electron back donation from oxygen to the electron-deficient sp^2 boron. Analogous trimerized cyclic boronic anhydride structures with various trigonal/tetrahedral boron atom arrangements have also been reported.[68-70] Hence, as part of the boronate anhydride, the N-B dative bond was observed.

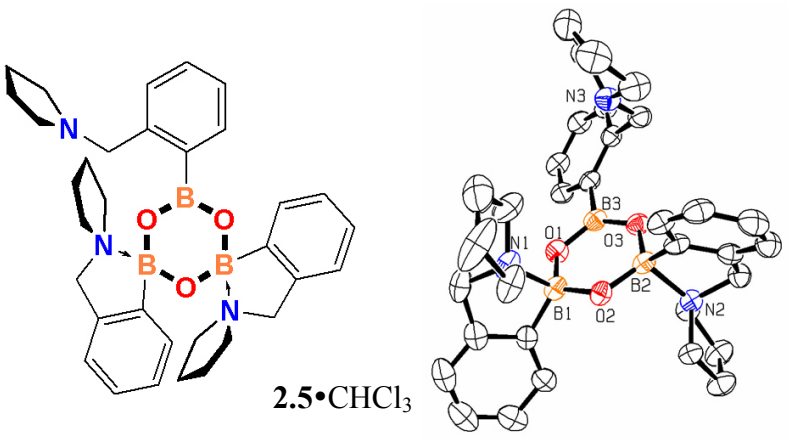

Figure 2.4: Left: Chemdraw presentation of the cyclic anhydride of **2.5**. Right: ORTEP diagrams (50% probability ellipsoids) of the cyclic anhydride of **2.5**. Hydrogen atoms are removed for clarity.

The existence of N-B bond formation in aprotic solvents was further corroborated by the structure of **2.6**, the complex between compound **2.5** and catechol. Complex **2.6** was prepared by mixing equal molar parts of **2.5** and catechol in chloroform followed by azeotropic removal of water. The product was recrystallized by diffusing pentane into a concentrated chloroform solution. In the single crystal structure two different isoforms were found (**Figure 2.5A**, one isoform is shown), differing in conformations of the pyrrolidinyl ring. In both, the nitrogen atom was coordinated with boron. The N-B bond lengths in the conformers are 1.683 Å and 1.700 Å, respectively. They are slightly shorter than observed in the trimeric structure of **2.5**, suggesting strengthened N-B interactions. The O-B-O bond angle is 105.70º, typical of a tetrahedral geometry. The average B-O bond length was 1.47Å, significantly longer than that observed in compounds **2.5** with sp^2 boron atoms. The observation of an N-B bond is also consistent with the chronicled structural studies by ^{1}H, ^{11}B, and ^{15}N NMRs on boronic acids with neighboring amine groups and diol complexes in aprotic solvents ($CDCl_3$, CD_2Cl_2).[45-48, 71-73]

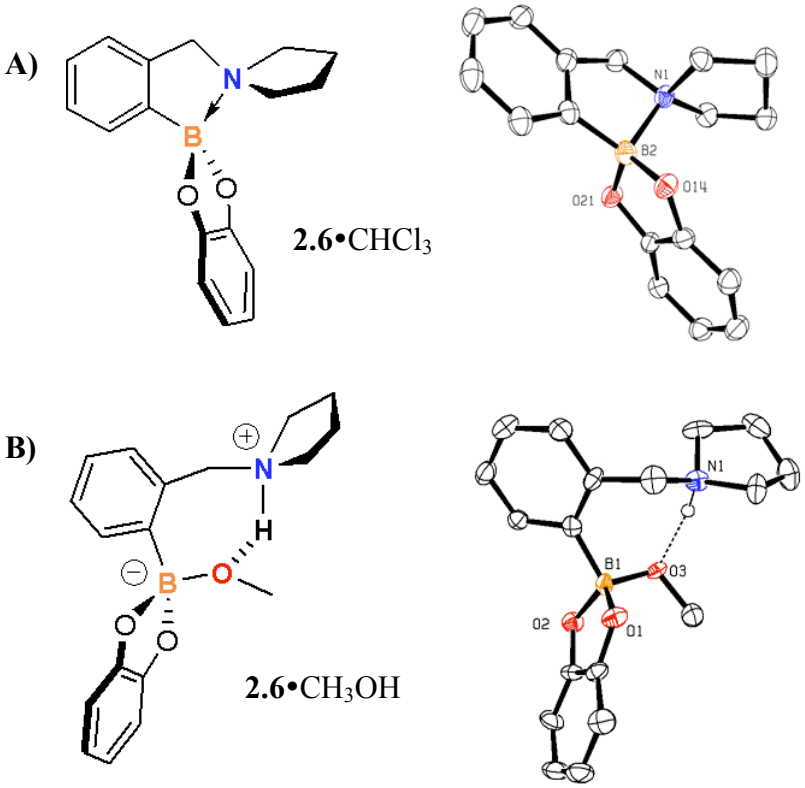

Figure 2.5: Left: Chemdraw presentations of the complexes between **2.5** and catechol. Right: OREP diagrams (50% probability ellipsoids) of arbitrary conformers of **2.6** and **2.6**·CH_3OH. Most hydrogen atoms are removed for clarity.

When complex **2.6** was crystallized from methanol, a protic solvent, instead of an N-B dative bond, the boron atom was coordinated with a methoxy group from the solvent, and the nitrogen atom was protonated (**Figure 2.5B**). Three conformers were observed in the crystal lattice. They differ slightly in their pyrrolidinyl ring conformations. The average B-O bond length is 1.50Å, and the O-B-O bond angle of the cyclic catechol boronate is 102.43º. In all the conformers, the nitrogen and boron atoms are associated through hydrogen bonds between N-H and B-OCH_3.

Zwitterionic ammonium boronate structures have been reported before. Reetz *et al*. prepared a crown ether phenyl boronate of catechol (**2.7**, **Figure 2.6**).[74, 75] When compound **2.7** was allowed to react with a 1:1 mixture of methanol and benzylamine in dichloromethane, a ternary complex (**2.8**) was formed. The crystal structure showed that methanol was deprotonated by benzylamine in this ternary complex and the methoxy group was coordinated with the boronate to afford a zwitterionic complex.[75] The ammonium ion was stabilized by both hydrogen bonding with the crown ether moiety and ion pairing with the boronate anion. As in the structures in **Figures 2.6**, the amino group in compound **2.8** forms an ammonium ion instead of coordinating with the boron atom. The substantial stabilization of the ammonium ion by a crown ether moiety apparently facilitates the zwitterion formation.

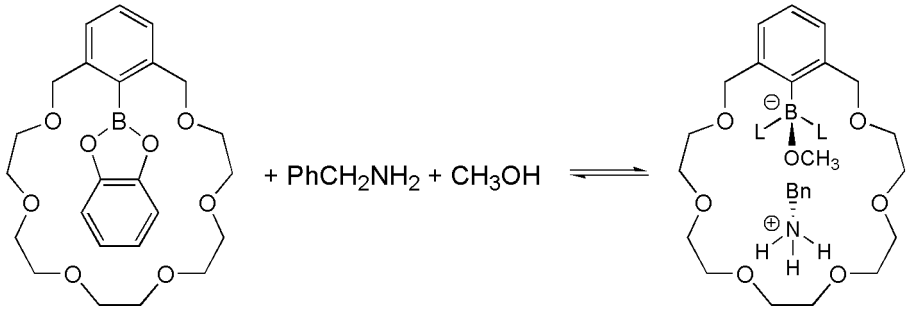

2.7 **2.8**

Figure 2.6: The formation of zwitterionic amino boronate **2.8** reported by Reetz, *et al.*

On the other hand, N-B bonded amino boronate has also been crystallized from protic solvents. We previously reported a crystal structure of *o*-(N-benzylaminomethyl)phenylboronic acid (**2.9**) obtained from methanol as a dimethyl boronate with an N-B bond of 1.665 Å (**Figure 2.7**).[25] The shortened N-B bond length comparing to that of **2.6** suggests stronger N-B coordination. The strengthened N-B interaction should be due to the more sterically accessible nitrogen lone pair of electrons

in a secondary amine than in a tertiary amine as in **2.6**. In support, steric hindrance has been invoked by Norrild *et al.* as the cause for the absence of a N-B bond in a ferrocene bisboronic acid complex with D-sorbitol.[54] Interestingly, ^{11}B NMR – pH profile of **2.9** in 10% CD_3OD in water indicates that the boron atom is solvated in solution (see the next section).[55] Therefore, as evidenced in the discrepancy between the structures of compound **2.9** in solid state and in solution, caution should be applied when solution behavior is predicted based upon solid state evidence.

Further evidence for steric effects comes from Reetz and co-workers. They reported a catechol phenylboronate structure with an N-B coordinating benzylamine.[76] The coordination of boron with this primary amine affords an N-B bond length of 1.612Å, shorter than that in compound **2.9**. The ^{11}B NMR chemical shift of the benzylamine complex in CD_2Cl_2 is 9 ppm, indicating a stronger sp^3 character of boron than that of the tertiary amino group-based compounds reported in this article, whose ^{11}B NMR chemical shifts range from 12-16 ppm (see the next section). Therefore, the balance between N-B coordination and the solvated analog is also influenced by steric interactions, likely favoring N-B coordination with primary amines and smaller alkyl groups, both in solution and solid states.

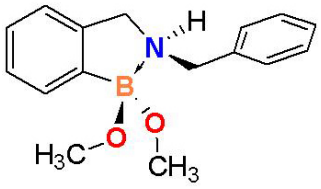

2.9•CH_3OH

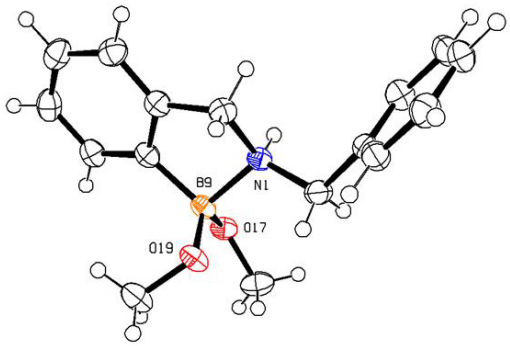

Figure 2.7: Chewdraw presentation and crystal structure (ORTEP, 50% probability ellipsoids) of dimethyl *o*-(*N*-benzylaminomethyl)phenylboronate (**2.9**).

Therefore, the conclusion drawn from the x-ray crystallographic analysis is that the formation of either N-B coordinated or solvated structures largely depends upon the solvent from which a boronate crystallizes.

2.2 Results and Discussion

2.2.1 X-ray Crystallographic Analysis

In our previous crystal structure of complex **2.6**, the hydrogen was approximated to be in between the nitrogen and the oxygen of methanol. In order to clearly identify the position of the hydrogen atom the crystal was resynthesized and analyzed using refined x-ray crystallography. A total of 525 frames of data were collected using ω-scans with a scan range of 0.8° and a counting time of 153 seconds per frame. The hydrogen atom was found to be on the nitrogen with an average bond length of N-H was 1.03 Å which is indicative of the N-H covalent bond (**Figure 2.8**).

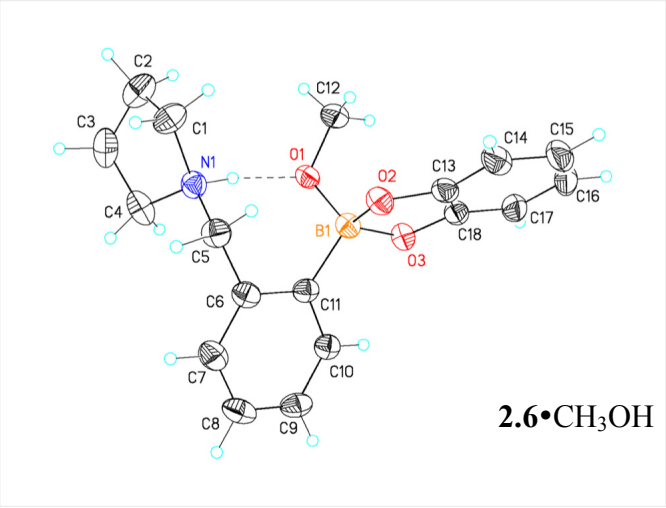

Figure 2.8: View of complex **2.6** showing the atom-labeling scheme. Displacement ellipsoids are scaled to the 50% probability level. The dashed line is indicative of a H-bonding interaction with geometry.

2.2.1 ^{11}B NMR Analysis

Structural characterization in solution

Structural studies using ^{11}B NMR were carried out to investigate the factors (e.g. solvent, pH) that affect the nature of the N-B interaction in solution. The same sample of crystals used to obtain the x-ray structure of **2.5** displays two ^{11}B signals at 26.8 ppm and 15.7 ppm in $CDCl_3$ (**Table 2.1**). The major signal accounting for ~66% of the sample at 15.7 ppm is assigned to the N-B coordinated tetrahedral boron, based on the comparison with literature data.[45, 46, 77] The minor signal (~34%) at 26.8 ppm is assigned to the trigonal planar boron species with no N-B bond. The relative abundance of the tetrahedral and trigonal planar boron species (roughly 2:1) correlates well to what was observed in the single crystal structure of the cyclic trianhydride (**Figure 2.4**). In CD_3OD, however, the same set of crystals of compound **2.5** shows a single peak at 8.3 ppm. This significantly downfield signal from the resonance of the N-B coordinated species is assigned to the fully solvated species,[78] analogous to other literature reports.[50, 55, 56, 79] The difference of ^{11}B NMR data of compound **2.5** with respect to NMR solvents suggests that the boron center is very prone to solvolysis, which is in agreement to the conclusion drawn from the solid state studies.

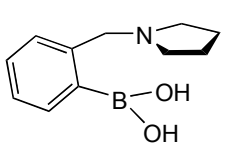

2.5

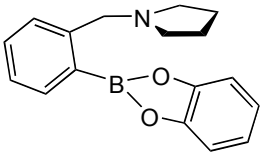

2.6

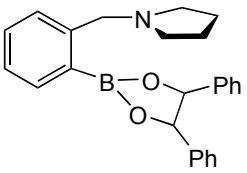

2.10

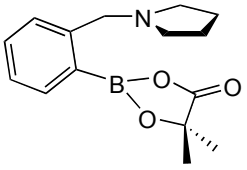

2.11

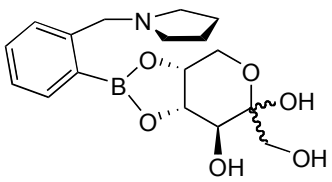

2.12

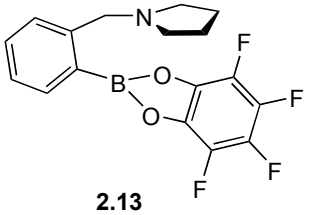

2.13

Table 2.1: ^{11}B NMR chemical shifts (δ/ppm) of selected boronic acids and esters in $CDCl_3$ and CD_3OD, respectively.[a] N. D.: not determined.

Compound No.	^{11}B NMR (δ/ppm, 160 MHz, ($CDCl_3$)	^{11}B NMR (δ/ppm, 160 MHz, (CD_3OD)
2.5	26.8 15.7*	8.3
2.6	14.7* 10.4	14.3 10.2* 8.2
2.10	13.2	9.0
2.11	12.0* 7.8	8.0
2.12	13.6	11.7, 6.2*
2.13	15.5* 11.6	11.8* 8.1
2.7[68]	30 (CD_2Cl_2)	N. D.
2.8[69]	9.0 (CD_2Cl_2)	N. D.
2.9[17]	N. D.	10.3

[a]: All ^{11}B NMR chemical shifts are referred to external standard BF_3-OEt_2. *: Major signals.

In the ^{11}B NMR spectrum of complex **2.6** in $CDCl_3$ (**Table 2.1**), the signal at 26.8 ppm found for the cyclic trimer of **2.5** disappears, indicating that the boron atom completely adopts a tetrahedral configuration upon associating with catechol. The major signal (~90%) at 14.7 ppm is assigned to the N-B coordinated species. The minor signal (~10%) at 10.4 ppm is assigned to the solvated species. The small extent of solvolysis is attributed to the adventitious wetting of $CDCl_3$. The assignment of the solvated species is based on the spectrum of complex **2.6** in CD_3OD, in which the major signal (~80%) of **2.6** appears at 10.2 ppm. Also in CD_3OD, a minor peak at 14.3 ppm (~10%) was

observed, which is indicative of a small portion of N-B coordinated species. Another minor species (~10%) was observed at 8.2 ppm, which is assigned to the solvated compound **2.5** from the dynamic dissociation of the complex **2.6** to **2.5** and catechol in CD_3OD. The ^{11}B NMR assignments of different species are summarized in **Figure 2.9**.

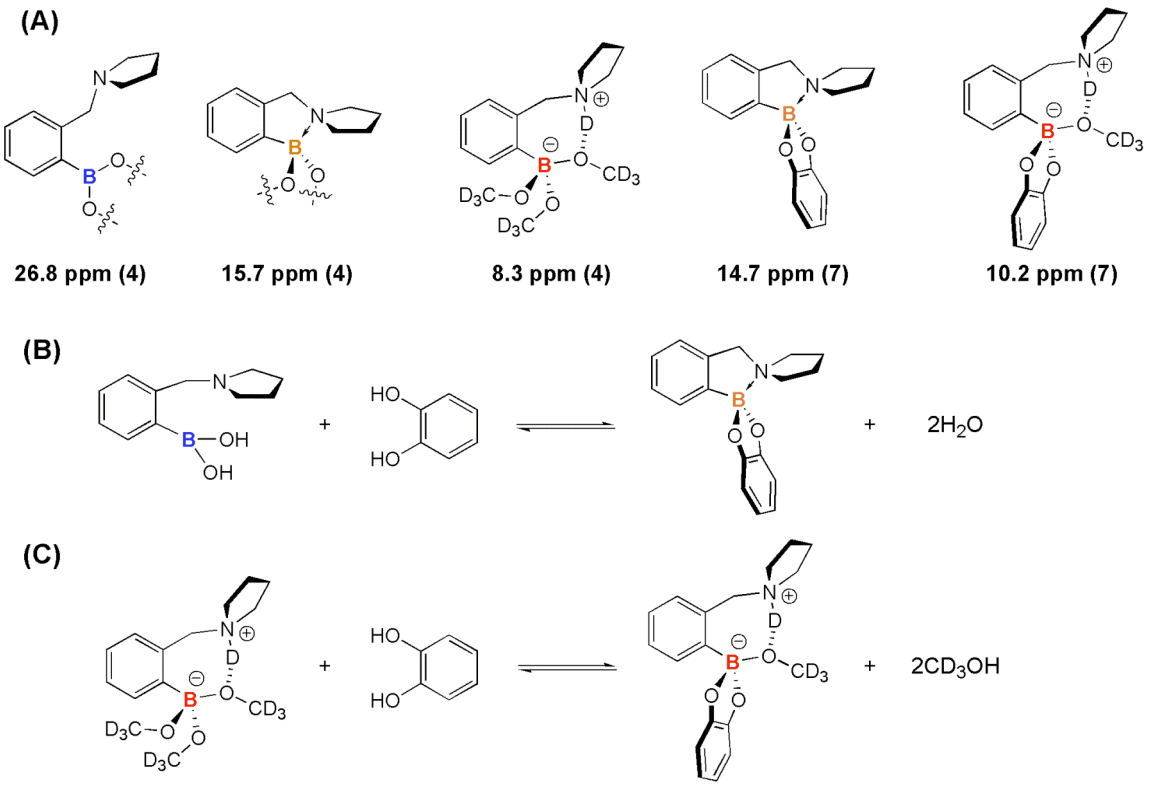

Figure 2.9: (**A**) The ^{11}B NMR assignments for different species in the equilibrium between **2.5** and **2.6** (blue: trigonal planar boron, orange: tetrahedral boron with an N-B dative bond, red: tetrahedral boronate anion). (**B**) The reversible association between **2.5** and catechol in $CDCl_3$ to create **2.6**. (**C**) The reversible association between **2.5** and catechol in CD_3OD to create **2.6**•CD_3OD.

The solvent-dependent ^{11}B NMR spectra of compounds **2.5** and **2.6** was in agreement with the solid state structural studies – the boron atom in this particular phenylboronate system is very prone to solvolysis. In the aprotic solvent chloroform, the

boron atom in free receptor **2.5** adopts N-B coordinated tetrahedral and/or N-B uncoordinated trigonal planar configurations. When compound **2.5** is associated with catechol to afford complex **2.6**, the complete formation of an N-B dative bond was observed (**Figure**. **2.9B**). The conversion of boron hybridization state from sp^2 to sp^3 was attributed to the increased electrophilicity of the boron atom upon association. Two factors contribute to the increased electrophilicity of the boron atom: 1. The electronic induction effect from the electron-withdrawing substrate catechol and **2.2**. the geometrical constraints to be tetrahedral upon associating with the vicinally bifunctionalized catechol molecule. In a protic solvent such as methanol, however, solvolysis appears to be the dominant pathway for both free receptor **2.5** and complex **2.6** (**Figure 2.9C**). The boronate anion is stabilized by the proximal tertiary ammonium ion.

^{11}B NMR titrations in aprotic and protic media

^{11}B NMR titrations were performed to investigate the correlation between the N-B bond strength and complex formation between **2.5** and substrates hydrobenzoin, catechol, and α-hydroxyisobutyric acid. These three molecules model three groups of physiologically important substances; saccharides, catecholamines, and α-hydroxycarboxylates that are common targets of boronic acid-based chemosensing applications. From the titration experiments, we wished to explore the modulation of N-B interactions in compound **2.5** upon associating with the aforementioned substrates under different experimental conditions and to further elucidate the underlining chemical events taking place upon association.

With the addition of hydrobenzoin (either enantiomer) in $CDCl_3$, the chemical shifts of boronic acid **2.5** (26.7 ppm and minor at 9.3 ppm from adventitiously hydrated **2.5**) disappeared and a peak at 13.4 ppm, which is characteristic of a nitrogen-coordinated

arylboronate, developed (**Figure 2.10A**). This titration clearly shows that in the aprotic solvent $CDCl_3$, the complex formation promotes the N-B coordination by raising the electrophilicity, or the Lewis acidity, of the boron atom. The Lewis acid-base interaction between the boronate and the tertiary amino group is strengthened as a result of complexation.

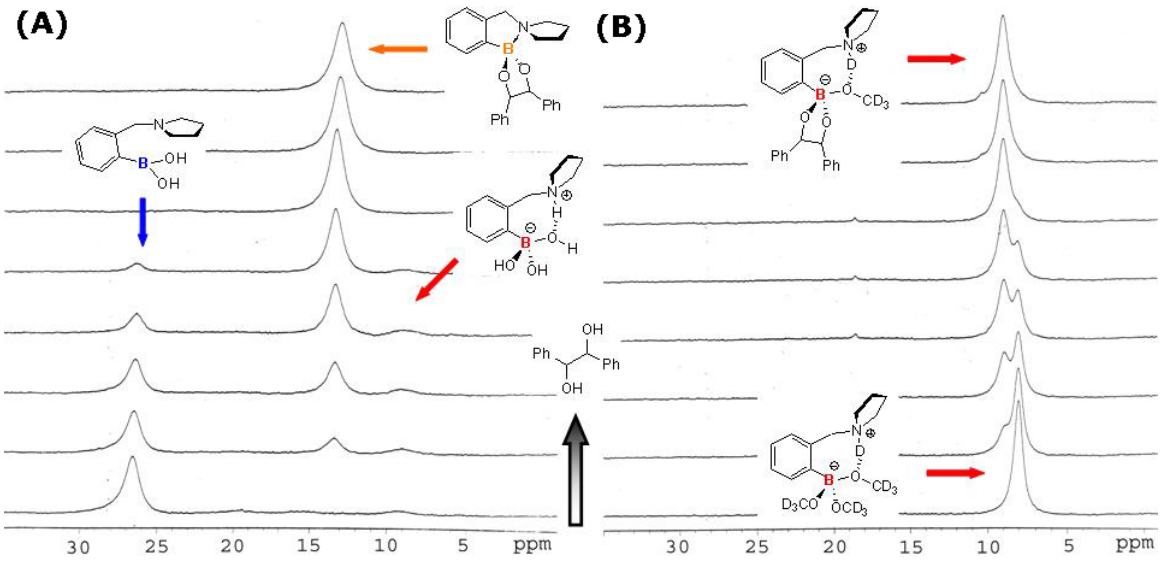

Figure 2.10: ^{11}B NMR spectra of compound **2.5** (10 mM) in the presence of 0 – 80 mM hydrobenzoin in $CDCl_3$ (**A**) and CD_3OD (**B**), respectively. The tiny signal at 19 ppm in B is from the non-interfering impurity boric acid. In (**A**), the free boronic acid **2.5** in $CDCl_3$ exists as a mixture of different aggregates, e.g. cyclic trianhydride in **Figure 2.5**.

The ^{11}B NMR titration in CD_3OD started with fully solvated compound **2.5** at 8.1 ppm (**Figure 2.10B**). This signal disappeared with concurrent appearance of a new signal at 9.1 ppm with the addition of hydrobenzoin. The peak at 9.1 ppm was assigned to the solvated complex **2.9**. No N-B coordinated species was observed. The ^{11}B NMR titration experiments in both $CDCl_3$ and CD_3OD support the conclusion that the complexation to form a 5-member-ring boronate increases the electrophilicity (or Lewis acidity) of the

boronate, which leads to N-B coordination in aprotic solvents. On the other hand, the solvolysis pathway is too dominant in protic solvents such as methanol for N-B coordination to occur to a significant extent in the complex of **2.5** and hydrobenzoin.

Catechol behaves similarly to hydrobenzoin as a substrate of **2.5** in a ^{11}B NMR titration experiment in $CDCl_3$ (**Figure 2.11A**). The signals of compound **2.5** (mixture of aggregates) at 26.7 and 9.2 ppm were reduced while the signal of the N-B coordinated complex (**2.6**) at 14.8 ppm grew in upon the addition of catechol. Interestingly, when the addition of catechol was over one equivalent, a new signal at 10.4 ppm appeared, which was assigned to a boronate triester species of a 1:2 complex. The underlining chemical event is that the Brønsted basicity of the nitrogen atom in **2.6** is less than that of **2.5** due to the strengthened N-B dative bond, the nature of which is a Lewis acid/base interaction. At the beginning of the titration, adventitious water in the NMR solvent ($CDCl_3$) was able to protonate a small percentage of free receptor **2.5** (9.2 ppm). With an increasing amount of catechol, N-B coordinated complex **2.6** was formed and the Brønsted basicity of the nitrogen atom in **2.5** was consequently lowered. Therefore, the miniscule amount of water was no longer acidic enough to give a detectable amount of solvated complex. However, when the catechol exceeded one equivalent, it acted as a Brønsted acid (pK_a 9.3) that was strong enough to protonate the nitrogen atom. The resulting ammonium ion facilitated the coordination of a second catechol molecule to compound **2.6** to afford the triester species. This situation with an excess of the protic substrate catechol in $CDCl_3$ simulates the solvolysis taking place in a protic solvent.

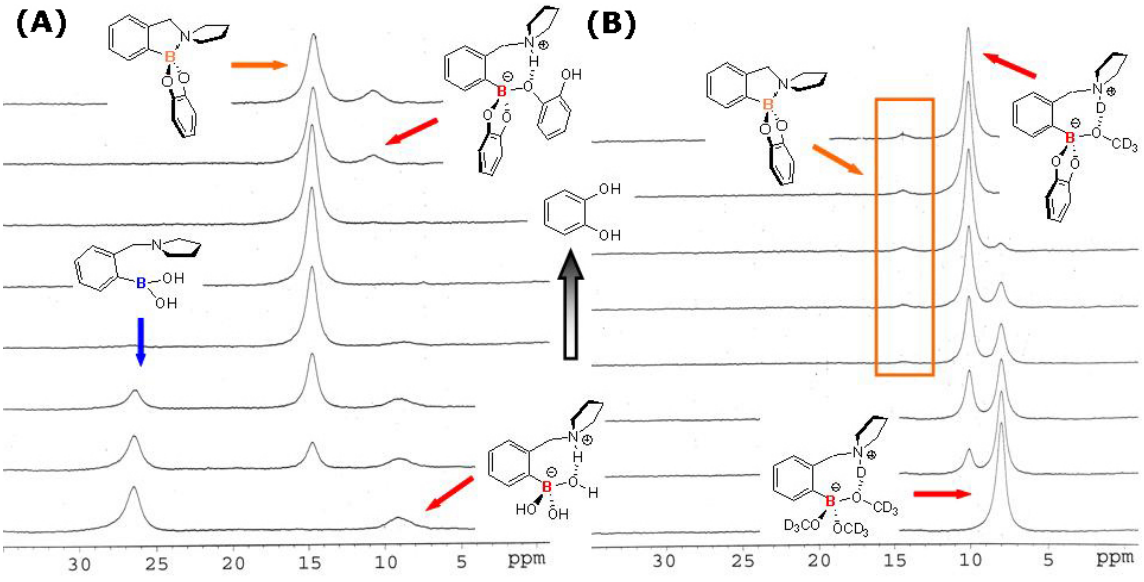

Figure 2.11: ^{11}B NMR spectra of compound **2.5** (10 mM) in the presence of 0 – 80 mM catechol to create complex **2.6** in $CDCl_3$ (A) and CD_3OD (B), respectively.

The ^{11}B NMR titration with catechol in CD_3OD (**Figure 2.11B**) was similar to that of hydrobenzoin, except that in addition to the solvated complex (10.3 ppm), a minor signal at 14.5 ppm also grew in with the addition of catechol. This peak was assigned to the N-B coordinated species by comparing the spectra in CD_3OD with previous characterization data of complex **2.6** and titration data in $CDCl_3$. Hence, the N-B coordinated and solvated species are found to be in equilibrium in this particular case. Therefore, although the solvolysis pathway is dominant in protic solvents, the N-B coordinated species can exist in equilibrium, and its extent of formation is dependent on the particular receptor and substrate structures. In fact, Norrild *et al*. examined an analog of **2.2** containing two boronic acid moieties and its complexation with glucose. They concluded that in this particular case the solvolysis and N-B containing structures both exist within the same complex in protic media.[53]

Finally, the ^{11}B NMR titration with α-hydroxyisobutyric acid was examined (**Figure 2.12A**). In $CDCl_3$, N-B bond formation occurred with the addition of α-hydroxyisobutyric acid to compound **2.5** to afford the N-B coordinated complex **2.11** (12.1 ppm). When the α-hydroxyisobutyric acid exceeded one equivalent, the triester species of the 1:2 complex (9.0 ppm) was observed as in the catechol case, however on a much larger scale. α-Hydroxyisobutyric acid is a much stronger Brønsted acid than both catechol and hydrobenzoin. It is able to protonate the pyrrolidinyl nitrogen of complex **11** completely, greatly favoring the formation of the anionic triester boronate. In CD_3OD (**Figure 2.12B**), the peaks of solvated receptor **2.5** and complex **2.11** coincided at 8.1 ppm. The diastereotopic methyl groups in the ^1H NMR of complex **2.11** in CD_3OD confirmed that the complex was formed in methanol. However, the existence of the N-B coordinated species was difficult to substantiate, because an exceedingly small bump at the proper ppm does grow in, but its level is so close to the background resonance of the experiment that our confidence in its existence is marginal (examine **Figure 2.13B** at the 12-13 ppm region).

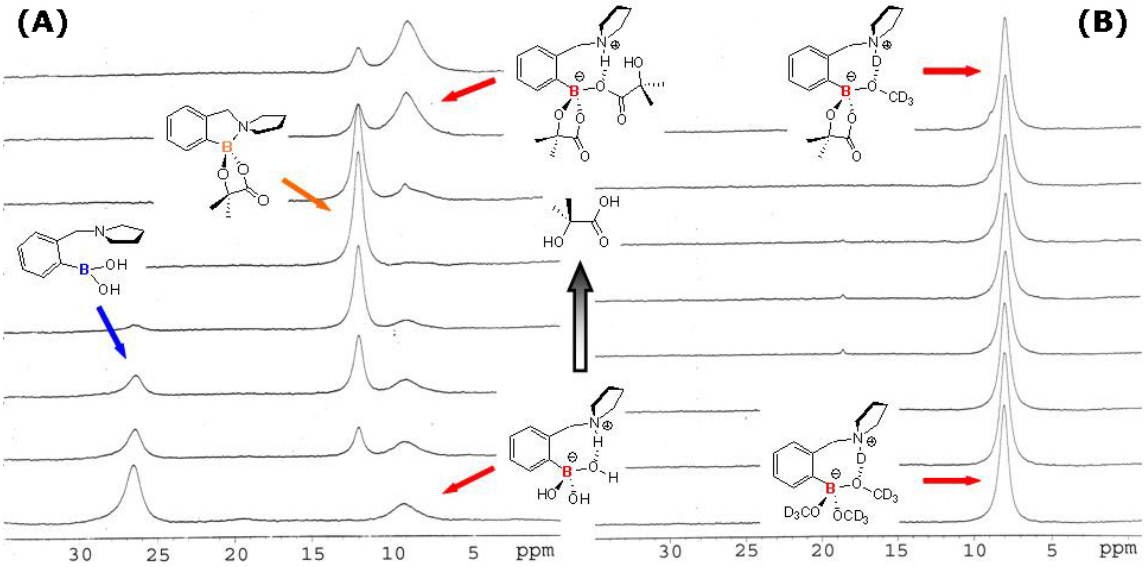

Figure 2.12: ^{11}B NMR spectra of compound **2.5** (10 mM) in the presence of 0 – 80 mMα-hydroxyisobutyric acid to afford complex **2.11** in $CDCl_3$ (**A**) and CD_3OD (**B**), respectively. The tiny signal at 19 ppm in B is from the non-interfering impurity boric acid. However, a signal at 12-13 ppm appears to grow in during the upper spectra of part B, possibly indicative of an N-B species at an exceedingly small fraction.

^{11}B NMR - pH profiles

^{11}B NMR – pH profiles of compound **2.5** and complex **2.6** in a 3:1 CH_3OH:H_2O solvent mixture were studied in an effort to characterize the solution species at various pH. As shown in **Figure 2.13**, the first pK_a (pK_{a1}) could be either from deprotonation of the ammonium ion if the deprotonated species has the N-B dative bond, or from hydroxylation of the sp^2 boron. Because there is a rapidly established equilibrium between the N-B coordinated and the solvated species, it cannot be determined from direct examination of the ^{11}B NMR spectra which structure is formed after the first deprotonation (**Figure 2.14A**). However, according to literature data, the second deprotonation of an *o*-(*N,N*-dialkylaminomethyl)phenylboronic acid should occur after

pH 9.[53, 55, 64] From the ^{11}B NMR – pH profile of **2.5**, no chemical shift transition was observed after pH 7, where the solvated species is dominant if not exclusive (**Figure 2.14A**). Therefore, the second pK_a should not be associated with hydroxylation of the sp^2 boron. It is therefore concluded that the first deprotonation event for compound **2.5** is primarily the hydroxylation of the sp^2 boron, where the ^{11}B chemical shift transition from sp^2 to sp^3 was observed at around pH 6.5, the value of pK_{a1}. Hence, the second pK_a primarily belongs to the deprotonation of the tertiary ammonium ion, which should be at its usual range of pH 9-10,[41] or shifted slightly higher due to the proximal boronate anion. The ratio of N-B coordinated to solvated boronate dictates the extent that each pK_a is dominated by boron solvation or ammonium deprotonation. In the cases we studied, the pK_a's are primarily attributed to the events just described above. Compared to arylboronic acids without *o*-(*N,N*-dialkylaminomethyl) groups, the pK_a of the boronate is decreased by more than 3 units.[41] Such pK_a reduction is caused by the ion-pairing stabilization of the anionic sp^3 boronate from the neighboring ammonium ion.

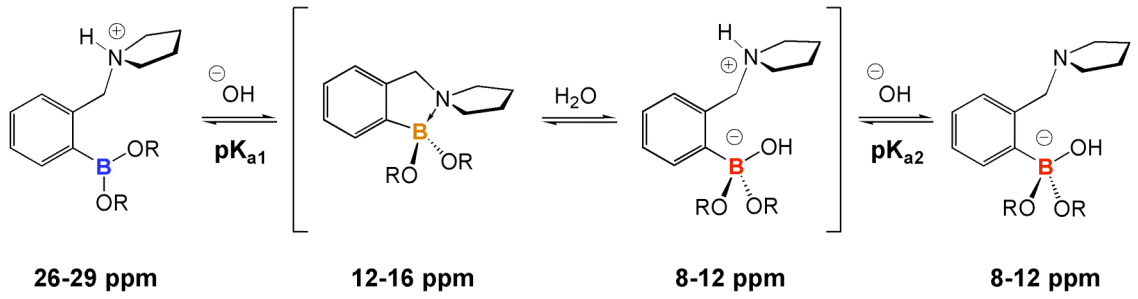

Figure 2.13: Deprotonation of a boronic ester in aqueous media (or acid when R = H). Different colors represent different ^{11}B NMR chemical shifts for respective species. The zwitterionic and fully deprotonated species have similar ^{11}B NMR resonances (red) due to similar chemical environments.

Similar pH profiles were reported for boronic acids in a previous study from our group,[55] and others.[54,58] The conclusion from our previous study on similar boronic acid

molecules stated that pK_{a1} was from the deprotonation of the ammonium ion. However, this was based upon the assumption that the N-B coordinated species was dominant in solution after the first deprotonation event.[55] In light of the new experimental data that revealed the nature of the N-B interaction in protic media, we hereby conclude that pK_{a1} of compound **2.5** in aqueous solution is primarily from the hydroxylation of the boronate, and pK_{a2} is primarily due to the deprotonation of the tertiary ammonium ion.[41]

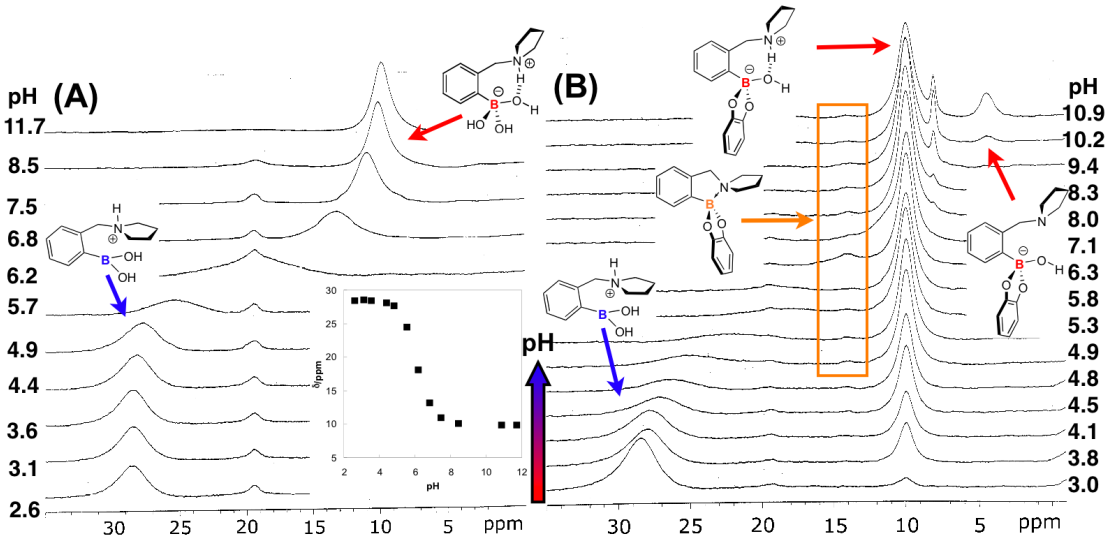

Figure 2.14: ^{11}B NMR spectra of compound **2.5** (20 mM, **A**) and **2.6** (20 mM, **B**) in 75% methanolic solution with HEPES (25 mM) with pH ranging from 3 to 12. The signals at 19 ppm are from the non-interfering impurity boric acid.

In the ^{11}B NMR – pH profile of complex **2.6** (**Figure 2.14B),** at pH 3 the boron atom in **2.6** was solvated to a small extent with an sp^3 configuration (10.0 ppm). This is due to the well-known fact that the association with catechol raises the acidity of the boronate.[81-83] In other words, complex formation promotes solvolysis. However, under

such acidic conditions, the affinity between **2.5** and catechol is low, and most of the complex is dissociated to **2.5** and catechol, with the boron in **2.5** having a trigonal planar geometry (~27 ppm).[53] With increasing pH, the signal of solvated complex **2.6** increased with concurrent disappearance of the chemical shift of **2.5**, suggesting enhanced affinity. When the pH was raised to 6.3, another minor species was observed at 14.4 ppm. This minor signal was assigned to an N-B coordinated species for three reasons: 1) its chemical shift at 14.4 ppm corresponds to the characterized N-B coordinated species (**Table 1.1**). 2) The occurrence of this signal at pH 6.3 matches well to the pH-dependent equilibrium of an N-B coordinated species in a protic medium with the solvated species. When the pH is too low, the nitrogen atom is primarily protonated; when the pH is too high, the boron atom is primarily hydroxlyated. Only when the pH is at an intermediate value can a subtle balance between Lewis acid-base and Brønsted acid-base interactions between the amino and boronate moieties be achieved (**Figure 2.13**). 3) The association between **2.5** and the vicinal bifunctionalized, electron-withdrawing substrate catechol stabilizes both the N-B coordinated species and the solvated species (see the next section). As a result two separated NMR signals corresponding to these two species were observed because their interconversion is slow relative the ^{11}B NMR time scale. For boronic acid **2.5**, however, the N-B bond stabilizing effect from catechol is absent. Instead a chemical shift transition from sp^2 to sp^3 solvated boron centers was observed (see inset, **Figure 2.14A**), with an interconversion rate faster than the ^{11}B NMR time scale.[50, 55]

The pH profiles of complexes between **2.5** and two other substrates – fructose (**2.12**) and tetrafluorocatechol (**2.13**) were also examined (**Figure 2.15-2.16**). The decreased pK_{a1} compared to that of **2.5** for both complexes was evident, and the solvated complexes dominated the species distributions. It was observed that complex **2.12** and

2.13 were not very stable at very high or low pH, too many possible isomeric species of the complex impede the resolution of the ^{11}B NMR spectrum. However, the N-B coordinated species could not be unequivocally identified in either case. Overall, the identification of an N-B coordinated species of **2.6** in an aqueous medium, albeit with a very small abundance, suggests that although the solvated species of arylboronates are dominant in aqueous media, the occurrence of the N-B coordinated species is still possible, and the abundance depends on the substrate and the solvent system.

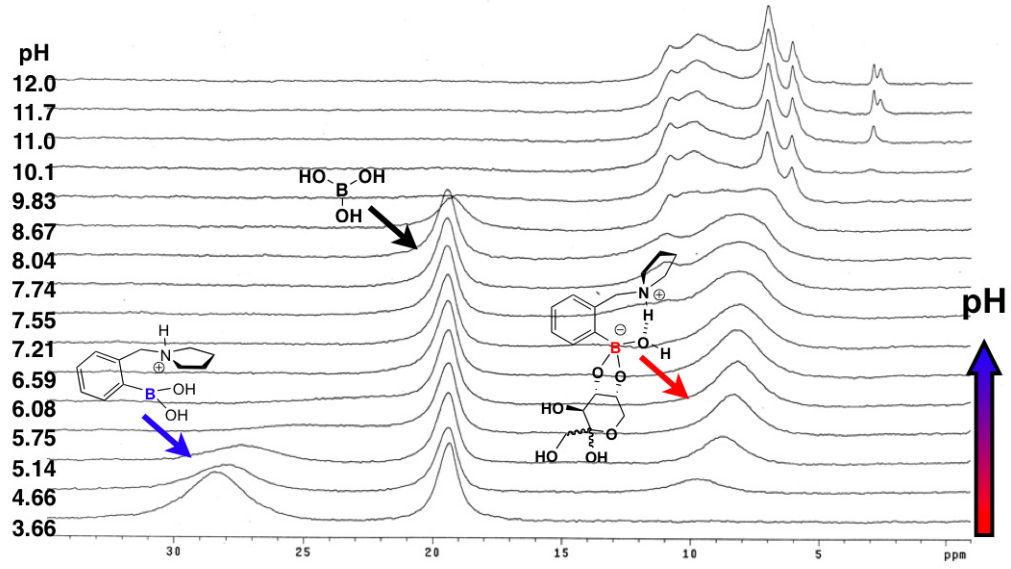

Figure 2.15: ^{11}B NMR spectra of compound **2.7 (**20 mM) **A**) and **2.12 (**20 mM) **B**) in 75% methanolic solution with HEPES (25 mM) with pH ranging from 3 to 12. The signals at 19 ppm are from impurity boric acid.

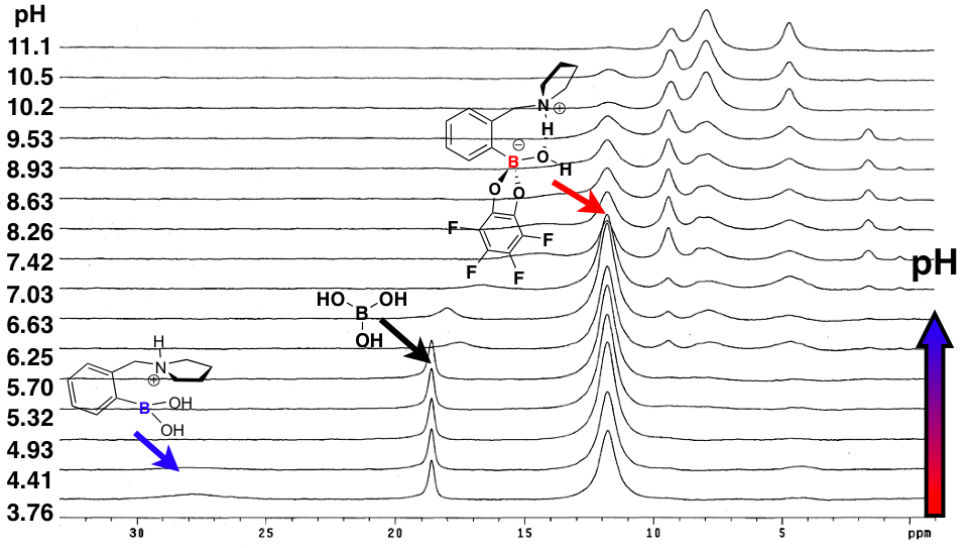

Figure 2.16: ^{11}B NMR spectra of compound **2.7 (**20 mM), **A**) and **2.13 (**20 mM), **B**) in 75% methanolic with pH ranging from 3 to 11. The signals at 19 ppm are from impurity boric acid.

2.3 CONCLUSION

Based on our structural investigation, we first conclude that in an aprotic solvent where the solvolysis pathway is absent, an N-B dative bond is usually present in an *o*-(*N,N*-dialkylaminomethyl)arylboronate. However, in a protic media, solvolysis of the boronate can dominate, which affords a hydrogen-bonded zwitterionic species with little or no N-B dative bond. Second, when a boronic acid associates with a vicinal bifunctionalized, electron-withdrawing substrate to afford a 5-member-ring cyclic boronate, both N-B bond formation and boronate solvolysis are promoted due to the increased electrophilicity/Lewis acidity of the boronate. The N-B coordinated and solvated species are in equilibrium. The abundances of the two species are decided by the relative strengths of the Brønsted acid/base interaction between an sp^2 boron and a protic solvent molecule and the Lewis acid/base interaction between the same boron atom and

neighboring nitrogen atom. Third, the first pK_a of an *o*-(*N,N*-dialkylaminomethyl)phenylboronate is primarily from hydroxylation of the sp^2 boronate, the second pK_a is primarily from the deprotonation of the neighboring tertiary ammonium ion. The markedly lowered boronic acid acidity[41] compared to unsubstituted arylboronic acids (e.g. phenylboronic acid – $pK_a \sim 8.8$) is due to the ion-pairing stabilization from the neighboring tertiary ammonium ion. Last, the N-B coordinated species can be observed at small abundance, but their presence depends on their structures and the solvent.

By providing a relatively complete picture of the structures of *o*-(*N,N*-dialkylaminomethyl)phenylboronates, a widely used motif in molecular receptor and sensor design, the correct interpretations of available data can be achieved and the designs of future sensing technologies will be facilitated.

2.4 EXPERIMENTAL

^1H and ^{13}C NMR spectra were recorded on a Varian Unity Plus 300 spectrometer, and ^{11}B NMR spectra were taken on a Bruker AMX-500 (160 MHz) spectrometer using $BF_3 \bullet OEt_2$ as an external reference. High-resolution mass spectra were measured with a VG Analytical ZAB2-E spectrometer. Chemical reagents were used as purchased from various commercial sources.

2.4.1 Synthesis

Boronic acid host **2.5** was synthesized by reductive amination according to the established literature procedure.[24]

Complex **2.6**. Compound **2.5** (0.5 mmol, 103 mg) and catechol (0.5 mmol, 55 mg) were dissolved in $CHCl_3$ (2.5 mL) and stirred with 1 g $MgSO_4$ suspension at room

temperature for 30 min. $MgSO_4$ was removed with vacuum filtration and the filtrate was concentrated. The crude product was dissolved in $CHCl_3$ (5 mL) and concentrated again in order to azeotropically remove the condensed water. The product was purified by crystallization by diffusing pentane into its concentrated $CHCl_3$ solution. The crystallized product was found to have low solubility in CH_3OH. The filtrated, clear methanolic solution was placed in the fridge (4 ºC) where crystals were formed overnight. The crystals from $CHCl_3$ and CH_3OH solutions respectively were submitted for x-ray crystallographic analysis.

Compound 2.6. m.p 100-101ºC ^{1}H NMR (300 MHz, $CDCl_3$) δ 7.58 (m, 1H), 7.37 (m, 2H), 7.18 (m, 1H), 6.85 (m, 2H), 6.79 (m, 2H), 4.19 (s, 2H), 3.43 (m, 2H), 2.83 (m, 2H), 1.96 (m, 4H); ^{13}C NMR (75.5 MHz, $CDCl_3$) δ 152.0, 140.3, 131.2, 128.8, 128.2, 122.7, 119.6, 109.9, 63.7, 55.4, 23.1; HRMS (FAB): calcd. $(M+H)^+$ 280.1503, found 280.1503.

2.4.2 X-ray Crystal Structure Determination

X-ray Experimental for **2.6** in methanol: Crystals grew as colorless prisms by slow evaporation from methanol. The data crystal was a prism that had approximate dimensions; 0.35 x 0.17 x 0.09 mm. The data were collected on a Nonius Kappa CCD diffractometer using a graphite monochromator with MoKα radiation (λ = 0.71073Å). A total of 525 frames of data were collected using ω-scans with a scan range of 0.8° and a counting time of 153 seconds per frame. The data were collected at 153 K using an Oxford Cryostream low temperature device. Details of crystal data, data collection and structure refinement are listed in **Table 1.1**. Data reduction were performed using DENZO-SMN.[84] The structure was solved by direct methods using SIR97[85]and refined by full-matrix least-squares on F^2 with anisotropic displacement parameters for the non-

H atoms using SHELXL-97.[86] The hydrogen atoms on carbon were calculated in ideal positions with isotropic displacement parameters set to 1.2xUeq of the attached atom (1.5xUeq for methyl hydrogen atoms). The hydrogen atoms on the nitrogen atoms were observed in a ΔF map and refined with isotropic displacement parameters. The function, $\Sigma w(|F_o|^2 - |F_c|^2)^2$, was minimized, where $w = 1/[(\sigma(F_o))^2 + (0.0332*P)^2 + (2.7466*P)]$ and $P = (|F_o|^2 + 2|F_c|^2)/3$. $R_w(F^2)$ refined to 0.122, with R(F) equal to 0.0558 and a goodness of fit, S, = 1.01. Definitions used for calculating R(F), $R_w(F^2)$ and the goodness of fit, S, are given below.[87] The data were checked for secondary extinction effects but no correction was necessary. Neutral atom scattering factors and values used to calculate the linear absorption coefficient are from the International Tables for X-ray Crystallography (1992).[88] All figures were generated using SHELXTL/PC.[89]

2.4.3 General Procedure for ^{11}B NMR Titrations

All the ^{11}B NMR experiments were done with quartz NMR tubes (Wilmad). Stock solutions of compound **2.5** (0.1 M) and catechol (0.1 M) in CD_3OD (or $CDCl_3$) were prepared. Each of the eight NMR tubes was loaded with 100 μL of solution **2.5** (0.1 M) first, followed with 0, 25 μL, 50 μL, 75 μL, 100 μL, 200 μL, 600 μL, and 800 μL of catechol solution (0.1 M) respectively. CD_3OD (or $CDCl_3$) was then added to take the total volume to 1.0 mL. Therefore, each tube contained 10 mM of **2.5**, with 0, 2.5 mM, 5 mM, 7.5 mM, 10 mM, 20 mM, 60 mM, and 80 mM of catechol respectively. Boron NMR were collected on Varian INOVA 500 with a sweep width of 51000 Hz, 131 k of data points, a 90º pulse width and a 1.2 second recycle time. Each spectrum was processed with 10 Hz line broadening, and a second order polynomial fitting routine was used to remove ^{11}B background. The temperature was regulated at 27ºC.

2.4.4 General Procedure for ^{11}B NMR – pH Profiles

Solutions of compound **5** (0.6 mL, 0.1 M in CH_3OH), HEPES (0.75 mL, 0.1 M in D_2O), and catechol (0.6 mL, 0.1 M in CH_3OH) were added in 16 vials and their pH values were adjusted with NaOH (2 M) or $HClO_4$ (2 M) in a range from 3 – 12. The total volume of the samples was adjusted to 3.0 mL. The final concentrations for **2.5**, HEPES, and catechol were 20 mM, 25 mM, and 20 mM, respectively.

Additional Information: The work presented in this chapter was a collaborated effort and additional information is available online at http://pubs.acs.org.[66]

2.5 References for Chapter 2

1. Marchi, S. D.; Cecchin, E.; Jengo, A.; Schinella, D.; Jus, A.; Villalta, D.; Santini, P. D. P.; Tesio, F., *Am. J. Nephrol* **1984,** 4, 280-286.

2. Elsas, L. J.; Rosenberg, L. E., Familial renal glycosuria: a genetic reappraisal of hexose transport by kidney and intestine. *J. Clinic. Invest.* **1969,** 48, 1845.

3. Baxter, P.; Goldhill, J.; Hardcastle, P. T.; Taylor, C. J., Enhanced intestinal glucose and alanine transport in cystic fibrosis. *Gut* **1990,** 31, 817-820.

4. Fedorak, R. N.; Gershon, M. D.; Field, M., *Gastroenterology* **1989,** 96, 37-44.

5. Yasuda, H.; Kurokawa, T.; Fujii, Y.; Yamashita, A.; Ishibashi, S., *Biochim. Biophys. Acta* **1990,** 1021, 114-118.

6. Yamamoto, T.; Seino, Y.; Fukumoto, H.; Koh, G.; Yano, H.; Inagaki, N.; Yamada, Y.; Inoue, K.; Manabe, T.; Imura, H., *Biochem. Biophyd. Res. Commun.* **1990,** 170, 223-230.

7. UK Prospective Diabetes Study Group. *Lancet* **1998,** 352, 2979-2996.

8. Hall, D. G., *Boronic Acids Preparation, Applications in Organic Synthesis and Medicine*. WILEY-VCH Verlag GmbH & Co. KGaA: Weinheim, 2005.

9. Kuivila, H. G.; Keough, A. H.; Soboczenski, E. J., Areneboronates from Diols and Polyols. *J. Org. Chem.* **1954,** 19, 780-783.

10. Dewar, M. J. S.; Kubba, V. P.; Pettit, R., New Heteroaromatic Compounds. Part II. Boron Compounds Isoconjugate with Indole, 2:3-Benzofuran, and Thionaphthen. *J. Chem. Soc., Abstracts* **1958**, 3076-3079.

11. Lorand, J. P.; Edwards, J. O., Polyol Complexes and Structure of the Benzeneboronate Ion. *J. Org. Chem.* **1959,** 24, 769-774.

12. Letsinger, R. L.; Hamilton, S. B., Organoboron Compounds. XII. Heterocyclic Compounds from Benzeneboronic Acid1. *J. Org. Chem.* **1960,** 25, 592-595.

13. Jensen, K. A.; Pedersen, T., Heterocyclic Boron Compounds I. *Acta Chem. Scand.* **1961,** 15, (8), 1780-1781.

14. Letsinger, R. L.; MacLean, D. B., Organoboron Compounds. XVI. Cooperative Functional Group Effects in Reactions of Boronoarylbenzimidazoles. *J. Am. Chem. Soc.* **1963,** 85, 2230-2236.

15. Kankare, J. J.; Varhiala, J., Selective Determination of Tartaric Acid in Aqueous Solution with 2-[1-(*o*-Dihydroxyborylphenyl)-2-phenylethyl]-2-imidazoline. *Anal. Chim. Acta* **1978,** 99, 151-156.

16. James, T. D.; Linnane, P.; Shinkai, S., Fluorescent Saccharide Receptors: A Sweet Solution to the Design, Assembly and Evaluation of Boronic Acid Derived PET Sensors. *Chem. Commun.* **1996**, 281-288.

17. James, T. D.; Sandanayake, K. R. A. S.; Shinkai, S., Saccharide Sensing with Molecular Receptors Based on Boronic Acid. *Angew. Chem. Int. Ed. Engl.* **1996,** 35, 1910-1922.

18. Wang, W.; Gao, X.; Wang, B., Boronic Acid-Based Sensors. *Curr. Org. Chem.* **2002,** 6, 1285-1317.

19. Striegler, S., Selective Carbohydrate Recognition by Synthetic Receptors in Aqueous Solution. *Curr. Org. Chem.* **2003,** 7, 81-102.

20. Fang, H.; Kaur, G.; Wang, B., Progress in Boronic Acid-Based Fluorescent Glucose Sensors. *J. Fluores.* **2004,** 14, 481-489.

21. Phillips, M. D.; James, T. D., Boronic Acid Based Modular Fluorescent Sensors for Glucose. *J. Fluores.* **2004,** 14, 549-559.

22. Cao, H.; Heagy, M. D., Fluorescent Chemosensors for Carbohydrates: A Decade's

Worth of Bright Spies for Saccharides in Review. *J. Fluores.* **2004,** 14, 569-584.

23. Gray Jr., C. W.; Houston, T. A., Boronic Acid Receptors for α-Hydroxycarboxylates: High Affinity of Shinkai's Glucose Receptor for Tartrate. *J. Org. Chem.* **2002,** 67, 5426-5428.

24. Zhu, L.; Anslyn, E. V., Facile Quantification of Enantiomeric Excess and Concentration with Indicator-Displacement Assays: An Example in the Analyses of a-Hydroxyacids. *J. Am. Chem. Soc.* **2004,** 126, (12), 3676-3677.

25. Wiskur, S. L.; Lavigne, J. J.; Matzger, A.; Tobey, S. L.; Lynch, V. M.; Anslyn, E. V., Thermodynamic Analysis of Receptors Based on Guanidinium/Boronic Acid for the

Complexation of Carboxylates, α-Hydroxylates, and Diols: Driving Force for Binding and Cooperativity. *Chem. Eur. J.* **2004,** 10, 3792-3804.

26. Nguyen, B. T.; Wiskur, S. L.; Anslyn, E. V., Using Indicator-Displacement Assays in Test Strips and to Follow Reaction Kinetics. *Org. Lett.* **2004,** 6, 2499-2501.

27. Zhao, J.; Fyles, T. M.; James, T. D., Chiral Binol-Bisboronic Acid as Fluorescence Sensor for Sugar Acids. *Angew. Chem. Int. Ed.* **2004,** 43, 3461-3464.

28. Zhao, J.; Davidson, M. G.; Mahon, M. F.; Kociok-Kohn, G.; James, T. D., An Enantioselective Fluorescent Sensor for Sugar Acids. *J. Am. Chem. Soc.* **2004,** 126, 16179-16186.

29. Zhu, L.; Zhong, Z.; Anslyn, E. V., Guidelines in Implementing Enantioselective Indicator-Displacement Assays for α-Hydroxycarboxylates and Diols. *J. Am. Chem. Soc.* **2005,** 127, 4260-4269.

30. Yoon, J.; Czarnik, A. W., Fluorescent Chemosensing of Catechol and Catecholamines in Water. *Bioorg. Med. Chem.* **1993,** 1, (4), 267-271.

31. Secor, K. E.; Glass, T. E., Selective Amine Recognition: Development of a Chemosensor for Dopamine and Norepinephrine. *Org. Lett.* **2004,** 6, 3727-3730.

32. Maue, M.; Schrader, T., A Color Sensor for Catecholamines. *Angew. Chem. Int. Ed.* **2005,** 44, 2265-2270.

33. Paugam, M.-F.; Valencia, L. S.; Boggess, B.; Smith, B. D., Selective Dopamine Transport Using a Crown Boronic Acid. *J. Am. Chem. Soc.* **1994,** 116, 11203-11204.

34. Paugam, M.-F.; Bien, J. T.; Smith, B. D.; Chrisstoffels, L. A. J.; de Jong, F.; Reinhoudt, D. N., Facilitated Catecholamine Transport through Bulk and Polymer-Supported Liquid Membranes. *J. Am. Chem. Soc.* **1996,** 118, 9820-9825.

35. Weith, H. L.; Wiebers, J. L.; Gilham, P. T., Synthesis of Cellulose Derivatives Containing the Dihydroxyboryl Group and a Study of Their Capacity to Form Specific Complexes with Sugars and Nucleic Acid Components. *Biochemistry* **1970,** 9, 4396-4401.

36. Rosenberg, M.; Wiebers, J. L.; Gilham, P. T., Studies on the Interactions of Nucleotides, Polynucleotides, and Nucleic Acids with Dihydroxyboryl-Substituted Celluloses. *Biochemistry* **1972,** 11, 3623-3628.

37. Barker, S. A.; Hatt, B. W.; Somers, P. J.; Woodbury, R. R., The Use of Poly(4-vinylbenzeneboronic Acid) Resins in the Fractionation and Interconversion of Carbohydrates. *Carbohydrate Res.* **1973,** 26, 55-64.

38. Reske, K.; Schott, H., Column-Chromatographic Separation of Neutral Sugars on a Dihydroxyboryl-Substituted Polymer. *Angew. Chem. Int. Ed.* **1973,** 12, 417-418.

39. Wulff, G.; Vesper, W., Preparation of Chromatogrphic Sorbents with Chiral Cavities for Racemic Resolution. *J. Chromatogr.* **1978,** 167, 171-186.

40. Glad, M.; Ohlson, S.; Hansson, L.; Mansson, M.-O.; Mosbach, K., High-Performance Liquid Affinity Chromatography of Nucleosides, Nucleotides and Carbohydrates with Boronic Acid-Substituted Microparticulate Silica. *J. Chromatogr.* **1980,** 200, 254-260.

41. Wulff, G., Selective Binding to Polymers via Covalent Bonds. The Construction of Chiral Cavities as Specific Receptor Sites. *Pure Appl. Chem.* **1982,** 54, 2093-2102.

42. Wulff, G., Molecular Imprinting in Cross-Linked Materials with the Aid of Molecular Templates - A Way towards Artificial Antibodies. *Angew. Chem. Int. Ed. Engl.* **1995,** 34, 1812-1832.

43. Suri, J. T.; Cordes, D. B.; Capuccio, F. E.; Wessling, R. A.; Singaram, B., Continuous Glucose Sensing with a Fluorescent Thin-Film Hydrogel. *Angew. Chem. Int. Ed.* **2003,** 42, 5857-5859.

44. Badugu, R.; Lakowicz, J. R.; Geddes, C. D., A Gluocose-Sensing Contact Lens: From Bench Top to Patient. *Curr. Opin. Biotechnol.* **2005,** 16, 100-107.

45. Burgemeister, T.; Grobe-Einsler, R.; Grotstollen, R.; Mannschreck, A.; Wulff, G., Fast Thermal Breaking and Formation of a B-N Bond in 2-(Aminomethyl)benzeneboronates. *Chem. Ber.* **1981,** 114, 3403-3411.

46. Wulff, G.; Lauer, M.; Bohnke, H., Rapid Proton Transfer as Cause of an Unusually Large Neighboring Group Effect. *Angew. Chem. Int. Ed. Engl.* **1984,** 23, (9), 741-742.

47. Lauer, M.; Bohnke, H.; Grotstollen, R.; Salehnia, M.; Wulff, G., *Chem. Ber.* **1985,** 118, 246-260.

48. Lauer, M.; Wulff, G., Complexation of Arylboronates with Nitrogen-containing Bases. *J. Chem. Soc., Perkin Trans. 2* **1987**, 745-749.

49. Bello-Ramírez, M. A.; Martínez, M. E. R.; Flores-Parra, A., Dioxaborolanes and borates derived from 2,3-butanediol, mandelic acid, and quinic acid [1]. *Heteroatom Chem.* **1993,** 4, 613-620.

50. Nagai, Y.; Kobayashi, K.; Toi, H.; Aoyama, Y., Stabilization of Sugar-Boronic Esters of Indolylboronic Acid in Water via Sugar–Indole Interaction: A Notable Selectivity in Oligosaccharides . *Bull. Chem. Soc. Jpn.* **1993,** 66, 2965-2971.

51. Norrild, J. C.; Eggert, H., Evidence for Mono- and Bisdentate Boronate Complexes of Glucose in the Furanose Form. Application of 1JC-C Coupling Constants as a Structural Probe. *J. Am. Chem. Soc.* **1995,** 117, 1479-1484.

52. Bielecki, M.; Eggert, H.; Norrild, J. C., A fluorescent glucose sensor binding covalently to all five hydroxy groups of -D-glucofuranose. A reinvestigation. *J. Chem. Soc., Perkin Trans. 2* **1999**, 449-455.

53. Norrild, J. C., An illusive chiral aminoalkylferroceneboronic acid. Structural assignment of a strong 1:1 sorbitol complex and new insight into boronate–polyol interactions. *J. Chem. Soc., Perkin Trans. 2* **2001**, 719-726.

54. Norrild, J. C.; Søtofte, I., Crystal structures of 2-(*N,N*-dimethylaminoalkyl)ferroceneboronic acids and their diol derivatives. The quest for a B–N intramolecular bond in the solid state. *J. Chem. Soc., Perkin Trans. 2* **2001**, 727-732.

55. Wiskur, S. L.; Lavigne, J. J.; Ait-Haddou, H.; Lynch, V. M.; Chiu, Y. H.; Canary, J. W.; Anslyn, E. V., PKa Values and Geometries of Secondary and Tertiary Amines Complexed to Boronic Acids - Implications for Sensor Design. *Org. Lett.* **2001,** 3, (9), 1311-1314.

56. Otsuka, H.; Uchimura, E.; Koshino, H.; Okano, T.; Kataoka, K., Anomalous Binding Profile of Phenylboronic Acid with N-Acetylneuraminic Acid (Neu5Ac) in Aqueous Solution with Varying pH. *J. Am. Chem. Soc.* **2003,** 125, 3493-3502.

57. Ni, W.; Kaur, G.; Springsteen, G.; Wang, B.; Franzen, S., Regulating the Fluorescence Intensity of an Anthracene Boronic Acid System: a B-N Bond or a Hydrolysis Mechanism? *Bioorg. Chem.* **2004,** 32, 571-581.

58. Bosch, L. I.; Fyles, T. M.; James, T. D., Binary and Ternary Phenylboronic Acid Complexes with Saccharides and Lewis Bases. *Tetrahedron* **2004,** 60, 11175-11190.

59. Paugam, M.-F.; Smith, B. D., Active Transport of Uridine through a Liquid Organic Membrane Mediated by Phenylboronic Acid and Driven by a Fluoride Ion Gradient. *Tetrahedron Lett.* **1993,** 34, 3723-3726.

60. Kubo, Y.; Kobayashi, A.; Ishida, T.; Misawa, Y.; James, T. D., Detection of Anions Using a Fluorescent Alizarin-Phenylboronic Acid Ensemble. *Chem. Commun.* **2005**, 2846-2848.

61. Soundararajan, S.; Badawi, M.; Kohlrust, C. M.; Hageman, J. H., Boronic acids for affinity chromatography: Spectral methods for determinations of ionization and diol-binding constants. *Analytical Biochemistry* **1989,** 178, (1), 125-134.

62. Kavarnos, G. J., Fundamentals of photoinduced electron transfer. In VCH Publishers: New York, 1993.

63. James, T. D.; Sandanayake, K. R. A. S.; Shinkai, S., Novel Photoinduced Electron-Transfer Sensor for Saccharides Based on the Interaction of Boronic Acid and Amine. *J. Chem. Soc., Chem. Commun.* **1994**, 477-478.

64. James, T. D.; Sandanayake, K. R. A. S.; Iguchi, R.; Shinkai, S., Novel Saccharide-Photoinduced Electron Transfer Sensors Based on the Interaction of Boronic Acid and Amine. *J. Am. Chem. Soc.* **1995,** 117, 8982-8987.

65. Franzen, S.; Ni, W.; Wang, B., Study of the Mechanism of Electron-Transfer Quenching by Boron-Nitrogen Adducts in Fluorescent Sensors. *J. Phys. Chem. B* **2003,** 107, 12942-12948.

66. Zhu, L.; Shabbir, S. H.; Gray, M.; Lynch, V. M.; Sorey, S.; Anslyn, E. V., A Structural Investigation of the N-B Interaction in an o-(*N,N*-Dialkylaminomethyl)arylboronate System. *J. Am. Chem. Soc.* **2006,** 128, (4), 1222-1232.

67. Höpfl, H., The Tetrahedral Character of the Boron Atom Newly Defined - A Useful Tool to Evaluate the N-B Bond. *J. Organomet. Chem.* **1999,** 581, 129-149.

68. Norrild, J. C.; Søtofte, I., Design, Synthesis and Structure of New Potential Electrochemically Active Boronic Acid-Based Gluocose Sensors. *J. Chem. Soc., Perkin Trans. 2* **2002**, 303-311.

69. Giles, R. L.; Howard, J. A. K.; Patrick, L. G. F.; Probert, M. R.; Smith, G. E.; Whiting, A., Synthesis and Structure of Potential Lewis Acid - Lewis Base Bifunctional Catalysts: 1-*N,N*-Dimethylamino-8-bororonaphthalene Derivatives. *J. Organomet. Chem.* **2003,** 680, 257-262.

70. Bosch, L. I.; Mahon, M. F.; James, T. D., The B-N Bond Controls the Balance between Locally Excited (LE) and Twisted Internal Charge Transfer (TICT) States Observed for Aniline Based Fluorescent Saccharide Sensors. *Tetrahedron Lett.* **2004,** 45, 2859-2862.

71. Biedrzycki, M.; Scouten, W. H.; Biedrzycka, Z., Derivatives of Tetrahedral Boronic Acids. *J. Organomet. Chem.* **1992,** 431, 255-270.

72. Lauer, M.; Wulff, G., *J. Organomet. Chem.* **1983,** 256, 1-9.

73. Brown, H. C.; Vara Prasad, J. V. N., Chiral synthesis via organoboranes. 9. Crystalline chelates from borinic and boronic esters. A simple procedure for upgrading borinates and boronates to materials approaching 100% optical purity. *J. Org. Chem.* **1986,** 51, 4526-4530.

74. Reetz, M. T.; Niemeyer, C. M.; Harms, K., Crown Ethers with a Lewis Acidic Center: A New Class of Heterotopic Host Molecules. *Angew. Chem. Int. Ed. Engl.* **1991,** 30, 1472-1474.

75. Reetz, M. T.; Niemeyer, C. M.; Harms, K., Heterotopic Host Molecules for Binding Two Different Guests. *Angew. Chem. Int. Ed. Engl.* **1991,** 30, 1474-1476.

76. Reetz, M. T.; Niemeyer, C. M.; Hermes, M.; Goddard, R., Molecular Recognition of Primary Amines by Three-Point Binding with Boron-Containing Host Molecules. *Angew. Chem. Int. Ed. Engl.* **1992,** 31, 1017-1019.

77. Arimori, S.; Ward, C. J.; James, T. D., The First Fluorescent Sensor for Boronic and Boric Acids with Sensitivity at Sub-micromolar Concentrations - A Cautionary Tale. *Chem. Commun.* **2001**, 2018-2019.

78. Zhong, S.; Jordan, F.; Kettner, C.; Polgar, L., *J. Am. Chem. Soc.* **1991,** 113, 9429-9435.

79. Singhal, R. P.; Ramamurthy, B.; Govindraj, N.; Sarwar, Y., New ligands for boronte affinity chromatography *1: Synthesis and propertiesa. *J. Chromatogr.* **1991,** 543, 17-38.

80. Yan, J.; Springsteen, G.; Deeter, S.; Wang, B., The Relationships among pKa, pH, and Binding Constants in the Interactions between Boronic Acids and Diols - It is not as Simple as It appears. *Tetrahedron* **2004,** 60, 11205-11209.

81. James, T. D.; Shinkai, S., Artificial Receptors as Chemosensors for Carbohydrates. *Top. Curr. Chem.* **2002,** 218, 159-200.

82. Springsteen, G.; Wang, B., A Detailed Examination of Boronic Acid - Diol Complexation. *Tetrahedron* **2002,** 58, 5291-5300.

83. Yoon, J.; Czarnik, A. W., Fluorescent Chemosensors of Carbohydrates. A Means of Chemically Communicating the Binding of Polyols in Water Based on Chelation-Enhanced Quenching. *J. Am. Chem. Soc.* **1992,** 114, 5874-5875.

84. Otwinowski, Z.; Minor, W.; Charles W. Carter, Jr., [20] Processing of X-ray diffraction data collected in oscillation mode. In *Methods in Enzymology*, Academic Press: 1997; Vol. Volume 276, pp 307-326.

85. Altomare, A.; Burla, M. C.; Camalli, M.; Cascarano, G. L.; Giacovazzo, C.; Guagliardi, A.; Moliterni, A. G. G.; Polidorib, G.; Spagnac, R., Computer Programs. *J. Appl. Cryst* **1999,** 32, 115-119.

86. Sheldrick, G. M. *Program for the Refinement of Crystal Structures*, University of Gottingen, Germany, 1994.

87. $R_W(F^2) = \{\Sigma w(|F_o|^2 - |F_c|^2)^2/\Sigma w(|F_o|)^4\}^{1/2}$ where w is the weight given each reflection.
$R(F) = \Sigma(|F_o| - |F_c|)/\Sigma|F_o|\}$ for reflections with $F_o > 4(\sigma(F_o))$.
$S = [\Sigma w(|F_o|^2 - |F_c|^2)^2/(n - p)]^{1/2}$, where n is the number of reflections and p is the number of refined parameter.

88. Wilson, A. J. C., *International Tables for X-ray Crystallography*. Kluwer Academic Press: Boston, 1992.

89. Sheldrick, G. M. *SHELXTL/PC (Version 5.03)*, Siemens Analytical X-ray Instruments, Inc.: Madison, Wisconsin, USA, 1994.

Chapter 3: Two Methods for the Determination of Enantiomeric Excess (*ee*) and Concentration of a Chiral Sample with a Single Spectroscopic Measurement

3.1 Enantioselective Indicator Displacement Assays (eIDAs)

Library screening approaches for the development of asymmetric catalysts are becoming standard protocols in both industry and academia[1, 2] for rapid quantification of yield and enantiomeric excess (*ee*) of chiral products in a high-throughput fashion.[3, 4] Currently, parallel chromatographic methods are mostly employed for that purpose.[5-9] The development of optical spectroscopic assays (e.g. absorption or fluorescence) should ease the instrumentation dependence and increase the speed of high-throughput screening assays.[1, 10]

We introduced the use of enantioselective indicator-displacement assays (eIDAs) to determine both concentration and *ee* of chiral samples.[11-13] Few other methods have been shown to have this capacity.[14-17] In an eIDA, two spectroscopic measurements are taken. First, the concentration of a chiral sample ($[G]_t$) is determined with an indicator-displacement assay (IDA)[18] using an achiral host (**Scheme 3.1A**). Second, an eIDA is carried out where a chiral host (H*) is used to generate a $[G]_t$ and *ee*-dependent optical signal (ΔAbs). Such a signal is related to $[G]_t$ and *ee* via a mathematical function of solution equilibrium constants and molar absorptivities (**Eq**. **3.2**, **Scheme 3.1**).[11] Because $[G]_t$ is known from the measurement using the achiral host H, the *ee* of the sample can be obtained by solving Eq. 2. We have used an arylboronic acid-based eIDA to quantitatively analyze chiral α-hydroxycarboxylates and diols.[11, 12] The accuracies for both concentration and *ee* are well within the requirement for a typical asymmetric catalysis screening project. The association constants between the host and indicator are

determined through 1:1 binding isotherms. The affinities of the receptor to the guest are determined with traditional competitive spectrophotometric method. The relationship between *ee* and *A* is derived mathematically.

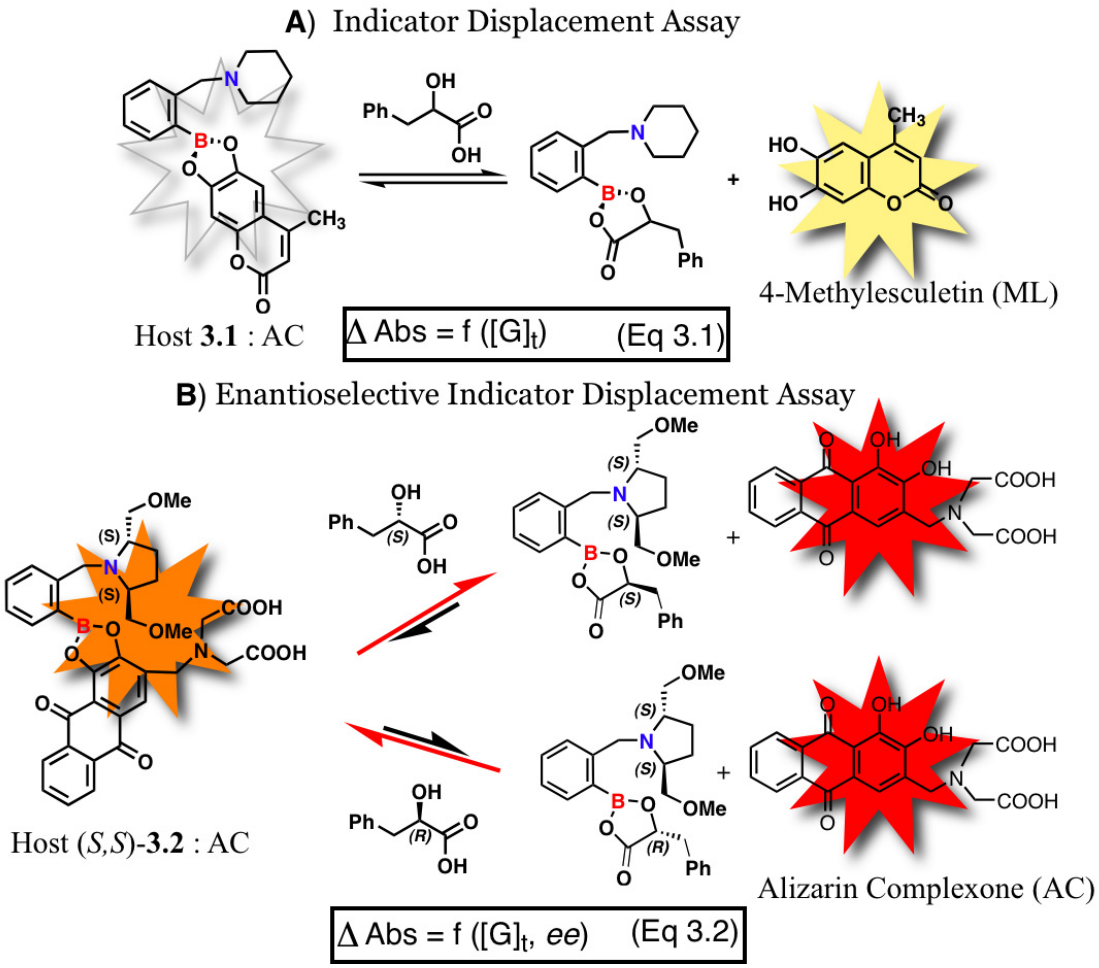

Scheme 3.1: Two-step enantioselective indicator-displacement assays (eIDAs). **A**) Achiral host– **3.1**; indicators–4-methylesculetin (ML); guest – α-hydroxycarboxylate phenylactate (PL). **B**) Chiral host – (*S,S*)-**3.2**; indicators – alizarin complexone (AC); guest – (*R*)α-hydroxycarboxylate phenylactate (D-PL) and (*S*)α-hydroxycarboxylate phenylactate (L-PL). ΔAbs – absorbance change; $[G]_t$ – guest concentration; *ee* – enantiomeric excess Eq. 3.1 is an empirical polynomial fit for an *A* vs. $[G]_t$ displacement curve. Eq. 3.2 is a theoretical function derived from solution multi-equilibria and Beer's Law analysis.

3.1:1 Binding Isotherm

To determine the binding constant K_{HI} between the host and the indicator a 1:1 binding isotherm is used. In this system a single 1:1 complex of Host:Indicator ([HI]) is formed. The [HI] complex and the free indicator ([I]) have significant different absorption spectra. It is assumed that Beer's law is followed by all the species present on solution. The equilibrium equation is written as:

$$H + I \rightleftharpoons HI \qquad (3.3)$$

without considering the activity coefficient at diluted solutions, the binding constant (K) can be expressed as

$$K_{HI} = \frac{[HI]}{[H] + [I]} \qquad (3.4)$$

Let the total concentration of [H] and [I] be $[H]_t$ and $[I]_t$, respectively, we have the following mass balance expression

$$[H]_t = [H] + [HI] \qquad (3.5)$$

$$[I]_t = [I] + [HI] \qquad (3.6)$$

Putting $[HI] = K[H][I]$ in Eq. 3.5 and solving for [H], gives

$$[H] = \frac{[H]_t}{(1 + K_{HI}[I])} \qquad (3.7)$$

Substituting [H] in Eq. 3.6 and solving for [HI] gives

$$[HI] = \frac{K_{HI}[I][H]_t}{(1 + K_{HI}[I])} \qquad (3.8)$$

Substituting equation 3.7 and 3.8 in equation gives a quadratic equation that is rearranged as

$$K_{HI}[I]^2 + (1-K_{HI}[I]_t + K_{HI}[H]_t)[I] - [I]_t = 0 \quad (3.9)$$

The real root of this equation is given by

$$[I] = \frac{-(1-K_{HI}[I]_t + K_{HI}[H]_t) + \{ (1-K_{HI}[I]_t + K_{HI}[H]_t)^2 + 4 K_{HI}[I]_t\}^{1/2}}{2K} \quad (3.10)$$

Once [I] is obtained [H] and [HI] can be easily calculated by using Eq. 3.7 and 3.8

According to Beer's law, the absorbance of the equilibrium solution can be expressed as

$$A = \varepsilon_H b[H] + \varepsilon_I b[I] + \varepsilon_{HG} b[H:I] \quad (3.11)$$

where A is the absorbance a the selected wavelength; ε_H, ε_I, ε_{HI}, are the molar absorptivity of the host, indicator and the host indicator complex at that wavelength. In the current study the boronic acid receptors are transparent at the observed wavelength. Therefore $\varepsilon_H = 0$, Eq 3.11 is simplified as

$$A = \varepsilon_I b[I] + \varepsilon_{HI} b[H:I] \quad (3.12)$$

Substituting the value of [I] and [H:I] values from equation 3.6 and 3.8 respectively, in Eq. 3.10 gives Eq. 3.13

$$A = \left\{ \varepsilon_I b + \frac{\varepsilon_{HI} b K_{HI}[H]_t}{1+0.5\{-(1=K_{HI}[I]_t + K_{HI}[H]_t) + \sqrt{(1-K_{HI}[I]_t + K_{HI}[H]_t)^2 + 4K_{HI}[I]_t}\}} \right\} \times \frac{-(1-K_{HI}[I]_t + K[H]_t) + \sqrt{(1-K[I]_t + K[H]_t)^2 + 4K[I]_t}}{2K}$$

where b = path length; ε_I = molar absorptivity of the indicator at that wavelength and $\varepsilon_{H:I}$ = molar absorptivity of the host indicator complex; K_{HI} = binding constant between the host and the indicator; $[H]_t$ = host total concentration; $[I]_t$ = indicator total concentration. $[H]_t$, $[I]_t$ and b are known variables the binding constant K_{HI} and the $\varepsilon_{H:I}$ can be determined from the titration data by non-linear curve fitting with Eq. 3.13.

3.1.2 Competitive Spectrophotometry

To determine the binding constant between the host and the guest K_{HG} competitive spectroscopy is used. If binding between the substrate and ligand does not produce a significant spectral change, the direct spectrophotometric method cannot be used. An alternative is to employ competitive spectrophotometry, in which the equilibrium is established between the host and the indicator, this equilibrium results in a spectral change. Then the guest molecule of interest is added to the solution resulting in a competition between the guest and the indicator for the host. The displacement of the indicator from the host causes a spectral change.

In indicator displacement assay, we consider a system where only indicator and the guest forms 1:1 complex with the host. The competitive complexation equilibrium is

$$HI + G \rightleftharpoons HG + I \tag{3.14}$$

The mass balance expressions are

$$[G]_t = [G] + [HG] \tag{3.15}$$

$$[H]_t = [H] + [HG] + [HI] \tag{3.16}$$

$$[I]_t = [I] + [HI] \tag{3.17}$$

and the binding constant are defined

$$K_{HG} = \frac{[HG]}{[H] + [G]} \tag{3.18}$$

$$K_{HI} = \frac{[HI]}{[H] + [I]} \tag{3.19}$$

From equation 3.15 and 3.18 we have

$$[HG] = \frac{K_{HG}[H]}{1 + K_{HG}[H]}[G]_t \tag{3.20}$$

From Eq. 3.17 and 3.19 we get

$$[HI] = \frac{K_{HI}[H]}{1 + K_{HI}[H]}[I]_t \tag{3.21}$$

Substituting Eq 3.20 and 3.21 in Eq 3.18 gives

$$[H]_t = [H] + \frac{K_{HG}[H]}{1 + K_{HG}[H]}[G]_t + \frac{K_{HI}[H]}{1 + K_{HI}[H]}[I]_t \tag{3.22}$$

This is a cubic equation for [H]. To numerically solve cubic equation 3.22 by Newton's method, we need to rearrange it to the polynomial form:

$$A[H]^3 + B[H]^2 + C[H] + D = 0 \tag{3.23}$$

where $A = K_{HI}K_{HG}$

$B = K_{HI} + K_{HG} + K_{HI}K_{HG}[I]_t + K_{HI}K_{HG}[G]_t - K_{HI}K_{HG}[H]_t$

$C = 1 + K_{HI}[I]_t + K_{HG}[G]_t - K_{HI}[H]_t - K_{HG}[H]_t$

$D = -[H]_t$

In the indicator displacement titration, the total concentrations of the host and indicator are kept constant, and the total concentration of the guest is increased. A titration curve is obtained by plotting the absorbance at specific wavelength ($A_{\lambda x}$) verses guest total concentration ($[G]_t$). Since the host and the guest molecule used are transparent at the observed wavelength, the absorbance is expressed as the function of the free indicator (I) and the complex indicator (HI):

$$A_{\lambda x} = \varepsilon_I b[I] + \varepsilon_{HI} b[HI] \tag{3.24}$$

where b is the path length of the cell.

Combining Eq. 3.17 and 3.19 we get

$$[I] = \frac{[I]_t}{(1 + K_{HI}[H])} \tag{3.25}$$

$$[\mathrm{HI}] = \frac{[\mathrm{I}]_t K_{\mathrm{HI}}}{(1 + K_{\mathrm{HI}}[\mathrm{H}])} \tag{3.26}$$

Substitution of Eq. 3.25 and 3.26 in Eq. 3.24 gives

$$A = \{[\mathrm{I}]_t/(1+K_{\mathrm{HI}}[\mathrm{H}])\}\ \{\varepsilon_{\mathrm{I}}b + \varepsilon_{\mathrm{HI}}bK_{\mathrm{HI}}[\mathrm{H}]\} \tag{3.1}$$

Origin is used to solve Eq. 3.23 for [H] by non-linear curve fitting using Eq. 3.1. Where K_{HI}, ε_{I}, and $\varepsilon_{\mathrm{HI}}$ are previously determine by curve-fitting the data of the titration of the host into a solution of the indicator, $[\mathrm{H}]_t$ and $[\mathrm{I}]_t$ are kept constant through out the titration and are known. The $[\mathrm{G}]_t$ (x) and the A (y) are read by Origin, and given the estimated initial values for K_{HG}, the fitter can iteratively find the value of K_{HG} best fitting the experimental data.

Another method that is used to confirm the binding constant (K_{HG}) that is obtained by Origin is by using a graphical approach by plotting $[\mathrm{G}]_t/P$ against Q where Q is defined as the indicator ratio [I]/[HI] which allows us to write $K_{\mathrm{HI}} = 1/Q[\mathrm{I}]$, which, substituted in Eq. 3.22 gives

$$[\mathrm{H}]_t = \frac{1}{QK_{\mathrm{HI}}} + \frac{[\mathrm{G}]_t K_{\mathrm{HG}}}{QK_{\mathrm{HI}} + K_{\mathrm{HG}}} + \frac{[\mathrm{I}]_t}{Q+1} \tag{3.27}$$

The quantity P is defined as

$$P = [\mathrm{H}]_t - \frac{1}{QK_{\mathrm{HI}}} - \frac{[\mathrm{I}]_t}{Q+1} \tag{3.28}$$

Therefore Eq. 3.27 can be written as

$$P = \frac{[\mathrm{G}]_t K_{\mathrm{HG}}}{(QK_{\mathrm{HI}} + K_{\mathrm{HG}})} \tag{3.29}$$

$$\frac{[\mathrm{G}]_t}{P} = (\frac{K_{\mathrm{HI}}}{K_{\mathrm{HG}}})Q + 1 \tag{3.30}$$

The indicator ratio Q can be obtained from Eq. 3.31

$$Q = (\varepsilon-\varepsilon_{HI})/(\varepsilon_I -\varepsilon) \quad (3.31)$$

where ε_I and ε_{HI} are the molar absorptivity of the free and complexed indicator, respectively , and ε is the apparent molar absorptivity in any solution containing both forms. If the total indicator concentration is constant in all solutions, the absorptivity can be replaced by absorbance. K_{HI} can be obtained by independent measurement on solutions of indicator and the host by conventional spectrophotometeric method. P is obtained by using Eq. 31. Adding a linear trendline to the graph of $[G]_t/P$ verses Q and varying the value of ε_{HI} the value K_{HG} can be obtained from the slope of the graph (slope = K_{HI}/K_{HG}).

3.1.3 *Ee* Measurement by Indicator-Displacement Assay

As enantioselective indicator displacement assay follow solution equilibrium a relationship between *ee* and the absorbance can be established. When a mixture of enantiomers are present, the concentration of all the solution species are defined by three solution equilibria.

$$H^* + I \rightleftharpoons H^*I \qquad K_{H^*I} = \frac{[H^*I]}{[H^*]+[I]} \quad (3.32)$$

$$H^* + G_R \rightleftharpoons H^*G_R \qquad K_{H^*G_R} = \frac{[H^*G_R]}{[H^*]+[G_R]} \quad (3.33)$$

$$H^* + G_S \rightleftharpoons H^*G_S \qquad K_{H^*G_S} = \frac{[H^*G_S]}{[H^*]+[G_S]} \quad (3.34)$$

The mass balance equations for the host ($[H^*]_t$), indicator ($[I]_t$), and the guest ($[G_R]$, $[G_S]$)

$$[H^*]_t = [H^*] + [H^*I] + [H^*G_R] + [H^*G_S] \quad (3.35)$$

$$[G]_t = [H^*G_R] + [H^*G_S] + [G_S] + [G_R] \quad (3.36)$$

$$[I]_t = [H^*I] + [I] \quad (3.37)$$

ee expression

$$ee_R = \frac{([G_R] + [H^*G_R]) - ([G_S] + [H^*G_S])}{[G]_t} \quad (3.38)$$

Beer's Law and indicator mass balance

$$A = \varepsilon_I b[I] + \varepsilon_{HI} b[H^*I] \quad (3.39)$$

From Eq 3.37 and 3.39 we get

$$[I] = \frac{\varepsilon_{HI} b[I]_t - A}{b\Delta\varepsilon} \quad (3.40)$$

$$[H^*I] = \frac{A - \varepsilon_I b[I]_t}{b\Delta\varepsilon} \quad (3.41)$$

$$\Delta\varepsilon = \varepsilon_{H^*I} - \varepsilon_I \quad (3.42)$$

From Eq. 3.32, 3.40 and 3.41

$$[H^*] = \frac{[H^*I]}{K_{H^*I}[I]} = \frac{\varepsilon_I b[I]_t - A}{K_{H^*I}(A - \varepsilon_{H^*I} b[I]_t)} \quad (3.43)$$

From Eq. 3.38

$$X \equiv [G_R] + [H^*G_R] \text{ , } Y \equiv [G_S] + [H^*G_S] \quad (3.44)$$

Then

$$X + Y = [G]_t \quad (3.45)$$

$$X - Y = [G]_t ee_R \quad (3.46)$$

Solving for X and Y give

$$X = [G_R] + [H^*G_R] = \frac{[G]_t}{2}(1 + ee_R) \quad (3.47)$$

$$Y = [G_s] + [H^*G_s] = \frac{[G]_t}{2}(1 - ee_R) \tag{3.48}$$

From Eq. 3.47

$$[G_R] + [H^*G_R] = \frac{[G]_t}{2}(1 + ee_R) \tag{3.49}$$

Substituting the value of $[H^*G_R]$ from Eq. 3.33 in Eq. 3.49

$$[H^*G_S] = \frac{(1 + ee_R)[G]_t[H^*]K_{HG_S}}{2(1 + [H^*]K_{H*G_R})} \tag{3.50}$$

Substituting the value of $[G_R]$ from Eq. 3.32 in Eq. 3.49

$$[H^*G_R] = \frac{(1 + ee_R)[G]_t[H^*]K_{H^*G_R}}{2(1 + [H^*]K_{H^*G_R})} \tag{3.51}$$

Substituting the value of $[H^*]$ from Eq. 3.43 in Eq. 3.51 gives

$$[H^*G_R] = \frac{K_{H^*G_R}[G]_t(1 + ee_R)(\varepsilon_I b[I]_t - A)}{2[A(K_{H^*I} - K_{H^*G_R}) - b[I]_t(\varepsilon_{H^*I}K_{H^*I} - \varepsilon_I K_{H^*G_R})]} \tag{3.52}$$

Likewise

$$[H^*G_S] = \frac{(1 + ee_R)[G]_t[H^*]K_{H^*G_S}}{2(1 + [H^*]K_{H^*G_R})} = \frac{K_{H^*G_S}[G]_t(1 + ee_R)(\varepsilon_I b[I]_t - A)}{2[A(K_{H^*I} - K_{H^*G_S}) - b[I]_t(\varepsilon_{H^*I}K_{H^*I} - \varepsilon_I K_{H^*G_S})]} \tag{3.53}$$

Substituting the value of $[H^*]$, $[H^*_I]$, $[H^*G_R]$, $[H^*G_S]$ in Eq. 3.35

$$[H^*]_t = [H^*] + [H^*I] + [H^*G_R] + [H^*G_S] \tag{3.35}$$

$$[H^*I] = \frac{A - \varepsilon_I b[I]_t}{b\Delta\varepsilon} \tag{3.41}$$

$$[H^*] = \frac{[H_*I]}{K_{H^*I}[I]} = \frac{\varepsilon_I b[I]_t - A}{K_{H*I}(A - \varepsilon_{H^*I} b[I]_t)} \tag{3.43}$$

$$[H^*G_R] = \frac{K_{H^*G_R}[G]_t(1+ee_R)(\varepsilon_I b[I]_t - A)}{2[A(K_{H^*I} - K_{H^*G_R}) - b[I]_t(\varepsilon_{H^*I}K_{H^*I} - \varepsilon_I K_{H^*G_R})]} \tag{3.52}$$

$$[H^*G_S] = \frac{K_{H^*G_S}[G]_t(1+ee_R)(\varepsilon_I b[I]_t - A)}{2[A(K_{H^*I} - K_{H^*G_S}) - b[I]_t(\varepsilon_{HI}K_{H^*I} - \varepsilon_I K_{H^*G_S})]} \tag{3.53}$$

The Absorbance (A) verses *ee* relationship is Eq. 3.2:

$$[H^*]_t = \frac{A - \varepsilon_I b[I]_t}{b\Delta\varepsilon} + \frac{\varepsilon_I b[I]_t - A}{K_{H^*I}(A - \varepsilon_{H^*I} b[I]_t)} + \frac{K_{H^*G_R}[G]_t(1+ee_R)(\varepsilon_I b[I]_t - A)}{2[A(K_{H^*I} - K_{H^*G_R}) - b[I]_t(\varepsilon_{H^*I}K_{H^*I} - \varepsilon_I K_{H^*G_R})]} + \frac{K_{H^*G_S}[G]_t(1+ee_R)(\varepsilon_I b[I]_t - A)}{2[A(K_{H^*I} - K_{H^*G_S}) - b[I]_t(\varepsilon_{HI}K_{H^*I} - \varepsilon_I K_{H^*G_S})]}$$

where, ε_I, ε_{H*I}, K_{H*I} is determined from the 1:1 binding isotherm of the host with the indicator. K_{H*R} K_{H*S} is calculated from the displacement isotherm. $[I]_t$, $[H^*]_t$, $[G]_t$ is known by the gravimetric analysis

The requirement for applying two spectroscopic measurements for analyzing one chiral sample prompted us to engineer the eIDA system further to eliminate the need of separate measurements for concentration and *ee*. We now report two critical improvements. The first is a reduction of the number of measurements from two to one by using a dual-chamber quartz cuvette (**Figure 3.1A**).[19] A single absorption spectrum of the dual-chamber cuvette represents a combined optical response from each individual chamber caused by the addition of a chiral sample. The absorption data can be collected at the isosbestic points or alternate transparent region of the individual chambers, thus reflecting optical changes that take place in the other chamber. The consequence here is that two independent equations can be established using data collected from a single

spectroscopic measurement to determine the values of two independent variables (concentration and *ee*) in these two equations. In an extension of our mathematical procedure mentioned above, we describe a judicious choice of indicator/host combinations that takes advantage of this feature to generate both concentration and *ee*-dependent calibration curves. Our second improvement uses the same dual-chamber cuvette to collect absorption data. However, we remove the requirement to measure equilibrium constants and molar absorptivities altogether via the use of an artificial neural network (ANN) where the data collection is not limited to just isosbestic points and transparent regions. We demonstrate both approaches using a previously reported boronic acid receptor **3.1** and (*S,S*)-**3.2** (**Figure 3.1**).[11] The work reported here represents a significant advancement in the accuracy and more importantly, the speed of our eIDA's methodologies.

3.1.4 Isosbestic Point Analysis

In the first approach, appropriate indicator/host combinations are added in respective chambers of the cuvette so that two independent equations regarding $[G]_t$ and *ee* can be established simultaneously with a single absorption measurement. The left chamber of the cuvette contained the achiral host **3.1** (H) and the colorless indicator 4-methylesculetin (ML); while the right chamber contained the chiral host (*S,S*)-**3.2** (H*) with the colorimetric indicator alizarin complexone (AC, **Figure 3.1**). Absorption modulations occur when the catechol-based ML and AC reversibly interact with boronic acid host **3.1** and (*S,S*)-**3.2**. The addition of the chiral α-hydroxycarboxylate phenyllactate (PL) enantioselectively alters the ratio of free and chiral host-bound indicators ([I] and [H*I]), hence also the absorbance.

A particularly attractive feature of this cuvette is that absorption data can be collected at the isosbestic points, or transparent regions, of the spectra recorded in each individual chamber, thereby only reflecting optical changes that occur in the other chamber. The absorption spectra of ML/1 (blue) and AC/(*S,S*)-**3.2** (red) titration experiments are overlaid in **Figure 3.1B**. The isosbestic point of AC at 387 nm (λ_1) overlaps with a receptor-responsive region of ML that has a large dynamic range. At 387 nm, the absorbance from the right chamber (A_R) is independent of both host ([H*]) and guest ($[G]_t$) concentrations, whereas the absorbance from the left chamber is only dependent on the guest concentration ($[G]_t$) because the residing host in the left chamber (1) is achiral. By combining the absorbance from both chambers at this wavelength, Eq. 3.54 is established (**Figure 3.1D**). In contrast, at 536 nm (λ_2) where indicator ML is transparent, the absorbance change is solely due to the chemical events taking place in the right chamber. The absorbance is dependent on both $[G]_t$ and *ee* because the right chamber is occupied by the chiral host (*S,S*)-**3.2** (Eq. 3.2). Putting these two equations together, the values of $[G]_t$ and *ee* can be solved. The overall spectroscopic modulation with the *ee* of PL ranging from -1 to 1, where the concentration of PL is fixed at 6.0 mM, is plotted in **Figure 3.1C**.

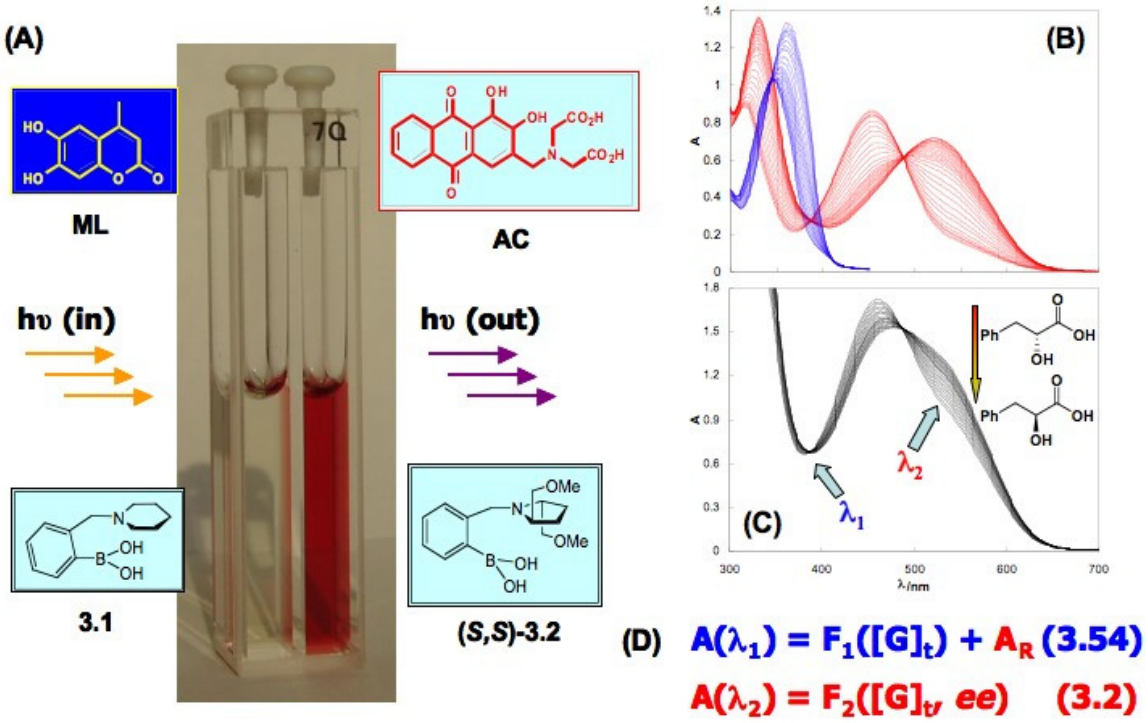

Figure 3.1: (**A**) A dual-chamber quartz cuvette containing indicators ML (left) and AC (right). (**B**) Overlay of two indicator-host isotherms. Blue: absorption spectra of ML (92.0 μM) in 75% methanolic aqueous solution buffered with 10 mM HEPES at pH 7.4 (default buffer) in the presence of 0 – 0.44 mM of 1; Red: absorption spectra of AC (115 μM) in the default buffer in the presence of 0 – 0.26 mM of (*S,S*)-**3.2**. (**C**) Absorption spectra of ML (198 μM), 1 (0.559 mM), AC (285 μM), and (*S,S*)-**3.2** (0.765 mM) in their designated chambers in the default buffer in the presence of PL (6.0 mM) with *ee* of D-PL varying from -1 to 1. (**D**) Two independent equations that correlate the absorbance (A) to $[G]_t$ and *ee* at wavelengths λ_1 (387 nm) and λ_2 (536 nm)

The parameters required for Eq. 3.54 and 3.2 (A_R, K_{H^*I}, ε_I, ε_{H^*I}, K_{H^*GR}, K_{H^*GS}, $[I]_t$, $[H^*]_t$, I = AC) are determined independently prior to the actual analysis. In short, the equilibrium constants and molar absorptivities (K_{H^*I}, ε_I, ε_{H^*I}, K_{H^*GR}, K_{H^*GS}) were determined by UV/vis titrations in the dual-chamber cuvette (b = 0.5 cm, while the other chamber was filled with buffer blank in these parameter-determination experiments) using entiomerically pure PL samples (for experimental procedures see ref 11) A_R was

also determined from the above-mentioned titrations by averaging the absorption values at 387 nm when AC was used as the indicator at 284.5 μM. The total concentration values ($[I]_t$, $[H^*]_t$) were determined gravimetrically.

A calibration curve for $[G]_t$ determination was generated as the following: A displacement isotherm at 387 nm was afforded by titrating PL (either enantiomer, 0 – 6.55 mM) into a solution of the achiral host **3.1** (0.307 mM) and indicator ML (202 μM) in the left chamber of the cuvette (the right chamber was filled with buffer). The isotherm was raised by adding A_R (Eq. 3.54). As described before, A_R is the absorbance at the isosbestic point (387 nm) of AC at the concentration of AC used in the right chamber (284.5 μM), which was determined to be 0.31. The empirical polynomial curve fitting afforded the A_{387} vs. $[G]_t$ relationship Eq. 54 as $y = 8\times10^{-6}\ x^6 - 0.0002\ x^5 + 0.0028\ x^4 - 0.0181\ x^3 + 0.0727\ x^2 - 0.2043\ x + 1.0318$ ($y = A$, $x = [G]_t$). The high-order (6^{th}) of the polynomial curve fitting allowed us to gain the maximum regression coefficient ($R^2 = 1$). This equation was subsequently used as a calibration equation for the accurate determination of $[G]_t$ (**Figure 3.2B**).

Three *ee* titration experiments were performed in the dual-chamber cuvette by using the 2-indicator-2-host system.[19] For each set of data, the concentration of PL ($[G]_t$) was fixed and the *ee* of D-PL was varied from -1 to 1. The actual titration spectra are similar to the ones shown in **Figure 3.1C**. The absorbance at 387 nm vs. *ee* values for all three sets of spectra is shown in **Figure 3.2A**. As expected, the absorbance at 387 nm is independent of *ee* values. However, it differs with respect to total concentration $[G]_t$ (**Figure 3.2A**). The average absorbance values for every $[G]_t$ are overlaid with the calibration curve at 387 nm (**Figure 3.2B**). The predictive power of the calibration curves is evident. The concentrations $[G]_t$ of 11 designated unknown PL samples (the "unknown" samples were randomly chosen from the 3 titration experiments). These 11

data points were not included in the 3 calibration curves in **Figure 3.3**, but instead determined by solving Eq. 3.54 using the software Mathematica 5.1.[20] The average absolute errors were limited to an average of ± 3.3 % (**Table 3.1**).

Table 3.1: Determination of concentration and *ee* of PL samples. IA: determined by isosbestic point analysis

No.	$[G]_t$/mM (actual)	$[G]_t$/mM (IA)	*ee*(actual)	*ee* (IA)
1	0.98	1.06	-0.90	-0.42
2	0.98	1.03	-0.49	-0.22
3	0.98	0.97	0.00	0.03
4	0.98	1.00	0.90	1.00
5	1.47	1.54	-1.00	-0.82
6	1.47	1.46	-0.30	-0.31
7	1.47	1.50	0.49	0.46
8	1.96	2.06	-0.69	-0.61
9	1.96	1.92	-0.10	-0.21
10	1.96	1.98	0.69	0.62
11	1.96	1.96	0.10	0.00

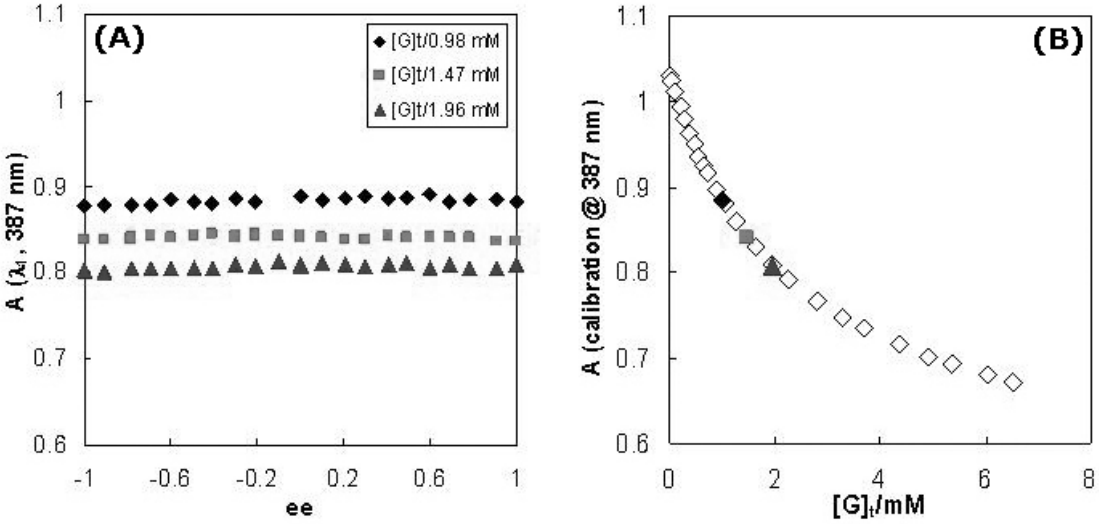

Figure 3.2: (**A**) Absorbance change at 387 nm of ML (202 μM), 1 (307 μM), AC (284.5 μM), and (*S,S*)-**2** (400 μM), in their designated chambers in the default buffer, upon increasing *ee* of D-PL. Diamonds: $[G]_t$ = 0.98 mM. Squares: $[G]_t$ = 1.47 mM. Triangles: $[G]_t$ = 1.96 mM. (**B**) Open diamonds: the absorbance change at 387 nm of the dual-chamber ensemble in **Figure 3.2A** upon increasing concentration of L-PL (D-PL produced an identical curve, not shown). The average absorbance from the *ee* titrations (coding scheme as in **Figure 3.2A** at three different $[G]_t$ values are overlaid on the calibration curve

The absorbance at 536 nm, where the bound indicator (H*I) absorbs, with regard to *ee* values at three different $[G]_t$ values are plotted in **Figure 3.3**. At a fixed $[G]_t$, the absorbance decreases (which indicates that the amount of free indicator AC is reduced) with increasing *ee* of D-PL, the enantiomer with lesser affinity. When the $[G]_t$ found from the measurement in the first chamber is used in Eq. 2, only a function of *ee* is obtained. Calculated *A* vs. *ee* curves were generated for the three $[G]_t$ values as shown in **Figure 3.2**. The overlay of the theoretical predictions with the experimental *ee* data for all three $[G]_t$ cases were shown in **Figure 3.3** (Parameters used for solving Eq. 3.2: b = 0.5 cm, ε_I = 4,600 M^{-1}/cm, ε_{H*I} = 128 M^{-1}/cm, K_{H*I} = 15,000 M^{-1}, K_{H*GR} = 2,174 M^{-1}, K_{H*GS} = 7,142 M^{-1}, $[H^*]_t = 0.40 \times 10^{-3}$ M^{-1}, $[I]_t = 284.5 \times 10^{-6}$ M^{-1}. ε_I and ε_{H*I} values were slightly

adjusted from values determined by AC and (*S,S*)-**3.2** 1:1 association titration experiment to gain satisfying curve fittings in **Figure 3.3**). **Eq. 3.2** was then used to determine the *ee* of the 11 unknown PL samples, where their concentrations ($[G]_t$) were determined by Eq. **3.54**. The average absolute error of the *ee* determination was ±7.9% (**Table 3.1**). The first 2 outliers, which lay on the least sensitive region of the A vs. *ee* calibration curve, were excluded in the error determination. Hence, the determination of both $[G]_t$ and *ee* of chiral samples using single spectroscopic measurements is possible using a dual-chamber cuvette. This work was performed by Dr. Lei Zhu a post doc in Anslyn's laboratories.[21]

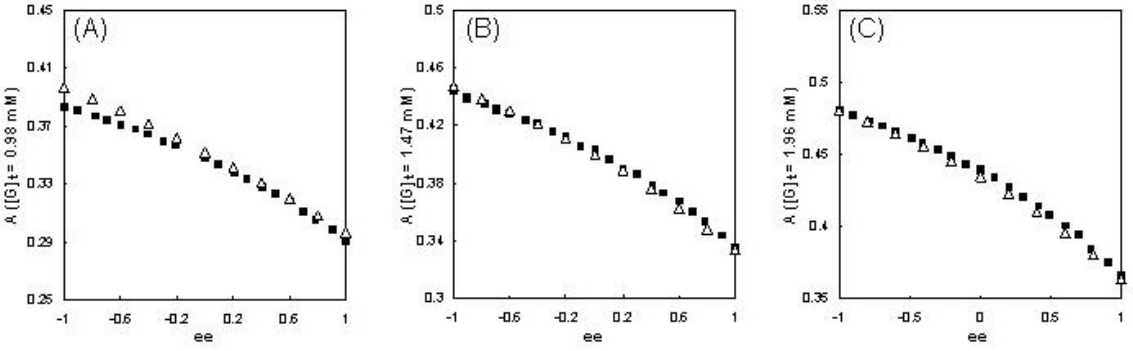

Figure 3.3: Filled squares: absorbance changes at 536 nm of the dual-chamber ensemble upon increasing *ee* of D-PL. (**A**) $[G]_t$ = 0.98 mM; (**B**) $[G]_t$ = 1.47 mM; (C) $[G]_t$ =1.96 mM. Empty triangles: data calculated from Eq. 3.2 by the computer program Mathematica 5.1

3.2 RESULTS AND DISCUSSION:

3.2.1 Artificial Neural Network Analysis

The second approach relies on an analysis using artificial neural networks (ANNs). An ANN is an information processing paradigm that simulates the way biological nervous systems, in particular the brain, process information. The computer programs that implement the ANN paradigm are able to solve problems by learning from

analogous existing examples. The theoretical foundation and the applications of ANNs in chemistry, mainly in the pattern recognition area, have been extensively reviewed.[22, 23]

The chiral analysis problem in this study can be solved with an ANN program. The general procedure included 3 steps. First, the absorbance data obtained with known $[G]_t$ and *ee* values are fed into the program. A network is subsequently generated which accurately models the unknown underlying function that relates the input variables to the output variables. Second, a successful training session establishes a hidden function in the form of $\{[G]_t, ee\} = f(A_{\lambda 1}, A_{\lambda 2}, A_{\lambda 3}, \text{etc.})$ within the network. Third, absorbance data from test samples are input into the network. After the new data are processed by the hidden function, the network will generate outputs, which in this case are the values of $[G]_t$ and *ee*.

As a simple demonstration, the absorbance at 387 nm and 536 nm (A_{387}, A_{536}) from the three *ee* titrations and corresponding $[G]_t$ and %*R* (the percentage of *R*(D)-PL in the sample) values, excluding the 11 data points in **Table 3.1**, were used as training sets. A_{387} and A_{536} were considered as inputs, and $[G]_t$ and %*R* were outputs. Thus, a total of 65 cases were imported into the STATISTICA Neural Networks 4.0 program,[24] 10 of these cases were randomly selected by the program for the cross-verification of the networks that are generated. In principle, a large number of networks are tested and the one with the best cross-verification error is selected. STATISTICA Neural Network has an embedded Intelligent Problem Solver (IPS) function, which is used to automatically create a network set that contains neural networks suitable for the designated problem. From the network set a multi-layer perceptron (MLP) with 2 inputs was selected based upon both its performance rating and our experience with MLP type of neural networks (**Figure 3.4A**).[25, 26] The selected MLP was subsequently trained with the back-propagation algorithm. By then, the learning process of the MLP network was completed

and a hidden function with predictive power specifically tailored for our problem was established.

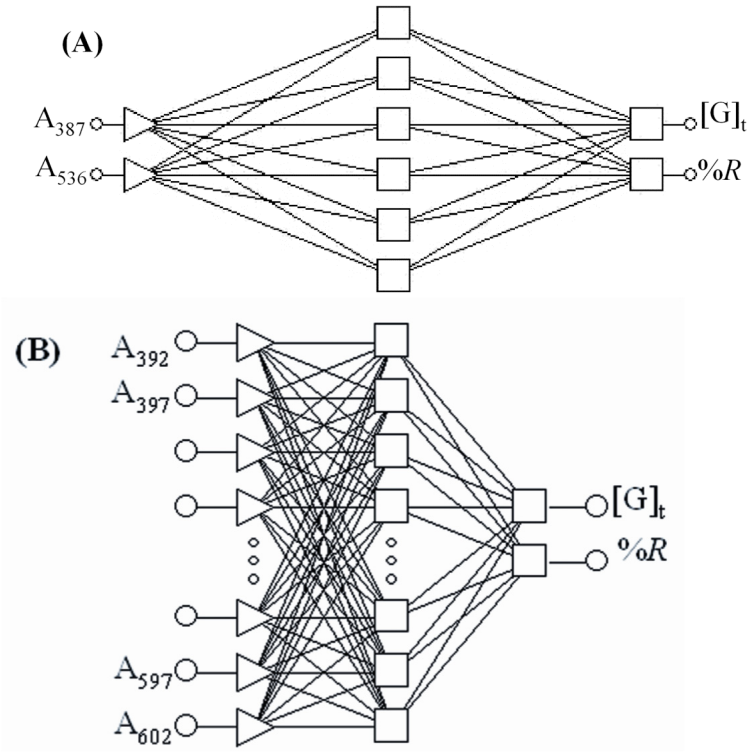

Figure 3.4: Structures of two MLP networks in this study. Both have three layers: (**A**) the input layer at left has 2 variables – A_{387} and A_{536}. The input layer is connected to, and processed by a hidden layer in the middle with 6 nodes. Two variables, $[G]_t$ and %R, are generated to the output layer at right; (**B**) the input layer has 43 variables from A_{392} to A_{602} with 5 nm intervals. The hidden layer has 11 nodes.

For unknown sample analysis, the trained network was switched to run "one-off" cases. The "one-off" case is a function of the ANN program that takes a new input to generate an output by the trained network. Two absorbance values, A_{387} and A_{536}, of the designated 11 unknown data were fed to the network to generate the output $[G]_t$ and %R.

The predicted $[G]_t$ and %*R* values for the 11 unknown samples are shown in **Table 3.2** with average absolute errors of ±0.45% and ±1.1%, respectively.

Table 3.2: Determination of concentration and %*R* of PL samples with a trained MLP network (**Figure 3.4B**).

No.	$[G]_t$/mM (actual)	$[G]_t$/mM (ANN)	%*R* (actual)	%*R* (ANN)
1	0.98	0.98	5	4
2	0.98	0.98	25	24
3	0.98	0.99	50	48
4	0.98	0.98	95	94
5	1.47	1.47	0.0	-2.0
6	1.47	1.47	35	35
7	1.47	1.47	75	75
8	1.96	1.96	15	14
9	1.96	1.93	45	43
10	1.96	1.96	85	84
11	1.96	1.95	55	54

However, strictly speaking, these unknown values are not technically unknown because they were obtained in the same set of titration experiments from which the training sets of data were generated. The trained MLP network should be able to predict $[G]_t$ and *ee* from independently prepared and measured samples, which would be true unknowns. Thus, to test the capability of the ANN-based model to respond to true unknown samples, we examined samples never used in network development. A new

MLP network was generated with only two *ee* training sets at two different $[G]_t$ values (0.98 mM and 1.96 mM). In this analysis, one independently determined *ee* data set with $[G]_t$ at 1.47 mM was used to represent unknown samples. The new network was constructed with absorbance values at 43 wavelengths, instead of 2, as inputs in order to enhance the quality of the trained network. Again, a network set was successfully generated by IPS, consisting of 34 training sets and 7 validation sets. The network with the best performance (structure in **Figure 3.4B**) was trained with back-propagation algorithm. The $[G]_t$ and %*R* of 5 samples from the data set with actual $[G]_t$ at 1.47 mM were predicted by the trained network within 11.4% and 4.2% average absolute errors, respectively, of the actual values (**Table 3.3**). Considering that the testing samples were prepared and data were collected under entirely independent conditions from those of the training set data, it is amazing that the ANN gained such predicting ability through learning. The relatively low accuracy in $[G]_t$ determination (determined average at 1.58 mM vs. the actual value of 1.47 mM) should be attributed to the lack of $[G]_t$ variations in the training set data. The accuracy will certainly increase should a larger body of training set data be used. Admittedly, the ANN study reported herein is a proof-of-principle demonstration of the promise as well as limitation of analytical protocols based on ANNs. In a practical implementation, 10 times more data than used in this study points would be needed to train the networks.

Table 3.3: Determination of concentration and %*R* of PL samples with a trained MLP network (**Figure 3.4B**). $[G]_t$ (actual) = 1.47 mM.

%*R* (actual)	20	45	75	50	100
%*R* (determined)	27	50	79	52	103
$[G]_t$/mM (determined)	1.62	1.58	1.58	1.57	1.57

The advantages of ANNs over the traditional spectroscopic approach based upon the analysis of solution thermodynamics and Beer's Law in determining concentration and %*R* (or *ee*) of a chiral sample are obvious. What is required for implementing an ANN analysis is simply a large body of existing data (training sets) that represent the behavior of the system in interest (the spectroscopic modulation with regard to $[G]_t$ and %*R*), and a computer program (STATISTICA Neural Networks) that can model and predict behavior of the system that is not included in the existing data. Thus, the laborious determination of thermodynamic and optical parameters is not needed, and the indicator choice and wavelengths for analysis are not as restricted as in the isosbestic analysis. Furthermore, the ANN approach described in this study can be extended to other mixture analysis amenable to indicator-displacement assays. However, one drawback of ANN analysis is that a large body of existing data has to be available. ANNs are at their best when they are trained with rich information for the system under study.

3.3 CONCLUSION

In summary, we developed two different approaches for determination of concentration $[G]_t$ and *ee* of a chiral sample with a single spectroscopic measurement. The analysis of PL samples by eIDAs based on a chiral boronic acid host was used to demonstrate the described methods. The experimental setup for both methods relies on a cuvette with two separate chambers. In practice, two independent IDAs, one of which used a chiral host, were carried out simultaneously with the addition of identical guest samples in both chambers. In the first approach, an isosbestic analysis led to the establishment of two independent equations for solving two desired variables $[G]_t$ and *ee*. In the second approach, an artificial neural network (ANN) analysis enabled by the computer program STATISTICA was used for determining $[G]_t$ and %*R*. Both approaches achieved satisfactory accuracy. The implementation of either approach will be determined by particular applications and/or practitioner's preferences. Both approaches are naturally extendable to high-throughput formats, potentially by using designer multi-well absorbance plate readers that simulate double-chamber cuvettes.

3.4 EXPERIMENTAL

3.4.1 Typical Procedure for Double-Chamber Cuvette *ee* Titration

Four ensemble solutions (A-D) were prepared. Their respective compositions are: solution A – ML (202 μM), 1 (307 μM), D-PL (0.982 mM); solution B – ML (202 μM), 1 (307 μM), L-PL (0.982 mM); solution C – AC (284 μM), (*S,S*)-**3.2** (400 μM), D-PL (0.982 mM); solution D – AC (284 μM), (*S,S*)-**3.2** (400 μM), L-PL (0.982 mM). Solutions B and D (500 μL each) were added into the left and right chambers of the cuvette respectively. Solutions A and C were incrementally titrated into the left and right

chambers, respectively, until 500 μL each of A and C were added, where the *ee* of PL reached 0 in both chambers. The absorption spectrum was recorded 3 minutes after each addition to allow the system to reach equilibrium. The titration was repeated with solutions B and D adding into solutions A and C in their respective chambers to complete the *ee* range from -1 to 1.

3.4.2 ANN Training Procedure

Among 65 data in the training set, 55 of which were designated as training data by the STATISTICA program, the rest 10 data were designated as verification data. The IPS was requested to search for MLP networks with 3 layers, input, hidden, and output, respectively. One search sequence was designed to last for 2 minutes, during which the number of units in the hidden layer was varied until the best network was found. The found network, which has 6 hidden layer units, was trained with back-propagation algorithm until the errors of training and verification data converged at ~1%.

Additional Information: The work presented in this chapter is available online at http:// interscience.wiley.com.[21]

3.5 REFERENCES FOR CHAPTER 3

1. Reetz, M. T., Combinatorial and Evolution-Based Methods in the Creation of Enantioselective Catalysts. *Angew. Chem. Int. Ed.* **2001,** 40, 284-310.

2. Wahler, D.; Reymond, J.-L., Novel Methods for Biocatalyst Screening. *Curr. Opin. Chem. Biol.* **2001,** 5, 152-158.

3. Tsukamoto, M.; Kagan, H. B., Recent Advances in the Measurement of Enantiomeric Excesses. *Adv. Synth. Catal.* **2002,** 344, (5), 453-463.

4. Finn, M. G., Emerging Methods for the Rapid Determination of Enantiomeric Excess. *Chirality* **2002,** 14, 534-540.

5. Welch, C. J.; Szczerba, T.; Perrin, S. R., Some recent high-performance liquid chromatography separations of the enantiomers of pharmaceuticals and other compounds using the Whelk-O 1 chiral stationary phase. *J. Chromatogr. A* **1997,** 758, 93-98.

6. Welch, C. J.; Grau, B.; Moore, J.; Mathre, D. J., A High-Throughput Screening Protocol for Fast Evaluation of Enantioselective Catalysts. *J. Org. Chem.* **2001,** 66, 6836-6837.

7. Welch, C. J.; Fleitz, F.; Antia, F.; Yehl, P.; Waters, R.; Ikemoto, N.; Amstrong, I., J. D.; Mathre, D. J., Chromatography as an Enabling Technology in Pharmaceutical Process Development: Expedited Multikilogram Preparation of a Candidate HIV Protease Inhibitor. *Org. Process Res. & Dev.* **2004,** 8, 186-191.

8. Sigman, M. S.; Jacobsen, E. N., Schiff Base Catalysts for the Asymmetric Strecker Reaction Identified and Optimized from Parallel Synthetic Libraries. *J. Am. Chem. Soc.* **1998,** 120, 4901-4902.

9. Wolf, C.; Hawes, P. A., A High-Throughput Screening Protocol for Fast Evaluation of Enantioselective Catalysts. *J. Org. Chem.* **2002,** 67, 2727-2729.

10. Reetz, M. T., New Methods for the High-Throughput Screening of Enantioselective Catalysts and Biocatalysts. *Angew. Chem. Int. Ed.* **2002,** 41, 1335-1338.

11. Zhu, L.; Anslyn, E. V., Facile Quantification of Enantiomeric Excess and Concentration with Indicator-Displacement Assays: An Example in the Analyses of α-Hydroxyacids. *J. Am. Chem. Soc.* **2004,** 126, (12), 3676-3677.

12. Zhu, L.; Zhong, Z.; Anslyn, E. V., Guidelines in Implementing Enantioselective Indicator-Displacement Assays for α-Hydroxycarboxylates and Diols. *J. Am. Chem. Soc.* **2005,** 127, 4260-4269.

13. Folmer-Andersen, J. F.; Lynch, V. M.; Anslyn, E. V., Colorimetric Enantiodiscrimination of α-Amino Acids in Protic Media. *J. Am. Chem. Soc.* **2005,** 127, 7986-7987.

14. Taran, F.; Gauchet, C.; Mohar, B.; Meunier, S.; Valleix, A.; Renard, P. Y.; Crèminon, C.; Grassi, J.; Wagner, A.; Mioskowski, C., High-Throughput Screening of Enantioselective Catalysts by Immunoassay. *Angew. Chem. Int. Ed.* **2002,** 41, (1), 124-127.

15. Chen, Y.; Shimizu, K. D., Measurement of Enantiomeric Excess Using Molecularly Imprinted Polymers. *Org. Lett.* **2002,** 4, (17), 2937-2940.

16. Li, Z.; Bütikofer, L.; Witholt, B., High-Throughput Measurement of the Enantiomeric Excess of Chiral Alcohols by Using Two Enzymes. *Angew. Chem. Int. Ed.* **2004,** 43, 1698-1702.

17. Dey, S.; Karukurichi, K. R.; Shen, W.; Berkowitz, D. B., Double-Cuvette ISES: In Situ Estimation of Enantioselectivity and Relative Rate for Catalyst Screening. *J. Am. Chem. Soc.* **2005,** 127, (24), 8610-8611.

18. Wiskur, S. L.; Aït-Haddou, H.; Lavigne, J. J.; Anslyn, E. V., Teaching Old Indicators New Tricks. *Acc. Chem. Res.* **2001,** 34, 963-972.

19. Starna Cells, I.

20. http://www.wolfram.com.

21. Zhu, L.; Shabbir, S. H.; Anslyn, E. V., Two methods for the determination of enantiomeric excess and concentration of a chiral sample with a single spectroscopic measurement. *Chem. Eur. J.* **2007,** 13, (1), 99-104.

22. Cirovic, D. A., Feed-Forward Artificial Neural Networks: Applications to Spectroscopy. *Trends Anal. Chem.* **1997,** 16, 148-155.

23. Burns, J. A.; Whitesides, G. M., Feed-Forward Neural Networks in Chemistry: Mathematical Systems for Classification and Pattern Recognition. *Chem. Rev.* **1993,** 93, 2583-2601.

24. StatSoft, I.

25. Wiskur, S. L.; Floriano, P. N.; Anslyn, E. V.; McDevitt, J. T., A Multicomponent Sensing Ensemble in Solution: Differentiation between Structurally Similar Analytes. *Angew. Chem. Int. Ed.* **2003,** 42, 2070-2072.

26. McCleskey, S. C.; Floriano, P. N.; Wiskur, S. L.; Anslyn, E. V.; McDevitt, J. T., Citrate and Calcium Determination in Flavored Vodkas Using Artificial Neural Networks. *Tetrahedron* **2003,** 59, (50), 10089-10092.

Chapter 4: A General Protocol for Creating High-throughput Screening Methods for Reaction Yield and Enantiomeric Excess Applied to Hydrobenzoin

4.1 High-Throughput Screening Protocol

The unique role of chiral bioactive therapeutic substances is a source of inspiration for the design of efficient asymmetric catalytic processes.[1] To this end, combinatorial synthesis, and stockpiles of chiral ligands, can afford large libraries of molecules as a potential source of new and improved catalysts.[2, 3] Traditionally, the search for asymmetric catalysts has relied on iterative approaches wherein a single catalyst is designed, synthesized, tested and optimized. This cycle is repeated until a catalytically active system is obtained with the desired level of enantioselectivity. Considerable time and effort is spent in the screening of catalysts and experimental conditions, particularly with regards to the *ee* of the enantioselective reactions. In contrast, a high-throughput screening strategy would enable one to rapidly identify catalytically active systems, thus allowing for a much broader range of catalyst candidates and experimental conditions to be evaluated.[4, 5]

In 1997, Reetz and coworkers introduced high-throughput screening (HTS) of reaction *ee* values.[6] Following their pioneering work, methods such as chiral HPLC,[7] liquid crystals,[8, 9] IR-thermography,[10, 11] circular dichroism,[12, 13] capillary electrophoresis,[14] fluorescence,[15, 16] mass spectrometry,[17, 18] chemosensing,[19] competitive immunoassay,[20] NMR,[21] and enzymatic methods have been employed.[22-27] However, most of these methods require prior derivatization of the analyte or require expensive instrumentation, and many are still quite slow. Herein, we report a colorimetric strategy

based on indicator displacement assays (IDAs) for creating HTS protocols that can be used for the rapid determination of molecular chirality as well as the yield of a reaction.

An IDA rely upon a colorimetric or fluorescent indicator that changes optical or electrochemical properties when bound to a host relative to being free in the bulk medium.[28] The most commonly used indicators are pH indicators.[29] The competition between an indicator and the guest of interest for the binding site of the host allows the determination of total guest (or analyte) concentration $[G]_t$ (**Scheme 4.1** (**Eq. 4.1**)). An IDA both eliminates the need to incorporate the chromophore or fluorophore into the structure of the host, thus simplifying the synthesis of the host molecule, and allows one to tune the sensitivity of the assay due to the ability to change the identity and concentration of the indicator.[30] Our research group, and others, have developed multicomponent optical sensors that function on the basis of an indicator displacement assay.[31-36]

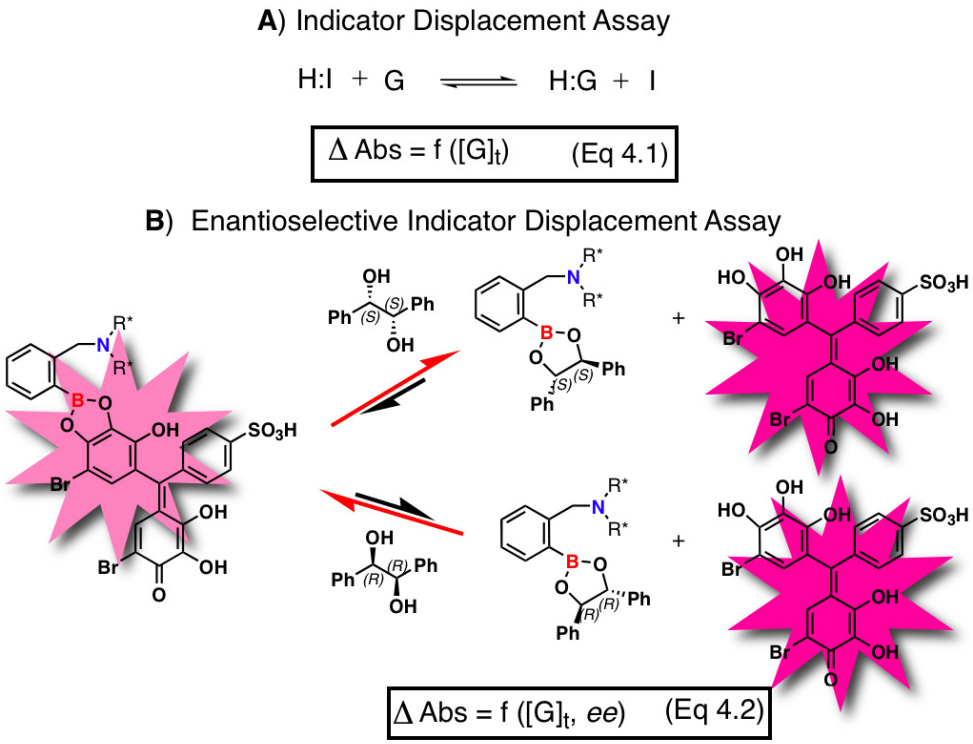

Scheme 4.1: **A**) Indicator displacement assay (IDA) **B**) Enantioselective indicator displacement assay (eIDA) using a chiral host for chiral diols with bromopyrogallol red (BPG) as the indicator, H: host, I: indicator, G: guest/analyte, Δ Abs: absorbance change, $[G]_t$: total guest concentration, *ee*: enantiomeric excess, *: indicates chiral center.

We recently expanded the scope of indicator displacement assays to enantioselective indicator displacement assays (eIDA's) by incorporating chirality into the host, which allows us to quantify *ee* in addition to the concentration of a chiral analyte (**Scheme 4.1**, (appropriate to the work described herein for hydrobenzoin in **Eq 4.2**).[37-43] This approach relies on the energetic difference of the two diastereomeric complexes that are formed when a chiral host interacts with the two enantiomers of the guest molecule. In our earlier work, chiral and achiral boronic acid hosts were used to determine *ee* and total guest concentration $[G]_t$ for chiral α-hydroxycarboxylic acids.[40]

We have also shown that artificial neural networks (ANNs) can be used to analyze the data obtained from cuvettes.[42]

Herein, we describe a general approach to using eIDA's for HTS of *ee* and reaction yield $[G]_t$ using ANN as the data analysis tool. Artificial neural networks (ANNs) are computational techniques that perform multifactorial analysis. ANN has been utilized to solve a wide array of problems ranging from character and voice recognition,[44] to modeling and data mapping.[45] These unique abilities are just beginning to be exploited by organic chemists. [46]

As described in the next section, the approach involves using a library of chiral receptors for the target analytes along with a series of three 96-well plates. The first two plates create the methodology, while a third plate contains unknowns for analysis. In principle there could actually be as many of these plates as are required to analyze potentially hundreds to thousands of samples. To show that the approach leads to a method that is accurate, sixteen samples of hydrobenzoin with unknown $[G]_t$ and *ee* values were determined in less then ten minutes with an average absolute error of ± 0.17 mM and 3.5% error in $[G]_t$ and *ee* values, respectively. Next, to show that the technique can be applied to catalyst discovery, the method developed for analyzing hydrobenzoin samples was applied to the analysis of the established Sharpless asymmetric dihydroxylation reactions. To our satisfaction the best cinchona alkaloid ligand known in literature was correctly identified.[47-49]

4.2 RESULTS AND DISCUSSION

4.2.1 Synthesis

As described above, one criteria we set for ourselves is an easy synthesis of the hosts. Thus, a series of boronic acid hosts (**Scheme 4.2A**) were synthesized by reductive amination of 2-formylphenylboronic acid with chiral amines which were commercially available (**Scheme 4.2B**). The general one pot procedure described in our previous publication[37] was used to make the achiral and chiral hosts (several of which are new), with the exception of host (*S*,*S*)-**4.5** (**Scheme 4.2C**). Host (*S*,*S*)-**4.5** was synthesized in two steps. The imine was first isolated by heating 2-acetylphenylboronic acid with the α-methylbenzylamine in toluene using a Dean Stark trap. The isolated imine was then reduced with $NaBH_4$ in methanol at 0°C (lower temperatures were employed to achieve asymmetric induction). The product was isolated in a 70% yield with a diastereomeric ratio (dr) of 1: 4 using alumina flash chromatography.

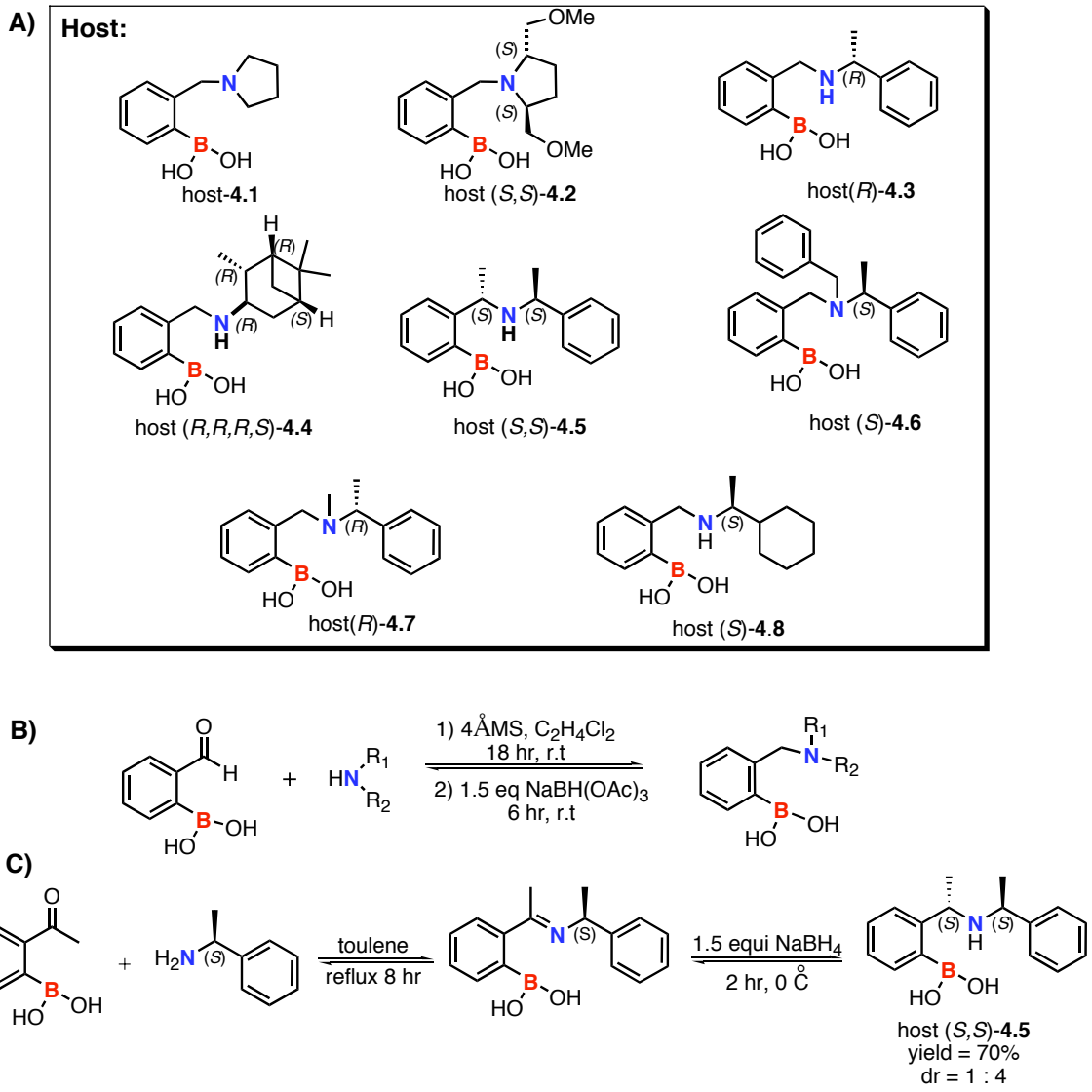

Scheme 4.2: **A**) Structures of the library of boronic acid hosts **B**) General reductive amination to synthesize chiral boronic acids **C**) Synthesis of host (*S*,*S*)-**4.5**.

4.2.2 Design Criteria

In this section we lay forth our vision for a general approach for creating HTS assays for *ee* and $[G]_t$, while the remainder of this paper describes our first successful implementation of the approach. We deemed that certain basic criteria must be met in

order for the approach to be adopted by others. First, the receptors must be easily synthesized, optimally in only one or two simple steps from commercially available and inexpensive starting materials (preferably in both enantiomeric forms). Second, the optical signaling should be simple and adaptable to screening and optimization without involving additional synthesis. This criteria is the strength of an IDA, which is modular and thereby allows one to mix and match commercially available pH indicators with the receptors to rapidly reveal the most accurate assays. Third, a general platform for HTS that is inexpensive, fast, and allows for the generation of large data sets for both training an ANN and analyzing unknowns is needed. To achieve this criteria, we used a 96-well plate (microtiter plate) analysis system.

Data collection in a 96-well plate format is significantly more rapid than in a standard bench-top UV-vis spectrophotometer. For example, after creation of the protocol (steps 1-3 below), a plate is loaded with host, indicator, buffer, and analyte solution using a microplate pipetting robotic system in approximately 10 minutes. A full absorption spectrum for each well is generated in approximately 30 minutes. The Absorption data is ported into a computer containing a trained ANN, resulting in essentially instantaneous output of the *ee* and $[G]_t$ values, making for a projected overall analysis time of around 40 minutes for 96 unknowns.

The creation of our overall protocol starts with the synthesis, characterization, and purification, of a series of chiral receptors for the chiral function group of interest. A small library of chiral receptors targeted to the analyte class of interest is created because it is likely that each and every new chiral analyte will not be best enantioselectively discriminated by a single chiral receptor. Therefore, we anticipate that it will be advantageous to screen each new analyte with a series of receptors to reveal the receptor most enantioselective for that new analyte. One strategy for creating a host-guest based

enantiomeric discrimination protocol would be to target highly enantioselective receptors. Yet, this has historically proven to be challenging, and often requires extensive synthesis in an iterative approach that optimizes a host's enantioselectivity.

Optimizing the host is not our approach. Rather, we aim to purchase our enantioselectivity in the form of simple chiral building blocks that can in one or two steps be incorporated into the receptors. Of course, this limits the potential enantioselectivity, but it does make the protocols more amenable to adoption by other researchers. To compensate for the limitation that we have set for ourselves, we use indicators and host combinations in our displacement assays that have large optical differences at a particular wavelength for enantiomeric analytes, thereby allowing us to make accurate assays, sometimes with even quite poor enantiomeric discrimination.

Once the chiral receptors are in-hand, the following protocol is followed:

Using traditional UV-vis titrations and standard binding isotherms, the proper concentrations for combining the receptors and indicators is determined as preparatory work required prior to screening for enantioselectivity.

The receptors and indicators are then screened in a 96-well plate to reveal the best indicator/receptor combination for reporting the *ee* of a chiral target. We call this the "screening plate" step.

Once the optimal receptor/indicator combination(s) are revealed, optical data for different concentrations and *ee* values of the analytes is collected in a 96-well plate format to train an ANN. We call this the "training plate" step.

Lastly, unknowns from reactions that were aimed at asymmetric induction or optimization of *ee* values are robotically loaded into 96-well plates for analysis. We refer to this as the "analysis plate(s)" step.

The data from the analysis plates is ported into a computer, analyzed with the trained ANN, and the values of *ee* and $[G]_t$ for the unknowns are revealed.

Step 1 involves a reasonable amount of work, yet we plan to ultimately automate this step. But, importantly, because this step does not involve the analyte, but rather only the hosts and indicators, it does not need to be repeated when creating assays using the same respective hosts and indicators for any new analytes. Steps 2 and 3 are those that lead to an analyte specific assay, and would need to be repeated for each new analyte; yet they are quick because they involve a 96-well plate screen. After steps 2 and 3 are accomplished, steps 4 and 5 can be repeated over and over for the analysis of numerous 96-well plates containing unknowns. We now describe the implementation of this protocol to the analysis of the chiral analyte hydrobenzoin, using boronic acid-based chiral receptors.

4.2.3 Indicator Displacement Assay Optimization (Step 1)

Our first goal was to determine the optimal concentrations of the various boronic acid hosts and indicator to be used in the HTS- eIDA. In our previous experience we have found that the best enantioselectivity is achieved when a host is 75-90% saturated with an indicator.[40] To obtain this information 1:1 binding isotherms of the synthesized boronic acid hosts with various indicators were determined with traditional UV-vis titrations. We were also able to calculate association constant K_{HI} between the hosts and the indicators from these 1:1 binding isotherms (**Table 4.1**).

The 1:1 binding isotherm of all host with PV is shown in **Figure 4.2-4.45**. As shown in **Figure 4.2B-4.45** the ideal concentration of host with PV (~ 90% saturation of host with indicator) for eIDA was determined from its 1:1 binding isotherm. In a similar fashion to determine the optimum ratio of each host to each indicator, UV-vis titrations

were performed between the enantioselective hosts and the indicators: Alizarin (A), Alizarin complexone dihydrate (AC), Bromopyrogallol red (BPG), 4-Methylesculetin (ML), Pyrogallol red (PG), and Pyrocatechol violet (PV). Their 1:1 binding isotherms with each host were generated (**Figure 4.2-4.45**), and their association constants are listed in **Table 4.1**. The optimal ratio of the host/indicator (~90% of host saturated with the indicator) for an eIDA was determined from their respective 1:1 binding isotherms. Based on previous results, it was assumed that the binding constants of the two enantiomers of host-**4.2** were the same for all the indicators, and that they would show opposite enantioselectivity with the two enantiomers of hydrobenzoin.[40] Step 1 in our protocol is time consuming, but it never needs to be repeated again (unless for verification and/or for reproducibility). After succeeding in the determination of the optimal ratios of hosts and indicator, we turned to step 2 to reveal the proper host/indicator duo for the enantiodifferentiation of hydrobenzoin.

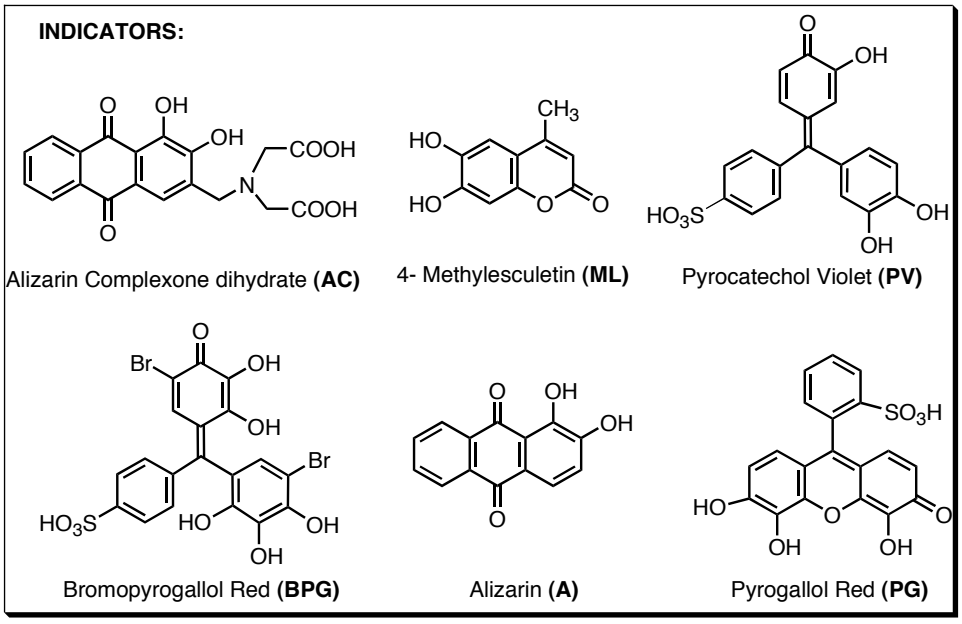

Figure 4.1: Structures of the selected catechol based indicators.

Table 4.1: Binding constant K_{HI} ($10^3 M^{-1}$) of boronic acid hosts with indicators. All titrations were carried out in 100% MeOH, 10 mM *para*-toluenesulfonic acid and Hunig's base buffer, pH =7.4. All measurements were taken at 25°C.

Indicators	**4.1**	(*S,S*)-**4.2**	(*R,R,R,S*)-**4.4**	(*R*)-**4.6**	(*S*)-**4.6**	(*R*)-**4.8**	(*S*)-**4.8**
A	19.0± 1.2	20.6± 2.5	32.7± 2.8	30.5± 3.3	27.8± 2.3	36.8± 2.6	35.7± 2.8
AC	132± 20	69.9± 4.3	128± 17	28.9± 4.1	22.8± 3.3	172± 55	192± 36
BPG	5.40± 0.1	108± 3.8	50.1± 4.9	210± 18	233± 27	34.8± 1.6	35.9± 1.9
ML	11.1± 0.1	24.1± 2.6	37.8± 1.5	118± 7.2	102± 5.4	53.6± 1.5	54.1± 1.5
PG	4.67± 0.2	24.7± 0.5	20.6± 1.3	188± 42	161± 25	11.3± 0.4	11.4± 0.4
PV	3.08± 0.01	53.2± 2.3	15.9± 0.4	27.8± 0.4	31.0± 0.9	14.8± 0.2	17.3± 0.3

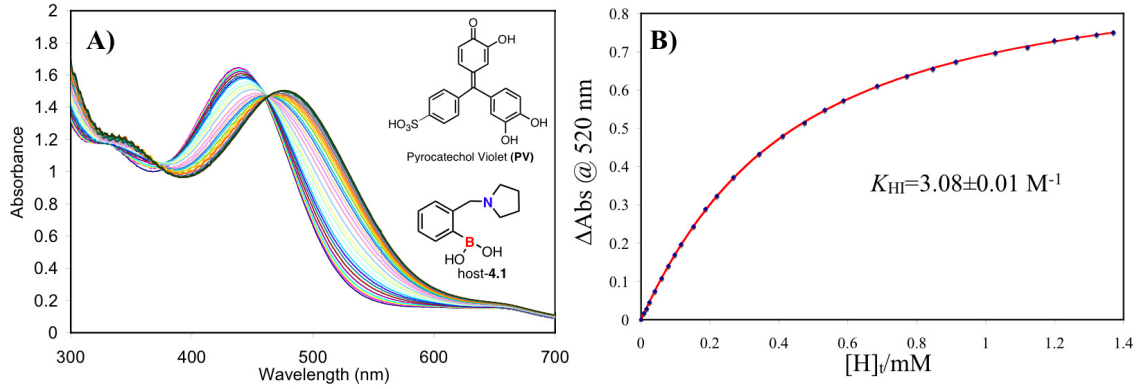

Figure 4.2: **A**) UV-visible titration of host-**4.1** with PV (150 μM) **B**) 1:1 binding isotherm (plot of the difference in absorbance at 520 nm with the addition of the host). All titrations were carried out in 100% MeOH, 10 mM *para*-toluenesulfonic acid and Hunig's base buffer, pH: 7.4, association constant K_{HI} (10^3 M^{-1}). All measurements were taken at 25°C. The solid line is the calculated curve resulting from iterative data fitting to a 1:1 binding isotherm.

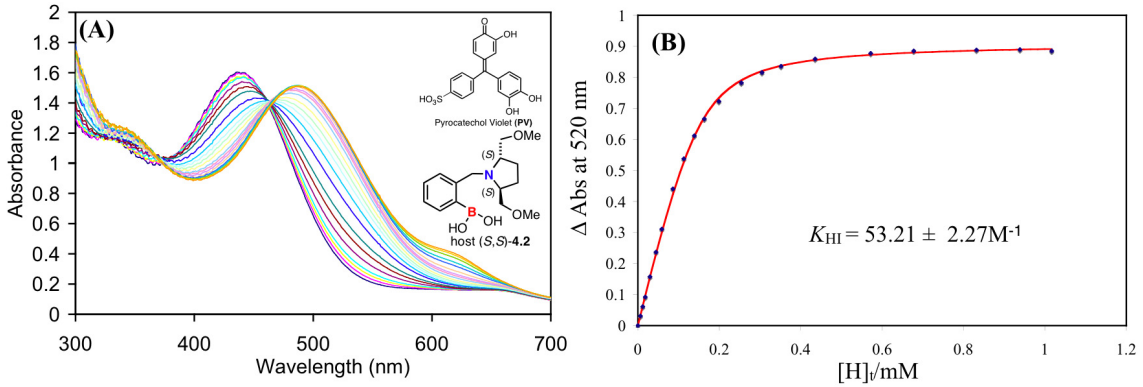

Figure 4.3: **A**) UV-visible titration of host (*S*,*S*)-**4.2** with PV (150 μM) **B**) 1:1 binding isotherm (plot of the difference in absorbance at 520 nm with the addition of the host). All titrations were carried out in 100% MeOH, 10 mM *para*-toluenesulfonic acid and Hunig's base buffer, pH: 7.4, association constant K_{HI} (10^3 M^{-1}). All measurements were taken at 25°C. The solid line is the calculated curve resulting from iterative data fitting to a 1:1 binding isotherm.

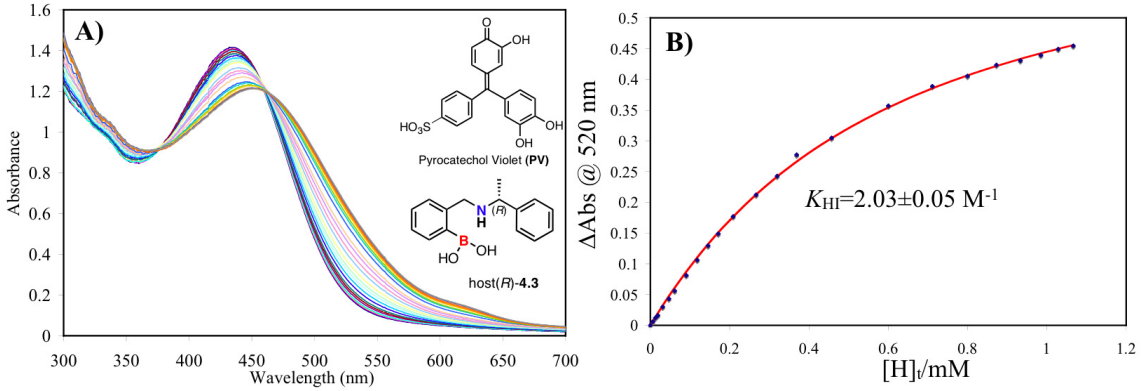

Figure 4.4: **A**) UV-visible titration of host (*R*)-**4.3** with PV (150 μM) **B**) 1:1 binding isotherm (plot of the difference in absorbance at 520 nm with the addition of the host). All titrations were carried out in 100% MeOH, 10 mM *para*-toluenesulfonic acid and Hunig's base buffer, pH: 7.4, association constant K_{HI} (10^3 M^{-1}). All measurements were taken at 25°C. The solid line is the calculated curve resulting from iterative data fitting to a 1:1 binding isotherm.

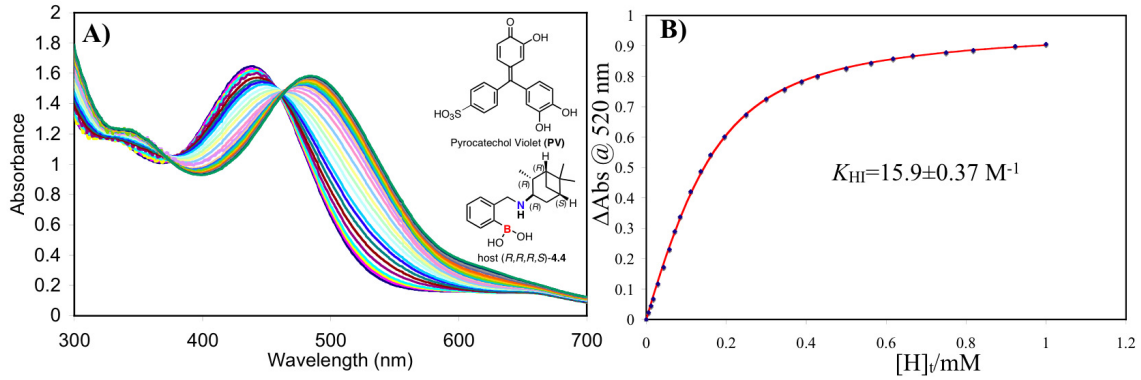

Figure 4.5: **A**) UV-visible titration of host (*R*,*R*,*R*,*S*)-**4.4** with PV (150 μM) **B**) 1:1 bindingisotherm (plot of the difference in absorbance at 520 nm with the addition of the host). All titrations were carried out in 100% MeOH, 10 mM *para*-toluenesulfonic acid and Hunig's base buffer, pH: 7.4, association constant K_{HI} (10^3 M^{-1}). All measurements were taken at 25°C. The solid line is the calculated curve resulting from iterative data fitting to a 1:1 binding isotherm.

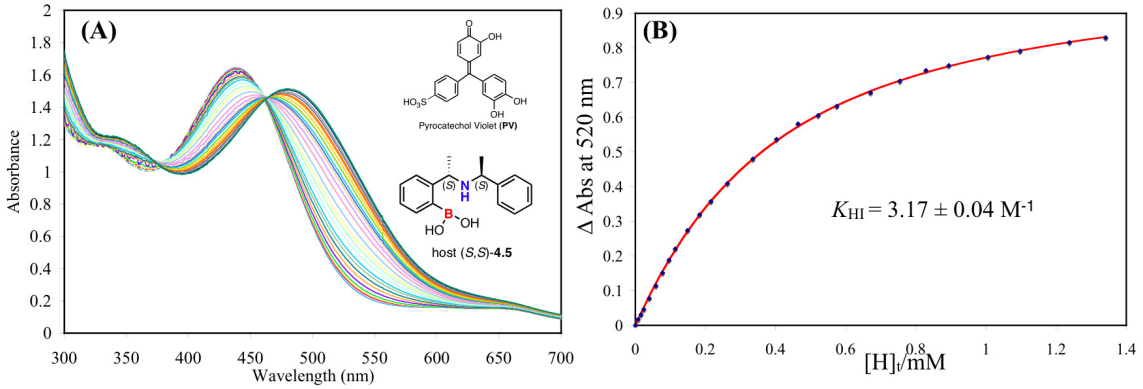

Figure 4.6: **A**) UV-visible titration of host (*S,S*)-**4.5** with PV (150 µM) **B**) 1:1 binding isotherm (plot of the difference in absorbance at 520 nm with the addition of the host). All titrations were carried out in 100% MeOH, 10 mM *para*-toluenesulfonic acid and Hunig's base buffer, pH: 7.4, association constant K_{HI} (10^3 M^{-1}). All measurements were taken at 25°C. The solid line is the calculated curve resulting from iterative data fitting to a 1:1 binding isotherm.

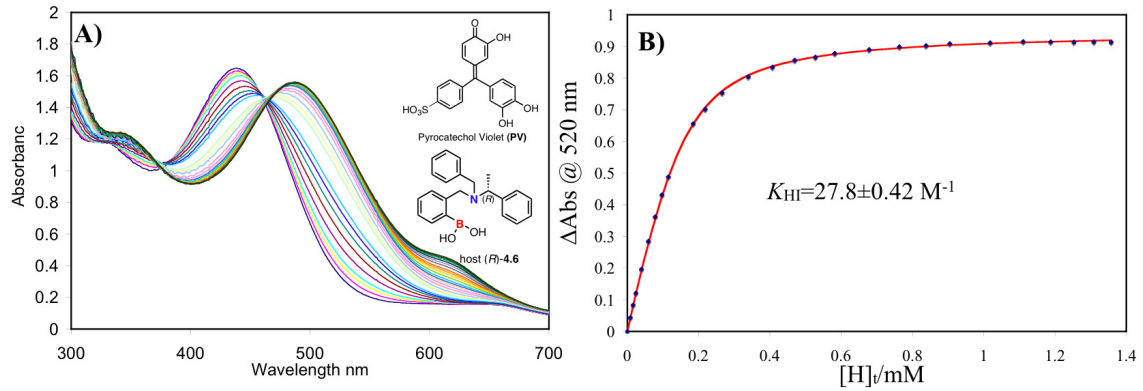

Figure 4.7: **A**) UV-visible titration of host (*R*)-**4.6** with PV (150 µM) **B**) 1:1 binding isotherm (plot of the difference in absorbance at 520 nm with the addition of the host). All titrations were carried out in 100% MeOH, 10 mM *para*-toluenesulfonic acid and Hunig's base buffer, pH: 7.4, association constant K_{HI} (10^3 M^{-1}). All measurements were taken at 25°C. The solid line is the calculated curve resulting from iterative data fitting to a 1:1 binding isotherm.

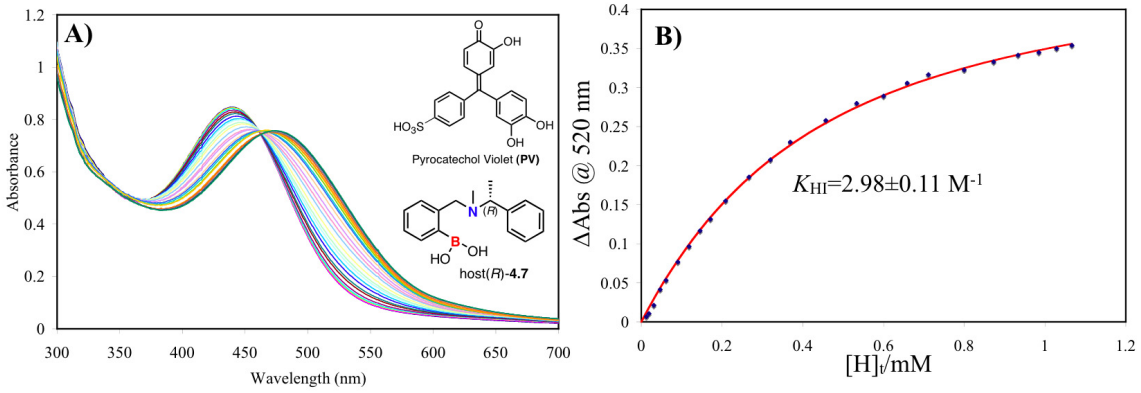

Figure 4.8: **A**) UV-visible titration of host (*R*)-**4.7** with PV (150 μM) **B**) 1:1 binding isotherm (plot of the difference in absorbance at 520 nm with the addition of the host). All titrations were carried out in 100% MeOH, 10 mM *para*-toluenesulfonic acid and Hunig's base buffer, pH: 7.4, association constant K_{HI} (10^3 M^{-1}). All measurements were taken at 25°C. The solid line is the calculated curve resulting from iterative data fitting to a 1:1 binding isotherm.

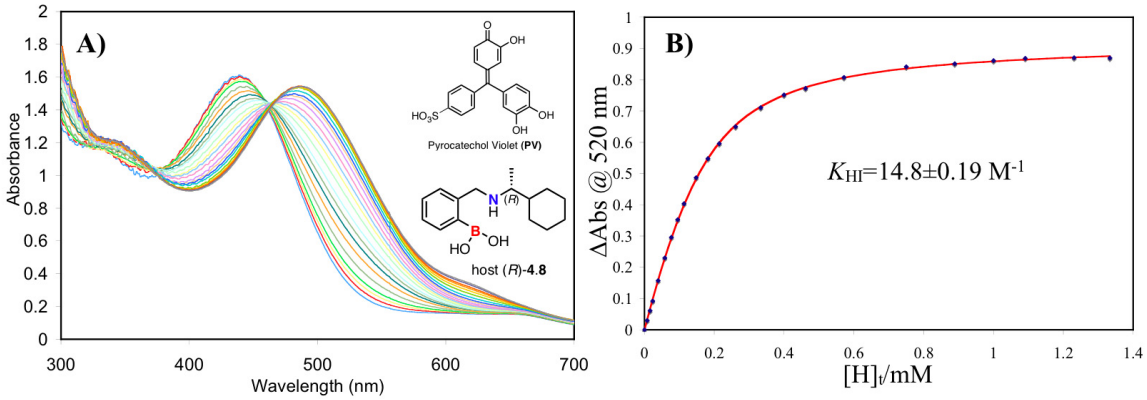

Figure 4.9: **A**) UV-visible titration of host (*R*)-**4.8** with PV (150 μM) **B**) 1:1 binding isotherm (plot of the difference in absorbance at 520 nm with the addition of the host). All titrations were carried out in 100% MeOH, 10 mM *para*-toluenesulfonic acid and Hunig's base buffer, pH: 7.4, association constant K_{HI} (10^3 M^{-1}). All measurements were taken at 25°C. The solid line is the calculated curve resulting from iterative data fitting to a 1:1 binding isotherm.

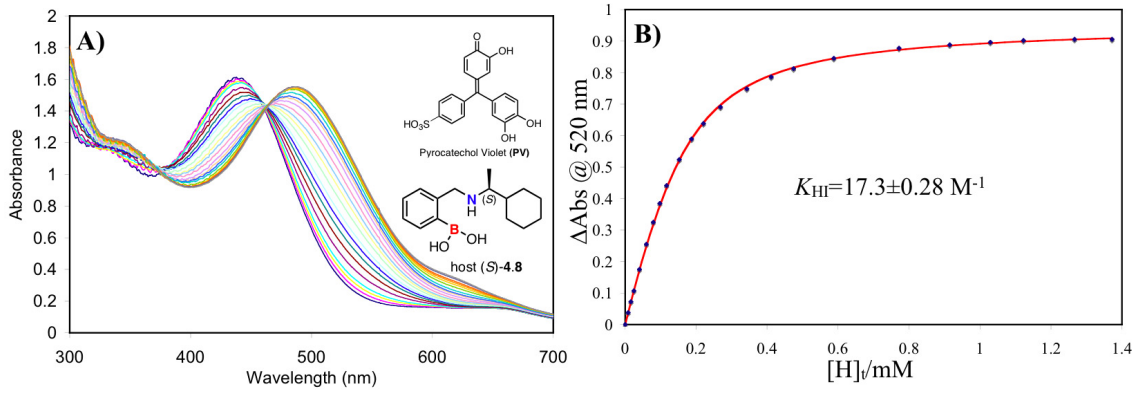

Figure 4.10: **A**) UV-visible titration of host (*S*)-**4.8** with PV (150 µM) **B**) 1:1 binding isotherm (plot of the difference in absorbance at 520 nm with the addition of the host). All titrations were carried out in 100% MeOH, 10 mM *para*-toluenesulfonic acid and Hunig's base buffer, pH: 7.4, association constant K_{HI} (10^3 M^{-1}). All measurements were taken at 25°C. The solid line is the calculated curve resulting from iterative data fitting to a 1:1 binding isotherm.

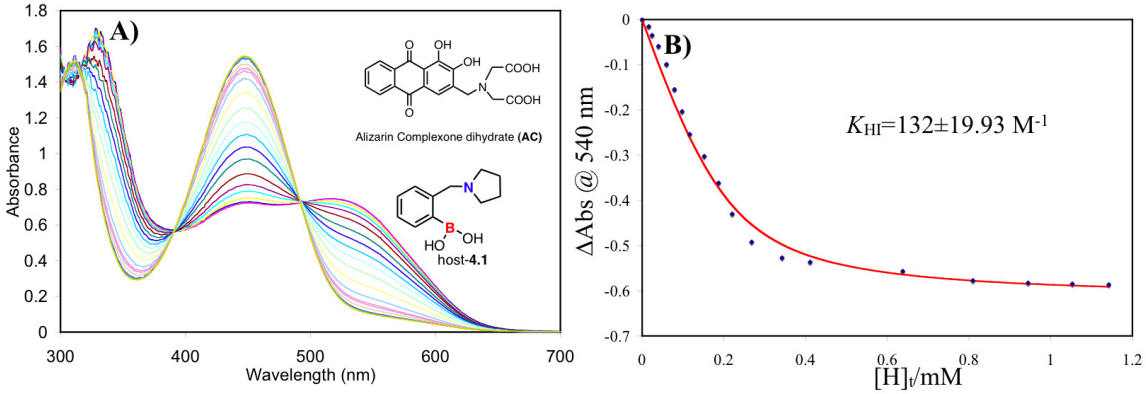

Figure 4.11: **A**) UV-visible titration of host-**4.1** with AC (200 µM) **B**) 1:1 binding isotherm (plot of the difference in absorbance at 540 nm with the addition of the host). All titrations were carried out in 100% MeOH, 10 mM *para*-toluenesulfonic acid and Hunig's base buffer, pH: 7.4, association constant K_{HI} (10^3 M^{-1}). All measurements were taken at 25°C. The solid line is the calculated curve resulting from iterative data fitting to a 1:1 binding isotherm.

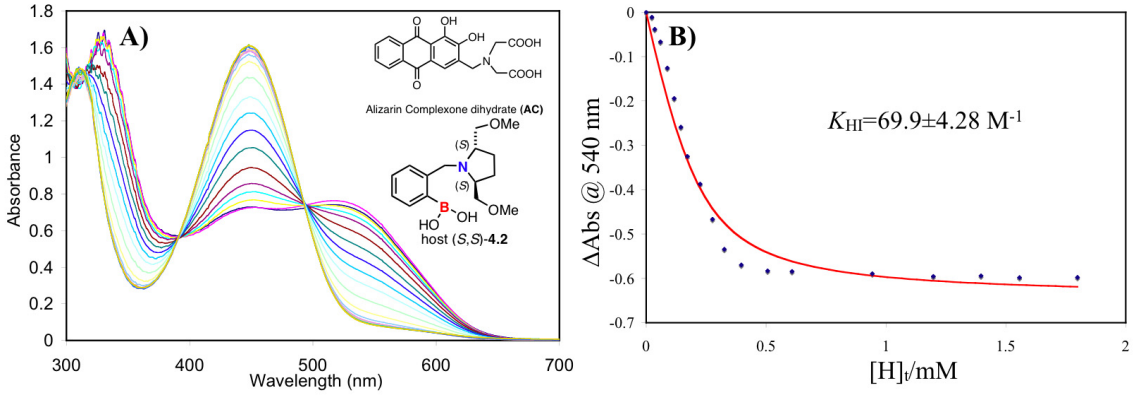

Figure 4.12: **A**) UV-visible titration of host (*S,S*)-**4.2** with AC (200 μM) **B**) 1:1 binding isotherm (plot of the difference in absorbance at 540 nm with the addition of the host). All titrations were carried out in 100% MeOH, 10 mM *para*-toluenesulfonic acid and Hunig's base buffer, pH: 7.4, association constant K_{HI} (10^3 M^{-1}). All measurements were taken at 25°C. The solid line is the calculated curve resulting from iterative data fitting to a 1:1 binding isotherm.

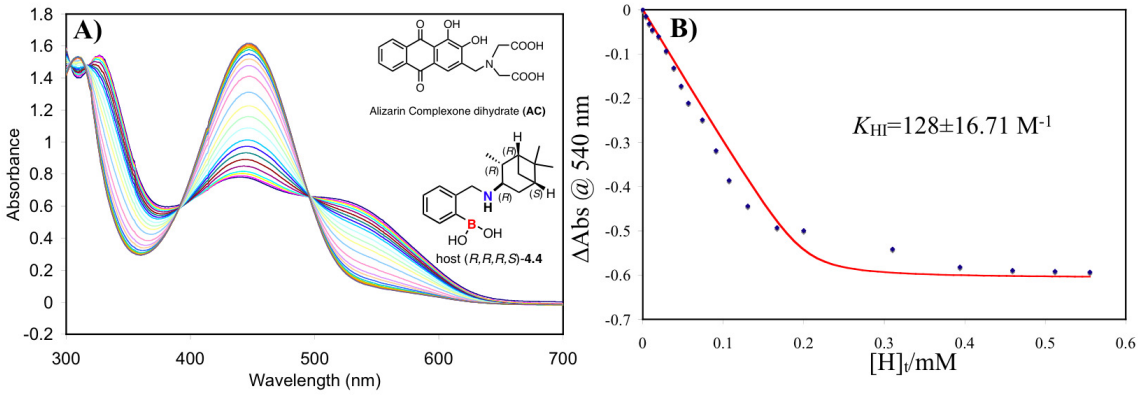

Figure 4.13: **A**) UV-visible titration of host (*R,R,R,S*)-**4.4** with AC (200 μM) **B**) 1:1 binding isotherm (plot of the difference in absorbance at 540 nm with the addition of the host). All titrations were carried out in 100% MeOH, 10 mM *para*-toluenesulfonic acid and Hunig's base buffer, pH: 7.4, association constant K_{HI} (10^3 M^{-1}). All measurements were taken at 25°C. The solid line is the calculated curve resulting from iterative data fitting to a 1:1 binding isotherm.

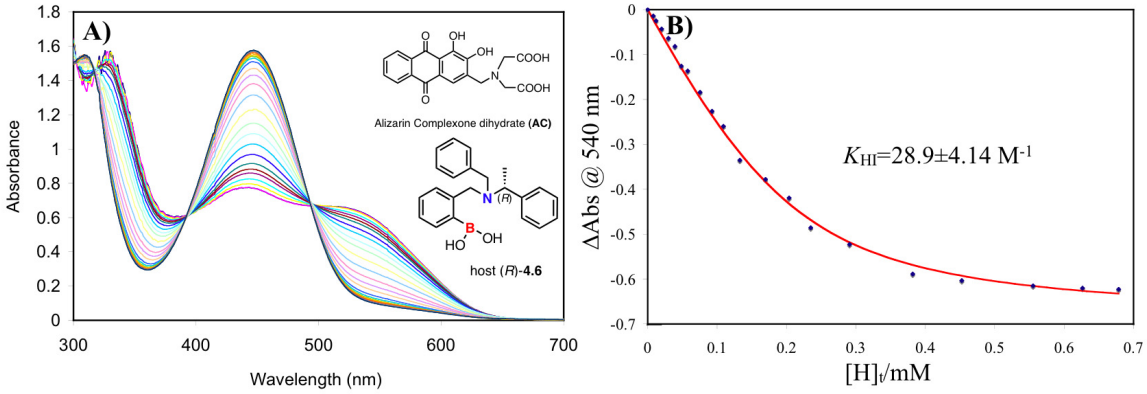

Figure 4.14: **A**) UV-visible titration of host (*R*)-**4.6** with AC (200 µM) **B**) 1:1 binding isotherm (plot of the difference in absorbance at 540 nm with the addition of the host). All titrations were carried out in 100% MeOH, 10 mM *para*-toluenesulfonic acid and Hunig's base buffer, pH: 7.4, association constant K_{HI} (10^3 M^{-1}). All measurements were taken at 25°C. The solid line is the calculated curve resulting from iterative data fitting to a 1:1 binding isotherm.

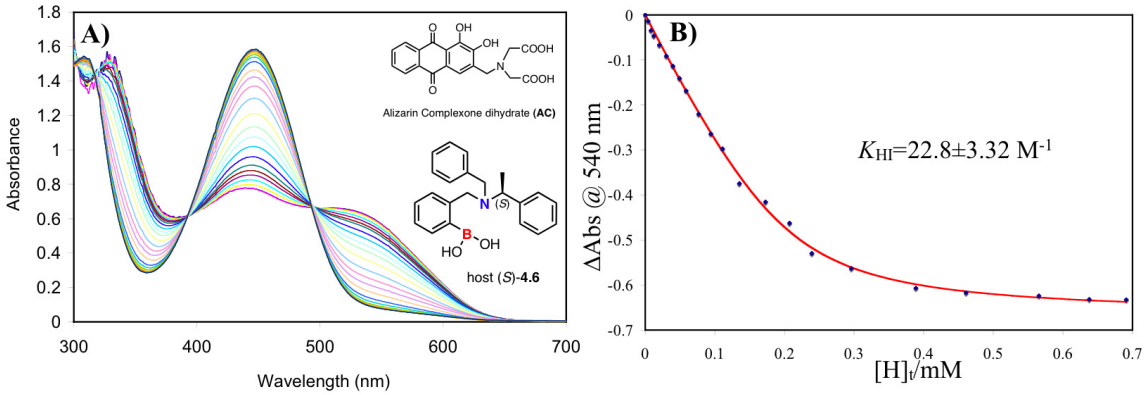

Figure 4.15: **A**) UV-visible titration of host (*S*)-**4.6** with AC (200 µM) **B**) 1:1 binding isotherm (plot of the difference in absorbance at 540 nm with the addition of the host). All titrations were carried out in 100% MeOH, 10 mM *para*-toluenesulfonic acid and Hunig's base buffer, pH: 7.4, association constant K_{HI} (10^3 M^{-1}). All measurements were taken at 25°C. The solid line is the calculated curve resulting from iterative data fitting to a 1:1 binding isotherm.

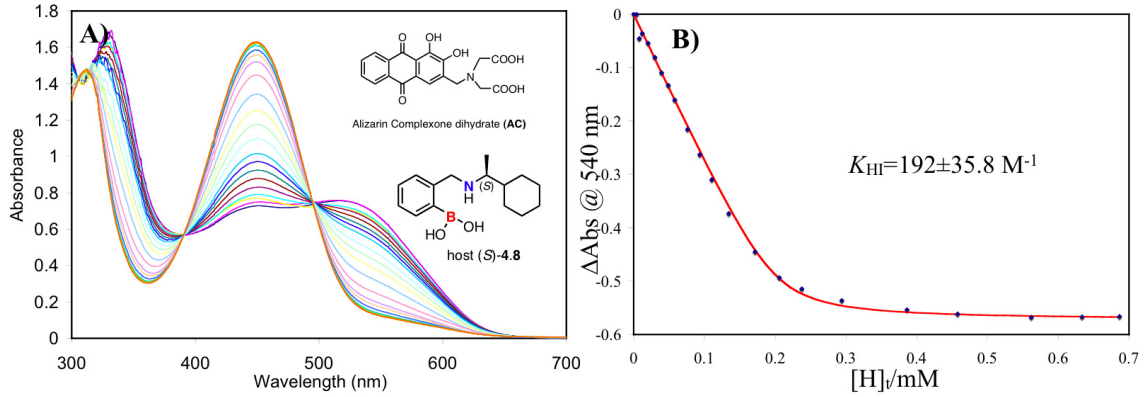

Figure 4.16: **A**) UV-visible titration of host (*S*)-**4.8** with AC (200 µM) **B**) 1:1 binding isotherm (plot of the difference in absorbance at 540 nm with the addition of the host). All titrations were carried out in 100% MeOH, 10 mM *para*-toluenesulfonic acid and Hunig's base buffer, pH: 7.4, association constant K_{HI} (10^3 M^{-1}). All measurements were taken at 25°C. The solid line is the calculated curve resulting from iterative data fitting to a 1:1 binding isotherm.

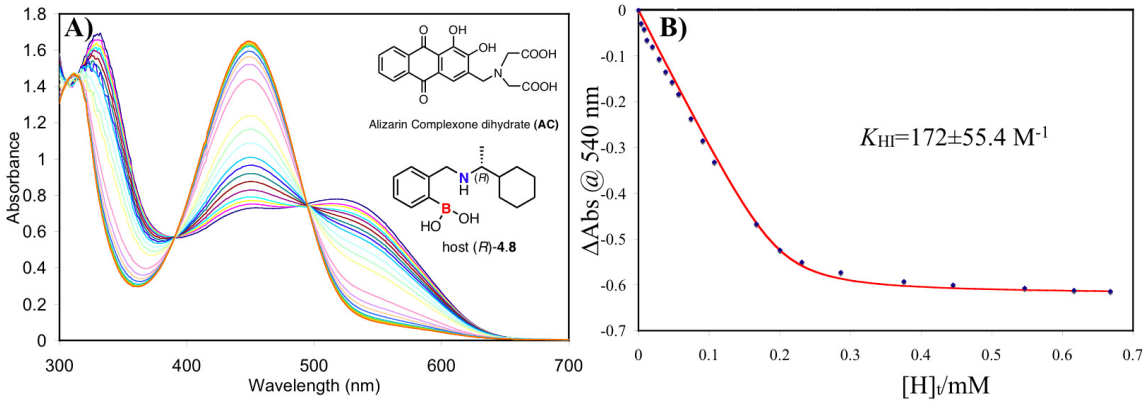

Figure 4.17: **A**) UV-visible titration of host (*R*)-**4.8** with AC (200 µM) **B**) 1:1 binding isotherm (plot of the difference in absorbance at 540 nm with the addition of the host). All titrations were carried out in 100% MeOH, 10 mM *para*-toluenesulfonic acid and Hunig's base buffer, pH: 7.4, association constant K_{HI} (10^3 M^{-1}). All measurements were taken at 25°C. The solid line is the calculated curve resulting from iterative data fitting to a 1:1 binding isotherm.

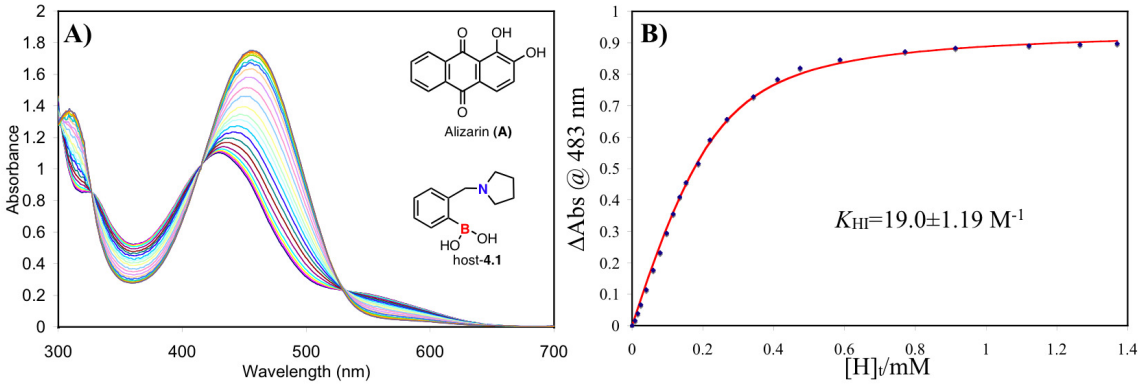

Figure 4.18: **A**) UV-visible titration of host-**4.1** with A (200 µM) **B**) 1:1 binding isotherm (plot of the difference in absorbance at 483 nm with the addition of the host). All titrations were carried out in 100% MeOH, 10 mM *para*-toluenesulfonic acid and Hunig's base buffer, pH: 7.4, association constant K_{HI} (10^3 M^{-1}). All measurements were taken at 25°C. The solid line is the calculated curve resulting from iterative data fitting to a 1:1 binding isotherm.

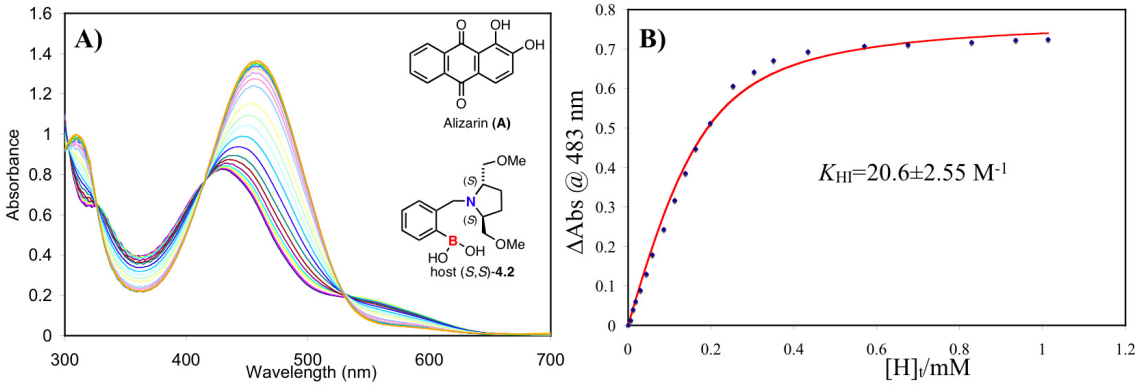

Figure 4.19: **A**) UV-visible titration of host (*S,S*)-**4.2** with A (200 µM) **B**) 1:1 binding isotherm (plot of the difference in absorbance at 483 nm with the addition of the host). All titrations were carried out in 100% MeOH, 10 mM *para*-toluenesulfonic acid and Hunig's base buffer, pH: 7.4, association constant K_{HI} (10^3 M^{-1}). All measurements were taken at 25°C. The solid line is the calculated curve resulting from iterative data fitting to a 1:1 binding isotherm.

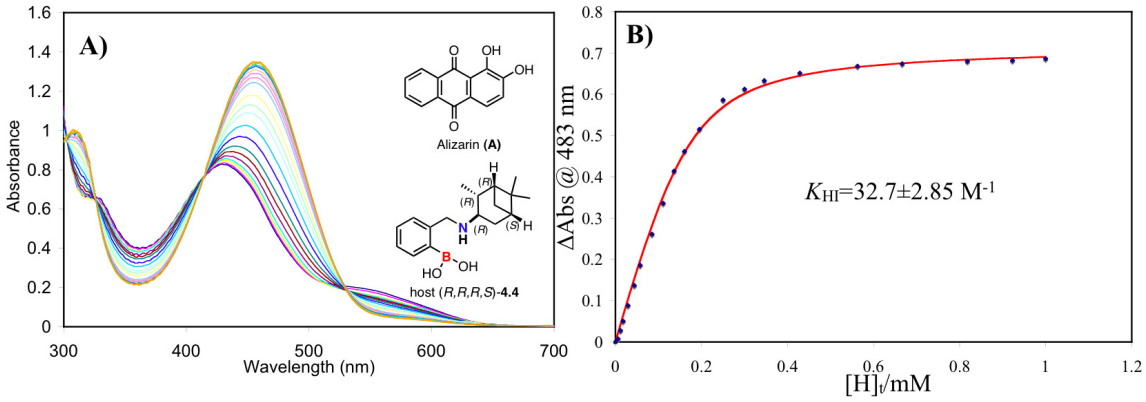

Figure 4.20: **A**) UV-visible titration of host (*R*,*R*,*R*,*S*)-**4.4** with A (200 μM) **B**) 1:1 binding isotherm (plot of the difference in absorbance at 483 nm with the addition of the host). All titrations were carried out in 100% MeOH, 10 mM *para*-toluenesulfonic acid and Hunig's base buffer, pH: 7.4, association constant K_{HI} (10^3 M^{-1}). All measurements were taken at 25°C. The solid line is the calculated curve resulting from iterative data fitting to a 1:1 binding isotherm.

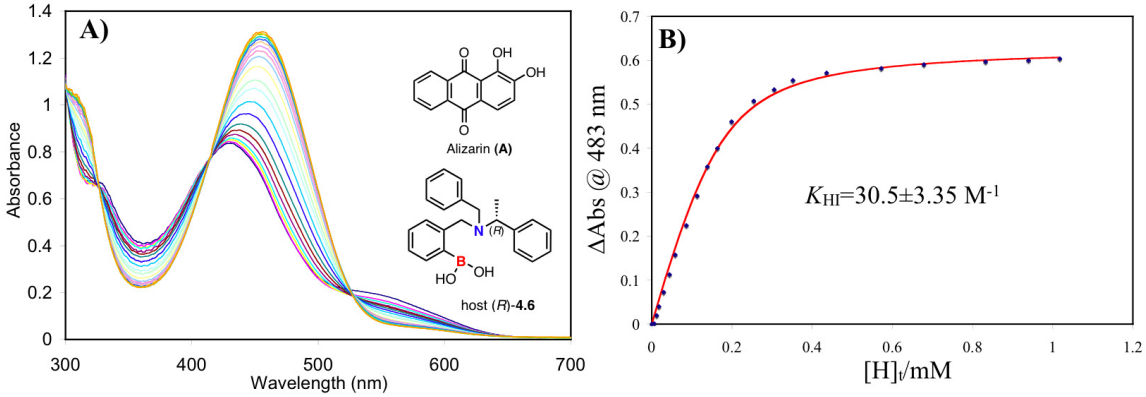

Figure 4.21: **A**) UV-visible titration of host (*R*)-**4.6** with A (200 μM) **B**) 1:1 binding isotherm (plot of the difference in absorbance at 483 nm with the addition of the host). All titrations were carried out in 100% MeOH, 10 mM *para*-toluenesulfonic acid and Hunig's base buffer, pH: 7.4, association constant K_{HI} (10^3 M^{-1}). All measurements were taken at 25°C. The solid line is the calculated curve resulting from iterative data fitting to a 1:1 binding isotherm.

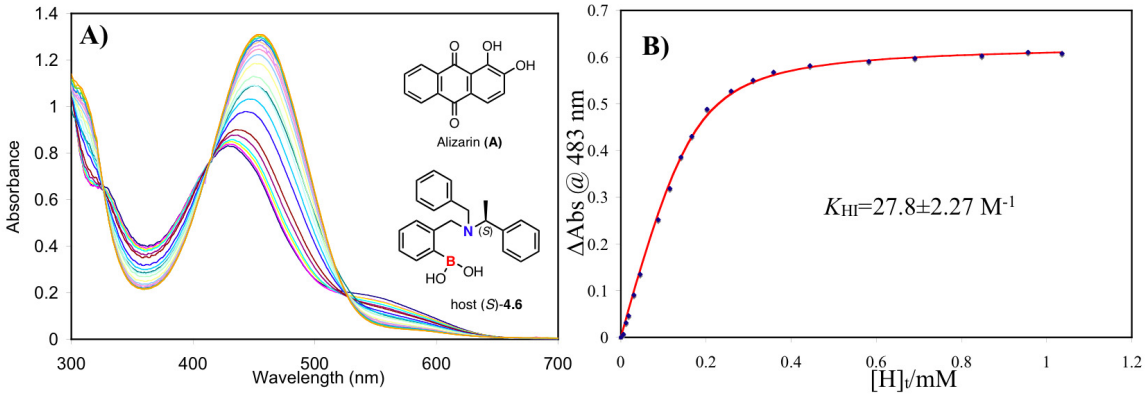

Figure 4.22: **A**) UV-visible titration of host (*S*)-**4.6** with A (200 µM) **B**) 1:1 binding isotherm (plot of the difference in absorbance at 483 nm with the addition of the host). All titrations were carried out in 100% MeOH, 10 mM *para*-toluenesulfonic acid and Hunig's base buffer, pH: 7.4, association constant K_{HI} (10^3 M^{-1}). All measurements were taken at 25°C. The solid line is the calculated curve resulting from iterative data fitting to a 1:1 binding isotherm.

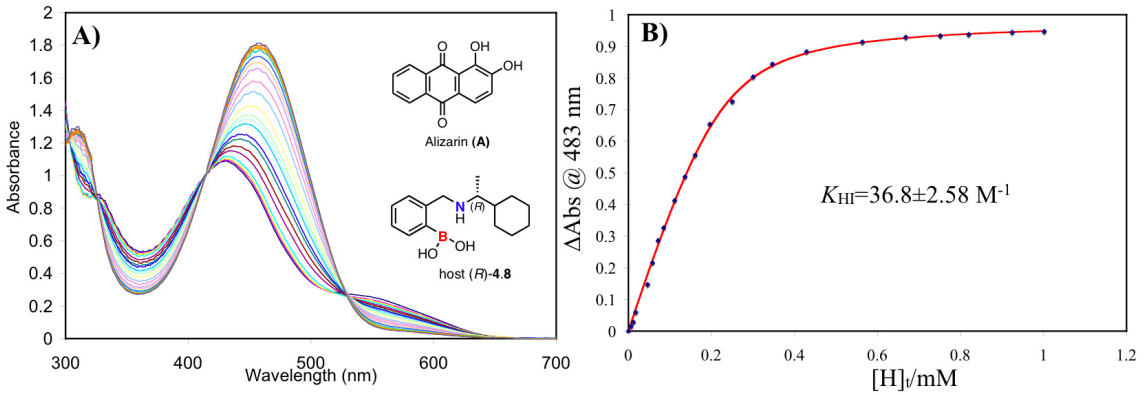

Figure 4.23: **A**) UV-visible titration of host (*R*)-**4.8** with A (200 µM) **B**) 1:1 binding isotherm (plot of the difference in absorbance at 483 nm with the addition of the host). All titrations were carried out in 100% MeOH, 10 mM *para*-toluenesulfonic acid and Hunig's base buffer, pH: 7.4, association constant K_{HI} (10^3 M^{-1}). All measurements were taken at 25°C. The solid line is the calculated curve resulting from iterative data fitting to a 1:1 binding isotherm.

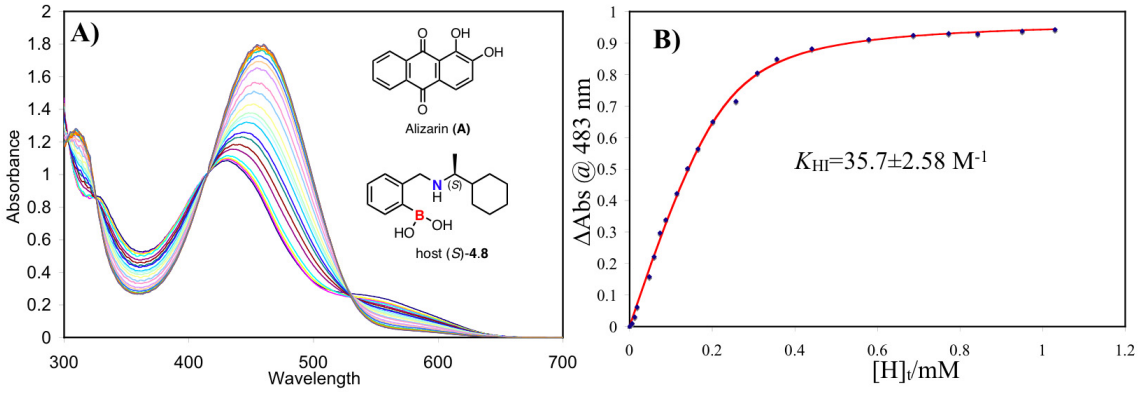

Figure 4.24: **A**) UV-visible titration of host (*S*)-**4.8** with A (200 µM) **B**) 1:1 binding isotherm (plot of the difference in absorbance at 483 nm with the addition of the host). All titrations were carried out in 100% MeOH, 10 mM *para*-toluenesulfonic acid and Hunig's base buffer, pH: 7.4, association constant K_{HI} (10^3 M^{-1}). All measurements were taken at 25°C. The solid line is the calculated curve resulting from iterative data fitting to a 1:1 binding isotherm.

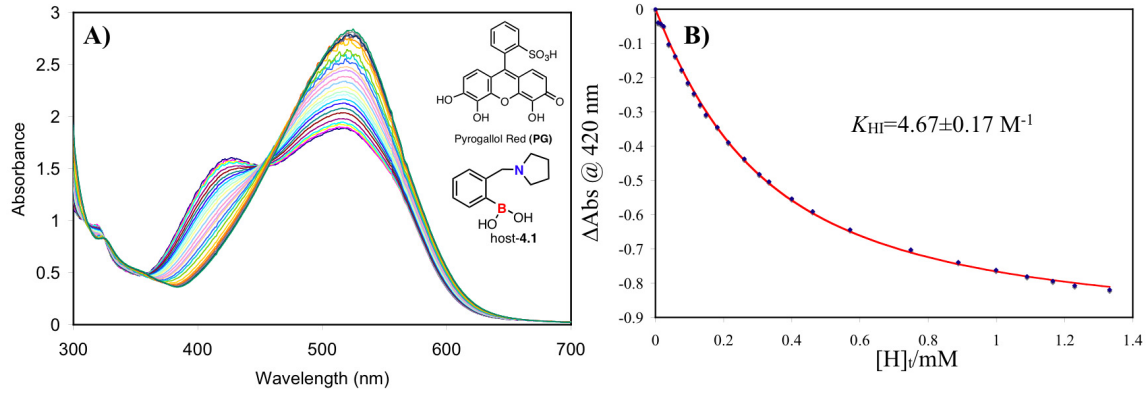

Figure 4.25: **A**) UV-visible titration of host-**4.1** with PG (75 µM) **B**) 1:1 binding isotherm (plot of the difference in absorbance at 420 nm with the addition of the host). All titrations were carried out in 100% MeOH, 10 mM *para*-toluenesulfonic acid and Hunig's base buffer, pH: 7.4, association constant K_{HI} (10^3 M^{-1}). All measurements were taken at 25°C. The solid line is the calculated curve resulting from iterative data fitting to a 1:1 binding isotherm.

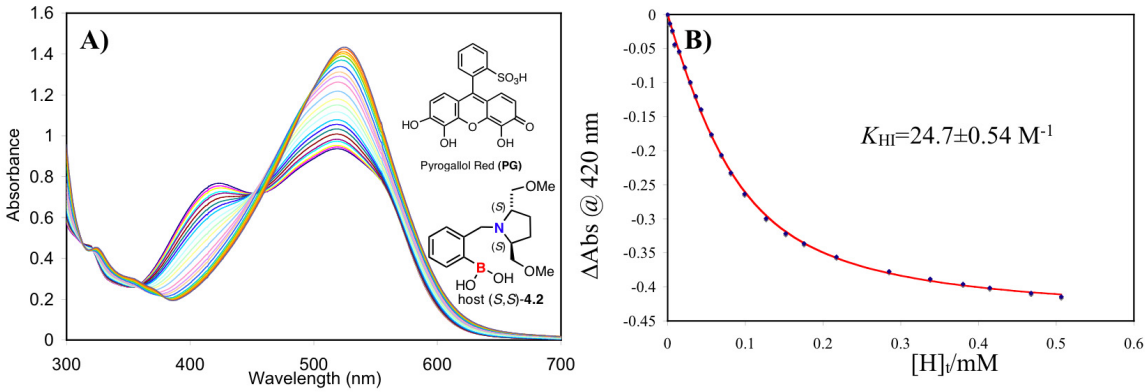

Figure 4.26: **A**) UV-visible titration of host (*S,S*)-**4.2** with PG (75 μM) **B**) 1:1 binding isotherm (plot of the difference in absorbance at 380 nm with the addition of the host). All titrations were carried out in 100% MeOH, 10 mM *para*-toluenesulfonic acid and Hunig's base buffer, pH: 7.4, association constant K_{HI} (10^3 M^{-1}). All measurements were taken at 25°C. The solid line is the calculated curve resulting from iterative data fitting to a 1:1 binding isotherm.

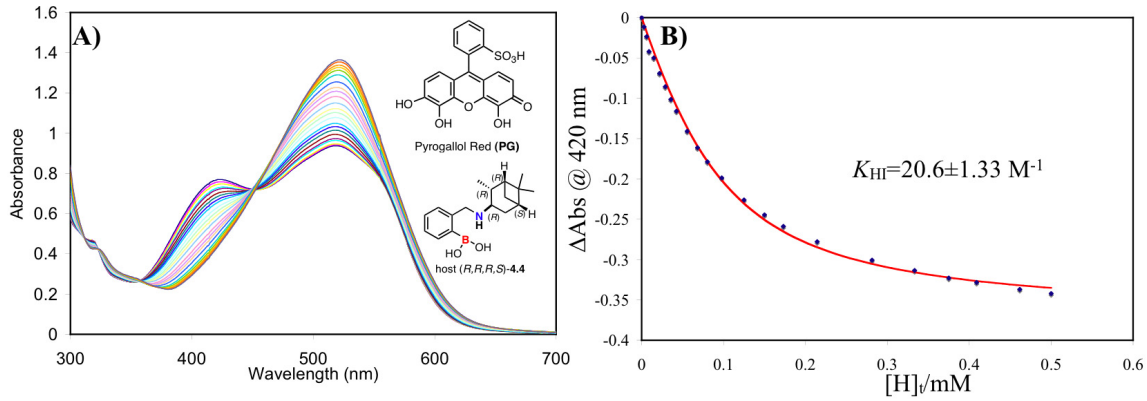

Figure 4.27: **A**) UV-visible titration of host (*R,R,R,S*)-**4.4** with PG (75 μM) **B**) 1:1 binding isotherm (plot of the difference in absorbance at 380 nm with the addition of the host). All titrations were carried out in 100% MeOH, 10 mM *para*-toluenesulfonic acid and Hunig's base buffer, pH: 7.4, association constant K_{HI} (10^3 M^{-1}). All measurements were taken at 25°C. The solid line is the calculated curve resulting from iterative data fitting to a 1:1 binding isotherm.

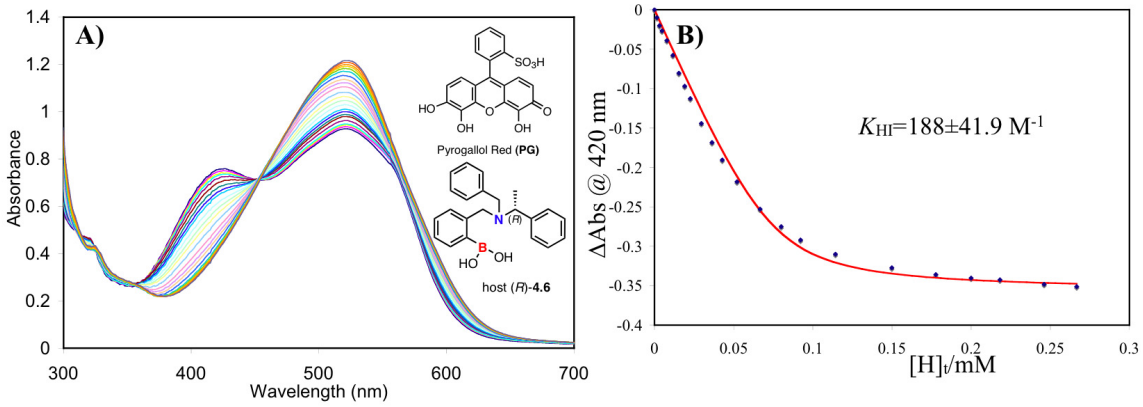

Figure 4.28: **A**) UV-visible titration of host (*R*)-**4.6** with PG (75 μM) **B**) 1:1 binding isotherm (plot of the difference in absorbance at 420 nm with the addition of the host). All titrations were carried out in 100% MeOH, 10 mM *para*-toluenesulfonic acid and Hunig's base buffer, pH: 7.4, association constant K_{HI} (10^3 M^{-1}). All measurements were taken at 25°C. The solid line is the calculated curve resulting from iterative data fitting to a 1:1 binding isotherm.

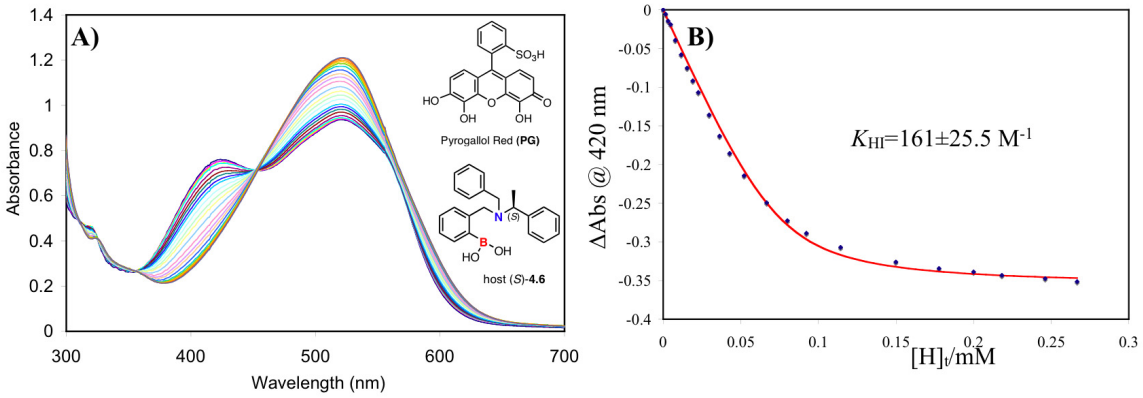

Figure 4.29: **A**) UV-visible titration of host (*S*)-**4.6** with PG (75 μM) **B**) 1:1 binding isotherm (plot of the difference in absorbance at 420 nm with the addition of the host). All titrations were carried out in 100% MeOH, 10 mM *para*-toluenesulfonic acid and Hunig's base buffer, pH: 7.4, association constant K_{HI} (10^3 M^{-1}). All measurements were taken at 25°C. The solid line is the calculated curve resulting from iterative data fitting to a 1:1 binding isotherm.

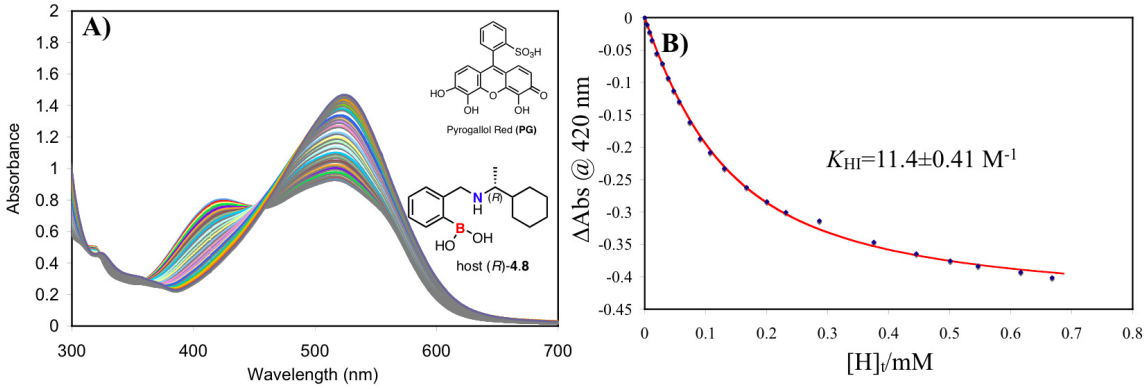

Figure 4.30: **A**) UV-visible titration of host (*R*)-**4.8** with PG (75 μM) **B**) 1:1 binding isotherm (plot of the difference in absorbance at 420 nm with the addition of the host). All titrations were carried out in 100% MeOH, 10 mM *para*-toluenesulfonic acid and Hunig's base buffer, pH: 7.4, association constant K_{HI} (10^3 M^{-1}). All measurements were taken at 25°C. The solid line is the calculated curve resulting from iterative data fitting to a 1:1 binding isotherm.

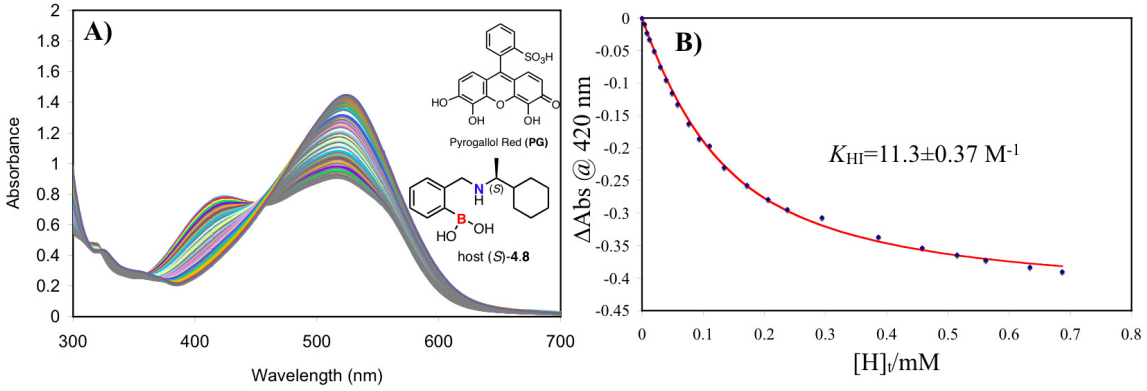

Figure 4.31: **A**) UV-visible titration of host (*S*)-**4.8** with PG (75 μM) **B**) 1:1 binding isotherm (plot of the difference in absorbance at 420 nm with the addition of the host). All titrations were carried out in 100% MeOH, 10 mM *para*-toluenesulfonic acid and Hunig's base buffer, pH: 7.4, association constant K_{HI} (10^3 M^{-1}). All measurements were taken at 25°C. The solid line is the calculated curve resulting from iterative data fitting to a 1:1 binding isotherm.

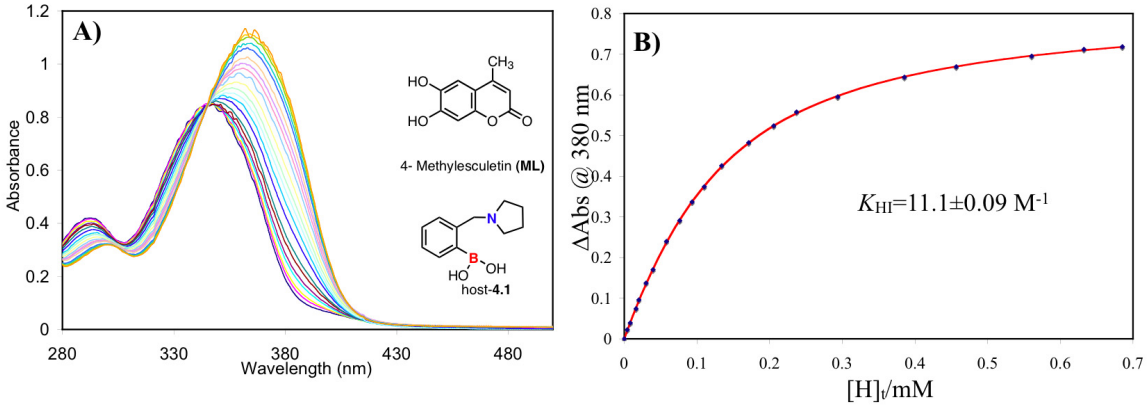

Figure 4.32: **A**) UV-visible titration of host-**4.1** with ML (75 µM) **B**) 1:1 binding isotherm (plot of the difference in absorbance at 380 nm with the addition of the host). All titrations were carried out in 100% MeOH, 10 mM *para*-toluenesulfonic acid and Hunig's base buffer, pH: 7.4, association constant K_{HI} (10^3 M^{-1}). All measurements were taken at 25°C. The solid line is the calculated curve resulting from iterative data fitting to a 1:1 binding isotherm.

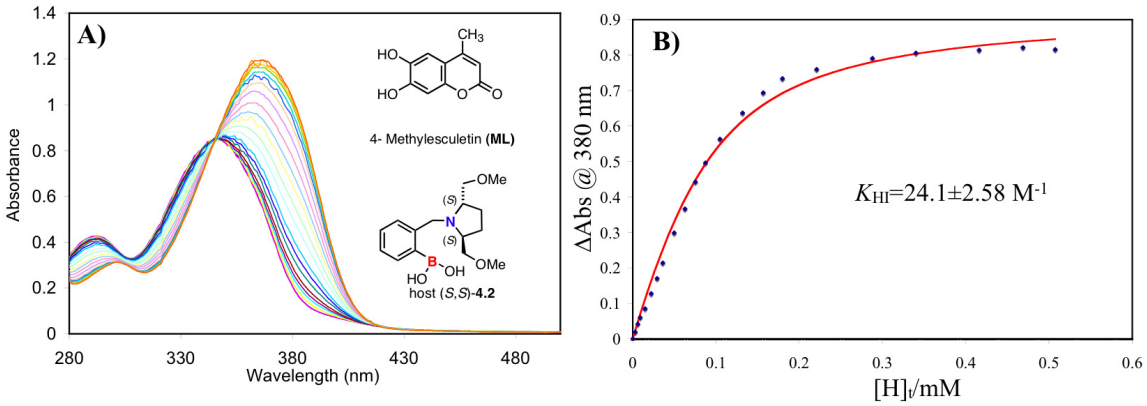

Figure 4.33: **A**) UV-visible titration of host (*S,S*)-**4.2** with ML (75 µM) **B**) 1:1 binding isotherm (plot of the difference in absorbance at 380 nm with the addition of the host). All titrations were carried out in 100% MeOH, 10 mM *para*-toluenesulfonic acid and Hunig's base buffer, pH: 7.4, association constant K_{HI} (10^3 M^{-1}). All measurements were taken at 25°C. The solid line is the calculated curve resulting from iterative data fitting to a 1:1 binding isotherm.

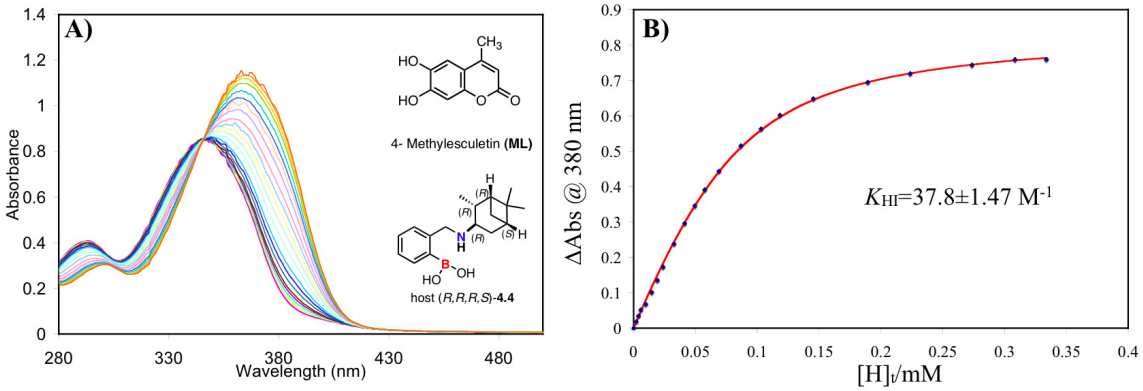

Figure 4.34: **A**) UV-visible titration of host (*R*,*R*,*R*,*S*)-**4.4** with ML (75 μM) **B**) 1:1 binding isotherm (plot of the difference in absorbance at 380 nm with the addition of the host). All titrations were carried out in 100% MeOH, 10 mM *para*-toluenesulfonic acid and Hunig's base buffer, pH: 7.4, association constant K_{HI} (10^3 M^{-1}). All measurements were taken at 25°C. The solid line is the calculated curve resulting from iterative data fitting to a 1:1 binding isotherm.

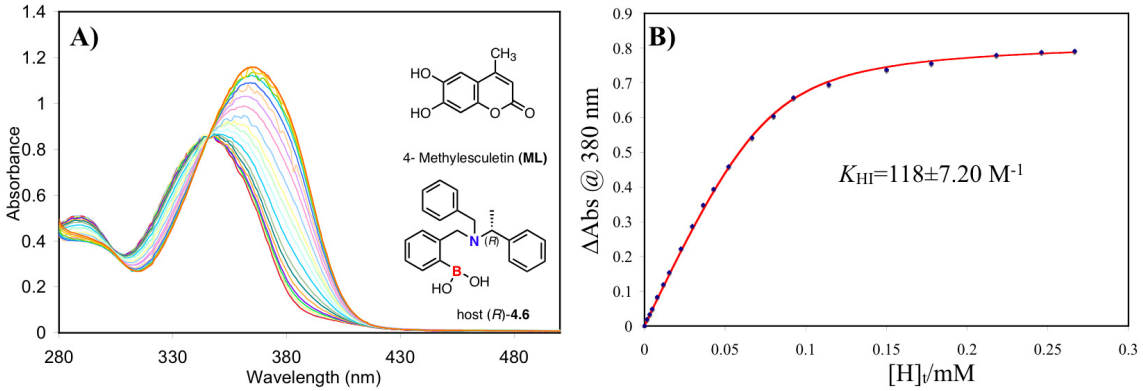

Figure 4.35: **A**) UV-visible titration of host (*R*)-**4.6** with ML (75 μM) **B**) 1:1 binding isotherm (plot of the difference in absorbance at 380 nm with the addition of the host). All titrations were carried out in 100% MeOH, 10 mM *para*-toluenesulfonic acid and Hunig's base buffer, pH: 7.4, association constant K_{HI} (10^3 M^{-1}). All measurements were taken at 25°C. The solid line is the calculated curve resulting from iterative data fitting to a 1:1 binding isotherm.

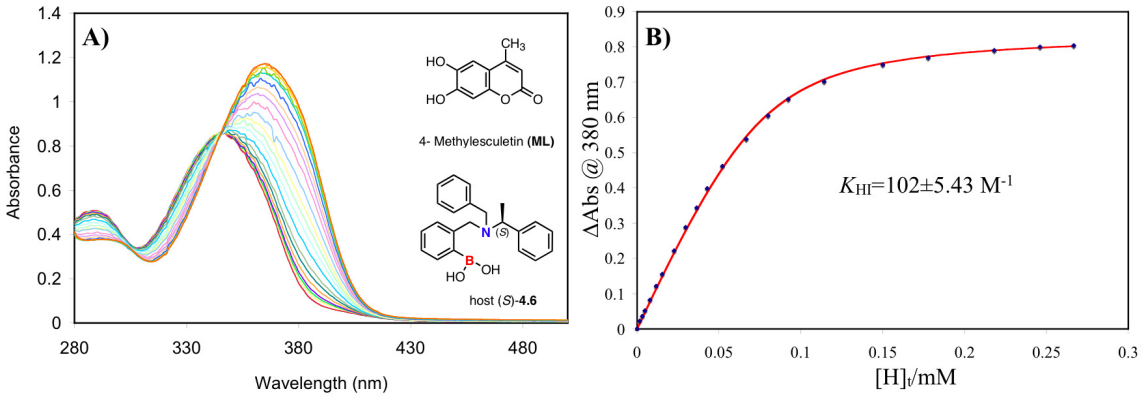

Figure 4.36: **A**) UV-visible titration of host (*S*)-**4.6** with ML (75 µM) **B**) 1:1 binding isotherm (plot of the difference in absorbance at 380 nm with the addition of the host). All titrations were carried out in 100% MeOH, 10 mM *para*-toluenesulfonic acid and Hunig's base buffer, pH: 7.4, association constant K_{HI} (10^3 M^{-1}). All measurements were taken at 25°C. The solid line is the calculated curve resulting from iterative data fitting to a 1:1 binding isotherm.

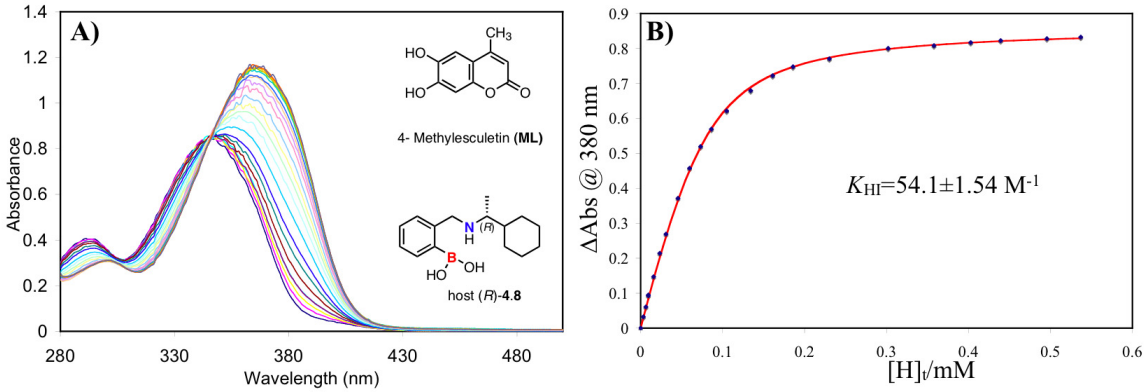

Figure 4.37: **A**) UV-visible titration of host (*R*)- **4.8** with ML (75 µM) **B**) 1:1 binding isotherm (plot of the difference in absorbance at 520 nm with the addition of the host). All titrations were carried out in 100% MeOH, 10 mM *para*-toluenesulfonic acid and Hunig's base buffer, pH: 7.4, association constant K_{HI} (10^3 M^{-1}). All measurements were taken at 25°C. The solid line is the calculated curve resulting from iterative data fitting to a 1:1 binding isotherm.

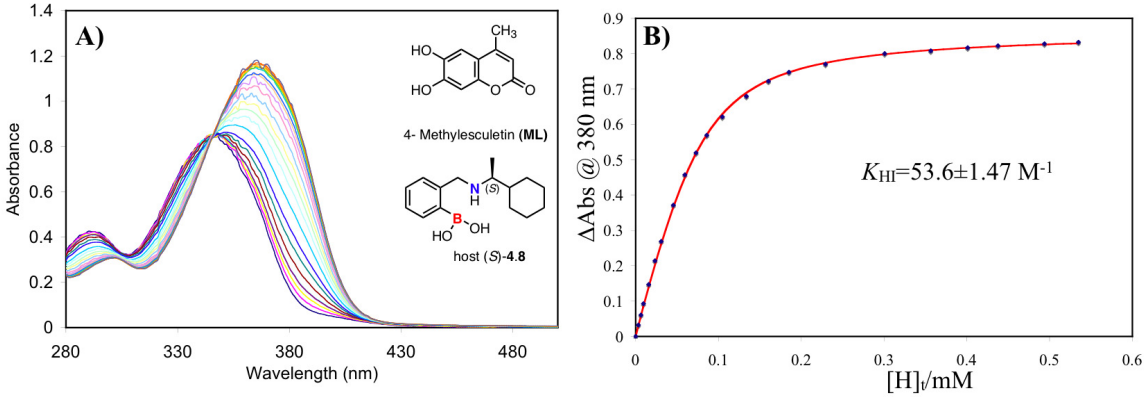

Figure 4.38: **A**) UV-visible titration of host (*S*)- **4.8** with ML (75 µM) **B**) 1:1 binding isotherm (plot of the difference in absorbance at 380 nm with the addition of the host). All titrations were carried out in 100% MeOH, 10 mM *para*-toluenesulfonic acid and Hunig's base buffer, pH: 7.4, association constant K_{HI} (10^3 M^{-1}). All measurements were taken at 25°C. The solid line is the calculated curve resulting from iterative data fitting to a 1:1 binding isotherm.

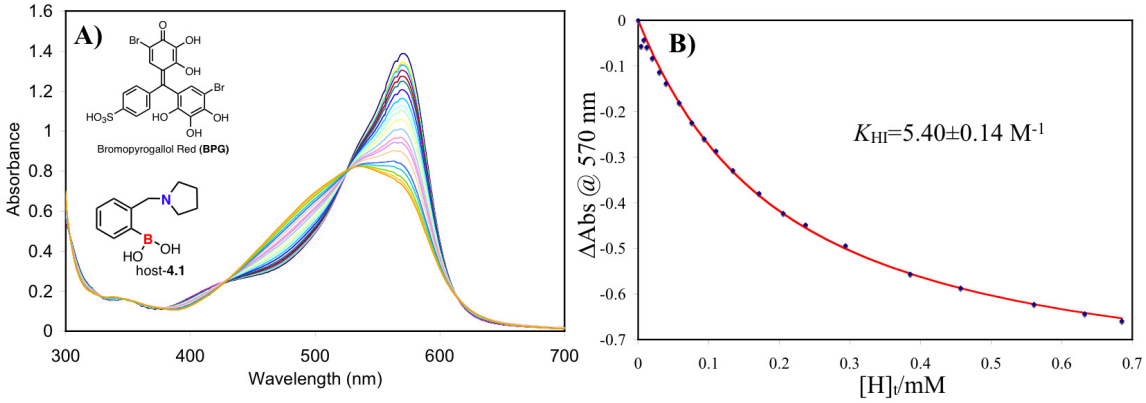

Figure 4.39: **A**) UV-visible titration of host-**4.1** with BPG (30 µM) **B**) 1:1 binding isotherm (plot of the difference in absorbance at 570 nm with the addition of the host). All titrations were carried out in 100% MeOH, 10 mM *para*-toluenesulfonic acid and Hunig's base buffer, pH: 7.4, association constant K_{HI} (10^3 M^{-1}). All measurements were taken at 25°C. The solid line is the calculated curve resulting from iterative data fitting to a 1:1 binding isotherm.

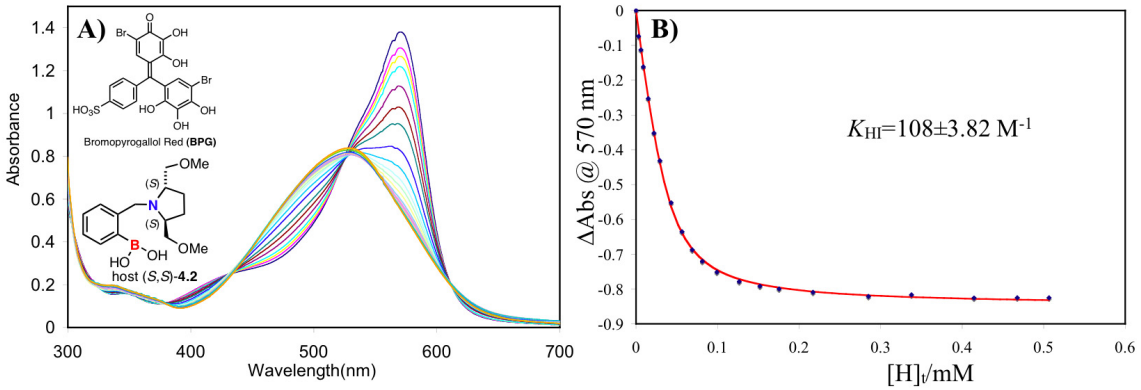

Figure 4.40: **A**) UV-visible titration of host (*S,S*)- **4.2** with BPG (30 μM) **B**) 1:1 binding isotherm (plot of the difference in absorbance at 570 nm with the addition of the host). All titrations were carried out in 100% MeOH, 10 mM *para*-toluenesulfonic acid and Hunig's base buffer, pH: 7.4, association constant K_{HI} (10^3 M^{-1}). All measurements were taken at 25°C. The solid line is the calculated curve resulting from iterative data fitting to a 1:1 binding isotherm.

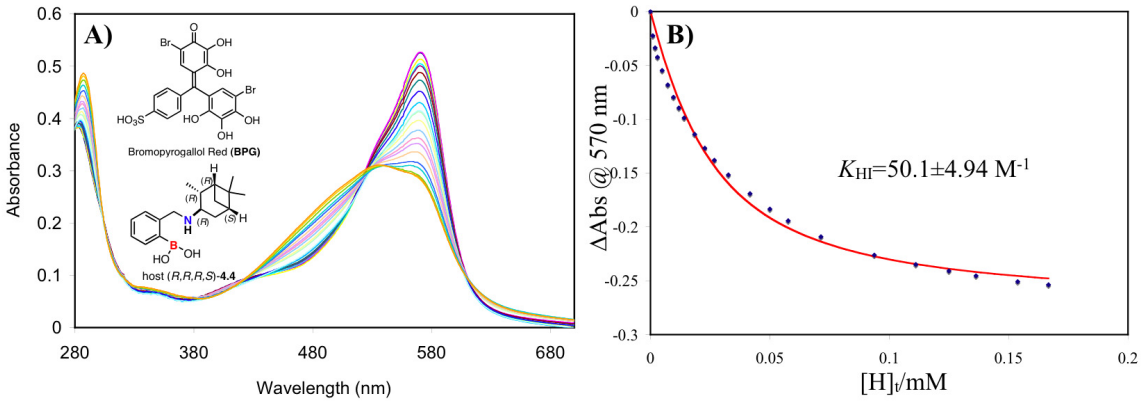

Figure 4.41: **A**) UV-visible titration of host (*R,R,R,S,S*)- **4.4** with BPG (30 μM) **B**) 1:1 binding isotherm (plot of the difference in absorbance at 570 nm with the addition of the host). All titrations were carried out in 100% MeOH, 10 mM *para*-toluenesulfonic acid and Hunig's base buffer, pH: 7.4, association constant K_{HI} (10^3 M^{-1}). All measurements were taken at 25°C. The solid line is the calculated curve resulting from iterative data fitting to a 1:1 binding isotherm.

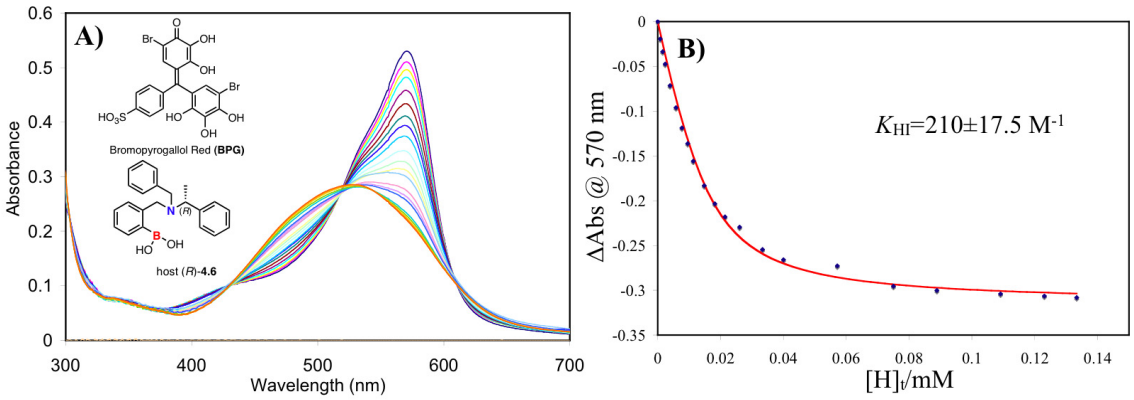

Figure 4.42: **A**) UV-visible titration of host (*R*)- **4.6** with BPG (30 µM) **B**) 1:1 binding isotherm (plot of the difference in absorbance at 520 nm with the addition of the host). All titrations were carried out in 100% MeOH, 10 mM *para*-toluenesulfonic acid and Hunig's base buffer, pH: 7.4, association constant K_{HI} (10^3 M^{-1}). All measurements were taken at 25°C. The solid line is the calculated curve resulting from iterative data fitting to a 1:1 binding isotherm.

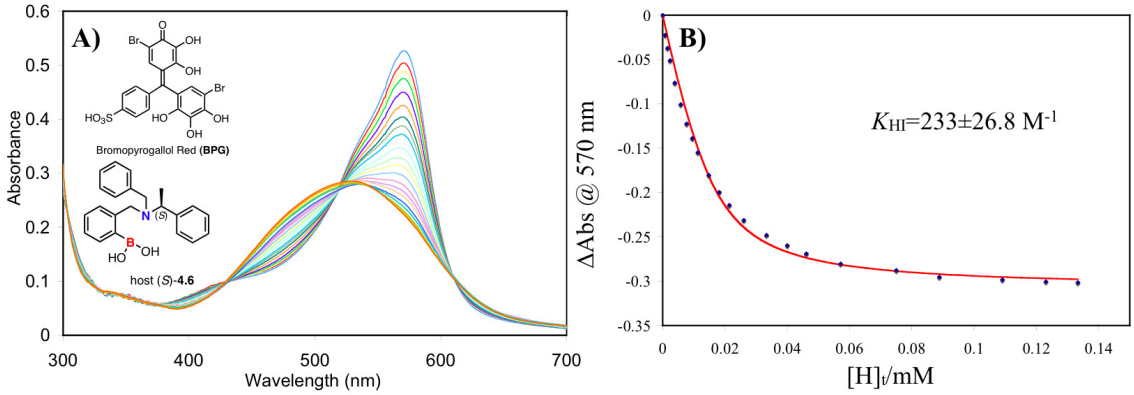

Figure 4.43: **A**) UV-visible titration of host (*S*)- **4.6** with BPG (30 µM) **B**) 1:1 binding isotherm (plot of the difference in absorbance at 570 nm with the addition of the host). All titrations were carried out in 100% MeOH, 10 mM *para*-toluenesulfonic acid and Hunig's base buffer, pH: 7.4, association constant K_{HI} (10^3 M^{-1}). All measurements were taken at 25°C. The solid line is the calculated curve resulting from iterative data fitting to a 1:1 binding isotherm.

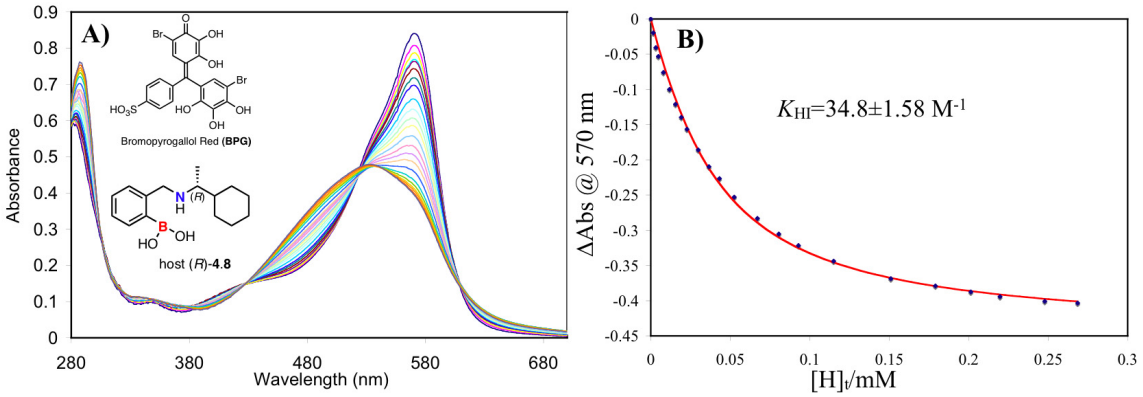

Figure 4.44: **A**) UV-visible titration of host (*R*)- **4.8** with BPG (30 μM) **B**) 1:1 binding isotherm (plot of the difference in absorbance at 570 nm with the addition of the host). All titrations were carried out in 100% MeOH, 10 mM *para*-toluenesulfonic acid and Hunig's base buffer, pH: 7.4, association constant K_{HI} (10^3 M^{-1}). All measurements were taken at 25°C. The solid line is the calculated curve resulting from iterative data fitting to a 1:1 binding isotherm.

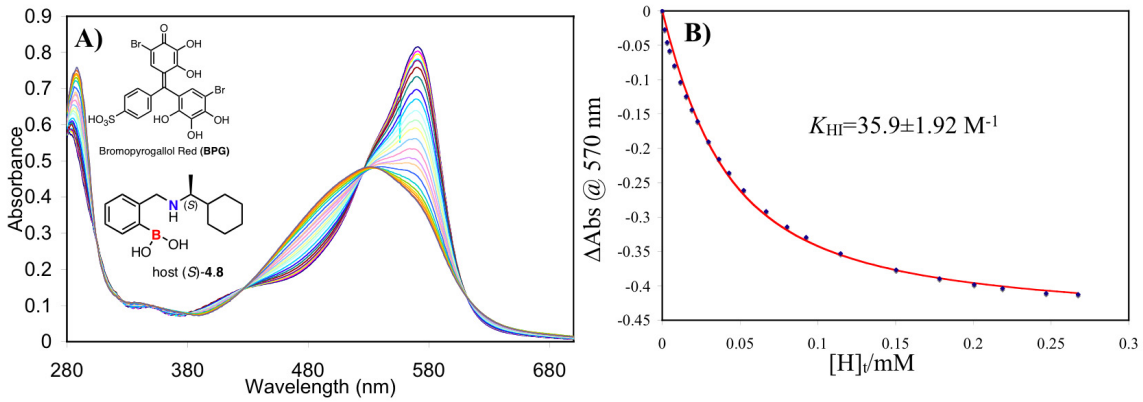

Figure 4.45: **A**) UV-visible titration of host (*S*)- **4.8** with BPG (30 μM) **B**) 1:1 binding isotherm (plot of the difference in absorbance at 570 nm with the addition of the host). All titrations were carried out in 100% MeOH, 10 mM *para*-toluenesulfonic acid and Hunig's base buffer, pH: 7.4, association constant K_{HI} (10^3 M^{-1}). All measurements were taken at 25°C. The solid line is the calculated curve resulting from iterative data fitting to a 1:1 binding isotherm.

4.2.4 Screening for Enantioselectivity (In Pre*para*tion of Step 2)

Because we have not previously performed a screen in a 96-well plate to reveal the most enantioselective receptor, we first checked the enantioselectivities of the chiral receptors we have synthesized (**Scheme 4.1A**) by using standard eIDA methods. The goal was to check the results we would ultimately obtain in Step 2 of our general protocol, to make sure that the screen reveals the correct receptor. Hence, we checked the enantioselectivity of our new chiral receptors using pyrocatechol violet (PV) as the indicator.

In the displacement assay the addition of the analyte (hydrobenzoin) to the indicator and the host solution causes a shift in absorbance of the resulting solution due to the displacement of the indicator from the host by the analyte. The displacement assay, of the host with the two enantiomers of hydrobenzoin is shown in **Figure 4.3**. As expected, the absorbance at 520 nm of the host (*S*)- **4.6** and PV complex [H:I] decreases to different extents with the two enantiomers. The association constants between the hosts and the two enantiomers can be calculated by traditional methods.[50, 51]

Similarly, the association constant of the synthesized boronic acid hosts (**4.1-4.8**) with (*R*,*R*)-hydrobenzoin and (*S*,*S*)-hydrobenzoin were determined (**Figure 4.46-4.53**). Of those synthesized boronic acid hosts, only host (*S,S*)-**4.2**, host (*R*,*R*,*R*,*S*)-**4.4**, host (*S*)-**4.6**, host (*R*)-**4.8** show significant discrimination between the two enantiomers of hydrobenzoin. Host (*S,S*)-**4.5** did not show any enantioselectivity suggesting that adding a stereocenter to the benzylic carbon does not improve enantioselectivity. The association constants ($K_{HG(R,R)}$ $K_{HG(S,S)}$) of the hosts that did show enantioselectivity with the two enantiomers of hydrobenzoin are listed in **Table 4.2**. As required by the first principles of stereochemistry, host (*R*)-**4.6** and host (*S*)-**4.6**, and, host (*R*)-**4.8** and host (*S*)-**4.8**, show equal and opposite enantioselectivity (**Figure 4.51, 4.53**). Host (*S,S*)-**4.2** shows the

highest enantioselectivity. Interestingly, this particular host is the only C_2 symmetric host, and apparently the CH_2OCH_3 groups on the pyrrolidine ring create a chiral environment that imparts the best enantioselectivity.

Given these results, we set out to determine if a 96-plate analysis would lead to the same conclusion and to find the optimal indicator host combination for hydrobenzoin as a means to use this combination in the HTS assay. This next stage of the study constitutes the implementation of Step 2 or our general protocol.

Table 4.2: Binding constant K_{HG} (10^3 M^{-1}) of boronic acid hosts, $K_{HG(S,S)}$with (*S*,*S*)-hydrobenzoin and $K_{HG(R,R)}$ with (*R*,*R*)-hydrobenzoin. All titrations were carried out in 100% MeOH, 10 mM *para*-toluenesulfonic acid and Hunig's base buffer, pH =7.4. All measurements were taken at 25°C. The error reported here results from the computer fit to the experimental isotherm. In our pervious experience, there is approximately 10% error at most in the reproducibility in the K_{HG} value.

Guest	**4.1**	(*S,S*)-**4.2**	(*R,R,R,S*)-**4.4**	(*R*)- **4.6**	(*S*)- **4.6**	(*R*)- **4.8**	(*S*)- **4.8**
$K_{HG(S,S)}$	1.42± 0.04	13.6± 0.13	3.55± 0.04	3.78± 0.06	6.38± 0.05	5.85± 0.06	4.17± 0.04
$K_{HG(R,R)}$	1.26± 0.03	4.77± 0.02	5.22± 0.07	5.93± 0.07	3.94± 0.04	3.96± 0.05	5.55± 0.06

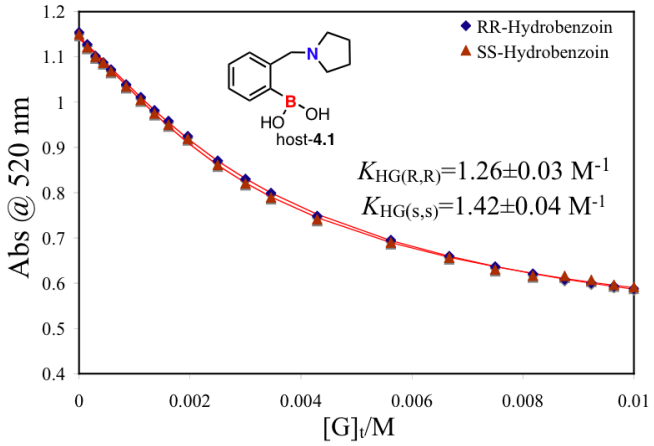

Figure 4.46: Enantioselective indicator displacement assay (eIDA) of host-**4.1** (700 µM) /PV (150 µM) with (*R*,*R*)-hydrobenzoin and (*S*,*S*)-hydrobenzoin. All titrations were carried out in 100% MeOH, 10 mM *para*-toluenesulfonic acid and Hunig's base buffer, pH =7.4, association constant K_{HI} (10^3 M^{-1}). All measurements were taken at 25°C. The solid lines are calculated curves resulting from iterative data fitting for displacement assay.[51]

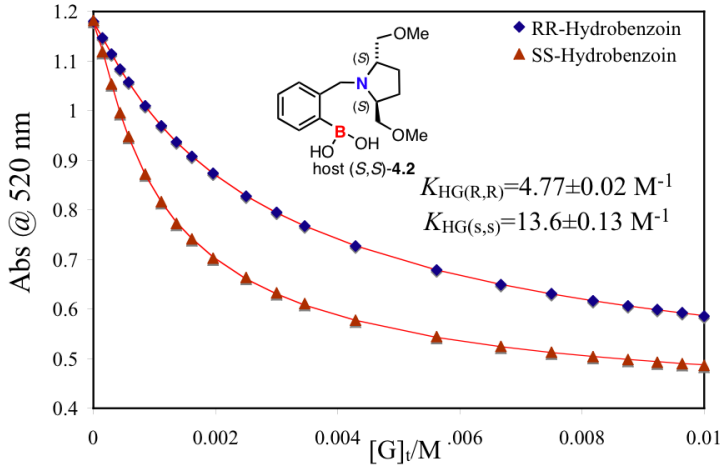

Figure 4.47: Enantioselective indicator displacement assay (eIDA) of host (*S*,*S*)-**4.2** (300 µM) /PV (150 µM) with (*R*,*R*)-hydrobenzoin and (*S*,*S*)-hydrobenzoin. All titrations were carried out in 100% MeOH, 10 mM *para*-toluenesulfonic acid and Hunig's base buffer, pH =7.4, association constant K_{HI} (10^3 M^{-1}). All measurements were taken at 25°C. The solid lines are calculated curves resulting from iterative data fitting for displacement assay.[51]

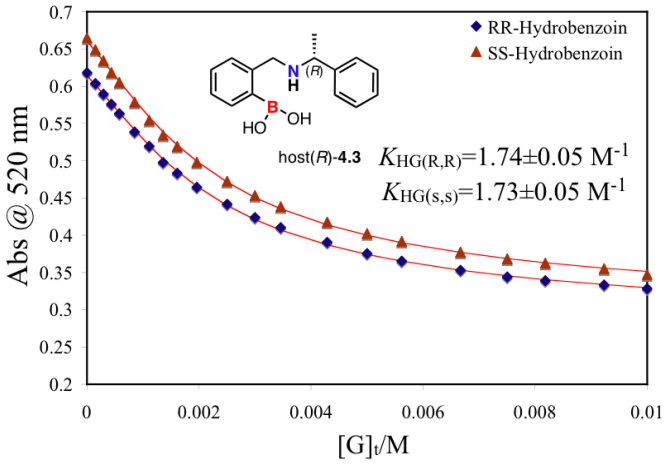

Figure 4.48: Enantioselective indicator displacement assay (eIDA) of host (*R*)-**4.3** (960 μM) /PV (150 μM) with (*R*,*R*)-hydrobenzoin and (*S*,*S*)-hydrobenzoin. All titrations were carried out in 100% MeOH, 10 mM *para*-toluenesulfonic acid and Hunig's base buffer, pH =7.4, association constant K_{HI} (10^3 M^{-1}). All measurements were taken at 25°C. The solid lines are calculated curves resulting from iterative data fitting for displacement assay.[51]

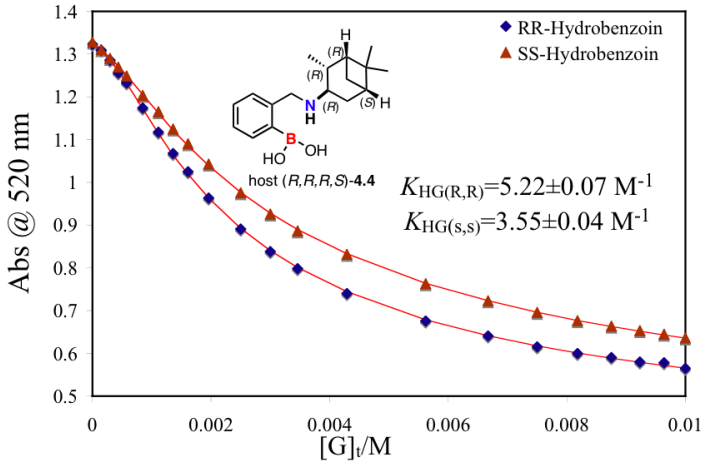

Figure 4.49: Enantioselective indicator displacement assay (eIDA) of host (*R*,*R*,*R*,*S*)-**4.4** (500 μM) /PV (150 μM) with (*R*,*R*)-hydrobenzoin and (*S*,*S*)-hydrobenzoin. All titrations were carried out in 100% MeOH, 10 mM *para*-toluenesulfonic acid and Hunig's base buffer, pH =7.4, association constant K_{HI} (10^3 M^{-1}). All measurements were taken at 25°C. The solid lines are calculated curves resulting from iterative data fitting for displacement assay.[51]

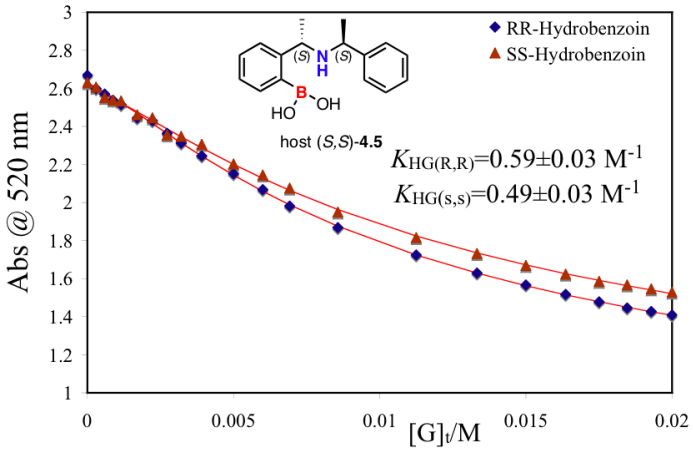

Figure 4.50: Enantioselective indicator displacement assay (eIDA) of host (*S,S*)-**4.5** (2010 µM) /PV (220 µM) with (*R,R*)-hydrobenzoin and (*S,S*)-hydrobenzoin. All titrations were carried out in 100% MeOH, 10 mM *para*-toluenesulfonic acid and Hunig's base buffer, pH =7.4, association constant K_{HI} (10^3 M^{-1}). All measurements were taken at 25°C. The solid lines are calculated curves resulting from iterative data fitting for displacement assay.[51]

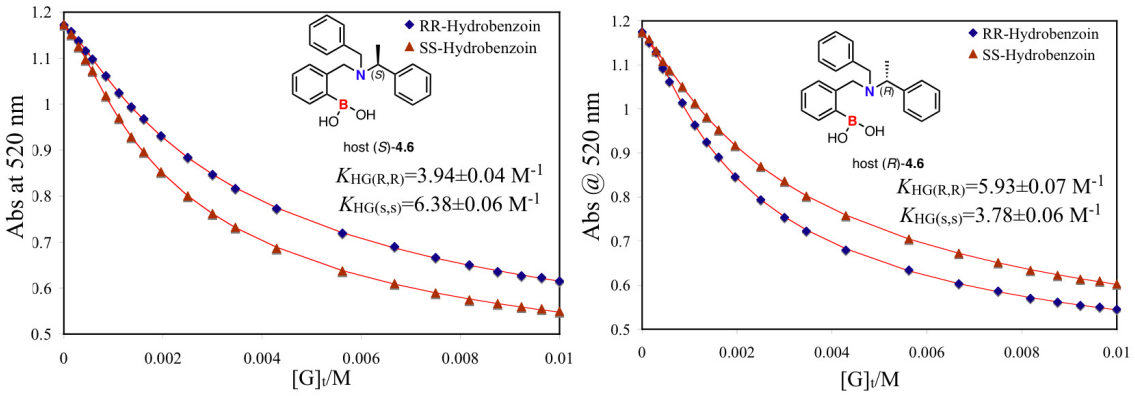

Figure 4.51: Enantioselective indicator displacement assay (eIDA) of host (*S*)-**4.6** and host (*R*)-**4.6** (400 µM) /PV (150 µM) with (*R,R*)-hydrobenzoin and (*S,S*)-hydrobenzoin. All titrations were carried out in 100% MeOH, 10 mM *para*-toluenesulfonic acid and Hunig's base buffer, pH =7.4, association constant K_{HI} (10^3 M^{-1}). All measurements were taken at 25°C. The solid lines are calculated curves resulting from iterative data fitting for displacement assay.[51]

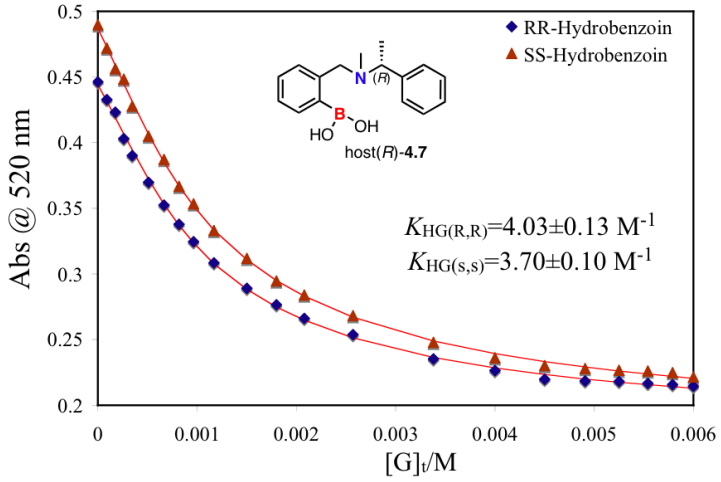

Figure 4.52: Enantioselective indicator displacement assay (eIDA) of host (*R*)-**4.7** (420 µM) /PV (75 µM) with (*R*,*R*)-hydrobenzoin and (*S*,*S*)-hydrobenzoin. All titrations were carried out in 100% MeOH, 10 mM *para*-toluenesulfonic acid and Hunig's base buffer, pH =7.4, association constant K_{HI} (10^3 M^{-1}). All measurements were taken at 25°C. The solid lines are calculated curves resulting from iterative data fitting for displacement assay.[51]

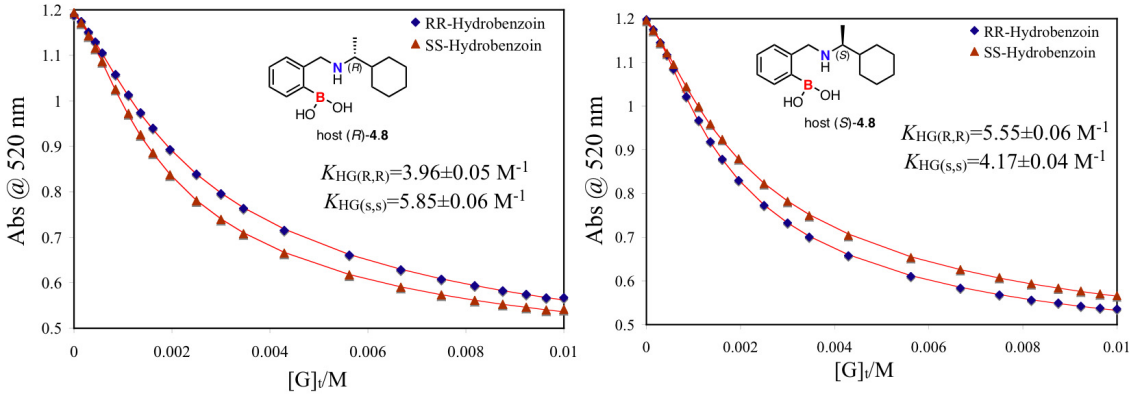

Figure 4.53: Enantioselective indicator displacement assay (eIDA) of host (*R*)-**4.8** and host (*S*)-**4.8** (400 µM)/PV (150 µM) with (*R*,*R*)-hydrobenzoin and (*S*,*S*)-hydrobenzoin. All titrations were carried out in 100% MeOH, 10 mM *para*-toluenesulfonic acid and Hunig's base buffer, pH =7.4, association constant K_{HI} (10^3 M^{-1}). All measurements were taken at 25°C. The solid lines are calculated curves resulting from iterative data fitting for displacement assay. [51]

4.2.5 Screening Plate (Step 2)

A screening plate was designed to determine which host and indicator combination shows the best discrimination between the two enantiomers of hydrobenzoin. Traditionally, acquiring this information would require several UV-titrations as described above, which we did in this one case as a means to check the following results. In the future the plan would be to skip these titrations and move directly to a 96-well screening plate as now described. In this study the screening plate was generated with one enantiomer of each hosts (host (*S,S*)-**4.2**, host (*R,R,R,S*)-**4.4**, host (*S*)-**4.6**, and host (*S*)-**4.8**) (**Figure 4.54**). In our experience,[40] the degree of enantioselectivity of a host is dependent on analyte concentration. Thus, two screening plates were designed, one at 5 mM, and the other at 10 mM concentration of the hydrobenzoin. The host/indicator combination that showed the best enantiodiscrimination of the two enantiomers of hydrobenzoin was determined to be host (*S,S*)-**4.2**, and bromopyrogallol red (BPG). A difference in absorbance of 0.237 was recorded at 570 nm with host (*S,S*)-**4.2** and BPG at 5 mM and 10 mM $[G]_t$ (**Figure 4.54B**). To validate the technique, the absorbance of a racemic mixture of hydrobenzoin was recorded. The ΔAbs of each host with the indicators are listed in **Table 4.3** and **4.4**. As described above host (*S,S*)-**4.2** was also found to be the most enantioselective host for hydrobenzoin by traditional methods, thereby verifying the reliability of the screening process.

Host (*S*)-**4.6** and host (*S*)-**4.8** also showed good enantioselectivity with BPG at 10 mM concentration of hydrobenzoin with a ΔAbs of 0.095 and 0.139 respectively. While host (*R,R,R,S*)-**4.4** showed reasonable enantioselectivity using ML with an ΔAbs of 0.064 at 5 mM concentration of hydrobenzoin. Another chiral 1-2 diol may show a good response with a different indicator and host combination.

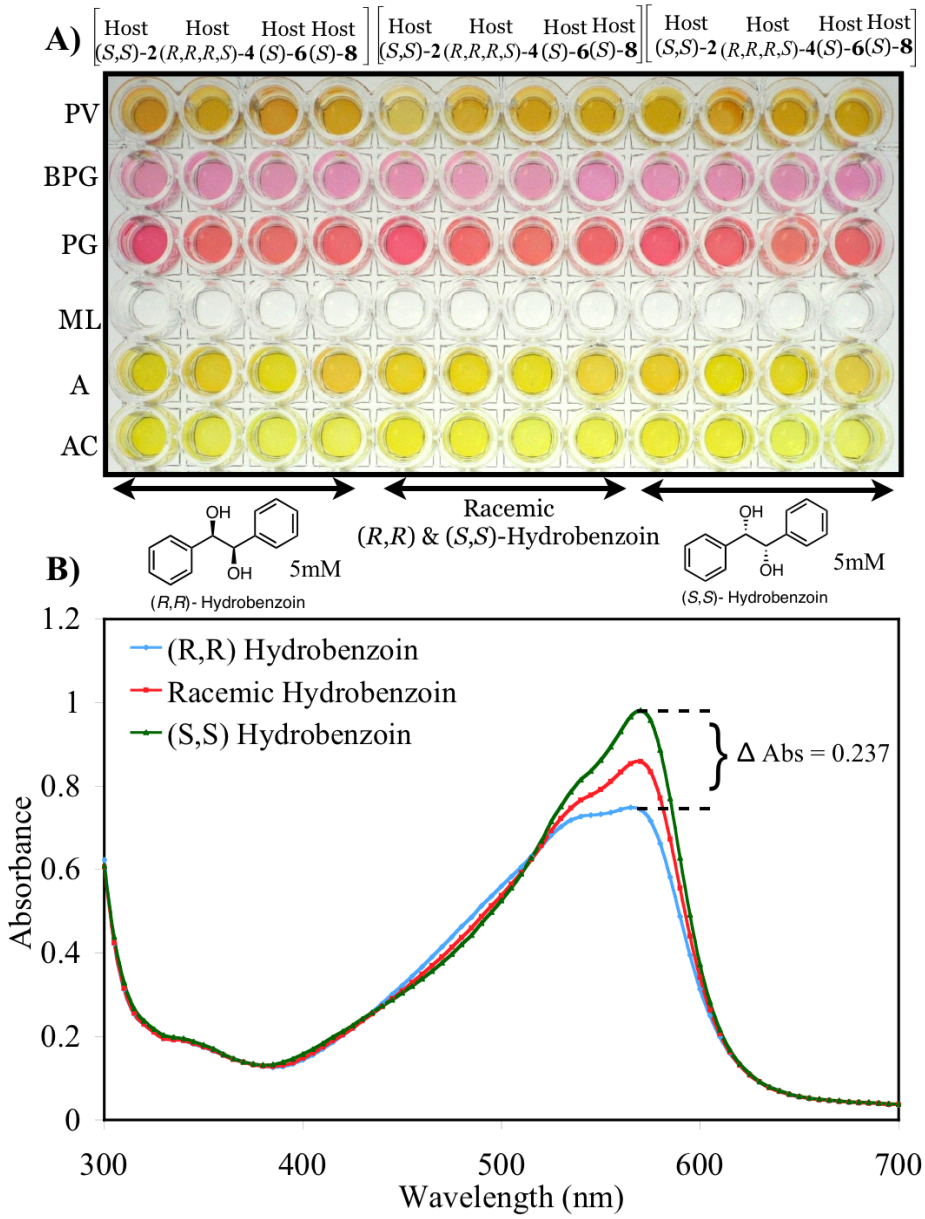

Figure 4.54. **A**) Screening plate with indicators, A: Alizarin (200 μM), AC: Alizarin complexone dihydrate (200 μM), BPG: Bromopyrogallol red (60 μM), ML: 4-Methylesculetin (125 μM), PG: Pyrogallol red (75 μM) PV: Pyrocatechol violet (150 μM) and host (*S,S*)-**4.2**, host (*R,R,R,S*)-**4.4**, host (*S*)-**4.6**, host (*S*)-**4.8** (See Table S1) and 5 mM hydrobenzoin **B**) Displacement of indicator BPG (60 μM) from host (*S,S*)-**4.2** (200 μM) with (*R,R*)-hydrobenzoin (5 mM), Racemic mixture (5 mM) and (*S,S*)-hydrobenzoin (5 mM). All solution were made in 100% MeOH, 10 mM *para*-toluenesulfonic acid and Hunig's base buffer, pH = 7.4. All measurements were taken at 25°C.

Table 4.3: Screening plate Δ Abs between (*R,R*)-hydrobenzoin & (*S,S*)-hydrobenzoin (5 mM) calculated for A at 480 nm, AC at 540 nm, ML at 380 nm, BPG at 570 nm, PG at 420 nm PV at 520 nm.

Indicators	**4.2**(*S,S*)	**4.4**(*R,R,R,S*)	**4.6**(*S*)	**4.8**(*S*)
A	0.015	0.004	0.003	0.023
AC	0.017	0.1	0.012	0.006
BPG	0.237	0.062	0.05	0.017
ML	0.103	0.064	0.048	0.027
PG	0.04	0.052	0.019	0.039
PV	0.107	0.045	0.046	0.025

Table 4.4: Screening plate Δ Abs between (*R,R*)-hydrobenzoin & (*S,S*)-hydrobenzoin (10 mM) calculated for A at 480 nm, AC at 540 nm, ML at 380 nm, BPG at 570 nm, PG at 420 nm, PV at 520 nm.

Indicators	**4.2**(*S,S*)	**4.4**(*R,R,R,S*)	**4.6**(*S*)	**4.8**(*S*)
A	0.033	0.019	0.01	0.038
AC	0.091	0.048	0.041	0.014
BPG	0.237	0.041	0.095	0.139
ML	0.064	0.053	0.066	0.039
PG	0.052	0.028	0.042	0.021
PV	0.083	0.026	0.032	0.007

4.2.6 Brief Description of ANN

Before describing the creation of our training plate, we start with a brief description of ANNs. ANN-based approaches have advantages that include a capacity to self-learn and to model complex data without the need for a detailed understanding of the underlying phenomena. There are many types of neural networks for various applications available in the literature. Multilayered Perceptron (MLP) is the simplest, and the most commonly used neural network with a feed-forward topology. In this study a simple three layered MLP network is utilized (**Figure 4.55**).[46, 52-54]

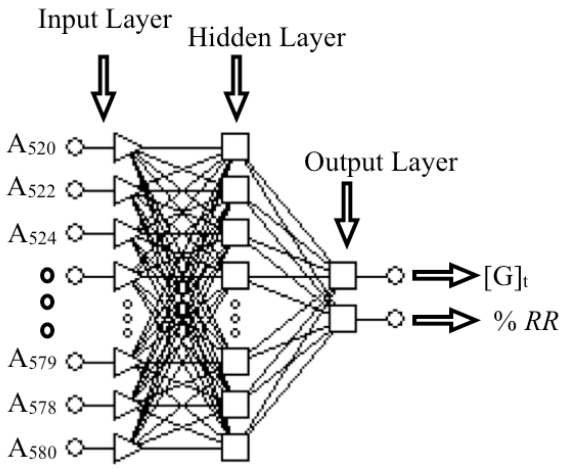

Figure 4.55. Three layered Multilayered Perceptron Artificial Neural Network, analyte concentration ($[G]_t$), percentage of (*R,R*)-hydrobenzoin (% *RR*).

The first layer is the input layer, which in our case contains absorbance values of several different solutions. The data in the input layer is transferred through a set of weighted connections to the second layer, called the hidden layer. The hidden layer is

made up of several processing units. Each processing unit computes the weighted sum of its inputs as shown below for unit j:

$$S_j = \sum_{i=0}^{j-1} a_i w_{ij}$$

where i represents unit in the pervious layer, a_i is the output of unit i, w_{ij} is the weight connecting it to unit j, and S_j is the weighted sum of its input.

Within the processing unit the weighted sum are passed through a sigmoidal "squashing function" as shown below:

$$\sigma(S_j) = \frac{1}{[1+\exp(-S_j)]}$$

The use of the sigmoidal function is to enable the network to be more adaptable, so as to need fewer hidden units to fit the data. The output of each unit in the hidden layer then passes to each unit of the next layer, which in this current study is the output layer ($[G]_t$, %*RR*). The output layer also sums and squashes its weighted inputs. Supervised training of a network consists of adjusting the weights to minimize disagreement between the outputs of the network and the desired output of the training set. The MLP network in this study is trained with back propagation algorithm, where the weights are optimized by minimizing the sum of squared differences between the desired and the actual values of the processing unit.

$$E = \frac{1}{2} \sum_j (y_{dj} - y_j)^2$$

where y_{dj} is the desired value of the output of the processing unit j and y_j is the actual output of that unit. Several training iterations are carried out until a satisfactory small value of error (E) is obtained.

4.2.7 Training the ANN (Step3)

The third step of our protocol calls for the training of an ANN. The results from the screening plate revealed that the enantiomers of host-**4.2** with BPG were the best pair for enantiomeric discrimination of hydrobenzoin. Therefore three training plates with three hosts (host-**4.1**, host (*S,S*)-**4.2** and host (*R,R*)-**4.2**) were made, all using BPG as the indicator. Two enantiomers of host-**4.2** were used in the assay as they are cross reactive, meaning their responses are equal and opposite to the change in *ee* of the analyte. For example host (*S,S*)-**4.2** is selective towards (*S,S*)-hydrobenzoin over (*R,R*)-hydrobenzoin, while host (*R,R*)-**4.2** is selective towards (*R,R*)-hydrobenzoin over (*S,S*)-hydrobenzoin, and from our previous studies we know that cross reactivity enhances the accuracy of the assay.[41] A training set consisting of eleven *ee* values (1, 0.8, 0.6, 0.4, 0.2, 0, -0.2, -0.4, -0.6, -0.8, -1), created at four different total concentrations of hydrobenzoin (2 mM, 4 mM, 6 mM, 10 mM), for each host, thereby generating a total of 44 cases. As host-**4.1** is achiral, it responds only to the change in concentration of the analyte while, host (*S,S*)-**4.2** and host (*R,R*)-**4.2** responds to both the change in concentration, as well as the change in *ee* of the analyte. The absorbance values at 570 nm recorded by a 96-well plate reader for the concentrations and *ee* values of hydrobenzoin described above are shown in **Figure 4.56**. As observed the absorbance values of the two enantiomeric host for the two enantiomeric complexes is not equal (i.e. the absorbance value of host (*S,S*)-**4.2** with (*R,R*) hydrobenzoin differs from the absorbance value of host (*R,R*)-**4.2** with (*S,S*) hydrobenzoin at utmost ±0.03 Abs). This loss in accuracy is due to the use of a 96-well plate and the robotic plate loader. Therefore by using both enantiomers of host-**4.2** we are able to cover this error in the analysis.

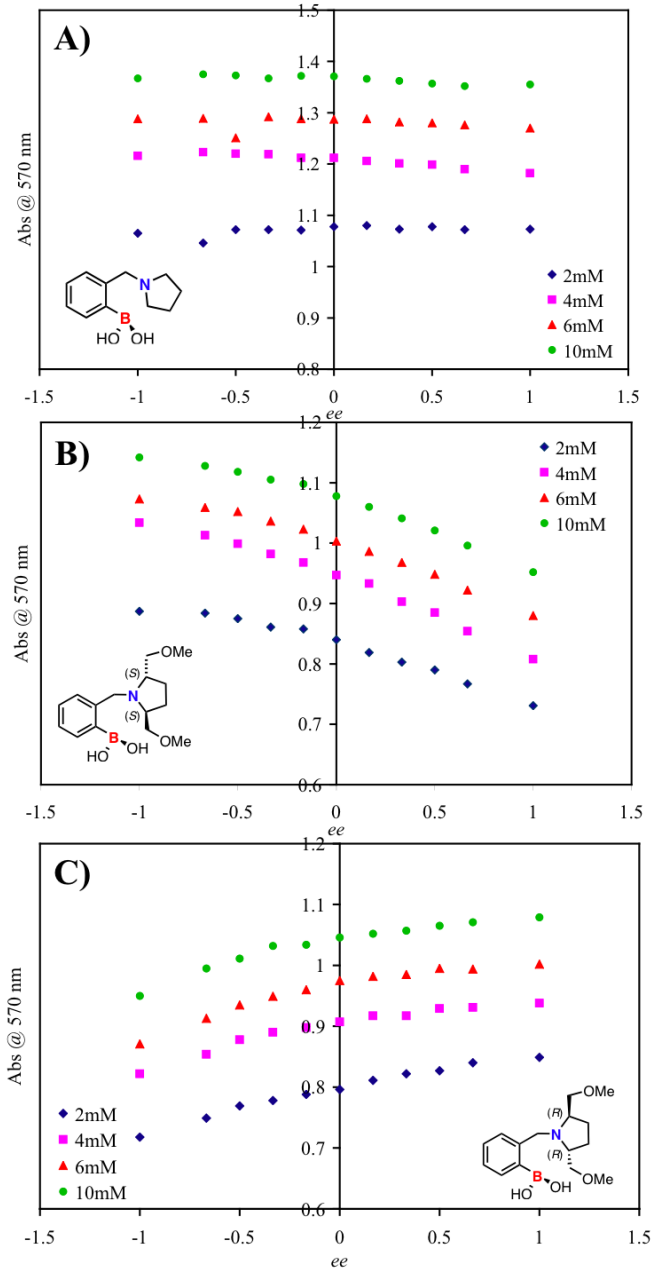

Figure 4.56. ANN training set, *ee* titration at 570 nm of (**A**) host-**1** (1200 μM) and BPG (60 μM), (**B**) host (*S,S*)-**4.2** (200 μM) with BPG (60 μM), and (**C**) host (*R,R*)-**4.2** (200 μM) with BPG (60 μM) at four different concentrations of hydrobenzoin (2 mM, 4 mM, 6 mM, 10 mM). All solution were made in 100% MeOH, 10 mM *para*-toluenesulfonic acid, and Hunig's base buffer, pH = 7.4. All measurements were taken at 25°C.

The data from these *ee* titrations was used as a training set for the development of an ANN.[55] The Statistica Neural Networks program has an embedded intelligent problem solver (IPS) function, which automatically generates several neural networks that are suitable for the designated problem. The input layer contains the absorbance of each *ee* titrations from 540-580 nm at an interval of 2 nm thus a total of 21 absorbance values. Multiple wavelengths were used to increase the accuracy of the analysis (i.e when only one wavelength was used in the analysis of unknown samples the error in $[G]_t$ and *ee* of unknown samples was ± 0.89 and 6.49% respectively). The wavelength range recorded for each host making a total of 63 absorbance values for each of the 44 cases that differ in *ee* and $[G]_t$. The outputs were total guest concentration $[G]_t$ and percentage of (*R*,*R*)-hydrobenzoin (%*RR*). As ANN does not work well with negative values, %*RR* was used instead of *ee* in the neural network. A three layered MLP network with 63 inputs, 46 hidden units and 2 outputs was used for the current study. Its selection was based upon both its performance rating and our experience with the MLP type of neural networks.[56,57]

Final Analysis Step 4 and 5: An analysis plate was made where unknown samples with varying *ee* and $[G]_t$ values were tested. Sixteen unknown samples were made completely independently, and their $[G]_t$ and *ee* values were not included in the training set. The unknown samples were placed in the same plate as the training set as shown in **Figure 4.57** to speed up the analysis. The absorbance values of the unknown samples were entered in the network and the network predicted $[G]_t$ and % *RR* of the unknown sample. % *RR* predicted by ANN is then converted into *ee*, which is reported in **Table 4.5**. The total time from sample preparation to prediction of *ee* and $[G]_t$ for the 16 unknown samples was ~ 32min. The error was calculated in the form of average absolute error and was determined to be ± 0.17 mM for $[G]_t$ in the range of 3mM to 8 mM and ± 3.5% for *ee*.

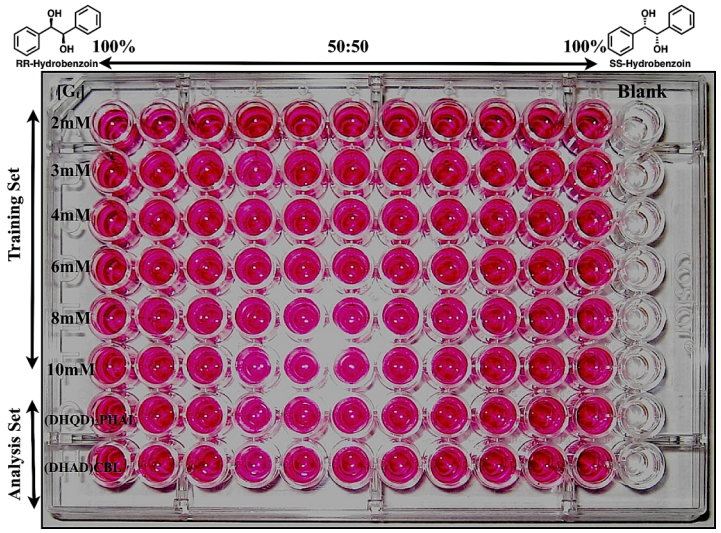

Figure 4.57: Layout of the training/ analysis plate, solvent 100% methanol, pH 7.4, 10 mM buffer (*para*-toluenesulfonic acid and Hunig's base), analyte (*R,R*)-hydrobenzoin and (*S,S*)-hydrobenzoin, host (*S,S*)-**2** (200 μM), BPG (60 μM).

Table 4.5. Determination of *ee* and $[G]_t$ of 16 unknown samples of hydrobenzoin. Average Absolute Error = (|Actual value|- |Experimental value|)

$[G]_t$ (mM)	ANN $[G]_t$ (mM)	Absolute Error $[G]_t$	*ee* (%)	ANN *ee* (%)	Absolute Error *ee* (%)
3.00	2.72	0.28	58.30	60.84	2.54
3.00	3.05	0.05	41.66	44.34	2.68
3.00	2.96	0.04	25.00	24.24	0.76
3.00	2.71	0.29	8.34	-3.20	5.14
3.00	2.99	0.01	-8.34	-14.12	5.78
3.00	3.11	0.11	-25.00	-30.00	5.00
3.00	2.80	0.20	-41.66	-39.04	2.62
3.00	2.92	0.08	-58.34	-52.86	5.48
8.00	7.92	0.08	58.30	54.94	3.36
8.00	7.93	0.07	41.66	33.52	8.14
8.00	8.07	0.07	25.00	21.92	3.08
8.00	8.23	0.23	8.34	4.18	4.16
8.00	8.48	0.48	-8.34	-9.44	1.10
8.00	8.05	0.05	-25.00	-24.18	0.82
8.00	8.07	0.07	-41.66	-38.48	3.18
8.00	8.59	0.59	-58.34	-60.96	2.62

4.2.8 Analysis of a Catalytic Asymmetric Dihydroxylation (Application of Steps 4 and 5)

Encouraged by the extremely high accuracy of our HTS protocol for the *ee* values of hydrobenzoin, we decided to test the method on an actual asymmetric reaction. Because our analysis was designed for a chiral diol, we naturally turned to the Sharpless dihydroxylation reaction.

Two different commercially available cinchona alkaloids ligands, hydroquinidine 1,4-phthalazinediyl diether $(DHQD)_2PHAL$ and hydroquinidine 4-chlorobenzoate (DHAD)CLB were examined (**Figure 4.58**). The literature reports that the reaction of *trans*- stilbene with $(DHQD)_2PHAL$ gives (*R*,*R*)-hydrobenzoin in 89% yield and 95% *ee* and the reaction of *trans*-stilbene with (DHAD)CLB also give (*R*,*R*)-hydrobenzoin but in a 89% yield and 85% *ee* before recrystallization.[47, 49]

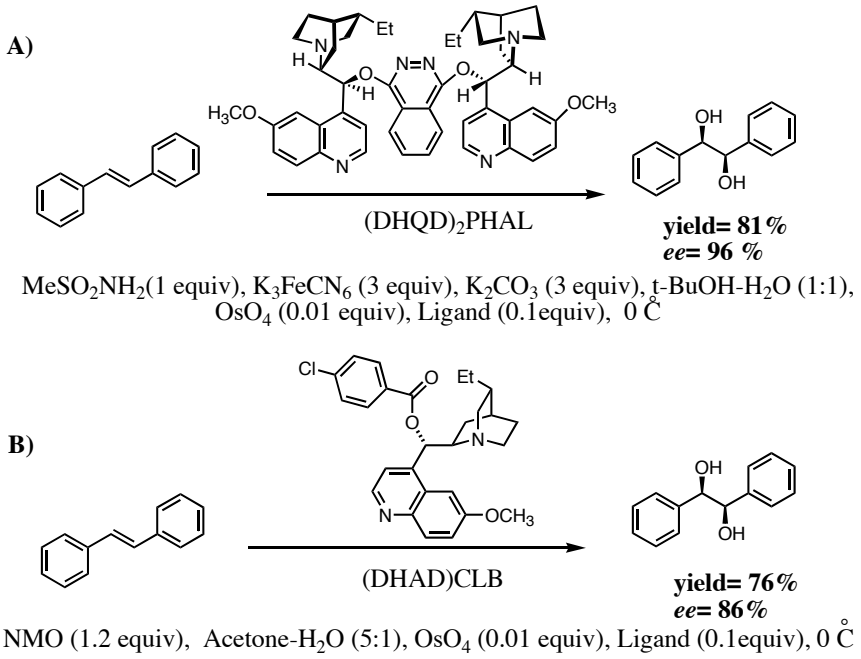

Figure 4.58. Asymmetric dihydroxylation of *trans*-stilbene with two cinchona alkaloids **A**) $(DHQD)_2PHAL$, **B**) (DHAD)CLB.

Prior to using the analyte from Sharpless asymmetric dihydroxylation reactions in the 96-well plate analysis, we wanted to verify the literature reported *ee* values of the reactions as a control. James, *et al*. has recently developed a three-component derivatization protocol for the determination of enantiomeric excess of chiral diols [58] using 1.0 equiv of racemic diol, 1.0 equiv of 2-formylphenylboronic acid, and 1.0 equiv. of (*R*)-(α)-methylamine were dissolved in $CDCl_3$ with 4 Å molecular sieves, and the ^1H NMR spectra of an aliquot acquired after 5 min was recorded. The resulting ^1H NMR revealed that a 50:50 mixture of the two diastereomers (*S*,*S*,*R*)-complex and (*R*,*R*,*R*)-complex (**Figure 4.59**). The comparison of the relative intensities of two different set of integrals of the ^1H NMR was used to accurately confirm the enantiopurity of the diol. The asymmetric dihydroxylation reactions with the two chinconoid ligand were analyzed by this method and their *ee* were determined to be 96% *ee* with $(DHQD)_2PHAL$ and 86%*ee* with (DHAD)CLB, similar to the literature values of 95% and 85% *ee*. With a confidant *ee* value in hand, we turned to testing of optical HTS-method.

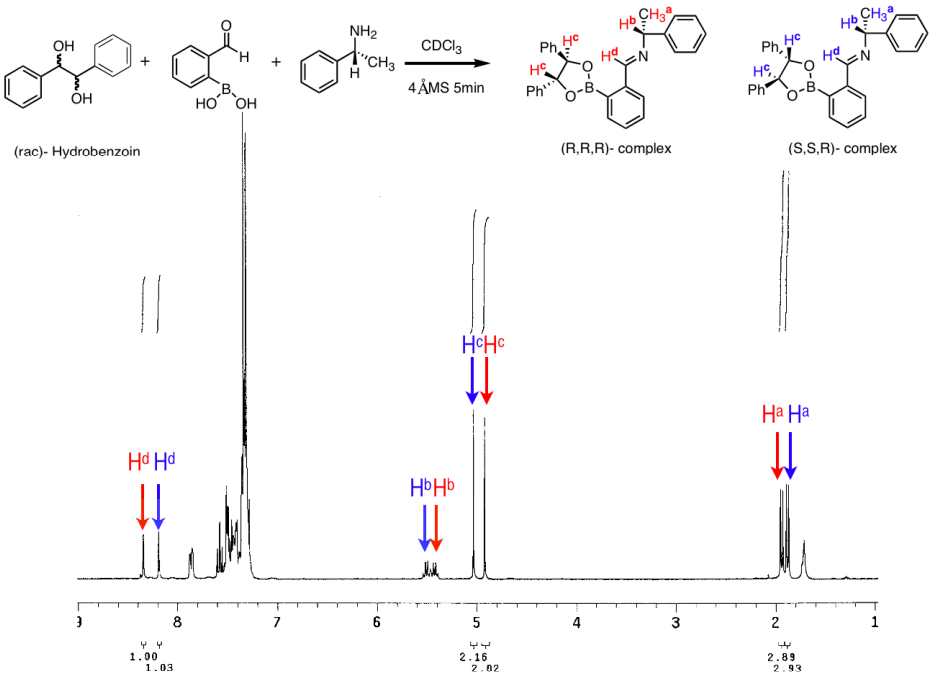

Figure 4.59. ^{1}H NMR 300 MHz on a Varian Mercury 300 spectrometer in $CDCl_3$ of the racemic mixture of hydrobenzoin after derivatization.

In addition to the analysis of the Sharpless reactions using our optical method, we desired to test an expanded training set that covers more concentration values as a means of lowering the error in $[G]_t$ and *ee* determination, and increase the reliability of the network which is directly related to the number of processing units in the hidden layer. Eleven *ee* values (1, 0.8, 0.6, 0.4, 0.2, 0, -0.2, -0.4, -0.6, -0.8, -1) at six different concentrations (2 mM, 3 mM, 4 mM, 6 mM, 8 mM, 10 mM) were placed in the 96-well plate with host-1, host (*S,S*)-**4.2**, and host (*R,R*)-**4.2** using BPG as the indicator; making a total of 66 training cases for the network (**Figure 4.60**). With the help of Statistica Neural Network Software a three layered MLP network was created with 166 inputs per each of the 66 training cases (absorbance values of each host from 550 nm to 600 nm at an interval of 1 nm), giving 35 processing units and 2 outputs (% *RR*, $[G]_t$). As predicted,

the number of processing units is significantly lower in this network as compared to the network generated before.

Asymmetric dihydroxylation reactions were performed according to the literature procedure,[47, 49] the products were isolated and dissolved in the MeOH buffer solutions. Two samples of each asymmetric dihydroxylation reaction were made at two different $[G]_t$'s (5 mM, 7 mM). These samples were then evaluated with all the three hosts (host-**4.1**, host (*S,S*)-**4.2**, host (*R,R*)- **4.2**) and BPG, and their absorbance values were analyzed by the MLP network generated. The *ee* and $[G]_t$ values predicted by the network are listed in **Table 4.4**. The $[G]_t$ and *ee* values predicted by the network were in excellent agreement with actual *ee* and $[G]_t$ values. The average absolute error for $[G]_t$ was ± 0.40 mM in the range of 5 mM to 7 mM and for *ee* it was ± 2.38 %. Slightly higher $[G]_t$ error could be due to the fact that the unknown were individually synthesized in lab, and the error may actually reside in the "known values". Thus, using this optical analysis we were able to easily discriminate between the 96% and 86% *ee*. Presumably dozens to hundreds of unknowns could be similarly analyzed in parallel with similar errors.

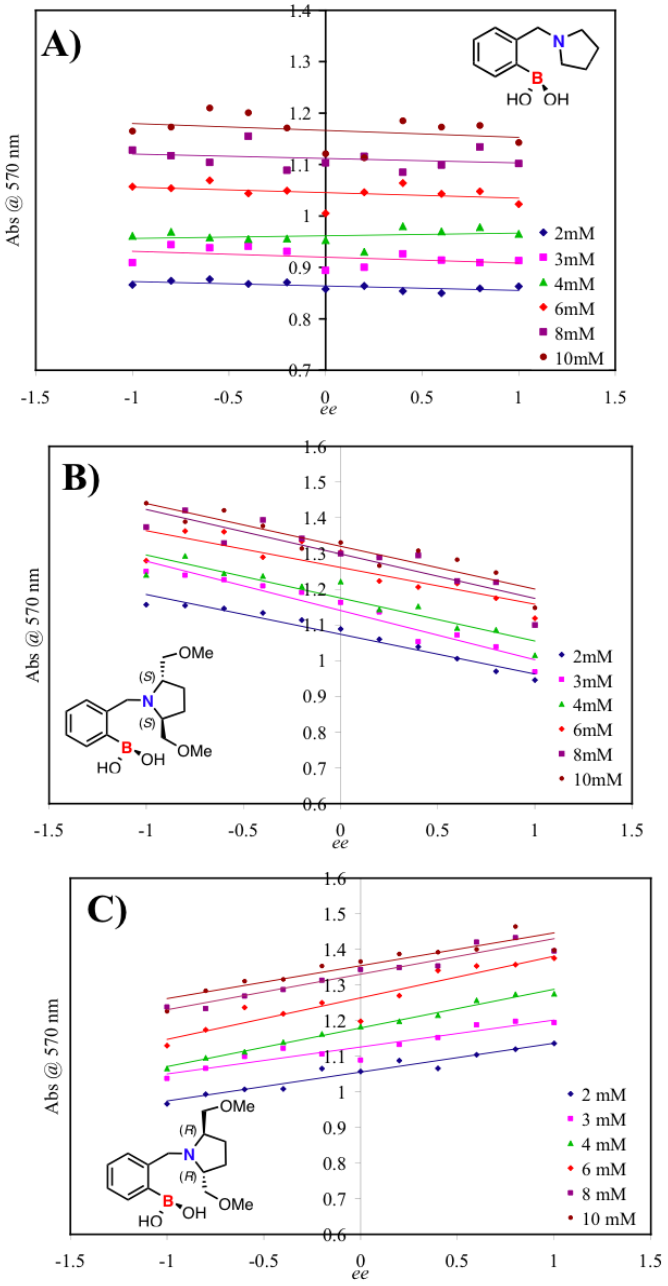

Figure 4.60. ANN training set, *ee* titration at 570 nm of (**A**) host-**4.1** (1200 μM) with BPG (60 μM), (**B**) host (*S,S*)-**4.2** (200 μM) with BPG (60 μM), (**C**) host (*R,R*)-**4.2** (200 μM) with BPG (60 μM) at six different concentrations of hydrobenzoin (2 mM, 3 mM, 4 mM, 6 mM, 8 mM, 10 mM). All solution were made in 100% MeOH, 10 mM *para*-toluenesulfonic acid and Hunig's base buffer, pH = 7.4. All measurements were taken at 25°C.

Table 4.4. Determination of *ee* and $[G]_t$ of Sharpless asymmetric dihydroxylation reaction, * as determined by ^{1}H NMR.

$[G]_t$ (mM)	ANN $[G]_t$ (mM)	Absolute Error $[G]_t$	*ee**(%)	ANN *ee* (%)	Absolute Error *ee*
5.00	4.51	0.49	96	94.44	1.56
7.00	7.09	0.09	96	96.42	0.42
5.00	4.49	0.51	86	93.24	7.24
7.00	6.49	0.51	86	86.28	0.28

4.3 SUMMARY

In summary, we have introduced a step-wise protocol for the creation of high-throughput screening methods using optical analyses in 96-well plates that exploit enantioselective indicator-displacement assays. The first step involves finding the optimal host to indicator ratios, which are set values to be used in any future analysis. The second and third steps are analysis specific, and involve finding the best host/indicator duo for enantiodiscrimination and training an artificial neural network, respectively. The fourth and fifth steps involve analysis plates containing samples of unknown *ee* and $[G]_t$ values and ANN data analysis. The errors in *ee* and $[G]_t$ resulting from the analysis of true unknowns were remarkably low, in the 3.5% range for *ee* and ± 0.17 mM for $[G]_t$. Just to prove the utility of the system for analysis of catalytic reactions, the method developed specifically for hydrobenzoin was used to analyze ligands for the Sharpless asymmetric dihydroxylation reaction, and we confirmed the literature values and even further lowered the errors in *ee* by using a larger training set. This work

expands the scope of enantioselective indicator displacement assays to a complete protocol amenable to HTS.

4.4 EXPERIMENTAL

General Procedure for UV- Vis titrations: UV-Vis measurements were performed on a Beckman DU-640 UV-vis spectrophotomer. pH measurements were performed on an Orion 720Aph meter with a glass electrode. The selected indicators were commercially available. All titrations were done in a 1 cm light path UV-vis quartz semi-micro cell, equipped with a silicon septum, and National Scientific gas-tight syringes were used to transfer solutions. Stock solutions of host, indicator and analytes were made in 10 mM solutions of *para*-toluenesulfonic acid and Hunig's base (*N,N*-diisopropylethylamine) in 100% spectral grade degassed methanol, and the pH of all the solutions were adjusted to 7.4. All measurements were taken at 25 °C.

4.4.1 Determination of K_{HI} Between Boronic Acid Hosts and Selected Indicators

The binding constant K_{HI} of the host to the indicator were calculated by measuring the change in the absorbance of the indicator with the addition of the host. The procedure described here is specifically for the indicator pyrocatechol violet.

Two solutions A and B were prepared. The compositions of the solutions were: solution A, 150 μM PV, and solution B, 150 μM PV, and 1.6 mM boronic acid host (~ 10 equiv of boronic acid host to the indicator). Initially 500 μL of solution A was added to a UV-vis cell, and the change in absorbance of the resulting solution was monitored with addition of solution B to solution A in the cell. In between the absorbance measurement the solution was allowed to equilibrate for 3 minutes. Typically, the

titration was carried out until the change in the absorbance of the resulting solution from one reading to the next was <0.03. The change in absorbance at 520 nm was plotted against the total host concentration and the isotherm was used to solve for 1:1 binding constants K_{HI} by multiple regressions using Origin (Microcal Software, Inc.). The math used to calculate the binding constant K_{HI} using indicator displacement assay is described in detail in our previous publications.[42] All titrations experiment for determing the 1:1 binding constant K_{HI} for all boronic acid hosts to the six selected indicators were carried out in a similar manner, except the concentration of each indicator used was adjusted so that the maximum absorbance from 300-600 nm was in the range of 0.2-1.4 over the course of a titration. The concentration of the indicators and the wavelength at which the 1:1 binding constants were determined were: A (200 μM Abs at 483 nm), AC (200 μM, Abs at 540 nm), BPG (30 μM, Abs at 570 nm), ML (75 μM, Abs at 380 nm) and PG (75 μM, Abs at 420 nm) (**Figure 4.2 –4.45**).

4.4.2 Determination of K_{HG} Between Boronic Acid Hosts and (*R*,*R*) & (*S*,*S*)-Hydrobenzoin

To gage the enantioselectivity of the chiral boronic acid hosts, enantioselective indicator displacement assays were utilized. The binding constant between the host and the analyte K_{HG} was determined by measuring the change in absorbance of the host indicator solution with the addition of the analyte. PV was the selected indicator for this analysis. The procedure described here is for host (*S*)-**4.6** and (*R*,*R*)-hydrobenzoin. The optimum ratio of host (*S*)-**4.6** to PV was used in the enantioselective displacement assay (~ 90% saturation) was determined by using the 1:1 binding isotherm of host (*S*)-**4.6** and PV.

Two solutions, C and D were made. The composition of the two solutions were: solution C 150 μM PV and 400 μM chiral host (*S*)-**4.6**, solution D 150 μM PV, 400 μM host (*S*)-**4.6** and 15 mM (*R*,*R*)-hydrobenzoin. The UV-vis titration was carried out with these two solutions in the similar manner as described above. To determine $K_{HG(S,S)}$ of host (*S*)-**6** with (*S*,*S*)-hydrobenzoin another titration was performed with (*S*,*S*)-hydrobenzoin. Similarly, the binding constant $K_{HG(R,R)}$ and $K_{HG(S,S)}$ between all the enantioselective host and (*R*,*R*)-hydrobenzoin and (*S*,*S*)-hydrobenzoin were determined, except the ratio of the host to the indicator (PV) was different in each case (**Figure 4.46 – 4.53).**

4.4.3 96-well Plate Analysis

Arrays were made by mixing hosts, indicators and analyte stock solutions within a Costar EIA/RIA polystyrene 96-well flat bottom plates. Absorbance spectra were recorded at ambient temperature on a BioTek Synergy™ 4 multi-detection microplate reader. BioTek Precision™ microplate pipetting system was used to add stock solution to the 96-well plate. Each well contained a total solution volume of 300 μL. After making the plate, it was sealed with a UC-500 sealing film to prevent solvent evaporation.

Screening Plate

Two different screening plates are designed at two different analyte (hydrobenzoin) concentrations 5 mM and 10 mM. The architecture of the screening plate was described in detail in Figure **4.54**. One enantiomer of the chiral host was analyzed in the screening plate, and the optimum ratios (~ 90% saturation) of each chiral host with each indicator were added in the 96-well plate (**Table 4.7**). 100% (*R*,*R*)-hydrobenzoin, racemic mixture of the two enantiomers, and 100% (*S*,*S*)-hydrobenzoin were added to

each combination. The plate is sealed with the sealing film and the absorbance spectra was recorded and analyzed.

Training/ Analysis Plate

The training and the analysis set for each host was combined together on one plate to speed up the analysis. The indicator used for this analysis was BPG and the concentration of the indicator was fixed at (60 μM) so that the maximum absorbance from 500-600 nm was in the range of 0.4-1.5. Three training /analysis plate were designed. First with host-**4.1** / BPG, second for host (*S*,*S*)-**4.2** / BPG and third for host (*R*,*R*)-**4.2** /BPG . The optimum ratio (~ 90% saturation) of the each host to the indicator was used in this assay as defined by their 1:1 binding isotherms (**Table 4.7**).

The procedure described here is for host (*S,S*)-**4.2** and BPG, the architecture of this training/analysis plate was described in detail in **Figure 4.60**. Host (*S,S*)-**4.2** (200 μM) and BPG (60 μM) was added to all the wells on the plate. The first four rows were the training set and the last two rows were the analysis set. The layout for the training set was such that the concentration of the analyte (*R*,*R*)-hydrobenzoin and (*S*,*S*)-hydrobenzoin would vary along each row of the plate while the *ee* of the solution, varied from (1) to (-1), where 1 is 100% (*R*,*R*)-hydrobenzoin and (-1) is 100% (*S*,*S*)-hydrobenzoin, along the columns. The last two rows contained the analysis set, which were the solutions with unknown concentrations and *ee*'s of analyte. The plate was sealed with a sealing film to prevent solvent evaporation and the absorbance spectra were recorded. The procedure was repeated for host (*R,R*)-**4.2** and host-**4.1**.

Table 4.7: The concentration of the indicators and the boronic acid host used in the 96-well plate analysis. The concentration of the indicators depends on the purity of the commercially available indicator.

Indicators	**4.1**	**4.2**(*S*,*S*)	**4.4**(*R*,*R*,*R*,*S*)	**4.6**(*S*)	**4.8**(*S*)
A (200 μM)	500 μM	400 μM	400 μM	300 μM	300 μM
AC (200 μM)	400 μM	300 μM	300 μM	400 μM	200 μM
BPG (60 μM)	1200 μM	200 μM	400 μM	200 μM	200 μM
ML (125 μM)	1170 μM	300 μM	500 μM	300 μM	300 μM
PG (75 μM)	500 μM	300 μM	400 μM	100 μM	500 μM
PV (150 μM)	700 μM	300 μM	500 μM	400 μM	400 μM

4.4.4 NMR Analysis of the Enantiomeric Purity of Hydrobenzoin

2-Formylphenylboronic acid (14.9 mg, 0.1 mole) and (*R*)-α methylbenzylamine (12.7 μL, 0.1 mole) was dissolved in $CDCl_3$ (1 mL), in a dry glass vial equipped with a few 4 Å molecular sieves. (21.4 mg, 0.1 mole) of the diol (hydrobenzoin) obtained from asymmetric dihydroxylation reactions was added to the solution. The mixture was allowed to stand with occasional shaking for 5 min. ^{1}H NMR of the resulting solution was recorded (**Figure 4.59**).

4.4.5 Synthesis of the Boronic Acid Hosts

Boronic acid hosts **4.1**-**4.8** were synthesized by reductive amination according to the established literature procedure.[37] ^{1}H NMR spectra were recorded at 300 MHz on a

Varian Mercury 300 spectrometer in CD_3OD. ^{13}C NMR spectra were recorded at 500 MHz on a Varian Mercury 500 spectrometer in DMSO–d_6.

Host (*S*,*S*)-**5** was synthesized in two steps. 2-Acetylphenylboronic acid (163.97 mg, 1 mM) and the (*S*)α-methyl benzylamine (228.7 μL, 1 mM) was dissolved in toluene (5 mL). The resulting mixture was allowed to stir overnight under reflux using a dean stark apparatus. The solvent was removed from the reaction mixture under vacuo and the imine was isolated as a yellow solid. The imine was re-dissolved in anhydrous methanol (5 mL) and the solution was cooled to 0°C, $NaBH_4$ (56.46 mg, 1.5 mmol) was added to the solution at 0°C, the resulting mixture and was allowed to stir vigorously at 0°C for 2 hr. After 2 hr the solvent was removed under vacuum followed by the addition of CH_2Cl_2 (25 mL). The resulting white precipitate was removed by vacuum filtration, and the filtrate was concentrated to give the crude product as a yellow oil. The yellow oil was further purified, using neutral alumina flash chromatography (0-2% MeOH in CH_2Cl_2). The product was isolated as a white powder, with a diastereomeric ratio (dr) of 1 : 4. The overall yield of the reaction was 70%.

Host (*R*)-**4.3**: mp 77 - 84 °C. ^1H NMR (300 MHz, CD_3OD) δ 7.53-7.38 (m, 6H), 7.23-7.02 (m, 2H), 7.01 (d, J = 7.0 Hz, 1H), 4.27 (q, J = 6.8 Hz, 1H), 3.84 (d, J = 13.6 Hz, 1H), 3.68 (d, J = 13.2 Hz, 1H),) 1.68 (d, J = 6.8Hz, 3H). ^{13}C NMR (125 MHz, DMSO) δ 149.60, 144.36, 136.42, 129.34, 128.42, 128.18, 127.13, 126.46, 125.76, 122.27, 51.26, 48.66, 19.62. HRMS calculated (M+H) calc 256.1509 found 256.1511.

Host (*R*,*R*,*R*,*S*)- **4.4**: mp 77 - 83 °C. ^1H NMR (300 MHz, CD_3OD) δ 7.64 (d, 7.69 Hz 1H), 7.27-7.16 (m, 3H), 4.21 (s, 2H), 3.43-3.40 (m, 1H), 2.58 (m, 1H), 2.47 (m, 1H), 2.19 (m, 1H), 2.05 (m, 3H), 1.29 (d, J = 7.48 Hz, 6 H), 1.15 (d, J = 10 Hz, 1H), 1.01 (s, 1H). ^{13}C

NMR (125 MHz, DMSO) δ 149.78, 136.56, 129.13, 127.98, 125.69, 122.38, 50.62, 47.35, 41.54, 40.83, 38.14, 33.95, 33.02, 27.99, 23.29, 20.43.HRMS calculated (M +H) 288.2131 found 288.2696.

Host (*S*,*S*)-**4.5**: mp 73 - 76 °C. ^{1}H NMR (300 MHz, CD_3OD) δ 7.54-7.06 (m, 9 H), 4.41 (q, J = 6.5Hz, 1H), 4.27 (q, J = 6.8 Hz, 1H), 1.55 (d, J = 6.8 Hz 3H), 1.27 (d, J = 6.8 Hz 3 Hz). ^{13}C NMR (125 MHz, DMSO) δ 155.15, 146.29, 129.27, 128.37, 128.09, 126.19, 125.85, 121.67, 57.45, 52.52, 22.10, 20.38. HRMS calculated (M+H) 270.1665 found 270.1663.

Host (*S*)-**4.6**: mp 64 - 66 °C. ^{1}H NMR (300 MHz, CD_3OD) δ 7.52-7.13 (m, 14H), 4.20 (m, 1H), 4.05 (m, 1H), 3.87 (m, 2H), 3.65 (m, 1H), 1.64 (d, J = 7.0 Hz 3H). ^{13}C NMR (125 MHz, DMSO) δ 142.16, 140.46, 138.44, 136.12, 134.48, 129.74, 129.19, 128.85, 128.39, 128.10, 127.99, 127.09, 126.87, 126.28, 56.75, 55.23, 52.90, 14.02. HRMS calculated. (M+H) 346.1978 found 346.1984.

Host (*R*)-**4.6**: mp 67 - 71 °C. ^{1}H NMR (300 MHz, CD_3OD) δ 7.53-7.13 (m, 14H), 4.18 (m, 1H), 4.05 (m, 1H), 3.99 (m, 2H), 3.64 (m, 1H), 1.62 (d, J = 7.0 Hz 3H). ^{13}C NMR (125 MHz, DMSO) δ 142.16, 140.45, 138.43, 136.14, 134.49, 129.74, 129.20, 128.85, 128.39, 128.10, 127.99, 127.09, 126.87, 126.28, 56.75, 55.23, 52.90, 14.02. HRMS calculated. (M+H) 346.1978 found 346.1982.

Host (*R*)-**4.7**: mp 120 - 122 °C. ^{1}H NMR (300 MHz, CD_3OD) δ 7.50-7.35 (m, 6H), 7.21-7.09 (m, 2H), 6.98 (d, J = 7.4 Hz, 1H), 4.43 (q, J = 6.9 Hz, 1H), 3.80 (d, J = 11.3 Hz, 1H), 3.66 (d, J = 13.5 Hz, 1H), 1.98 (s, 3H) 1.66 (d, J = 6.7Hz, 3H). ^{13}C NMR (125 MHz,

DMSO) δ 142.06, 140.61, 136.09, 135.38, 130.08, 129.33, 128.15, 128.06, 127.26, 126.65, 61.13, 60.14, 35.30, 16.07. (M+H) calc 270.1665 found 270.1667.

Host (*S*)-**4.8**: mp 67 - 69 °C. ^{1}H NMR (300 MHz, CD_3OD) δ 7.63 (d, J = 6.6 Hz 1H), 7.26-7.17 (m, 3H), 4.25 (d, J = 12.3 Hz 1H), 4.10 (d, J = 12 Hz 1H), 3.08-3.05 (m, 1H), 1.85-1.64 (m, 6H), 1.41-1.13 (m, 8H). ^{13}C NMR (125 MHz, DMSO) δ 149.82, 136.66, 129.22, 127.91, 125.66, 122.24, 52.40, 47.61, 41.22, 30.19, 29.90, 26.04, 2.71, 25.61, 18.41. HRMS calculated. (M+H) 262.1978 found 2.62.1984.

Host (*R*)-**4.8**: mp 62 - 65 °C. ^{1}H NMR (300 MHz, CD_3OD) δ 7.62 (d, J = 7.7 Hz 1H), 7.24-7.15 (m, 3H), 4.24 (d, J = 12.3 Hz 1H), 4.09 (d, J = 12.3 1H), 3.07 (m, 1H), 1.85-1.68 (m, 6H), 1.36-1.13 (m, 8H). ^{13}C NMR (125 MHz, DMSO) δ 149.78, 136.66, 129.16, 127.87, 125.62, 122.20, 52.38, 47.64, 41.21, 30.14, 29.86, 26.01, 25.74, 25.57, 18.35. HRMS calculated. (M+H) 262.1978 found 262.198.

4.5 REFERENCES FOR CHAPTER 4

1. Jaroch, S.; Weinmann, H.; Zietler, K., Asymmetric Organocatalysis. *Chem. Med. Chem.* **2007,** 2, 1261-1264.

2. Hoveyda, A. H., Catalyst discovery through combinatorial chemistry. *Chem. Biol.* **1998,** 5, (8), R187-R191.

3. Ding, K.; Du, H.; Yuan, Y.; Long, J., Combinatorial chemistry approach to chiral catalyst engineering and screening: Rational design and serendipity. *Chem. Eur. J.* **2004,** 10, (12), 2872-2884.

4. Traverse, J. F.; Snapper, M. L., High-throughput methods for the development of new catalytic asymmetric reactions. *Drug. Discovery. Today.* **2002,** 7, (19), 1002-1012.

5. Stambuli James, P.; Hartwig John, F., Recent advances in the discovery of organometallic catalysts using high-throughput screening assays. *Curr. Opin. Chem. Biol.* **2003,** 7, (3), 420-6.

6. Reetz, M. T.; Zonta, A.; Schimossek, K.; Leibeton, K.; Jaeger, K.-E., Creation of Enantioselective Biocatalysts for Organic Chemistry by In Vitro Evolution. *Angew. Chem., Int. Ed. Engl.* **1997,** 36, 2830-2832.

7. Mikami, K.; Angelaud, R.; Ding, K.; Ishii, A.; Tanaka, A.; Sawada, N.; Kudo, K.; Senda, M., Asymmetric activation of chiral alkoxyzinc catalysts by chiral nitrogen activators for dialkylzinc addition to aldehydes: super high-throughput screening of combinatorial libraries of chiral ligands and activators by HPLC-CD/UV and HPLC-OR/RIU systems. *Chem. Eur. J.* **2001,** 7, (3), 730-737.

8. Eelkema, R.; van Delden, R. A.; Feringa, B. L., Direct visual detection of the stereoselectivity of a catalytic reaction. *Angew. Chem., Int. Ed.* **2004,** 43, (38), 5013-5016.

9. Walba, D. M.; Eshdat, L.; Korblova, E.; Shao, R.; Clark, N. A., A general method for measurement of enantiomeric excess by using electrooptics in ferroelectric liquid crystals. *Angew. Chem., Int. Ed.* **2007,** 46, (9), 1473-1475.

10. Reetz, M. T.; Becker, M. H.; Kuhling, K. M.; Holzwarth, A., Time-Resolved IR-Thermographic Detection and Screening of Enantioselectivity in Catalytic Reactions. *Angew. Chem., Int. Ed.* **1998,** 37, 2647-2650.

11. Tielmann, P.; Boese, M.; Luft, M.; Reetz, M. T., A practical high-throughput screening system for enantioselectivity by using FTIR spectroscopy. *Chem. Eur. J.* **2003,** 9, (16), 3882-3887.

12. Ding, K.; Ishii, A.; Mikami, K., Super High Throughput Screening (SHTS) of Chiral ligands and Activators: Asymmetric Activation of Chiral Diol- Zinc Catalyst by Chiral Nitrogen Acitivators for the Enantioselective Addition pf Diethylzinc to Aldehydes. *Angew. Chem., In. Ed.* **1999,** 38, 497-501.

13. Reetz, M. T.; Kuhling, K. M.; Hinrichs, H.; Deege, A., Circular dichroism as a detection method in the screening of enantioselective catalysts. *Chirality.* **2000,** 12, (5/6), 479-482.

14. Reetz, M. T.; Kuhling, K. M.; Deege, A.; Hinrichs, H.; Belder, D., Super-High-Throughput Screening of Enantioselective Catalysts by Using Capillary Array Electrophoresis *Angew. Chem., Int. Ed.* **2000,** 39, 3891-3893.

15. G.Klein; Reymond, J.-L., Enantioselective Fluorogenic Assay of Acetate Hydrolysis for Detecting Lipase Catalytic Antibodies *Helv. Chim. Acta.* **1999,** 82, 400-407.

16. M. Matsushita; Yoshida, K.; Yamamoto, N.; Wirsching, P.; Lerner, R. A.; Janda, K. D., High-Throughput Screening by Using a Blue-Fluorescent Antibody Sensor. *Angew.Chem. Int. Ed.* **2003,** 42, 5984-5987.

17. Guo, J.; Wu, J.; Siuzdak, G.; Finn, M. G., Measurement of Enantiomeric Excess by Kinetic Resolution and Mass Spectrometry. *Angew. Chem., Int. Ed.* **1999,** 38, 1755-1758.

18. Reetz, M. T.; H.Becker, M.; H.-W.Klein; Stockigt, D., A Method for High-Throughput Screening of Enantioselective Catalysts. *Angew. Chem., Int. Ed.* **1999,** 38, 1758-1761.

19. Copelan, G. T.; Miller, S. J., A Chemosensor-Based Approach to Catalyst Discovery in Solution and on Solid Support. *J. Am. Chem. Soc.* **1999,** 121, 4306-4307.

20. Taran, F.; Gauchet, C.; B.Mohar; S.Meunier; A.Valleix; Renard, P. Y.; Grassi, C. C. J.; A.Wagner; Mioskowski, C., High-Throughput Screening of Enantioselective Catalysts by Immunoassay *Angew. Chem., Int. Ed.* **2002,** 41, 124-127.

21. Reetz, M. T.; Eipper, A.; Tielmann, P.; Mynott, R., A practical NMR-based high-throughput assay for screening enantioselective catalysts and biocatalysts. *Adv. Synth. Catal.* **2002,** 344, (9), 1008-1016.

22. P.Abato; C.T.Seto, EMDee: An Enzymatic Method for Determining Enantiomeric Excess. *J. Am. Chem. Soc.* **2001,** 123, 9206-9207.

23. Li, Z.; Buetikofer, L.; Witholt, B., High-throughput measurement of the enantiomeric excess of chiral alcohols by using two enzymes. *Angew. Chem., Int. Ed.* **2004,** 43, (13), 1698-1702.

24. Abato, P.; Seto, C. T., EMDee: An enzymatic method for determining enantiomeric excess. *J. Am. Chem. Soc.* **2001,** 123, (37), 9206-9207.

25. Hamberg, A.; Lundgren, S.; Penhoat, M.; Moberg, C.; Hult, K., High-throughput enzymatic method for enantiomeric excess determination of O-acetylated cyanohydrins. *J. Am. Chem. Soc.* **2006,** 128, (7), 2234-2235.

26. Onaran, M. B.; Seto, C. T., Using a Lipase as a High-Throughput Screening Method for Measuring the Enantiomeric Excess of Allylic Acetates. *J. Org. Chem.* **2003,** 68, (21), 8136-8141.

27. Dey, S.; Karukurichi, K. R.; Shen, W.; Berkowitz, D. B., Double-Cuvette ISES: In Situ Estimation of Enantioselectivity and Relative Rate for Catalyst Screening. *J. Am. Chem. Soc.* **2005,** 127, (24), 8610-8611.

28. Anslyn, E. V., Supramolecular analytical chemistry. *J. Org. Chem.* **2007,** 72, (3), 687-699.

29. Rancke-Madsen, E., *Indicators*. 1st ed.; Pergamon Press: New York, 1972.

30. Piatek, A. M.; Bomble, Y. J.; Wiskur, S. L.; Anslyn, E. V., Threshold detection using indicator-displacement assays: an application in the analysis of malate in pinot noir grapes. *J. Am. Chem. Soc* **2004,** 126, (19), 6072-6077.

31. Nguyen, B. T.; Wiskur, S. L.; Anslyn, E. V., Using Indicator-Displacement Assays in Test Strips and To Follow Reaction Kinetics. *Org. Lett.* **2004,** 6, (15), 2499-2501.

32. Zhang, T.; Anslyn, E. V., Molecular recognition and indicator-displacement assays for phosphoesters. *Tetrahedron.* **2004,** 60, (49), 11117-11124.

33. Nguyen, B. T.; Anslyn, E. V., Indicator-displacement assays. *Coord. Chem. Rev.* **2006,** 250, (23+24), 3118-3127.

34. Zhang, T.; Anslyn, E. V., A colorimetric boronic acid based sensing ensemble for carboxy and phospho sugars. *Org. Lett.* **2006,** 8, (8), 1649-1652.

35. Zhang, T.; Anslyn, E. V., Using an Indicator Displacement Assay to Monitor Glucose Oxidase Activity in Blood Serum. *Org. Lett.* **2007,** 9, (9), 1627-1629.

36. Mei, X.; Wolf, C., Determination of enantiomeric excess and concentration of unprotected amino acids, amines, amino alcohols, and carboxylic acids by competitive binding assays with a chiral scandium complex. *J. Am. Chem. Soc.* **2006,** 128, (41), 13326-13327.

37. Zhu, L.; Anslyn, E. V., Facile quantification of enantiomeric excess and concentration with indicator-displacement assays: An example in the analyses of alpha -hydroxyacids. *J. Am. Chem. Soc.* **2004,** 126, (12), 3676-3677.

38. Folmer-Andersen, J. F.; Lynch, V. M.; Anslyn, E. V., "Naked-eye" detection of histidine by regulation of CuII coordination modes. *Chem. Eur. J.* **2005,** 11, (18), 5319-5326.

39. Folmer-Andersen, J. F.; Lynch, V. M.; Anslyn, E. V., Colorimetric enantiodiscrimination of alpha -amino acids in protic media. *J. Am. Chem. Soc.* **2005,** 127, (22), 7986-7987.

40. Zhu, L.; Zhong, Z.; Anslyn, E. V., Guidelines in implementing enantioselective indicator-displacement assays for alpha -hydroxycarboxylates and diols. *J. Am. Chem. Soc.* **2005,** 127, (12), 4260-4269.

41. Folmer-Andersen, J. F.; Kitamura, M.; Anslyn, E. V., Pattern-based discrimination of enantiomeric and structurally similar amino acids: an optical mimic of the mammalian taste response. *J. Am. Chem. Soc.* **2006,** 128, (17), 5652-5653.

42. Zhu, L.; Shabbir, S. H.; Anslyn, E. V., Two methods for the determination of enantiomeric excess and concentration of a chiral sample with a single spectroscopic measurement. *Chem. Eur. J.* **2007,** 13, (1), 99-104.

43. Anslyn, E. V.; Frantz-folmer-Andersen, J.; Zhu, L. Determining enantiomeric excess using indicator-displacement assays. 2005-36642 2006003459, 20050114., 2006.

44. Gventer, B. Production pattern-recognition artificial neural net (ann) with event-response expert system (es)--yieldshieldtm. 2001-923215 2003028353, 20010806., 2003.

45. Deeb, O.; Hemmateenejad, B., ANN-QSAR model of drug-binding to human serum albumin. *Chem. Biol. Drug Des.* **2007,** 70, (1), 19-29.

46. Burns, J. A.; Whitesides, G. M., Feed-forward neural network in chemistry: mathmatical system for classification and pattern recognition. *Chem. Rev.* **1993,** 93, (8), 2583-2601.

47. Jacobsen, E. N.; Marko, I.; Mungall, W. S.; Schroeder, G.; Sharpless, K. B., Asymmetric dihydroxylation via ligand-accelerated catalysis. *J. Am. Chem. Soc.* **1988,** 110, (6), 1968-70.

48. Walsh, P. J.; Sharpless, K. B., Asymmetric dihydroxylation (AD) of alpha ,beta - unsaturated ketones. *Synlett.* **1993**, (8), 605-6.

49. Siedel, M. C.; Smits, R.; Stark, C. B. W.; Frackenpohl, J.; Gaertzen, O.; Hoffmann, H. M. R., Studies on the asymmetric dihydroxylation of advance bryostatin C-ring. *Synthesis.* **2004,** 9, 1391-1398.

50. Zhong, Z.; Anslyn Eric, V., A colorimetric sensing ensemble for heparin. *J. Am. Chem. Soc.* **2002,** 124, (31), 9014-5.

51. Connors, K. A., *Binding Constant, The Measurment of Molecular Complex Stability*. John Wiley and Sons: New York, 1987.

52. Dayhoff, J. E.; DeLeo, J. M., Artificial neural networks: opening the black box. *Cancer.* **2001,** 91, (8 Suppl), 1615-35.

53. Jansson, P. A., Neural networks an overview. *Anal. Chem.* **1991,** 63, (6), 357A-362A.

54. Konstantinos Petritis, L. J. K., Patrick L. Ferguson, Gordon A. Anderson, Ljiljana Paa-Toli, Mary S. Lipton, Kenneth J. Auberry, Eric F. Strittmatter, Yufeng Shen, Rui Zhao, and Richard D. Smith, Use of Artificial Neural Networks for the Accurate Prediction of Peptide Liquid Chromatography Elution Times in Proteome Analyses. *Anal. Chem.* **2003,** 75, (5), 1039 - 1048;.

55. StatSoft, I. *StatSoft, Inc*.

56. McCleskey, S. C.; Floriano, P. N.; Wiskur, S. L.; Anslyn, E. V.; McDevitt, J. T., Citrate and calcium determination in flavored vodkas using artificial neural networks. *Tetrahedron* **2003,** 59, (50), 10089-10092.

57. Wiskur, S. L.; Floriano, P. N.; Anslyn, E. V.; McDevitt, J. T., A multicomponent sensing ensemble in solution: Differentiation between structurally similar analytes. *Angew. Chem., Int. Ed.* **2003,** 42, (18), 2070-2072.

58. Kelly, A. M.; Perez-Fuertes, Y.; Arimori, S.; Bull, S. D.; James, T. D., Simple protocol for NMR analysis of the enantiomeric purity of diols. *Org. Lett.* **2006,** 8, (10), 1971-1974.

Chapter 5: Pattern-Based Recognition for the Rapid Determination of Identity, Concentration, and Enantiomeric Excess of Subtly Different Diols

5.1 PATTERN RECOGNITION SENSOR ARRAY

Animals are constantly surveying via their olfactory system, the external environment for chemicals that indicate food sources and habitats, as well as chemical signals controlling social interactions and reproductive behavior.[1] The olfactory system involves a broad pattern recognition protocol where the detectors/sensors generate a pattern that is recognized and classified by the brain.[2] Inspired by the olfactory system, the use of multivariate data analysis combined with sensors with partially overlapping selectivity has become a powerful tool in the field of molecular recognition. [3-17]

In an analogous fashion, a novel optical recognition scheme is described here for the rapid determination of the identity, enantiomeric excess (*ee*), and concentration ($[G]_t$) of chiral vicinal diols of close structural similarity. The sensor array used involved differential receptors and signaling units. The differential receptors were chiral boronic acids, which are responsible for the sensor's chemoselective and enantioselective discriminatory properties. The signaling relies upon indicator displacement assays (IDAs) to provide a colorimetric response. The assay was developed by using combinations of three differential receptors and three different indicators within a single array, which resulted in finger printing of each diol analyzed.

Indicator displacement assays rely on colorimetric or fluorescence indicators that reversibly interact with a receptor and upon binding to the receptor change their optical properties. A competition between the analyte and the indicator for the binding site of the

receptor generates an equilibrium in solution that can be monitored optically and related to $[G]_t$.[18] Our group has pioneered the development of enantioselective indicator displacement assays that utilize a chiral receptor where the color change is related to *ee* and $[G]_t$.[19, 20]

The data generated by each sensor array was processed by supervised and non-supervised pattern recognition algorithms. A major unsupervised technique is principle component analysis (PCA), while artificial neural network (ANN) is a supervised technique. PCA reduces multidimensional and partly correlated data to two, three or more dimensions. This is achieved by projecting the data onto fewer dimensions that represent variance relationships between variables.[21] ANN programs are based on a simplified model of the brain. ANN requires a training set that consists of a collection of known parameters. The training set creates a neural network suitable for the analysis in hand. This network is then used to analyze unknown samples.[22, 23]

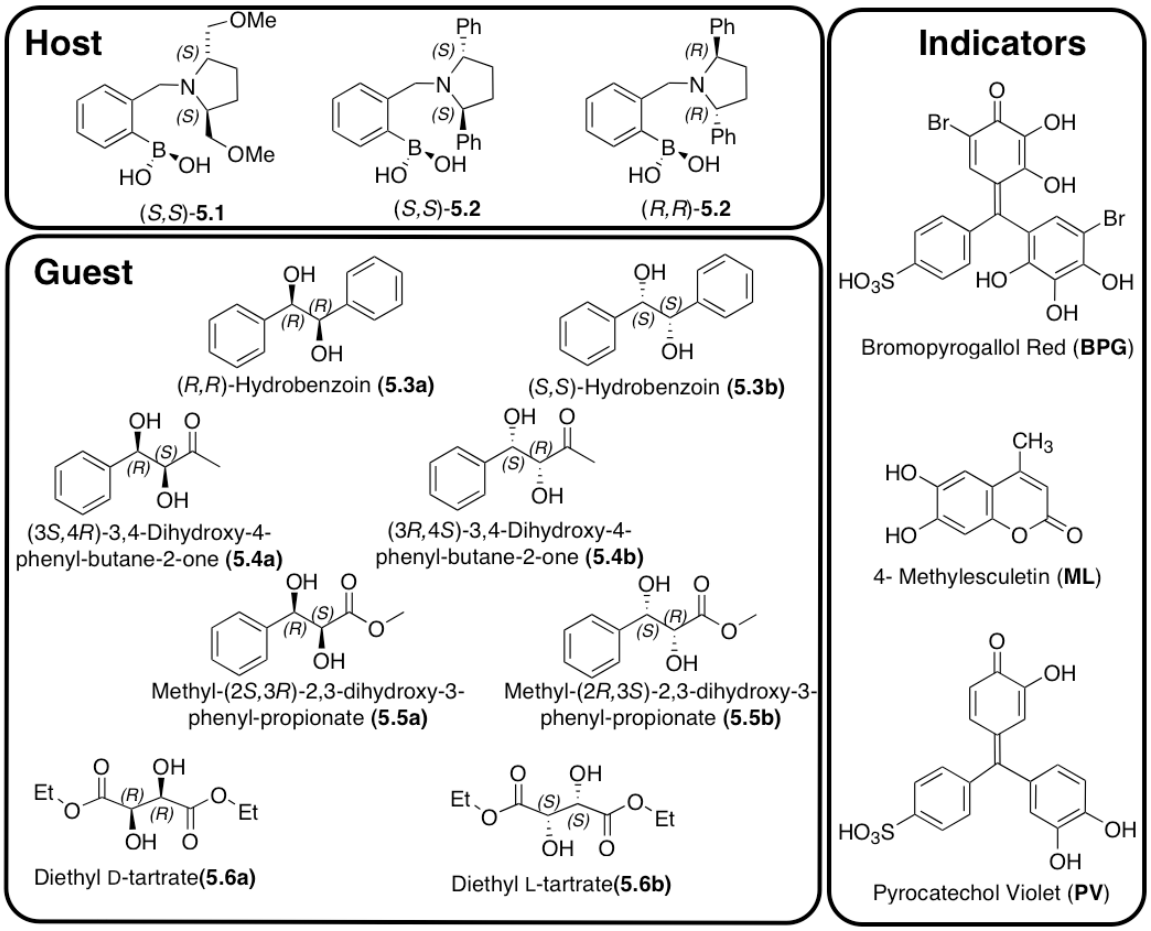

Scheme 5.1. Structures of hosts, guests/analyte and indicators used in this study.

To demonstrate the ability to distinguish chirality as well chemical identity, diols **5.3-5.6** were selected as analytes (**Scheme 5.1**). Analyte **5.3** has two phenyl groups, in contrast to **5.4** and **5.5**. Analyte **5.4** and **5.5** differ in a ketone relative to an ester, respectively. Lastly, analyte **5.6** has two esters. Hence, we are challenging our array approach by using four analytes and their enantiomers all possessing electron withdrawing groups of only subtle difference.

Our previous studies have shown that the use of cross-reactive sensors in a single array enhances the fingerprinting of the analytes, allowing one to determine structural similarities and chirality simultaneously.[24] Furthermore, increasing the enantioselectivity of the receptors improves chiral discrimination. Due to previous results which showed that C_2-symmetric chiral secondary amines on the boronic acid give excellent enantioselectivity, host-**5.1** was chosen.[25] With this guiding principle we now introduce host-**5.2,** which is also C_2-symmetric about the pyrrolidine ring (**Scheme 5.1**). The aim was to develop a second highly enantioselective host that can be used in conjunction with host-**5.1** in our pattern recognition protocol. To study the interactions that pertains to the enantioselectivity of the boronic acid receptor with chiral diols in methanol. Complexes of host (*R,R*)-**5.2** and (*S,S*)-hydrobenzoin (**5.3b**) was analyzed by x-ray crystallography an ^{11}B NMR.

5.2 RESULT AND DISCUSSION

5.2.1 Synthesis

Boronic acid host-**5.1** and host-**5.2** was easily synthesized by reductive amination according to published literature procedure (host-**5.2** is a new receptor).[26]

The diols used in this analysis are commercially available except for **5.4,** which was synthesized by a previously established Sharpless asymmetric dihydroxylation reaction.[27] Diol (3*S*,4*R*)-3,4 dihydroxy-4-phenyl-butane-2-one (**5.4a**) was isolated in 70% yield and 93% *ee* while (3*R*,4*S*)-3,4 dihydroxy-4-phenyl-butane-2-one (**5.4b**) was obtained in a 76% yield and 86 % *ee*. The *ee* of **5.4a** and **5.4b** was determined by using the James. *et al.* NMR analysis (**Figure 5.1**).[28]In the NMR analysis, the boronic acid

interacts with the chiral amine and chiral diol, to form two diastereomeric complexes. The ratio of these two complexes was easily determined by integrating the NMR peaks (**Figure 5.1**).

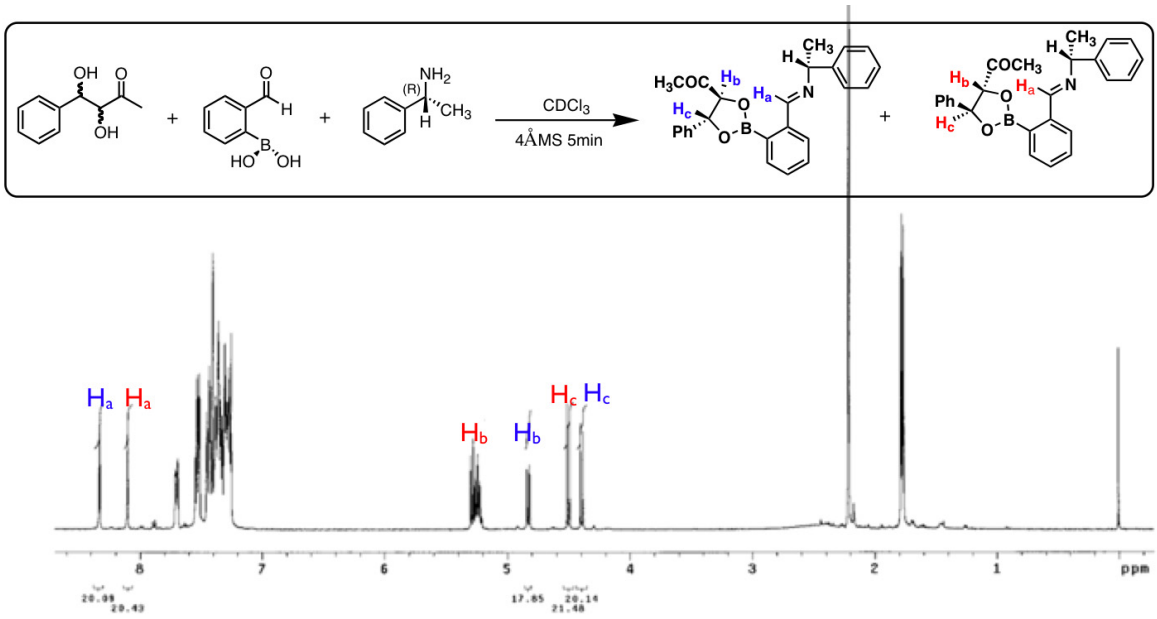

Figure 5.1: ^{1}H NMR 300 MHz on a Varian Mercury 300 spectrometer in $CDCl_3$ of the racemic mixture of **4.4** after derivatization.

5.2.2 X-ray Crystallographic Analysis:

An x-ray quality crystal of the complex (**5.7**) of host (*R*,*R*)-**5.2** with (*S*,*S*)-hydrobenzoin was isolated by diffusing methanol into a concentrated solution of the complex in dichloromethane (**Figure 5.2**). Previously, in our group we have analyzed the free boronic acid host *o*-(pyrrolidin-1-ylmethyl)phenylboronic acid and its complexes with catechol by x-ray crystallography.[29] It was shown that in these complexes the presence of the N-B bond is solvent dependent. Aprotic solvent ($CHCl_3$) facilitates the

formation of the N-B bond while in protic solvent (CH_3OH) solvolysis pathway is operative. When the complex **5.7** was crystallized from methanol, instead of the solvent inserted structure the boron atom was found to be near sp^2 hybridized. The average B-O bond length is 1.366Å and O-B-O angle of the cyclic (*S*,*S*)-hydrobenzoin boronate is 113.23°. As expected there is no intramolecular B-N bond observed in the complex the N-B bond distance of 4.43Å is observed, whereas the optimal distance for a N-B bond, is 1.5-1.8Å as reported for other boronic acid molecules with similar configurations.[30, 31] The absence of the solvent inserted structure could be due to the more sterically inaccessible nitrogen lone pair of electron in the tertiary amine as in host-**5.2**(*R*,*R*). Interestingly the ^{11}B NMR profile of the complex in CD_3OD indicates that the boron atom is solvated in solution (see next section). Therefore, there is a discrepancy between the structure of complex in solid state and in solution.

Although, we cannot estimate the exact solution behavior of host (*R*,*R*)-**5.2** with chiral diols. The competitive binding study of host-**5.2**(*S*,*S*) with **5.3a** and **5.3b** using PV as an indicator shows that the host (*S*,*S*)-**5.2** has a lower affinity for **5.3a** (K_{HG3b}1.4±0.04) than **5.3b** (K_{HG3a} 8.9±0.11) (**Figure 5.3**). Therefore host (*R,R*)-**5.2** would have a lower affinity for **5.3b** than **5.3a**. This can also be explained by the crystal structure where the phenyl group on the pyrrolidine ring of the host has an unfavorably steric interaction with the phenyl group of **5.3b**. This unfavorable interaction would not be present in the complex of host (*R*,*R*)-**5.2** and **5.3a**.

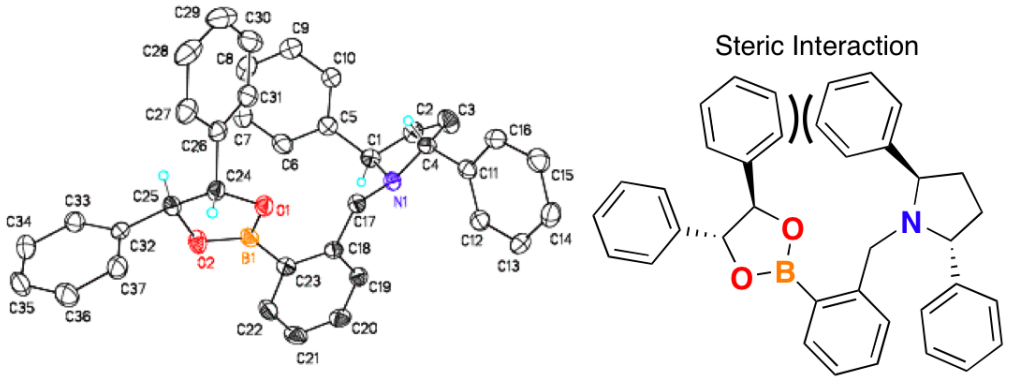

Figure 5.2: Left: Crystal structure of host (*R*,*R*)-**5.2** complex with (*S*,*S*)-hydrobenzoin (**5.3b**). Right: ChemDraw representation of the crystal structure.

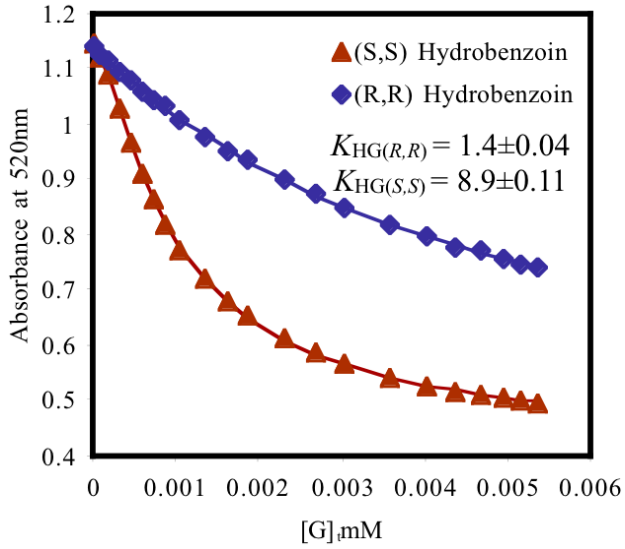

Figure 5.3: Enantioselective indicator displacement assay (eIDA) of host (*S*,*S*)-**5.2** and (0.48 mM) /PV (150 μM) with (*R*,*R*)-hydrobenzoin and (*S*,*S*)-hydrobenzoin. All titrations were carried out in 100% MeOH, 10 mM *para*-toluenesulfonic acid and Hunig's base buffer, pH =7.4, association constant K_{HI} (10^3 M^{-1}). All measurements were taken at 25°C. The solid lines are calculated curves resulting from iterative data fitting for displacement assay.

5.2.3 Structural Characterization in Solution by ^{11}B NMR

Structural studies using ^{11}B NMR were carried out to investigate the effect of solvent on the nature of the N-B interaction of complex 5.7 in solution. The ^{11}B NMR signals of the complex and the receptor are assigned based on the comparision with our pervious analysis of the *o*-(*N,N*-dialkylaminomethyl)arylboronate system.[29]

The sample of crystals used to obtain the x-ray structure of complex **5.7** displays one ^{11}B signals at 31.3 ppm in $CDCl_3$ (**Figure 5.4A**). The signal at 31.3 ppm is assigned to the trigonal planar boron species with no N-B bond. In CD_3OD (**Figure 5.4B**) however, the same set of crystals of complex **5.7** shows two peaks. The major peak (~90%) at 8.1 ppm is assigned to the fully solvated species. The minor signal (~20%) at 23.3 ppm corresponds to the ^{11}B NMR signal of the free receptor **5.2** in methanol.

The free receptor (**5.2)** has a chemical shift of 23.3 ppm in CD_3OD and 28.8 ppm in $CDCl_3$. The signal at 28.8 ppm was assigned to the trigonal planar boron in $CDCl_3$. The signal at 23.3 ppm in CD_3OD could not be assigned to a single boron species in solution. It is assumed that there is a fast exchange between the N-B coordinated sp^3 boron and the sp^2 hybridized boron of the free receptor (**5.2)** in methanol. The difference of ^{11}B NMR data of complex **5.7** with respect to NMR solvents suggests that the boron center is very prone to solvolysis, which contradicts the conclusion drawn from the solid state studies.

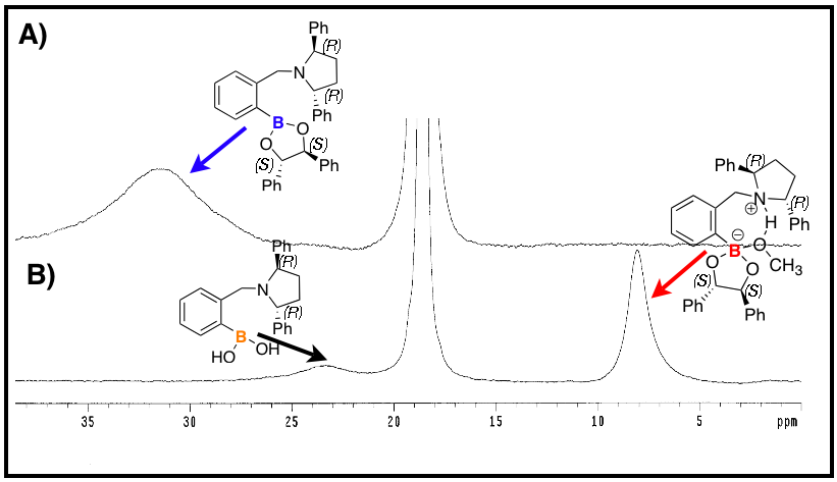

Figure 5.4: ^{11}B NMR spectra of compound **5.5** host (*R*,*R*)-**5.2** complex with (*S*,*S*)-hydrobenzoin in $CDCl_3$ (**A**) and CD_3OD (**B**). The signal at 18.6 ppm is the external standard trimethyl borate.

5.2.4 Generating a Chemo and Enantioselective Array

Before creating our pattern based recognition procedures, we needed to establish the proper pairings of hosts and indicators as described below. However, we first determined binding constants of the hosts with indicators because we have found that the optical response of an enantioselective IDA is best when the host is about 90% saturated with an indicator.[25] Six catechol based indicators were used in the study described herein: alizarin (**A**), alizarin complexone dihydrate (**AC**), bromopyrogallol red (**BPG**), 4-methylesculetin (**ML**), pyrogallol red (**PG**), and pyrocatechol violet (**PV**). Host-**5.1** has been studied previously, and thus the ratio to achieve 90% of saturated host-**5.1** with each of the six indicators was calculated from literature binding constants.[25] The binding constants for the indicators with host-**5.2**, are given in **Table 5.1** (**Figures 5.5-5.10**).

Table 5.1: Binding constant K (10^4 M^{-1}) of the host (*S*,*S*)-**5.2** with the indicators.

Indicators	A	AC	BPG	ML	PG	PV
(*S*,*S*)-**5.2**	8.42±1.76	6.41±2.21	191±131	3.61±0.13	1.02±00.7	1.36±0.02

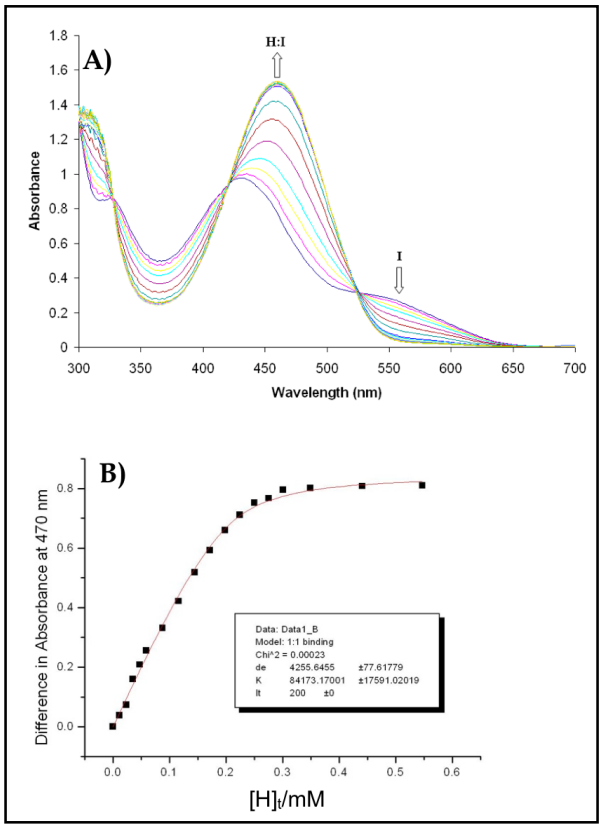

Figure 5.5: A) UV-visible titration of host (*S*,*S*)-**5.2** with A (200 μM), Host:Indicator complex (H:I), free indicator (I) **B)** 1:1 binding isotherm (plot of the difference in absorbance at 470 nm with the addition of the host). Stock solutions were prepared in 100% degassed spectral grade MeOH, using 10 mM *para*-toluenesulfonic acid and Hunig's base buffer, pH 7.4. Association constant: *K*, difference in molar absorptivity between the H:I complex and free I: de, total indicator concentration: It. The solid line is the calculated curve resulting from iterative data fitting to a 1:1 binding isotherm. All measurements were taken at 25ºC.

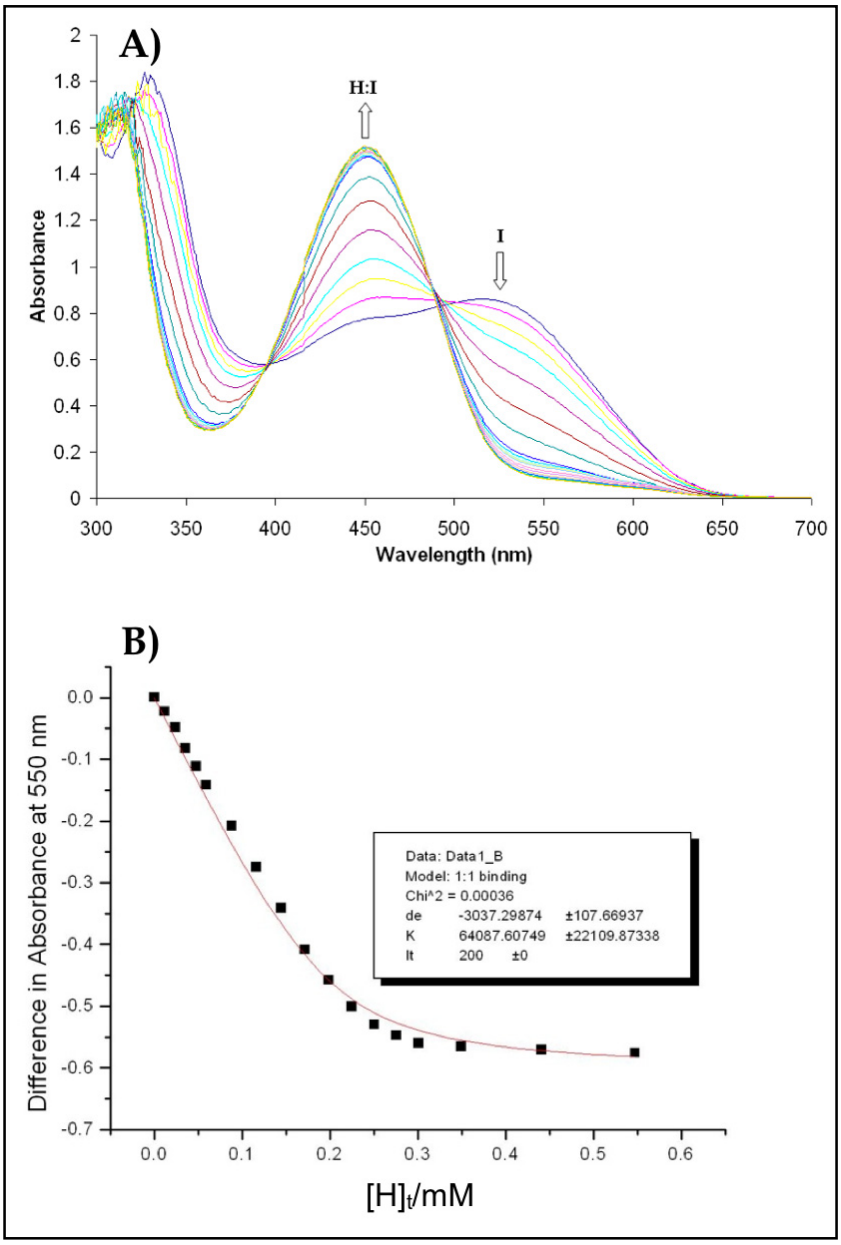

Figure 5.6: A) UV-visible titration of host (*S*,*S*)-**5.2** with AC (200 μM), Host:Indicator complex (H:I), free indicator (I) **B)** 1:1 binding isotherm (plot of the difference in absorbance at 550 nm with the addition of the host). Stock solutions were prepared in 100% degassed spectral grade MeOH, using 10 mM *para*-toluenesulfonic acid and Hunig's base buffer, pH 7.4. Association constant: *K*, difference in molar absorptivity between the H:I complex and free I: de, total indicator concentration: It. The solid line is the calculated curve resulting from iterative data fitting to a 1:1 binding isotherm. All measurements were taken at 25ºC.

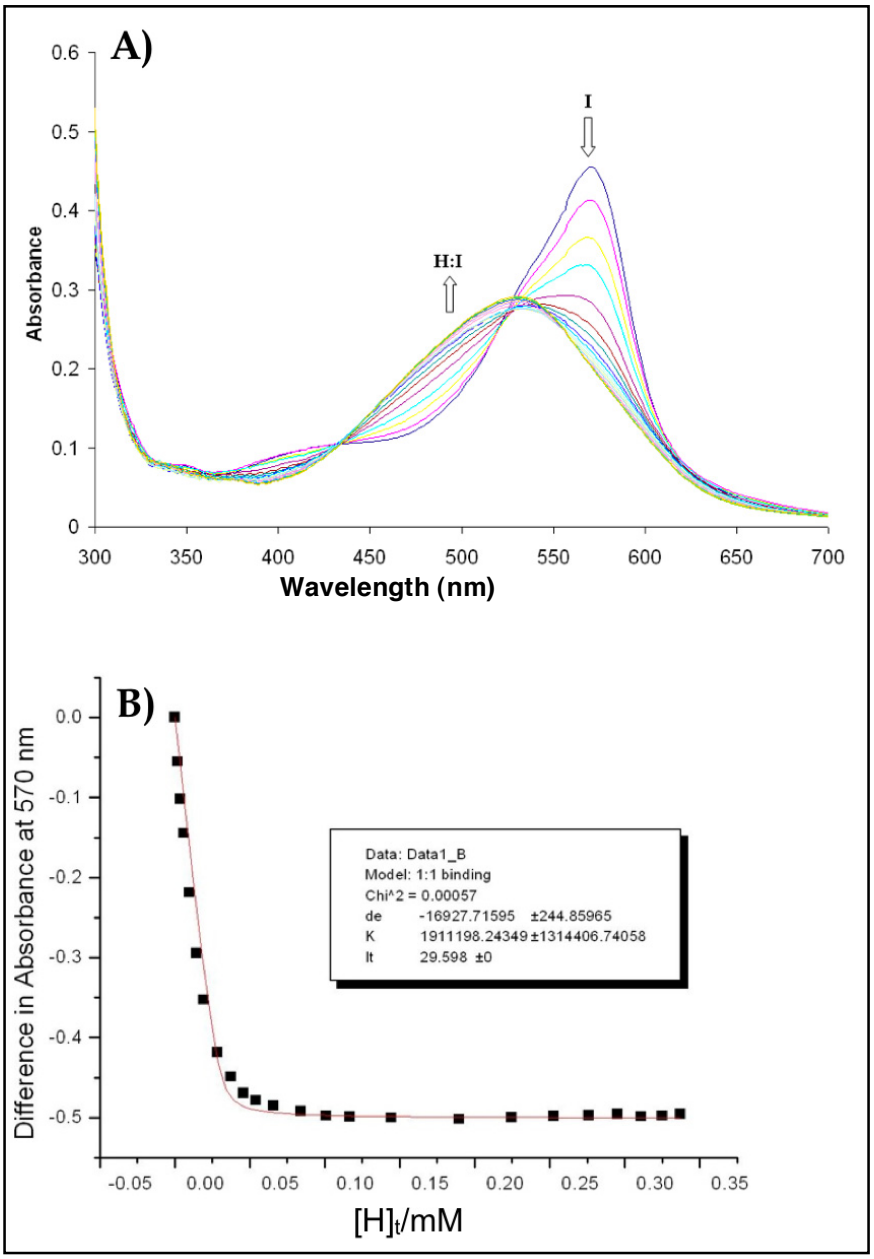

Figure 5.7: A) UV-visible titration of host (*S*,*S*)-**5.2** with BPG (29.59 μM), Host/Indicator complex (H:I), free indicator (I) **B)** 1:1 binding isotherm (plot of the difference in absorbance at 570 nm with the addition of the host). Stock solutions were prepared in 100% degassed spectral grade MeOH, using 10 mM *para*-toluenesulfonic acid and Hunig's base buffer, pH 7.4. Association constant: *K*, difference in molar absorptivity between the H:I complex and free I: de, total indicator concentration: It. The solid line is the calculated curve resulting from iterative data fitting to a 1:1 binding isotherm. All measurements were taken at 25ºC.

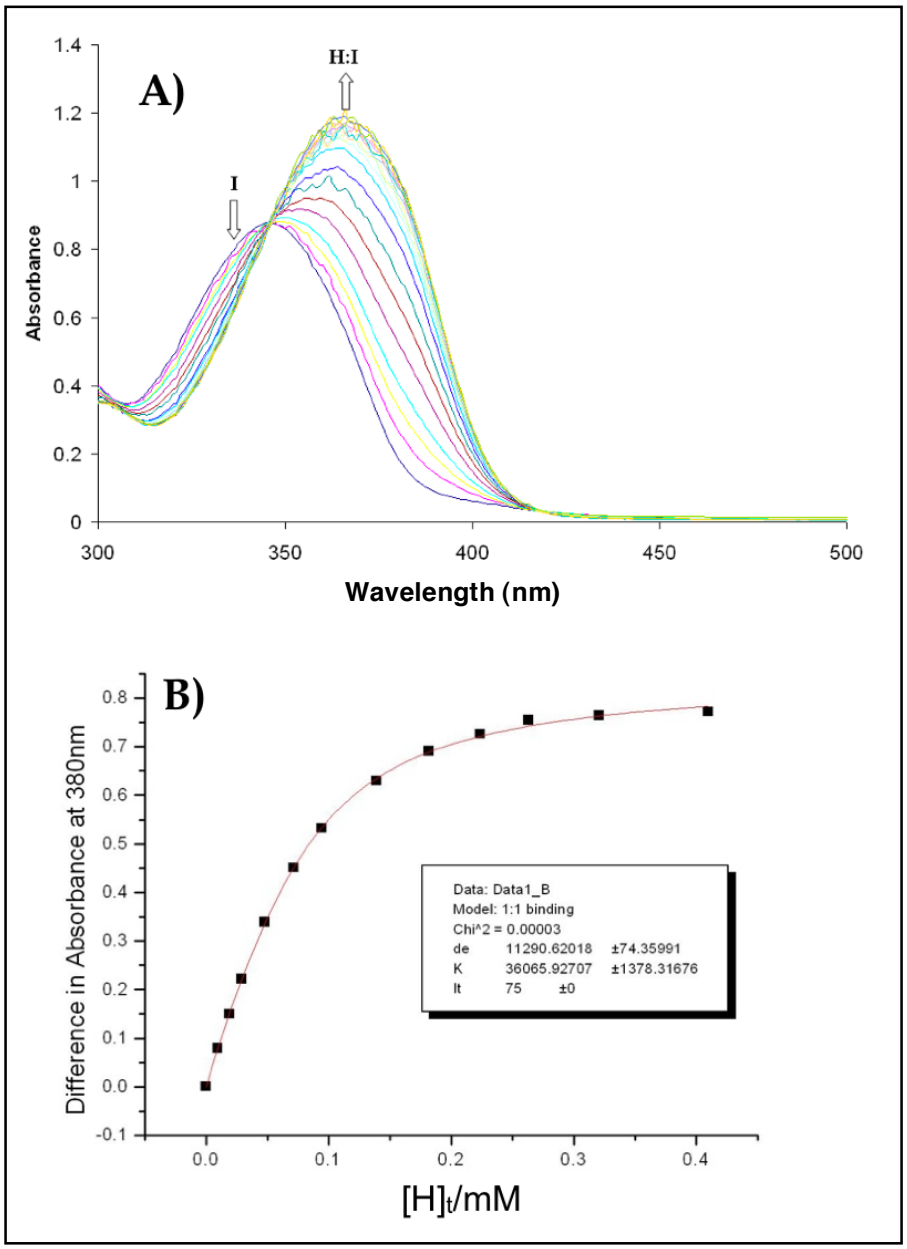

Figure 5.8: A) UV-visible titration of host (*S*,*S*)-**5.2** with ML (75 μM), Host:Indicator complex (H:I), free indicator (I) **B)** 1:1 binding isotherm (plot of the difference in absorbance at 380 nm with the addition of the host). Stock solutions were prepared in 100% degassed spectral grade MeOH, using 10 mM *para*-toluenesulfonic acid and Hunig's base buffer, pH 7.4. Association constant: *K*, difference in molar absorptivity between the H:I complex and free I: de, total indicator concentration: It. The solid line is the calculated curve resulting from iterative data fitting to a 1:1 binding isotherm. All measurements were taken at 25ºC.

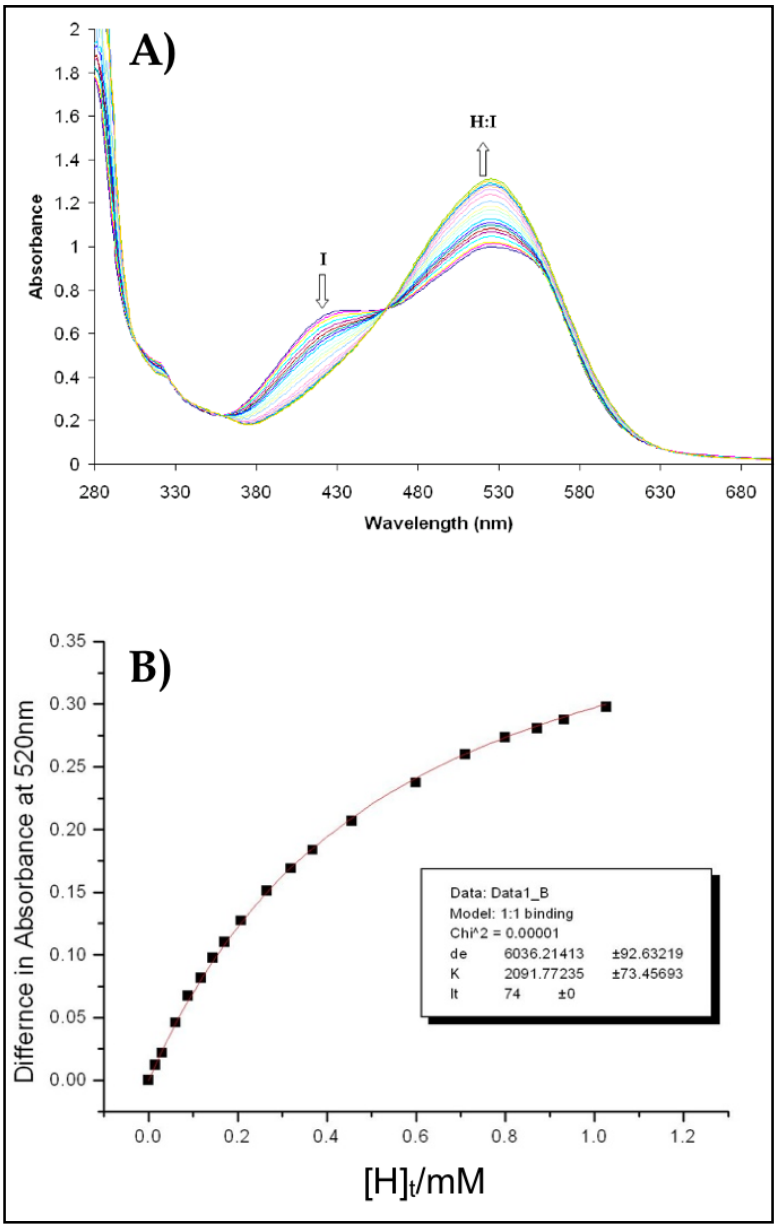

Figure 5.9: A) UV-visible titration of host (*S,S*)-**5.2** with PG (74 µM), Host:Indicator complex (H:I), free indicator (I) **B)** 1:1 binding isotherm (plot of the difference in absorbance at 520 nm with the addition of the host). Stock solutions were prepared in 100% degassed spectral grade MeOH, using 10 mM *para*-toluenesulfonic acid and Hunig's base buffer, pH 7.4. Association constant: *K*, difference in molar absorptivity between the H:I complex and free I: de, total indicator concentration: It. The solid line is the calculated curve resulting from iterative data fitting to a 1:1 binding isotherm. All measurements were taken at 25ºC.

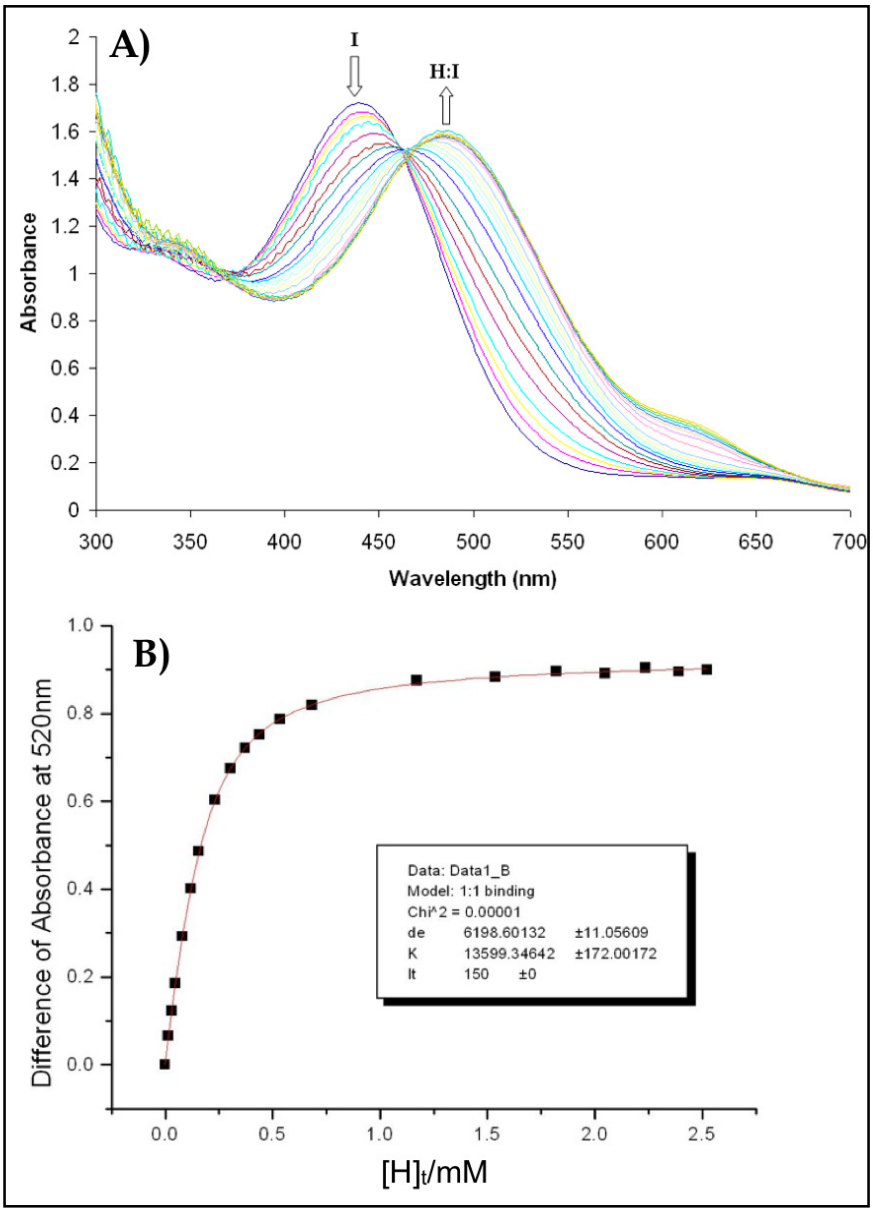

Figure 5.10: A) UV-visible titration of host (*S,S*)-**5.2** with PV (150 µM), Host:Indicator complex (H:I), free indicator (I) **B)** 1:1 binding isotherm (plot of the difference in absorbance at 520 nm with the addition of the host). Stock solutions were prepared in 100% degassed spectral grade MeOH, using 10 mM *para*-toluenesulfonic acid and Hunig's base buffer, pH 7.4. Association constant: *K*, difference in molar absorptivity between the H:I complex and free I: de, total indicator concentration: It. The solid line is the calculated curve resulting from iterative data fitting to a 1:1 binding isotherm. All measurements were taken at 25ºC.

To establish the proper host:indicator pairings we screened to seek the best host and indicator duos for colorimetric difference between analytes. The concentration of each host that yields 90% saturation with each indicator was used in a 96-well plate (**Table 5.1**). Each receptor/indicator pair was treated with each diol solution (**Figure 5.11**) such, that the concentration of the diol was 5mM. The results of these plates identified three basic combinations: host-**5.1**:PV, host-**5.2**:PV and host-**5.2**:ML as good host:indicator duos for enantiomeric discrimination for all the diols, showing a ΔAbs of 0.18 on average (**Table 5.2-5.3**). Host-**5.1**:BPG also shows good discrimination, ΔAbs of 0.23 and ΔAbs of 0.16, between the two enantiomers of **5.3** and **5.5** respectively, but the discrimination is poor for the enantiomers of diols **5.4** and **5.6**. This process allows us to rapidly identify the best host indicator combination for the enantiodiscrimination of each chiral diol, and eliminate the need to develop 1:1 binding isotherms of hosts and guests with each indicator.

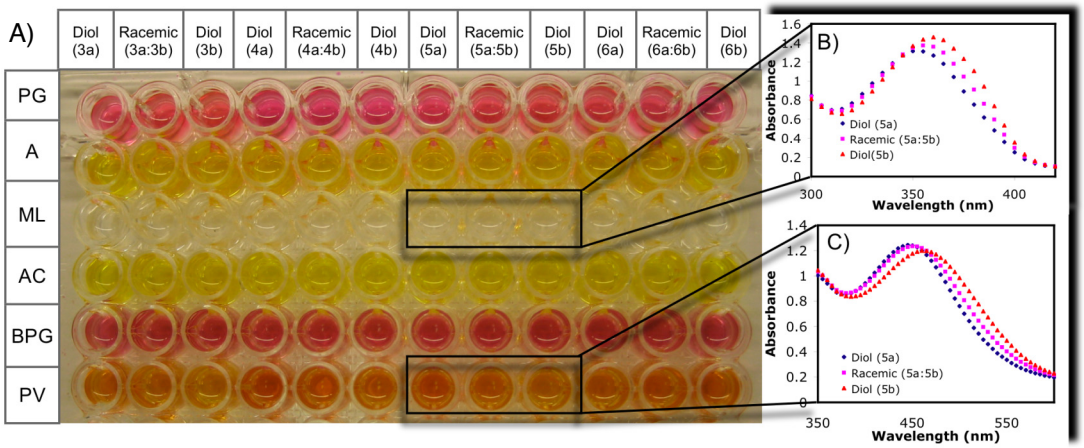

Figure 5.11 A) Method used to screen for host (*R*,*R*)-**5.2** with indicators: pyrogallol red (**PG**), alizarin (**A**), 4-methylesculetin (**ML**), alizarin complexone dihydrate (**AC**), bromopygallol red (**BPG**), and pyrocatechol violet (**PV**). The concentration of the indicators and the host are listed in **Table 5.5**. (*R*,*R*)-hydrobenzoin (**5.3a**), (*S*,*S*)-hydrobenzoin (**5.3b**), (3*S*,4*R*)-2,3-dihydroxy-4-phenyl-butane-2-one (**5.4a**), (3*R*,4*S*)-2,3-dihydroxy-4-phenyl-butane-2-one (**5.4b**), methyl(2*S*,3*R*)-2,3-dihydroxy-3-phenyl-propionate (**5.5a**), methyl(2*R*,3*S*)-2,3-dihydroxy-3-phenyl-propionate (**5.5b**), diethyl D-tartrate (**5.6a**), diethyl L-tartrate (**5.6b**) B) Absorption spectrum of host (*R*,*R*)- **5.2**:ML with diol **5.5a**:Racemic mixture (**5.5a:5.5b**): **5.5b**. C) Absorption spectrum of host (*R*,*R*)-**5.2**:PV with diol **5.5a**:Racemic mixture (**5.5a: 5.5b**):**5.5b**. All studies were carried out in 100% MeOH, 10 mM buffered solution of Hunig's base and *para*-toluenesulfonic acid to pH 7.4 at 25°C.

Table 5.2: Screening plate Δ Abs between the enantiomeric guests (5 mM) with host (S,S)- **5.1** and the indicators calculated for, A at 450 nm, AC at 550 nm, ML at 380 nm, BPG at 570 nm, PG at 520 nm and PV at 520 nm.

Indicators	Diol (**5.3**)	Diol (**5.4**)	Diol (**5.5**)	Diol (**5.6**)
A	0.007	0.035	0.024	0.007
AC	0.026	0.025	0.008	0.014
BPG	0.233	0.054	0.119	0.038
ML	0.145	0.061	0.102	0.043
PG	0.031	0.031	0.03	0.007
PV	0.107	0.08	0.072	0.057

Table 5.3: Screening plate Δ Abs between the two enantiomeric guests (5 mM) with host (*R*,*R*)-**5.2** and the indicators calculated for, A at 450 nm, AC at 550 nm, ML at 380 nm, BPG at 570 nm, PG at 520 nm and PV at 520 nm.

Indicators	Diol (**5.3**)	Diol (**5.4**)	Diol (**5.5**)	Diol (**5.6**)
A	0.176	0.092	0.158	0.043
AC	0.161	0.042	0.107	0.002
BPG	0.251	0.046	0.156	0.018
ML	0.357	0.208	0.352	0.126
PG	0.005	0.01	0.031	0.112
PV	0.216	0.166	0.232	0.139

5.2.5 Principal Component Analysis (PCA)

Our first goal was to demonstrate chemo and enantioselective discrimination of our analytes. As identified by the screening, our assay utilized three host:indicator combinations: (*S*,*S*)-**5.1**:PV, (*R*,*R*)-**5.2**:ML, and (*S*,*S*)-**5.2**:PV. Each diol at 5 mM concentration was treated with these three host:indicator combinations. The experiment was repeated four times to ensure reproducibility. A full spectrum of each sample was recorded, and the data was analyzed at nine different wavelengths: (496, 500, 516 nm) for host (*S*,*S*)-**5.1**:PV, (362, 366, 374 nm) for host (*R*,*R*)-**5.2**:ML, and (496, 500, 516 nm) for host (*S*,*S*)-**5.2**:PV. These wavelengths were chosen based on the largest change in absorbance. A PCA plot was then generated, which showed excellent discrimination for all the diols and their enantiomers (**Figure 5.12**). Tight clustering of identical samples and good spatial resolution for all the analytes was achieved. A slight rotation of the PCA axes showed chemoselectivity separated along PC1', while chirality is correlated along PC2'. *S* stereochemistry on the stereocenter near the phenyl (or ester of **5.6**) have positive scores along PC2', while *R* stereochemistry has negative score.

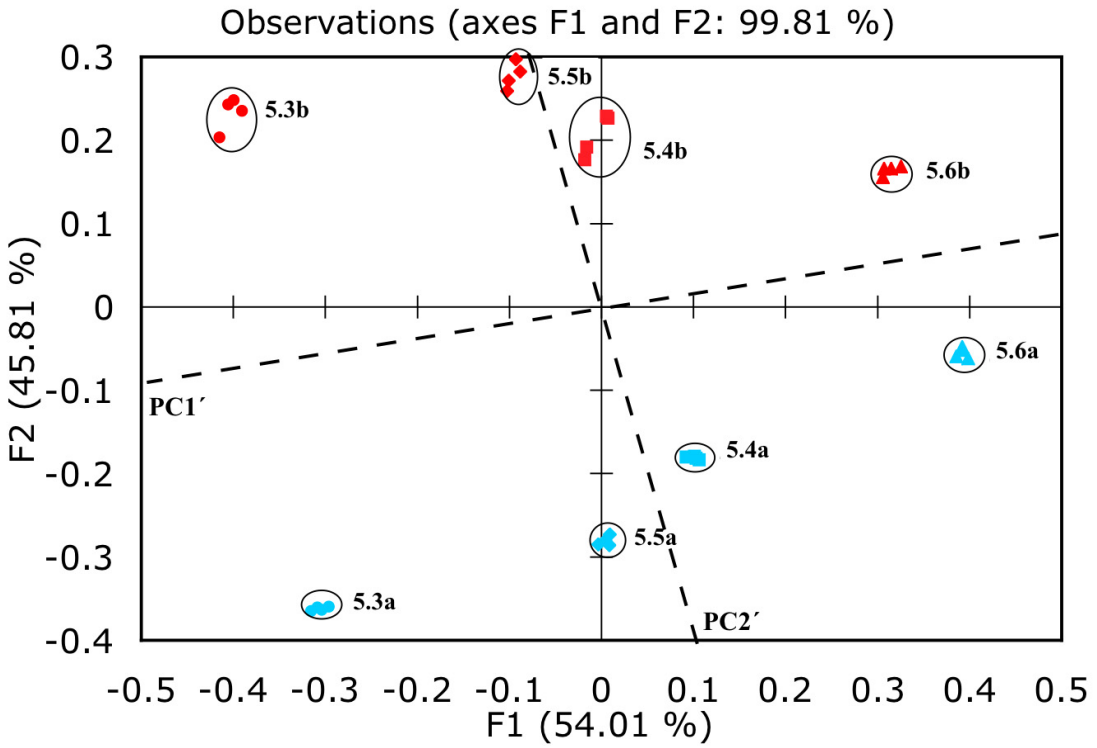

Figure 5.12. PCA of the enantiomers of the four diols analyzed with host (*S*,*S*)-**5.1**:PV host (*R*,*R*)-**5.2**:ML, and host (*S*,*S*)-**5.2**:PV. The diols are labeled on the PCA plot. All studies were carried out in 100% MeOH, 10 mM buffered solution of Hunig's base and *para*-toluenesulfonic acid to pH 7.4 at 25 °C.

Having found excellent chemo and enantioselectivity, the next goal was to explore the ability to simultaneously determine $[G]_t$ and *ee*. For this purpose we analyzed diol **5.5** with three different host indicator combinations. The earlier screening experiment discussed above for diol **5.5** determined that the best enantiomeric discrimination between **5.5a** and **5.5b** was achieved by host-**5.1**:BPG (Δ Abs 0.119), host-**5.2**:ML (Δ Abs 0.352) and host-**5.2**:PV (Δ Abs 0.232). Thus, *ee* titrations of diol-**5.5** with only these three combinations of host and indicators were carried out at three different concentrations (2 mM, 4 mM and 5 mM) and eight different *ee* values (-1.0, -

0.6, -0.2, 0, 0.2, 0.4, 0.6, 1.0), where 1.0 is 100% **5.5a** and -1.0 is 100% **5.5b**. Each *ee* titration was carried out at one concentration, and repeated three times. The data set consisting of wavelengths (570, 572, 574, 576, 578 nm) for host (*S*,*S*)-**5.1**:BPG, (512, 514, 516, 518 nm) for host (*S*,*S*)-**5.2**:PV, and (376, 378, 380, 382, 384 nm) for host (*R*,*R*)-**5.2**:ML was analyzed using PCA (**Figure 5.13A**). Good spatial resolution was obtained in the PCA plot showing clustering of identical samples and spatial resolution of concentration and *ee*. The data sets of varying *ee* values at the same concentration were clustered together in smooth curves in **Figure 5.13A**. *Ee* values range within the stripe from +1 to -1 left to right respectively. In this analysis we did not have to use an achiral host to determine concentration of analytes in contrast to our previous studies. Using data from different host and indicator combinations enabled us to eliminate the achiral host from our sensor array, thus simplifying the analysis.[19]

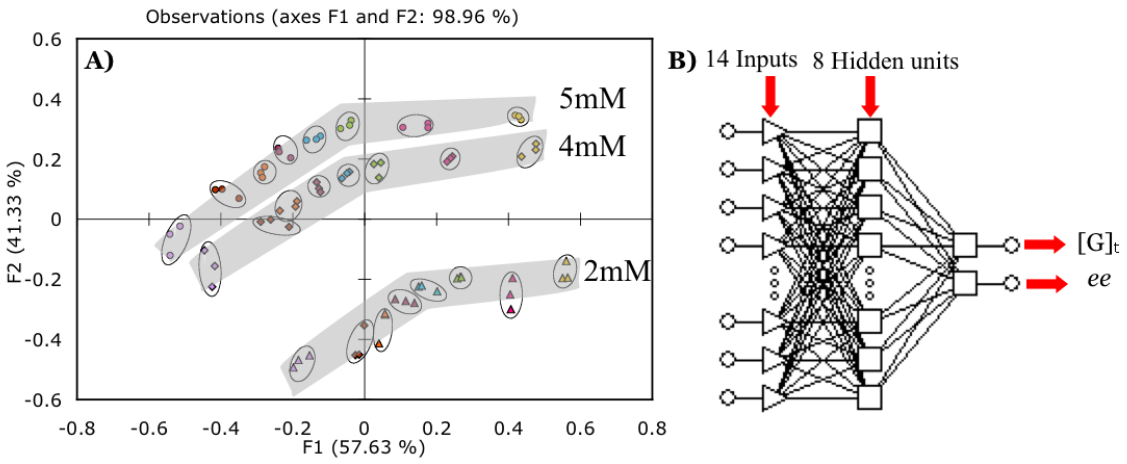

Figure 5.13. **A**) PCA of diol **5.5** *ee* titration at three different concentrations △: 2 mM, ◇: 4 mM, ◯: 5 mM. *ee*, yellow: -1, pink: -0.6, green: -0.2, blue: 0, red: 0.2, orange: 0.4, brown: 0.6, purple: 1, where 1 is 100% methyl(2*S*,3*R*)-(-)-2,3- dihydroxy-3-phenylpropionate (**5.5a**) and -1 is 100% methyl(2*R*,3*S*)-(-)-2,3- dihydroxy-3-phenylpropinate (**5.5b**) **B**) Multilayer perceptron (MLP) artificial neural network generated for the determination of *ee* and analyte total concentration ($[G]_t$). All studies were carried out in 100% MeOH, 10mM buffered solution of Hunig's base and *para*-toluenesulfonic acid to pH 7.4 at 25 °C.

5.2.6 Artificial Neural Networks (ANN's) Analysis

The last goal was to analyze unknown samples for concentration and *ee*. A neural network was generated by using the data set that was used to generate the PCA plot for diol **5.5** as the training set (**Figure 5.13B**). The repeated data set was not included in the training set as ANN does not work well with redundant values. Statistica Neural Network software was used to develop the ANN. It has an embedded intelligent problem solver (IPS) function, which automatically generates several networks that are suitable for the designated problem at hand. The input layer contains the absorbance of each *ee* titration giving a total of 14 absorbance values. The outputs are $[G]_t$ and % **5.5a**. ANN does not

work well with negative values, therefore % **5.5a** was used instead of *ee* values. A multilayered perceptron (MLP) network with 14 inputs, 8 processing units in the hidden layer, and 2 outputs was selected for our analysis. The network was trained by back-propagation algorithms, which minimize the discrepancy between the input and the outputs. True unknown samples, prepared completely independent of the training set, were then treated with the same sensor array and their $[G]_t$ and % **5.5a** values predicted by the network. The % **5.5a** values predicted by the network were converted to *ee* and are listed in **Table 5.4**. The average absolute error for $[G]_t$ was ± 0.08 mM and for *ee* was 6.72%. The *ee* error is high because of a single outlier that has an *ee* error of 19.38%. Without including the outlier, the average absolute error in *ee* drops to 3.57%.

Table 5.4: Artificial Neural Network Analysis of unknown solutions.

$[G]_t$ mM	ANN $[G]_t$ mM	Error $[G]_t$ mM	% *ee*	ANN % *ee*	Error % *ee*
3.00	3.07	0.07	50.00	69.38	19.38
3.00	3.04	0.04	30.00	33.10	3.10
3.00	3.05	0.05	10.00	8.47	1.53
3.00	3.04	0.04	-30.00	-20.64	9.36
3.00	2.79	0.21	-50.00	-50.27	0.27

Overall, the time required for this entire analysis; from screening, to training, to analysis by ANN and PCA, required approximately 24 hrs of work. However, after

establishing the protocol, identity, concentration and *ee* values of 96 samples can be determined in 40 minutes. In effect, this assay is a powerful tool which we are now transitioning to a high-throughput study to determine identity, $[G]_t$, and *ee* of unknown samples of chiral vicinal diols.

5.3 CONCLUSION

We have described a technique that fingerprints chemical identity, concentration, and chirality of chiral vicinal diols. Pattern recognition protocols were used to analyze the data. Excellent fingerprinting was obtained where the diols are chemoselectively and enantioselectively separated. This was achieved by using a diverse sensor array made up of different host and indicator combinations. Unknown samples were rapidly analyzed using ANN for their concentration and *ee* with high accuracy. In addition, a new enantioselective boronic acid host-**5.2** has been designed and synthesized in one step that showed excellent enantioselectivity for several chiral vicinal diols.

5.4 EXPERIMENTAL SECTION

5.4.1 Synthesis

Boronic acid host-**5.2** was synthesized by reductive amination according to a published procedure.[26]

Complex **5.7**. Compound **5.2** (0.5 mmol, 178.6 mg) and (*S,S*)-hydrobenzoin (0.5 mmol, 107.1 mg) were dissolved in $CHCl_3$ (2.5 mL) and stirred with 1 g $MgSO_4$ suspension at room temperature for 30 min. $MgSO_4$ was removed with vacuum filtration and the filtrate was concentrated. The crude product was dissolved in $CHCl_3$ (5 mL) and concentrated again in order to azeotropically remove the condensed water. The product

was purified by crystallization by diffusing methanol into its concentrated $CHCl_3$ solution. The crystals from CH_3OH solutions respectively were submitted for x-ray crystallographic analysis.

Host (*S*,*S*)-**5.2**: mp 118 - 128 °C. ^{1}H NMR (600 MHz, CD_3OD) δ 7.29-7.21 (m, 10H), 7.13-7.06 (m, 3H), 6.79 (b, 1H), 4.39 (m, 1H), 3.57 (d, J = 13.6 Hz, 1H), 3.26 (d, J = 13.7 Hz, 1H),) 2.59-2.54 (m, 2H), 2.17-2.12 (m, 2H) ppm. ^{13}C NMR (150 MHz, DMSO) δ 141.79, 133.72, 130.05, 129.24, 128.65, 127.40, 67.89, 55.66, 33.04, 30.65 ppm. HRMS calculated (M+H) calc 358.1934 found 358.1973

Host (*R*,*R*)-**5.2**: mp 98 - 117 °C. ^{1}H NMR (600 MHz, CD_3OD) δ 7.29-7.21 (m, 10H), 7.14-7.06 (m, 3H), 6.81 (b, 1H), 4.39 (m, 1H), 3.57 (d, J = 13.6 Hz, 1H), 3.29 (d, J = 13.7 Hz, 1H),) 2.58-2.54 (m, 2H), 2.17-2.13 (m, 2H) ppm. ^{13}C NMR (150 MHz, DMSO) δ 141.73, 133.45, 130.06, 129.24, 128.67, 127.41, 67.89, 55.46, 33.02, 30.65 ppm. HRMS calculated (M+H) calc 358.1934 found 358.1973.

Complex **5.7**: mp 162-169 °C ^{1}H NMR (500 MHz, $CDCl_3$) δ 7.87 7.84 (m, 2H), 7.52-7.49 (m, 1H), 7.37-7.32 (m, 6H), 7.27-7.17 (m, 12H), 7.12-7.09 (m, 4H), 4.37-4.35 (m, 2H), 3.80 (d, J = 16.1 Hz, 1H), 3.74 (d, J = 16.2 Hz, 1H), 2.61-2.54 (m, 2H), 2.03-1.97 (m, 2H) ppm. ^{13}C NMR (125 MHz, $CDCl_3$) δ 147.16, 143.83, 140.29, 135.87, 131.33, 128.61, 128.12, 128.09, 128.05, 128.01, 126.73, 125.80, 125.40, 86.52, 65.19, 50.55, 33.14 ppm. HRMS calculated (M+H) calc 536.2761 found 536.2755

5.4.2 NMR Analysis of the Enantiomeric Purity of 5.4:

2-Formylphenylboronic acid (14.9 mg, 0.1 mole) and (*R*)-α methylbenzylamine (12.7 μL, 0.1 mole) were dissolved in $CDCl_3$ (1 mL), in a dry glass vial equipped with a few 4 Å molecular sieves. (18.02 mg, 0.1 mole) of the diol (3,4 dihydroxy-4-phenyl-butane-2-one) obtained from asymmetric dihydroxylation reactions was added to the solution. The mixture was allowed to stand with occasional shaking for 5 min. ^{1}H NMR of the resulting solution was recorded (**Figure 5.1**).

5.4.3 Standard UV-vis Titrations:

UV-vis titrations were performed on a Beckman DU-640 UV-vis spectrophotometer. Stock solutions of the hosts, indicators, and diols were made in 10 mM buffer solution pH 7.4 (Hunig's base and *para*-toluenesulfonic acid) in 100% spectral grade degassed methanol. All measurements were taken at 25 °C.

The ideal host and indicator combinations for enantiomeric discrimination were determined by generating 1:1 binding isotherms via UV-vis titration between the host and the indicator. During the titration, the solution was allowed to equilibrate for 3 min after each addition, and the absorbance spectra was recorded until the change in absorbance from one reading to the next was < 0.03. The concentrations and the wavelengths of the indicators used are listed in **Table 5.3**. The binding constants (K_{HI}) between the host and the indicators were determined from a 1:1 binding isotherm (**Table 5.1**).

5.4.4 96-well Plate Analysis:

Arrays were made by mixing host, indicator, and guest stock solutions within a Costar EIA/RIA polystyrene 96-well flat bottom plate. BioTek Precision™ microplate

pipetting system was used to add stock solution to the 96-well plate. Each well contained a total solution volume of 300 μL. After making the plate, it was sealed with a UC-500 sealing film to prevent solvent evaporation. The absorbance spectra of the 96-well plate were recorded on a BioTek Synergy™ 4 multi-detection microplate reader.

Table 5.5: Concentration of the hosts and the indicators used in the 96-well plate. The concentration of the indicators used depends upon the purity of the commercially available indicators.

Indicator	Host **5.1**-(*S*,*S*)	Host -**5.2** (*S*,*S*)
A (200 μM)	300 μM	400 μM
AC (200 μM)	446 μM	300 μM
BPG (60 μM)	180 μM	200 μM
ML (125 μM)	380 μM	340 μM
PG (150 μM)	546 μM	300 μM
PV (150 μM)	680 μM	300 μM

5.4.5 X-ray Crystal Structure Determination

X-ray Experimental for $C_{37}H_{34}BNO_2$: Crystals grew as colorless prisms by diffusion of methanol into a DCM solution. The data crystal was cut from a larger crystal and had approximate dimensions; 0.33 x 0.25 x 0.17 mm. The data were collected on a Nonius Kappa CCD diffractometer using a graphite monochromator with MoKα radiation (λ = 0.71073Å). A total of 166 frames of data were collected using ω-scans

with a scan range of 2° and a counting time of 98 seconds per frame. The data were collected at 153 K using an Oxford Cryostream low temperature device. Data reduction were performed using DENZO-SMN.[32] The structure was solved by direct methods using SIR97[33] and refined by full-matrix least-squares on F^2 with anisotropic displacement parameters for the non-H atoms using SHELXL-97.[34] The hydrogen atoms on carbon were calculated in ideal positions with isotropic displacement parameters set to 1.2xUeq of the attached atom (1.5xUeq for methyl hydrogen atoms). The absolute configuration was determined from the known configuration of the ammine portion of the molecule. The function, $\Sigma w(|F_o|^2 - |F_c|^2)^2$, was minimized, where $w = 1/[(\sigma(F_o))^2 + (0.0439*P)^2 + (0.2884*P)]$ and $P = (|F_o|^2 + 2|F_c|^2)/3$. $R_w(F^2)$ refined to 0.0910, with R(F) equal to 0.0424 and a goodness of fit, S, = 1.07. Definitions used for calculating R(F), $R_w(F^2)$ and the goodness of fit, S, are given in reference 35.[35] The data were corrected for secondary extinction effects. The correction takes the form: $F_{corr} = kF_c/[1 + (2.5(7)x10^{-6})* F_c^2 \lambda^3/(\sin 2\theta)]^{0.25}$ where k is the overall scale factor. Neutral atom scattering factors and values used to calculate the linear absorption coefficient are from the International Tables for X-ray Crystallography (1992).[36] All figures were generated using SHELXTL/PC.[37]

5.5 REFERENCES FOR CHAPTER 5

1. Breer, H.; Fleischer, J.; Strotmann, J., The sense of smell: multiple olfactory subsystems. *Cell. Mol. Life Sci.* **2006,** 63, (13), 1465-1475.

2. Doty, R. L., *Handbook of Olfaction and Gustation* 2nd ed.; Marcel Dekker: New York, 2003.

3. Simeonov, A.; Masayuki Matsushita; Juban, E. A.; Thompson, E. H. Z.; Hoffman, T. Z.; IV, A. E. B.; Taylor, M. J.; Wirsching, P.; Rettig, W.; McCusker, J. K.; Stevens, R. C.; Millar, D. P.; Schultz, P. G.; Lerner, R. A.; Janda, K. D., Blue-Fluorescent Antibodies. *Science* **2000,** 290, 307.

4. Johnson, S. R.; Sutter, J. M.; Engelhardt, H. L.; Jurs, P. C.; White, J.; Kauer, J. S.; Dickinson, T. A.; Walt, D. R., Identification of multiple analytes using an optical sensor array and pattern recognition neural networks. *Anal. Chem.* **1997,** 69, (22), 4641-4648.

5. Rakow, N. A.; Suslick, K. S., A colorimetric sensor array for odour visualization. *Nature* **2000,** 406, 710.

6. Lavigne, J. J.; Anslyn, E. V., Sensing a paradigm shift in the field of molecular recognition: from selective to differential receptors. *Angew. Chem., Int. Ed.* **2001,** 40, (17), 3118-3130.

7. Wiskur, S. L.; Floriano, P. N.; Anslyn, E. V.; McDevitt, J. T., A multicomponent sensing ensemble in solution: Differentiation between structurally similar analytes. *Angew. Chem., Int. Ed.* **2003,** 42, (18), 2070-2072.

8. Zhou, H.; Baldini, L.; Hong, J.; Wilson, A. J.; Hamilton, A. D., Pattern Recognition of Proteins Based on an Array of Functionalized Porphyrins. *J. Am. Chem. Soc.* **2006,** 128, (7), 2421-2425.

9. Palacios, M. A.; Nishiyabu, R.; Marquez, M.; Anzenbacher, P., Jr., Supramolecular Chemistry Approach to the Design of a High-Resolution Sensor Array for Multianion Detection in Water. *J. Am. Chem. Soc.* **2007,** 129, (24), 7538-7544.

10. Nieto, S.; Lynch, V. M.; Anslyn, E. V.; Kim, H.; Chin, J., High-throughput screening of identity, enantiomeric excess, and concentration using MLCT transitions in CD spectroscopy. *J. Am. Chem. Soc.* **2008,** 130, (29), 9232-9233.

11. Ponnu, A.; Edwards, N. Y.; Anslyn, E. V., Pattern recognition based identification of nitrated explosives. *New J. Chem.* **2008,** 32, (5), 848-855.

12. Reetz, M. T.; Zonta, A.; Schimossek, K.; Leibeton, K.; Jaeger, K.-E., Creation of Enantioselective Biocatalysts for Organic Chemistry by In Vitro Evolution. *Angew. Chem., Int. Ed.* **1997,** 36, 2830-2832.

13. Masayuki Matsushita; Yamamoto, K. Y. N.; Wirsching, P.; Lerner, R. A.; Janda, K. D., High-Throughput Screening by Using a Blue-Fluorescent Antibody Sensor13. *Angew. Chem., Int. Ed.* **2003,** 42, (48), 5984-5987.

14. Dey, S.; Karukurichi, K. R.; Shen, W.; Berkowitz, D. B., Double-Cuvette ISES: In-Situ Estimation of Enantioselectivity and Relative Rate for Catalyst Screening. *J. Am. Chem. Soc.* **2005,** 127, 8610-8611.

15. Abato, P.; Seto, C. T., EMDee: An Enzyme Method for Determination Enantiomeric Excess. *J. Am. Chem. Soc.* **2001,** 123, 9206-9207.

16. Li, Z.-B.; Lin, J.; Qin, Y.-C.; Pu, L., Enantioselective Fluorescent Recognition of a soluble "Supported" Chiral Acid: Towards a New Method for Chiral Catalyst Screening. *Org. Lett.* **2005,** 7, (16), 3441-3444.

17. Rienk Eelkema, R. A. v. D. B. L. F., Direct Visual Detection of the Stereoselectivity of a Catalytic Reaction13. *Angewandte Chemie International Edition* **2004,** 43, (38), 5013-5016.

18. Nguyen, B. T.; Anslyn, E. V., Indicator-displacement assays. *Coord. Chem. Rev.* **2006,** 250, (23+24), 3118-3127.

19. Zhu, L.; Shabbir, S. H.; Anslyn, E. V., Two methods for the determination of enantiomeric excess and concentration of a chiral sample with a single spectroscopic measurement. *Chem. Eur. J.* **2007,** 13, (1), 99-104.

20. Leung, D.; Anslyn, E. V., Transitioning Enantioselective Indicator Displacement Assays for alpha -Amino Acids to Protocols Amenable to High-Throughput Screening. *J. Am. Chem. Soc.* **2008,** 130, (37), 12328-12333.

21. Jurs, P. C.; Bakken, G. A.; McClelland, H. E., Computational Methods for the Analysis of Chemical Sensor Array Data from Volatile Analytes. *Chem. Rev.* **2000**, 2649-2678.

22. Jansson, P. A., Neural networks an overview. *Anal. Chem.* **1991,** 63, (6), 357A-362A.

23. Burns, J. A.; Whitesides, G. M., Feed-forward neural network in chemistry: mathmatical system for classification and pattern recognition. *Chem. Rev.* **1993,** 93, (8), 2583-2601.

24. Folmer-Andersen, J. F.; Kitamura, M.; Anslyn, E. V., Pattern-based discrimination of enantiomeric and structurally similar amino acids: an optical mimic of the mammalian taste response. *J. Am. Chem. Soc.* **2006,** 128, (17), 5652-5653.

25. Zhu, L.; Zhong, Z.; Anslyn, E. V., Guidelines in implementing enantioselective indicator-displacement assays for alpha -hydroxycarboxylates and diols. *J. Am. Chem. Soc.* **2005,** 127, (12), 4260-4269.

26. Zhu, L.; Anslyn, E. V., Facile quantification of enantiomeric excess and concentration with indicator-displacement assays: An example in the analyses of alpha -hydroxyacids. *J. Am. Chem. Soc.* **2004,** 126, (12), 3676-3677.

27. Walsh, P. J.; Sharpless, K. B., Asymmetric dihydroxylation (AD) of alpha ,beta -unsaturated ketones. *Synlett.* **1993**, (8), 605-6.

28. Kelly, A. M.; Perez-Fuertes, Y.; Arimori, S.; Bull, S. D.; James, T. D., Simple protocol for NMR analysis of the enantiomeric purity of diols. *Org. Lett.* **2006,** 8, (10), 1971-1974.

29. Zhu, L.; Shabbir, S. H.; Gray, M.; Lynch, V. M.; Sorey, S.; Anslyn, E. V., A Structural Investigation of the N-B Interaction in an o-(*N,N*-Dialkylaminomethyl)arylboronate System. *J. Am. Chem. Soc.* **2006,** 128, (4), 1222-1232.

30. Wiskur, S. L.; Lavigne, J. J.; Ait-Haddou, H.; Lynch, V. M.; Chiu, Y. H.; Canary, J. W.; Anslyn, E. V., PKa Values and Geometries of Secondary and Tertiary Amines Complexed to Boronic Acids - Implications for Sensor Design. *Org. Lett.* **2001,** 3, (9), 1311-1314.

31. Wiskur, S. L.; Lavigne, J. J.; Matzger, A.; Tobey, S. L.; Lynch, V. M.; Anslyn, E. V., Thermodynamic Analysis of Receptors Based on Guanidinium/Boronic Acid for the

Complexation of Carboxylates, α-Hydroxylates, and Diols: Driving Force for Binding and Cooperativity. *Chem. Eur. J.* **2004,** 10, 3792-3804.

32. Otwinowski, Z.; Minor, W.; Charles W. Carter, Jr., Processing of X-ray diffraction data collected in oscillation mode. In *Methods in Enzymology*, Academic Press: 1997; Vol. Volume 276, pp 307-326.

33. Altomare, A.; Burla, M. C.; Camalli, M.; Cascarano, G. L.; Giacovazzo, C.; Guagliardi, A.; Moliterni, A. G. G.; Polidorib, G.; Spagnac, R., Computer Programs. *J. Appl. Cryst* **1999,** 32, 115-119.

34. Sheldrick, G. M. *Program for the Refinement of Crystal Structures*, University of Gottingen, Germany, 1994.

35. $R_w(F^2) = \{\Sigma w(|F_o|^2 - |F_c|^2)^2/\Sigma w(|F_o|)^4\}^{1/2}$ where w is the weight given each reflection.
$R(F) = \Sigma(|F_o| - |F_c|)/\Sigma|F_o|\}$ for reflections with $F_o > 4(\sigma(F_o))$.
$S = [\Sigma w(|F_o|^2 - |F_c|^2)^2/(n - p)]^{1/2}$, where n is the number of reflections and p is the number of refined parameter.

36. Wilson, A. J. C., *International Tables for X-ray Crystallography*. Kluwer Academic Press: Boston, 1992.

37. Sheldrick, G. M. *SHELXTL/PC (Version 5.03)*, Siemens Analytical X-ray Instruments, Inc.: Madison, Wisconsin, USA, 1994.

Bibilography

Abato, Paul, and Christopher T. Seto. "Emdee: An Enzyme Method for Determination Enantiomeric Excess." *J. Am. Chem. Soc.* 123 (2001): 9206-07.

Altomare, Angela, Maria Cristina Burla, Mercedes Camalli, Giovanni Luca Cascarano, Carmelo Giacovazzo, Antonietta Guagliardi, Anna Grazia Giuseppina Moliterni, Giampiero Polidorib, and Riccardo Spagnac. "Computer Programs." *J. Appl. Cryst* 32 (1999): 115-19.

Angelaud, Remy, Yousuke Matsumoto, Toshinobu Korenaga, Kenichi Kudo, Masaaki Senda, and Koichi Mikami. "Optical Rotation Per Refractive Index Unit, or Enantiomeric (E) Factor, for Screening Enantioselective Catalysts through Asymmetric Activation or Carbohydrates." *Chirality.* 12, no. 5/6 (2000): 544-47.

Anslyn, Eric V. "Supramolecular Analytical Chemistry." *J. Org. Chem.* 72, no. 3 (2007): 687-99.

Anslyn, Eric V., J. Frantz-Folmer-Andersen, and Lei Zhu. "Determining Enantiomeric Excess Using Indicator-Displacement Assays." 48 pp. US: (University of Texas At Austin, USA). 2006.

Anslyn, Eric V., Aaron T. Wright, and Zhenlin Zhong. "Fluorescent Synthetic Receptors for the Detection of Analytes, Especially Heparin." 25 pp. US: (USA). 2006.

Arimori, S., C. J. Ward, and Tony. D. James. "The First Fluorescent Sensor for Boronic and Boric Acids with Sensitivity at Sub-Micromolar Concentrations - a Cautionary Tale." *Chem. Commun.* (2001): 2018-19.

Badugu, R., J. R. Lakowicz, and C. D. Geddes. "A Gluocose-Sensing Contact Lens: From Bench Top to Patient." *Curr. Opin. Biotechnol.* 16 (2005): 100-07.

Barker, S. A., B. W. Hatt, P. J. Somers, and R. R. Woodbury. "The Use of Poly(4-Vinylbenzeneboronic Acid) Resins in the Fractionation and Interconversion of Carbohydrates." *Carbohydrate Res.* 26 (1973): 55-64.

Barry M. Trost, David L. Van Vranken. "Asymmetric Ligands for Transition-Metal-Catalyzed Reactions: 2-Diphenylphosphinobenzoyl Derivatives of C_2 Symmetric Diols and Diamines." *Angewandte Chemie International Edition in English* 31, no. 2 (1992): 228-30.

Barry M. Trost, Richard C. Bunt. "On Ligand Design for Catalytic Outer Sphere Reactions: A Simple Asymmetric Synthesis of Vinylglycinol." *Angew. Chem., Int. Ed.* 35, no. 1 (1996): 99-102.

Baxter, P., J. Goldhill, P. T. Hardcastle, and C. J. Taylor. "Enhanced Intestinal Glucose and Alanine Transport in Cystic Fibrosis." *Gut* 31 (1990): 817-20.

Beer, G., K. Rurack, and J. Daub. "Chiral Discrimination with a Fluorescent Boron-Dipyrromethene Dye." *Chem. Commun.* (2001): 1138-39.

Bello-Ramírez, Mara Angélica, M. Elena Rodríguez Martínez, and Angelina Flores-Parra. "Dioxaborolanes and Borates Derived from 2,3-Butanediol, Mandelic Acid, and Quinic Acid [1]." *Heteroatom Chem.* 4 (1993): 613-20.

Benkovic, Stephen J., and Sharon Hammes-Schiffer. "A Perspective on Enzyme Catalysis." *Science (Washington, DC, U. S.)* 301, no. 5637 (2003): 1196-202.

Bhattacharya, Santani, and Saubhik Halder. "Interaction between Cholesterol and Lipids in Bilayer Membranes. Role of Lipid Headgroup and Hydrocarbon Chain-Backbone Linkage." *Biochimca et Biophysica Acta* 1467 (2000): 39-53.

Biedrzycki, M., W. H. Scouten, and Z. Biedrzycka. "Derivatives of Tetrahedral Boronic Acids." *J. Organomet. Chem.* 431 (1992): 255-70.

Bielecki, M., H. Eggert, and J. C. Norrild. "A Fluorescent Glucose Sensor Binding Covalently to All Five Hydroxy Groups of -D-Glucofuranose. A Reinvestigation." *J. Chem. Soc., Perkin Trans. 2* (1999): 449-55.

Billington, David Charles. *The Inosital Phosphate. Chemical Synthesis and Biological Significance*. Germany: Wiley VCH, 1992.

Bosch, L. I., M. F. Mahon, and T. D. James. "The B-N Bond Controls the Balance between Locally Excited (Le) and Twisted Internal Charge Transfer (Tict) States Observed for Aniline Based Fluorescent Saccharide Sensors." *Tetrahedron Lett.* 45 (2004): 2859-62.

Breer, H., J. Fleischer, and J. Strotmann. "The Sense of Smell: Multiple Olfactory Subsystems." *Cell. Mol. Life Sci.* 63, no. 13 (2006): 1465-75.

Breslow, Ronald, Ying Huang, Xiaojun Zhang, and Jerry Yang. "An Artificial Cytochrome P450 That Hydroxylates Unactivated Carbon with Regio- and Stereoselectivity and Useful Catalytic Turnovers." *Proc. Natl. Acad. Sci. U. S. A.* 94 (1997): 11156-58.

Breuer, Michael, Klaus Ditrich, Tilo Habicher, Bernhard Hauer, Maria Kefleler, Rainer StÜrmer, and Thomas Zelinski. "Industrial Methods for the Production of Optically Active Intermediates." *Angew. Chem., Int. Ed.* 43, no. 7 (2004): 788-824.

Brown, H. C., and J. V. N. Vara Prasad. "Chiral Synthesis Via Organoboranes. 9. Crystalline Chelates from Borinic and Boronic Esters. A Simple Procedure for Upgrading Borinates and Boronates to Materials Approaching 100% Optical Purity." *J. Org. Chem.* 51 (1986): 4526-30.

Burgemeister, T., R. Grobe-Einsler, R. Grotstollen, A. Mannschreck, and G. Wulff. "Fast Thermal Breaking and Formation of a B-N Bond in 2-(Aminomethyl)Benzeneboronates." *Chem. Ber.* 114 (1981): 3403-11.

Burgess, K., and A. M. Porte. "A Reagent for Determining Optical Purities of Diols by Formation of Diasteromeric Arylboronate Esters." *Angew. Chem. Int. Ed. Engl.* 33, no. 11 (1994): 1182-84.

Burns, John A., and George M. Whitesides. "Feed-Forward Neural Network in Chemistry: Mathmatical System for Classification and Pattern Recognition." *Chem. Rev.* 93, no. 8 (1993): 2583-601.

Burns, J. A., and G. M. Whitesides. "Feed-Forward Neural Networks in Chemistry: Mathematical Systems for Classification and Pattern Recognition." *Chem. Rev.* 93 (1993): 2583-601.

Cao, H., and M. D. Heagy. "Fluorescent Chemosensors for Carbohydrates: A Decade's Worth of Bright Spies for Saccharides in Review." *J. Fluores.* 14 (2004): 569-84.

Caselli, E., C. Danieli, S. Morandi, B. Bonfiglio, A. Forni, and F. Prati. "(*S*)-(+)-*N*-Acetylphenylglycineboronic Acid: A Chiral Derivatizing Agent for Ee Determination of 1,2-Diols." *Org. Lett.* 5, no. 25 (2003): 4863-66.

Chakraborty, T. K., K. Azhar Hussain, and G. Venkat Reddy. "[Alpha]-Phenylglycinol as Chiral Auxiliary in Diastereoselective Strecker Synthesis of [Alpha]-Amino Acids." *Tetrahedron* 51, no. 33 (1995): 9179-90.

Chen, Y., and K. D. Shimizu. "Measurement of Enantiomeric Excess Using Molecularly Imprinted Polymers." *Org. Lett.* 4, no. 17 (2002): 2937-40.

Cirovic, D. A. "Feed-Forward Artificial Neural Networks: Applications to Spectroscopy." *Trends Anal. Chem.* 16 (1997): 148-55.

Connors, K. A. *Binding Constants, the Measurement of Molecular Complex Stability.* New York: John Wiley and Sons, 1987.

Copelan, G.T., and S.J. Miller. "A Chemosensor-Based Approach to Catalyst Discovery in Solution and on Solid Support." *J. Am. Chem. Soc.* 121 (1999): 4306-07.

Copeland, Gregory T., and Scott J. Miller. "Selection of Enantioselective Acyl Transfer Catalysts from a Pooled Peptide Library through a Fluorescence-Based Activity

Assay: An Approach to Kinetic Resolution of Secondary Alcohols of Broad Structural Scope." *J. Am. Chem. Soc.* 123 (2001): 6496-502.

Curey, Theodore E., Adrian Goodey, Andrew Tsao, John Lavigne, Youngsoo Sohn, John T. McDevitt, Eric V. Anslyn, Dean Neikirk, and Jason B. Shear. "Characterization of Multicomponent Monosaccharide Solutions Using an Enzyme-Based Sensor Array." *Anal. Biochem.* 293, no. 2 (2001): 178-84.

Dayhoff, J. E., and J. M. DeLeo. "Artificial Neural Networks: Opening the Black Box." *Cancer.* 91, no. 8 Suppl (2001): 1615-35.

Deeb, Omar, and Bahram Hemmateenejad. "Ann-Qsar Model of Drug-Binding to Human Serum Albumin." *Chem. Biol. Drug Des.* 70, no. 1 (2007): 19-29.

Dewar, M. J. S., V. P. Kubba, and R. Pettit. "New Heteroaromatic Compounds. Part Ii. Boron Compounds Isoconjugate with Indole, 2:3-Benzofuran, and Thionaphthen." *J. Chem. Soc., Abstracts* (1958): 3076-79.

Dey, Sangeeta, Kannan R Karukurichi, Weijun Shen, and David B Berkowitz. "Double-Cuvette Ises: In-Situ Estimation of Enantioselectivity and Relative Rate for Catalyst Screening." *J. Am. Chem. Soc.* 127 (2005): 8610-11.

Ding, Kuiling, Haifeng Du, Yu Yuan, and Jiang Long. "Combinatorial Chemistry Approach to Chiral Catalyst Engineering and Screening: Rational Design and Serendipity." *Chem. Eur. J.* 10, no. 12 (2004): 2872-84.

Ding, Kuiling, Akihira Ishii, and Koichi Mikami. "Super High Throughput Screening (Shts) of Chiral Ligands and Activators: Asymmetric Activation of Chiral Diol-Zinc Catalyst by Chiral Nitrogen Acitivators for the Enantioselective Addition Pf Diethylzinc to Aldehydes." *Angew. Chem., In. Ed.* 38 (1999): 497-501.

Ding, Kuiling, Akihiro Ishii, and Koichi Mikami. "Super High Throughput Screening (Shts) of Chiral Ligands and Activators: Asymmetric Activation of Chiral Diol-Zinc Catalysts by Chiral Nitrogen Activators for the Enantioselective Addition of Diethylzinc to Aldehydes." *Angew. Chem., Int. Ed.* 38, no. 4 (1999): 497-501.

Doty, Richard L. *Handbook of Olfaction and Gustation* Edited by Richard L. Doty. 2nd ed. New York: Marcel Dekker, 2003. Reprint, 2nd.

Eelkema, Rienk, Richard A. van Delden, and Ben L. Feringa. "Direct Visual Detection of the Stereoselectivity of a Catalytic Reaction." *Angew. Chem., Int. Ed.* 43, no. 38 (2004): 5013-16.

Elsas, L. J., and L. E. Rosenberg. "Familial Renal Glycosuria: A Genetic Reappraisal of Hexose Transport by Kidney and Intestine." *J. Clinic. Invest.* 48 (1969): 1845.

Fang, H., G. Kaur, and B. Wang. "Progress in Boronic Acid-Based Fluorescent Glucose Sensors." *J. Fluores.* 14 (2004): 481-89.

Fang, Zhenglai, and Ronald Breslow. "Metal Coordination-Directed Hydroxylation of Steroids with a Novel Artificial P-450 Catalyst." *Org. Lett.* 8 (2006): 251-54.

Fedorak, R. N., M. D. Gershon, and M. Field. *Gastroenterology* 96 (1989): 37-44.

Finn, M. G. "Emerging Methods for the Rapid Determination of Enantiomeric Excess." *Chirality* 14 (2002): 534-40.

Fisher, E., and Ber. Dtsch. 27 (1894): 3189.

Folmer-Andersen, J. Frantz, Masanori Kitamura, and Eric V. Anslyn. "Pattern-Based Discrimination of Enantiomeric and Structurally Similar Amino Acids: An Optical Mimic of the Mammalian Taste Response." *J. Am. Chem. Soc.* 128, no. 17 (2006): 5652-53.

Folmer-Andersen, J. Frantz, Vincent M. Lynch, and Eric V. Anslyn. "Colorimetric Enantiodiscrimination of Alpha -Amino Acids in Protic Media." *J. Am. Chem. Soc.* 127, no. 22 (2005): 7986-87.

Folmer-Andersen, J. Frantz, Vincent M. Lynch, and Eric V. Anslyn. "Naked-Eye" Detection of Histidine by Regulation of Cuii Coordination Modes." *Chem. Eur. J.* 11, no. 18 (2005): 5319-26.

Franzen, S., W. Ni, and B. Wang. "Study of the Mechanism of Electron-Transfer Quenching by Boron-Nitrogen Adducts in Fluorescent Sensors." *J. Phys. Chem. B* 107 (2003): 12942-48.

G.Klein, and J.-L. Reymond. "Enantioselective Fluorogenic Assay of Acetate Hydrolysis for Detecting Lipase Catalytic Antibodies " *Helv. Chim. Acta.* 82 (1999): 400-07.

Gardossi, Lucia, Daniele Bianchi, and Alexander M. Klibanov. "Selective Acylation of Peptide Catalyzed by Lipases in Organic Solvent." *J. Am. Chem. Soc.* 113 (1991): 6328-29.

Giles, R. L., J. A. K. Howard, L. G. F. Patrick, M. R. Probert, G. E. Smith, and A. Whiting. "Synthesis and Structure of Potential Lewis Acid - Lewis Base Bifunctional Catalysts: 1-*N,N*-Dimethylamino-8-Bororonaphthalene Derivatives." *J. Organomet. Chem.* 680 (2003): 257-62.

Glad, M., S. Ohlson, L. Hansson, M.-O. Mansson, and K. Mosbach. "High-Performance Liquid Affinity Chromatography of Nucleosides, Nucleotides and Carbohydrates with Boronic Acid-Substituted Microparticulate Silica." *J. Chromatogr.* 200 (1980): 254-60.

Gray, Jr., C. W.; Houston, T. A. "Boronic Acid Receptors for α-Hydroxycarboxylates: High Affinity of Shinkai's Glucose Receptor for Tartrate." *J. Org. Chem.* 67 (2002): 5426-28.

Guo, J., J. Wu, G. Siuzdak, and M.G. Finn. "Measurement of Enantiomeric Excess by Kinetic Resolution and Mass Spectrometry." *Angew. Chem., Int. Ed.* 38 (1999): 1755-58.

Gventer, Brian. "Production Pattern-Recognition Artificial Neural Net (Ann) with Event-Response Expert System (Es)--Yieldshieldtm." US: (USA). 2003.

Hall, Dennis G., ed. *Boronic Acids Preparation, Applications in Organic Synthesis and Medicine*. Weinheim: WILEY-VCH Verlag GmbH & Co. KGaA, 2005.

Halpern, Jack. "Mechanism and Seteroselectivity of Asymmetric Hydrogenation." *Science* 217, no. 4558 (1982): 401-07.

Hamberg, Anders, Stina Lundgren, Mael Penhoat, Christina Moberg, and Karl Hult. "High-Throughput Enzymatic Method for Enantiomeric Excess Determination of O-Acetylated Cyanohydrins." *J. Am. Chem. Soc.* 128, no. 7 (2006): 2234-35.

Höpfl, H. "The Tetrahedral Character of the Boron Atom Newly Defined - a Useful Tool to Evaluate the N-B Bond." *J. Organomet. Chem.* 581 (1999): 129-49.

Hoveyda, Amir H. "Catalyst Discovery through Combinatorial Chemistry." *Chem. Biol.* 5, no. 8 (1998): R187-R91.

J. Guo, J.. Wu, G. Siuzdak, M.G. Finn. "Measurement of Enantiomeric Excess by Kinetic Resolution and Mass Spectrometry." *Angew. Chem., Int. Ed.* 38 (1999): 1755-58.

Jacobsen, Eric N., Istvan Marko, William S. Mungall, Georg Schroeder, and K. Barry Sharpless. "Asymmetric Dihydroxylation Via Ligand-Accelerated Catalysis." *J. Am. Chem. Soc.* 110, no. 6 (1988): 1968-70.

James, T. D., P. Linnane, and S. Shinkai. "Fluorescent Saccharide Receptors: A Sweet Solution to the Design, Assembly and Evaluation of Boronic Acid Derived Pet Sensors." *Chem. Commun.* (1996): 281-88.

James, T. D., K. R. A. S. Sandanayake, R. Iguchi, and S. Shinkai. "Novel Saccharide-Photoinduced Electron Transfer Sensors Based on the Interaction of Boronic Acid and Amine." *J. Am. Chem. Soc.* 117 (1995): 8982-87.

James, T. D., K. R. A. S. Sandanayake, and S. Shinkai. "Novel Photoinduced Electron-Transfer Sensor for Saccharides Based on the Interaction of Boronic Acid and Amine." *J. Chem. Soc., Chem. Commun.* (1994): 477-78.

James, T. D., K. R. A. S. Sandanayake, and S. Shinkai. "Chiral Discrimination of Monosaccharides Using a Fluorescent Molecular Sensor." *Nature* 374 (1995): 345-47.

James, T. D., K. R. A. S. Sandanayake, and S. Shinkai. "Saccharide Sensing with Molecular Receptors Based on Boronic Acid." *Angew. Chem. Int. Ed. Engl.* 35 (1996): 1910-22.

James, T. D., and S. Shinkai. "Artificial Receptors as Chemosensors for Carbohydrates." *Top. Curr. Chem.* 218 (2002): 159-200.

Jansson, Peter A. "Neural Networks an Overview." *Anal. Chem.* 63, no. 6 (1991): 357A-62A.

Jaroch, Stefan, Hilmar Weinmann, and Kirsten Zietler. "Asymmetric Organocatalysis." *Chem. Med. Chem.* 2 (2007): 1261-64.

Jensen, K. A., and T. Pedersen. "Heterocyclic Boron Compounds I." *Acta Chem. Scand.* 15, no. 8 (1961): 1780-81.

Johnson, Stephen R., Jon M. Sutter, Heidi L. Engelhardt, Peter C. Jurs, Joel White, John S. Kauer, Todd A. Dickinson, and David R. Walt. "Identification of Multiple Analytes Using an Optical Sensor Array and Pattern Recognition Neural Networks." *Anal. Chem.* 69, no. 22 (1997): 4641-48.

Jurs, P. C., G. A. Bakken, and H. E. McClelland. "Computational Methods for the Analysis of Chemical Sensor Array Data from Volatile Analytes." *Chem. Rev.* (2000): 2649-78.

Kankare, J. J., and J. Varhiala. "Selective Determination of Tartaric Acid in Aqueous Solution with 2-[1-(*O*-Dihydroxyborylphenyl)-2-Phenylethyl]-2-Imidazoline." *Anal. Chim. Acta* 99 (1978): 151-56.

Kavarnos, George J. "Fundamentals of Photoinduced Electron Transfer." New York: VCH Publishers, 1993.

Kelly, Andrew M., Yolanda Perez-Fuertes, Susumu Arimori, Steven D. Bull, and Tony D. James. "Simple Protocol for Nmr Analysis of the Enantiomeric Purity of Diols." *Org. Lett.* 8, no. 10 (2006): 1971-74.

Knowles, William S. "Asymmetric Hydrogenation." *Acc. Chem. Res.* 16, no. 3 (1983): 106-12.

Knowles, William S. "Asymmetric Hydrogenation (Nobel Lecture 2001)." *Adv. Synth. Catal* 345, no. 1-2 (2001): 3-13.

Knowles, William S. "Asymmetric Hydrogenations (Nobel Lecture) " *Angew. Chem., Int. Ed.* 41 (2002): 1998-2007.

Konstantinos Petritis, Lars J. Kangas, Patrick L. Ferguson, Gordon A. Anderson, Ljiljana Paa-Toli, Mary S. Lipton, Kenneth J. Auberry, Eric F. Strittmatter, Yufeng Shen, Rui Zhao, and Richard D. Smith. "Use of Artificial Neural Networks for the Accurate Prediction of Peptide Liquid Chromatography Elution Times in Proteome Analyses." *Anal. Chem.* 75, no. 5 (2003): 1039 - 48;.

Koshland, D. E. "How a Non-Conformist Theory Beat Scepticism and Got into the Textbooks." *Nature* 432 (2004): 447.

Kubo, Kanji. "Pet Sensors." *Top. Fluoresc. Spectrosc.* 9, no. Advanced Concepts in Fluorescence Sensing, Part A (2005): 219-47.

Kubo, Y., A. Kobayashi, T. Ishida, Y. Misawa, and T. D. James. "Detection of Anions Using a Fluorescent Alizarin-Phenylboronic Acid Ensemble." *Chem. Commun.* (2005): 2846-48.

Kuivila, H. G., A. H. Keough, and E. J. Soboczenski. "Areneboronates from Diols and Polyols." *J. Org. Chem.* 19 (1954): 780-83.

Kuntz, K. W., M. L. Snapper, and A. H. Hoveyda. "Combinatorial Catalyst Discovery." *Curr. Opin. Chem. Biol.* 3, no. 3 (1999): 313-9.

Lad, C., N.H. Willaims, and R. Wolfenden. "The Rate of Hydrolysis of Phosphomonoester Dianions and the Exceptional Catalytic Proficiencies of Protein and Inositol Phosphatases." *Proc. Natl. Acad. Sci. U. S. A.* 100 (2003): 5607.

Lauer, M., H. Bohnke, R. Grotstollen, M. Salehnia, and G. Wulff. *Chem. Ber.* 118 (1985): 246-60.

Lauer, M., and G. Wulff. *J. Organomet. Chem.* 256 (1983): 1-9.

Lauer, M., and G. Wulff. "Complexation of Arylboronates with Nitrogen-Containing Bases." *J. Chem. Soc., Perkin Trans. 2* (1987): 745-49.

Lavigne, John J., and Eric V. Anslyn. "Sensing a Paradigm Shift in the Field of Molecular Recognition: From Selective to Differential Receptors." *Angew. Chem., Int. Ed.* 40, no. 17 (2001): 3118-30.

Letsinger, R. L., and S. B. Hamilton. "Organoboron Compounds. Xii. Heterocyclic Compounds from Benzeneboronic Acid1." *J. Org. Chem.* 25 (1960): 592-95.

Letsinger, R. L., and D. B. MacLean. "Organoboron Compounds. Xvi. Cooperative Functional Group Effects in Reactions of Boronoarylbenzimidazoles." *J. Am. Chem. Soc.* 85 (1963): 2230-36.

Leung, Diana, and Eric V. Anslyn. "Transitioning Enantioselective Indicator Displacement Assays for Alpha -Amino Acids to Protocols Amenable to High-Throughput Screening." *J. Am. Chem. Soc.* 130, no. 37 (2008): 12328-33.

Leung, Diana, J. Frantz Folmer-Andersen, Vincent M. Lynch, and Eric V. Anslyn. "Using Enantioselective Indicator Displacement Assays to Determine the Enantiomeric Excess of Alpha -Amino Acids." *J. Am. Chem. Soc.* 130, no. 37 (2008): 12318-27.

Li, Z., L. Bütikofer, and B. Witholt. "High-Throughput Measurement of the Enantiomeric Excess of Chiral Alcohols by Using Two Enzymes." *Angew. Chem. Int. Ed.* 43 (2004): 1698-702.

Li, Zi-Bo, Jing Lin, and Lin Pu. "A Cyclohexyl-1,2-Diamines-Derived Bis(Binaphthyl) Macrocycle: Enhanced Sensitivity and Enantioselectivity in the Fluorescent Recognition of Mandelic Acid." *Angew. Chem., Int. Ed.* 44 (2005): 1690-93.

Li, Zi-Bo, Jing Lin, Ying-Chuan Qin, and Lin Pu. "Enantioselective Fluorescent Recognition of a Soluble "Supported" Chiral Acid: Towards a New Method for Chiral Catalyst Screening." *Org. Lett.* 7, no. 16 (2005): 3441-44.

Lin, J., H.-C. Zhang, and L. Pu. "Bisbinaphthyl Macrocycle-Based Highly Enantioselective Fluorescent Sensors for α-Hydroxycarboxylic Acids." *Org. Lett.* 4, no. 19 (2002): 3297-300.

Lober, Oliver, Motoi Kawatsura, and John F. Hartwig. "Palladium-Catalyzed Hydroamination of 1,3-Dienes: A Colorimetric Assay and Enantioselective Addition." *J. Am. Chem. Soc.* 123 (2001): 4366-67.

Long, Jiang, Jieyu Hu, Xiaoqiang Shen, Baoming Ji, and Kuiling Ding. "Discovery of Exceptionally Efiicient Catalysts for Solvent Free Enantioselectivity Hetero-Diel-Alder Reaction." *J. Am. Chem. Soc.* 124, no. 1 (2002): 10-11.

Lorand, J. P., and J. O. Edwards. "Polyol Complexes and Structure of the Benzeneboronate Ion." *J. Org. Chem.* 24 (1959): 769-74.

Lundgren, Stina, Erica Wingstrand, Mael Penhoat, and Christina Moberg. "Dual Lewis Acid & Lewis Base Activation in Enantioselective Cyanation of Aldehydes Using Acetyl Cyanide and Cyanoformate as Cyanide Sources." *J. Am. Chem. Soc.* 127, no. 33 (2005): 11592-93.

M. Matsushita, K. Yoshida, Noboru Yamamoto, P. Wirsching, R. A. Lerner, and K. D. Janda. "High-Throughput Screening by Using a Blue-Fluorescent Antibody Sensor." *Angew.Chem. Int. Ed.* 42 (2003): 5984-87.

Marchi, S. De, E. Cecchin, A. Jengo, D. Schinella, A. Jus, D. Villalta, P. De PaoliG. Santini, and F. Tesio. *Am. J. Nephrol* 4 (1984): 280-86.

Masayuki Matsushita, Kazuhiro Yoshida Noboru Yamamoto, Peter Wirsching, Richard A. Lerner, and Kim D. Janda. "High-Throughput Screening by Using a Blue-Fluorescent Antibody Sensor13." *Angew. Chem., Int. Ed.* 42, no. 48 (2003): 5984-87.

Maue, M., and T. Schrader. "A Color Sensor for Catecholamines." *Angew. Chem. Int. Ed.* 44 (2005): 2265-70.

Mei, Xuefeng, and Christian Wolf. "Determination of Enantiomeric Excess and Concentration of Unprotected Amino Acids, Amines, Amino Alcohols, and Carboxylic Acids by Competitive Binding Assays with a Chiral Scandium Complex." *J. Am. Chem. Soc.* 128, no. 41 (2006): 13326-27.

Metzger, Axel, and Eric V. Anslyn. "A Chemosensor for Citrate in Beverages." *Angew. Chem., Int. Ed.* 37, no. 5 (1998): 649-52.

Metzger, A., V. M. Lynch, and E. V. Anslyn. "A Synthetic Receptor Selective for Citrate." *Angew. Chem. Int. Ed.* 36, no. 8 (1997): 862-65.

Mikami, Koichi, Remy Angelaud, Kuiling Ding, Akihiro Ishii, Akito Tanaka, Naotaka Sawada, Kenichi Kudo, and Masaaki Senda. "Asymmetric Activation of Chiral Alkoxyzinc Catalysts by Chiral Nitrogen Activators for Dialkylzinc Addition to Aldehydes: Super High-Throughput Screening of Combinatorial Libraries of Chiral Ligands and Activators by HPLC-CD/UV and HPLC-OR/RIU Systems." *Chem. Eur. J.* 7, no. 3 (2001): 730-37.

Nagai, Y., K. Kobayashi, H. Toi, and Y. Aoyama. "Stabilization of Sugar-Boronic Esters of Indolylboronic Acid in Water Via Sugar–Indole Interaction: A Notable Selectivity in Oligosaccharides." *Bull. Chem. Soc. Jpn.* 66 (1993): 2965-71.

Nguyen, Binh T., and Eric V. Anslyn. "Indicator-Displacement Assays." *Coord. Chem. Rev.* 250, no. 23+24 (2006): 3118-27.

Nguyen, B. T., S. L. Wiskur, and E. V. Anslyn. "Using Indicator-Displacement Assays in Test Strips and to Follow Reaction Kinetics." *Org. Lett.* 6 (2004): 2499-501.

Ni, W., G. Kaur, G. Springsteen, B. Wang, and S. Franzen. "Regulating the Fluorescence Intensity of an Anthracene Boronic Acid System: A B-N Bond or a Hydrolysis Mechanism?" *Bioorg. Chem.* 32 (2004): 571-81.

Nieto, Sonia, Vincent M. Lynch, Eric V. Anslyn, Hyunwoo Kim, and Jik Chin. "High-Throughput Screening of Identity, Enantiomeric Excess, and Concentration Using Mlct Transitions in Cd Spectroscopy." *J. Am. Chem. Soc.* 130, no. 29 (2008): 9232-33.

Norrild, J. C. "An Illusive Chiral Aminoalkylferroceneboronic Acid. Structural Assignment of a Strong 1:1 Sorbitol Complex and New Insight into Boronate–Polyol Interactions." *J. Chem. Soc., Perkin Trans. 2* (2001): 719-26.

Norrild, J. C., and H. Eggert. "Evidence for Mono- and Bisdentate Boronate Complexes of Glucose in the Furanose Form. Application of 1jc-C Coupling Constants as a Structural Probe." *J. Am. Chem. Soc.* 117 (1995): 1479-84.

Norrild, J. C., and I. Søtofte. "Crystal Structures of 2-(*N,N*-Dimethylaminoalkyl)Ferroceneboronic Acids and Their Diol Derivatives. The Quest for a B–N Intramolecular Bond in the Solid State." *J. Chem. Soc., Perkin Trans. 2* (2001): 727-32.

Norrild, J. C., and I. Søtofte. "Design, Synthesis and Structure of New Potential Electrochemically Active Boronic Acid-Based Gluocose Sensors." *J. Chem. Soc., Perkin Trans. 2* (2002): 303-11.

Noyori, R. "Asymmetric Catalysis: Science and Opportunities (Nobel Lecture)." *Angew. Chem., Int. Ed.* 41 (2002): 2008-22.

Ohshima, Takashi, Takanori Iwasaki, Yusuke Maegawa, Asako Yoshiyama, and Kazushi Mashima. "Enzyme-Like Chemoselective Acylation of Alcohols in the Presence of Amines Catalyzed by a Tetranuclear Zinc Cluster." *J. Am. Chem. Soc.* 130 (2008): 2944-45.

Onaran, M. Burak, and Christopher T. Seto. "Using a Lipase as a High-Throughput Screening Method for Measuring the Enantiomeric Excess of Allylic Acetates." *J. Org. Chem.* 68, no. 21 (2003): 8136-41.

Otsuka, H., E. Uchimura, H. Koshino, T. Okano, and K. Kataoka. "Anomalous Binding Profile of Phenylboronic Acid with N-Acetylneuraminic Acid (Neu5ac) in Aqueous Solution with Varying Ph." *J. Am. Chem. Soc.* 125 (2003): 3493-502.

Otwinowski, Zbyszek, Wladek Minor, and Charles W. Carter, Jr. "[20] Processing of X-Ray Diffraction Data Collected in Oscillation Mode." In *Methods in Enzymology*, 307-26: Academic Press, 1997.

Palacios, Manuel A., Ryuhei Nishiyabu, Manuel Marquez, and Pavel Anzenbacher, Jr. "Supramolecular Chemistry Approach to the Design of a High-Resolution Sensor Array for Multianion Detection in Water." *J. Am. Chem. Soc.* 129, no. 24 (2007): 7538-44.

Paugam, M.-F., J. T. Bien, B. D. Smith, L. A. J. Chrisstoffels, F. de Jong, and D. N. Reinhoudt. "Facilitated Catecholamine Transport through Bulk and Polymer-Supported Liquid Membranes." *J. Am. Chem. Soc.* 118 (1996): 9820-25.

Paugam, M.-F., and B. D. Smith. "Active Transport of Uridine through a Liquid Organic Membrane Mediated by Phenylboronic Acid and Driven by a Fluoride Ion Gradient." *Tetrahedron Lett.* 34 (1993): 3723-26.

Paugam, M.-F., L. S. Valencia, B. Boggess, and B. D. Smith. "Selective Dopamine Transport Using a Crown Boronic Acid." *J. Am. Chem. Soc.* 116 (1994): 11203-04.

Pauling, L. *Eng. News* 24 (1946): 1375.

Phillips, M. D., and T. D. James. "Boronic Acid Based Modular Fluorescent Sensors for Glucose." *J. Fluores.* 14 (2004): 549-59.

Piatek, A. M., Y. J. Bomble, S. L. Wiskur, and E. V. Anslyn. "Threshold Detection Using Indicator-Displacement Assays: An Application in the Analysis of Malate in Pinot Noir Grapes." *J. Am. Chem. Soc.* 126, no. 19 (2004): 6072-77.

Ponnu, Aravindan, Nicola Y. Edwards, and Eric V. Anslyn. "Pattern Recognition Based Identification of Nitrated Explosives." *New J. Chem.* 32, no. 5 (2008): 848-55.

Pu, Lin. "Fluorescence of Organic Molecules in Chiral Recognition." *Chemical Reviews* 104, no. 3 (2004): 1687-716.

Rakow, Neal A., and Kenneth S. Suslick. "A Colorimetric Sensor Array for Odour Visualization." *Nature* 406 (2000): 710.

Rancke-Madsen, E. *Indicators*. Edited by Edmund Bishop. 1st ed, *The History of Indicators*. New York: Pergamon Press, 1972.

Reetz, Manfred T. "Combinatorial and Evolution-Based Method in the Creation of Enantioselective Catalyst." *Angew. Chem., Int. Ed.* 40 (2001): 284-310.

Reetz, Manfred T. "New Methods for the High-Throughput Screening of Enantioselective Catalysts and Biocatalysts." *Angew. Chem. Int. Ed.* 41 (2002): 1335-38.

Reetz, Mansfred T., Micheal H. Becker, Klaus M. Kuhling, and Arnold Holzwarth. "Time-Resolved Ir-Thermographic Detection and Screening of Enantioselectivity in Catalytic Reactions." *Angew. Chem., Int. Ed.* 37 (1998): 2647-50.

Reetz, Manfred T., Andreas Eipper, Patrick Tielmann, and Richard Mynott. "A Practical Nmr-Based High-Throughput Assay for Screening Enantioselective Catalysts and Biocatalysts." *Adv. Synth. Catal.* 344, no. 9 (2002): 1008-16.

Reetz, Manferd T., Micheal H. Becker, H.-W.Klein, and D. Stockigt. "A Method for High-Throughput Screening of Enantioselective Catalysts." *Angew. Chem., Int. Ed.* 38 (1999): 1758-61.

Reetz, Mansfred T., Klaus M. Kuhling, Alfred Deege, Heike Hinrichs, and Detlev Belder. "Super-High-Throughput Screening of Enantioselective Catalysts by Using Capillary Array Electrophoresis " *Angew. Chem., Int. Ed.* 39 (2000): 3891-93.

Reetz, Manfred T., Klaus M. Kuhling, Heike Hinrichs, and Alfred Deege. "Circular Dichroism as a Detection Method in the Screening of Enantioselective Catalysts." *Chirality.* 12, no. 5/6 (2000): 479-82.

Reetz, Manfred T., C. M. Niemeyer, and K. Harms. "Crown Ethers with a Lewis Acidic Center: A New Class of Heterotopic Host Molecules for Binding Two Different Guests." *Angew. Chem. Int. Ed. Engl.* 30 (1991): 1472-74.

Reetz, Manfred T., C. M. Niemeyer, M. Hermes, and R. Goddard. "Molecular Recognition of Primary Amines by Three-Point Binding with Boron-Containing Host Molecules." *Angew. Chem. Int. Ed. Engl.* 31 (1992): 1017-19.

Reetz, Manfred T., Thorsten Sell, Andreas Meiswinkel, and Gerlinde Mehler. "A New Principle in Combinatorial Asymmetric Transition-Metal Catalysis: Mixture of Chiral Monodentate P Ligands." *Angew. Chem., Int. Ed.* 42, no. 7 (2003): 790-93.

Reetz, Manfred T., Albin Zonta, Klau Schimossek, Klaus Leibeton, and Karl-Erich Jaeger. "Creation of Enantioselective Biocatalysts for Organic Chemistry by in Vitro Evolution." *Angew. Chem., Int. Ed.* 36 (1997): 2830-32.

Rienk Eelkema, Richard A. van Delden Ben L. Feringa. "Direct Visual Detection of the Stereoselectivity of a Catalytic Reaction13." *Angewandte Chemie International Edition* 43, no. 38 (2004): 5013-16.

Rosenberg, M., J. L. Wiebers, and P. T. Gilham. "Studies on the Interactions of Nucleotides, Polynucleotides, and Nucleic Acids with Dihydroxyboryl-Substituted Celluloses." *Biochemistry* 11 (1972): 3623-28.

Schaus, S. E., B. D. Brandes, J. F. Larrow, M. Tokunaga, K. B. Hansen, A. E. Gould, M. E. Furrow, and E. N. Jacobsen. "Highly Selective Hydrolytic Kinetic Resolution of Terminal Epoxides Catalyzed by Chiral (Salen)Coiii Complexes. Practical Synthesis of Enantioenriched Terminal Epoxides and 1,2-Diols." *J. Am. Chem. Soc.* 124, no. 7 (2002): 1307-15.

Sculimbrene, Bianca R., and Scott J. Miller. "Discovery of a Catalytic Asymmetric Phosphorylation through Selection of a Minimal Kinase Mimic: A Concise Total Synthesis of D-Myo-Inositol-1-Phosphate." *J. Am. Chem. Soc.* 123, no. 41 (2001): 10125-26.

Secor, K. E., and T. E. Glass. "Selective Amine Recognition: Development of a Chemosensor for Dopamine and Norepinephrine." *Org. Lett.* 6 (2004): 3727-30.

Sharpless, K. B. "Searching for New Reactivity (Nobel Lecture)." *Angew. Chem., Int. Ed.* 41 (2002): 2024-32.

Program for the Refinement of Crystal Structures, University of Gottingen, Germany.

Shelxtl/Pc (Version 5.03). Siemens Analytical X-ray Instruments, Inc., Madison, Wisconsin, USA.

Shenoy, Siddhartha R., Fernando R. Pinacho Crisóstomo, Tetsuo Iwasawa, and Julius Rebek. "Organocatalysis in a Synthetic Receptor with an Inward Directed Carboxylic Acid." *J. Am. Chem. Soc.* 130, no. 17 (2009): 5658-59.

Shimizu, Ken D., Marc L Snapper, and Amir L Hoveyda. "High-Throughput Strategies for the Discovery of Catalysis." *Chem. Eur. J* 4, no. 10 (1998): 1885-89.

Shinkai, S., and M. Takeuchi. "Molecular Design of Synthetic Receptors with Dynamic, Imprinting, and Allosteric Functions." *Bull. Chem. Soc. Jpn.* 78 (2005): 40-51.

Siedel, Martin C., Rene Smits, Christian B. W. Stark, Jens Frackenpohl, Oliver Gaertzen, and H. Martin R. Hoffmann. "Studies on the Asymmetric Dihydroxylation of Advance Bryostatin C-Ring." *Synthesis.* 9 (2004): 1391-98.

Sigman, M. S., and E. N. Jacobsen. "Schiff Base Catalysts for the Asymmetric Strecker Reaction Identified and Optimized from Parallel Synthetic Libraries." *J. Am. Chem. Soc.* 120 (1998): 4901-02.

Simeonov, Anton, Masayuki Matsushita, Eric A. Juban, Elizabeth H. Z. Thompson, Timothy Z. Hoffman, Albert E. Beuscher IV, Matthew J. Taylor, Peter Wirsching, Wolfgang Rettig, James K. McCusker, Raymond C. Stevens, David P. Millar, Peter G. Schultz, Richard A. Lerner, and Kim D. Janda. "Blue-Fluorescent Antibodies." *Science* 290 (2000): 307.

Singhal, R. P., B. Ramamurthy, N. Govindraj, and Y. Sarwar. "New Ligands for Boronte Affinity Chromatography *1: Synthesis and Propertiesa." *J. Chromatogr.* 543 (1991): 17-38.

Soundararajan, Soundaramani, Mohamed Badawi, Cathy MontaÒo Kohlrust, and James H. Hageman. "Boronic Acids for Affinity Chromatography: Spectral Methods for

Determinations of Ionization and Diol-Binding Constants." *Analytical Biochemistry* 178, no. 1 (1989): 125-34.

Springsteen, G., and B. Wang. "Alizarin Red S. As a General Optical Reporter for Studying the Binding of Boronic Acids with Carbohydrates." *Chem. Commun.* (2001): 1608-09.

Springsteen, G., and B. Wang. "A Detailed Examination of Boronic Acid-Diol Complexation." *Tetrahedron* 58 (2002): 5291-300.

Stambuli J, P., and F. Hartwig J. "Recent Advances in the Discovery of Organometallic Catalysts Using High-Throughput Screening Assays." *Curr. Opin. Chem. Biol.* 7, no. 3 (2003): 420-6.

Striegler, S. "Selective Carbohydrate Recognition by Synthetic Receptors in Aqueous Solution." *Curr. Org. Chem.* 7 (2003): 81-102.

Summer, J. B. "The Isolation and Crystallization of the Enzyme Urease. Prelimanry Paper." *J. Biol. Chem* 69 (1926): 435.

Suri, J. T., D. B. Cordes, F. E. Capuccio, R. A. Wessling, and B. Singaram. "Continuous Glucose Sensing with a Fluorescent Thin-Film Hydrogel." *Angew. Chem. Int. Ed.* 42 (2003): 5857-59.

Taran, Frederic, Cecile Gauchet, Barbara Mohar, Stephane Meunier, Alain Valleix, Pierre Yves Renard, Christophe Creminon, Jacques Grassi, Alain Wagner, and Charles Mioskowski. "Communications: High-Throughput Screening of Enantioselective Catalysts by Immunoassay." *Angew. Chem., Int. Ed.* 41, no. 1 (2002): 124-27.

Tielmann, Patrick, Matthias Boese, Martin Luft, and Manfred T. Reetz. "A Practical High-Throughput Screening System for Enantioselectivity by Using Ftir Spectroscopy." *Chem. Eur. J.* 9, no. 16 (2003): 3882-87.

Tobey, S. L., and E. V. Anslyn. "Determination of Inorganic Phosphate in Serum and Saliva Using a Synthetic Receptor." *Org. Lett.* 5, no. 12 (2003): 2029-31.

Traverse, John F., and Marc L. Snapper. "High-Throughput Method for the Development of New Catalytic Asymmetric Reaction." *Drug Discovery Today* 2002, 1002-12.

Tsukamoto, M., and H. B. Kagan. "Recent Advances in the Measurement of Enantiomeric Excesses." *Adv. Synth. Catal.* 344, no. 5 (2002): 453-63.

Voet, Donald, and Judith G. Voet. *Biochemistry*. 3rd ed: John Wiley & Sons, inc, 2004.

Wahler, D., and J.-L. Reymond. "Novel Methods for Biocatalyst Screening." *Curr. Opin. Chem. Biol.* 5 (2001): 152-58.

Walba, David M., Lior Eshdat, Eva Korblova, Renfan Shao, and Noel A. Clark. "A General Method for Measurement of Enantiomeric Excess by Using Electrooptics in Ferroelectric Liquid Crystals." *Angew. Chem., Int. Ed.* 46, no. 9 (2007): 1473-75.

Walsh, Patrick J., and K. Barry Sharpless. "Asymmetric Dihydroxylation (AD) of Alpha, Beta-Unsaturated Ketones." *Synlett.*, no. 8 (1993): 605-6.

Wang, W., X. Gao, and B. Wang. "Boronic Acid-Based Sensors." *Curr. Org. Chem.* 6 (2002): 1285-317.

Warshel, A., and M. Levitt. "Theoretical Studies of Enzymic Reactions: Dielectric, Electrostatic and Steric Stabilization of the Carbonium Ion in the Reaction of Lysozyme." *J. Mol. Biol* 103 (1976): 227.

Weith, H. L., J. L. Wiebers, and P. T. Gilham. "Synthesis of Cellulose Derivatives Containing the Dihydroxyboryl Group and a Study of Their Capacity to Form Specific Complexes with Sugars and Nucleic Acid Components." *Biochemistry* 9 (1970): 4396-401.

Welch, C. J., F. Fleitz, F. Antia, P. Yehl, R. Waters, N. Ikemoto, III Amstrong, J. D., and D. J. Mathre. "Chromatography as an Enabling Technology in Pharmaceutical Process Development: Expedited Multikilogram Preparation of a Candidate Hiv Protease Inhibitor." *Org. Process Res. & Dev.* 8 (2004): 186-91.

Welch, C. J., B. Grau, J. Moore, and D. J. Mathre. "A High-Throughput Screening Protocol for Fast Evaluation of Enantioselective Catalysts." *J. Org. Chem.* 66 (2001): 6836-37.

Welch, C. J., T. Szczerba, and S. R. Perrin. "Some Recent High-Performance Liquid Chromatography Separations of the Enantiomers of Pharmaceuticals and Other Compounds Using the Whelk-O 1 Chiral Stationary Phase." *J. Chromatogr. A* 758 (1997): 93-98.

Wennemers, H. "Combinatorial Chemistry: A Tool for the Discovery of New Catalysts." *Comb. Chem. High Throughput Screen.* 4, no. 3 (2001): 273-85.

Westheimer, F. H., Harvey F. Fisher, Eric E. Conn, and Birgit Vennesland. "The Enzymatic Transfer of Hydrogen from Alcohol to Dpn." *J. Am. Chem. Soc.* 73, no. 5 (1951): 2403-03.

Westmark, Pamela R., Stephen J. Gardiner, and Bradley D. Smith. "Selective Monosaccharide Transport through Lipid Bilayers Using Boronic Acid Carriers." *J. Am. Chem. Soc* 118 (1996): 11093-100.

Wilson, A. J. C., ed. *International Tables for X-Ray Crystallography*. Boston: Kluwer Academic Press, 1992.

Wiskur, S. L., H. Aiet-Haddou, J. J. Lavigne, and Eric V. Anslyn. "Teaching Old Indicators New Tricks." *Acc. Chem. Res.* 34 (2001): 963-72.

Wiskur, S. L., H. Aït-Haddou, J. J. Lavigne, and Eric V. Anslyn. "Teaching Old Indicators New Tricks." *Acc. Chem. Res.* 34 (2001): 963-72.

Wiskur, S. L., and Eric V. Anslyn. "Using a Synthetic Receptor to Create an Optical-Sensing Ensemble for a Class of Analytes: A Colorimetric Assay for the Aging of Scotch." *J. Am. Chem. Soc.* 123, no. 41 (2001): 10109-10.

Wiskur, S. L., P. N. Floriano, Eric V. Anslyn, and J. T. McDevitt. "A Multicomponent Sensing Ensemble in Solution: Differentiation between Structurally Similar Analytes." *Angew. Chem. Int. Ed.* 42 (2003): 2070-72.

Wiskur, S. L., J. J. Lavigne, H. Ait-Haddou, V. M. Lynch, Y. H. Chiu, J. W. Canary, and E. V. Anslyn. "Pka Values and Geometries of Secondary and Tertiary Amines Complexed to Boronic Acids - Implications for Sensor Design." *Org. Lett.* 3, no. 9 (2001): 1311-14.

Wiskur, S. L., J. J. Lavigne, A. Matzger, S. L. Tobey, V. M. Lynch, and Eric V. Anslyn. "Thermodynamic Analysis of Receptors Based on Guanidinium/Boronic Acid for the Complexation of Carboxylates, α-Hydroxylates, and Diols: Driving Force for Binding and Cooperativity." *Chem. Eur. J.* 10, no. 1-14 (2004).

Wolf, C., and P. A. Hawes. "A High-Throughput Screening Protocol for Fast Evaluation of Enantioselective Catalysts." *J. Org. Chem.* 67 (2002): 2727-29.

Wulff, G. "Selective Binding to Polymers Via Covalent Bonds. The Construction of Chiral Cavities as Specific Receptor Sites." *Pure Appl. Chem.* 54 (1982): 2093-102.

Wulff, G. "Molecular Imprinting in Cross-Linked Materials with the Aid of Molecular Templates - a Way Towards Artificial Antibodies." *Angew. Chem. Int. Ed. Engl.* 34 (1995): 1812-32.

Wulff, G., M. Lauer, and H. Bohnke. "Rapid Proton Transfer as Cause of an Unusually Large Neighboring Group Effect." *Angew. Chem. Int. Ed. Engl.* 23, no. 9 (1984): 741-42.

Wulff, G., and W. Vesper. "Preparation of Chromatogrphic Sorbents with Chiral Cavities for Racemic Resolution." *J. Chromatogr.* 167 (1978): 171-86.

Yamamoto, T., Y. Seino, H. Fukumoto, G. Koh, H. Yano, N. Inagaki, Y. Yamada, K. Inoue, T. Manabe, and H. Imura. *Biochem. Biophyd. Res. Commun.* 170 (1990): 223-30.

Yan, J., G. Springsteen, S. Deeter, and B. Wang. "The Relationships among Pka, Ph, and Binding Constants in the Interactions between Boronic Acids and Diols - It Is Not as Simple as It Appears." *Tetrahedron* 60 (2004): 11205-09.

Yasuda, H., T. Kurokawa, Y. Fujii, A. Yamashita, and S. Ishibashi. *Biochim. Biophys. Acta* 1021 (1990): 114-18.

Yoon, J., and A. W. Czarnik. "Fluorescent Chemosensors of Carbohydrates. A Means of Chemically Communicating the Binding of Polyols in Water Based on Chelation-Enhanced Quenching." *J. Am. Chem. Soc.* 114 (1992): 5874-75.

Zhang, Tianzhi, and Eric V. Anslyn. "Molecular Recognition and Indicator-Displacement Assays for Phosphoesters." *Tetrahedron.* 60, no. 49 (2004): 11117-24.

Zhang, Tianzhi, and Eric V. Anslyn. "A Colorimetric Boronic Acid Based Sensing Ensemble for Carboxy and Phospho Sugars." *Org. Lett.* 8, no. 8 (2006): 1649-52.

Zhang, Tianzhi, and Eric V. Anslyn. "Using an Indicator Displacement Assay to Monitor Glucose Oxidase Activity in Blood Serum." *Org. Lett.* 9, no. 9 (2007): 1627-29.

Zhao, Jianzhang., Matthew G. Davidson, Mary F. Mahon, Gabriele Kociok-Kohn, and Tony D. James. "An Enantioselective Fluorescent Sensor for Sugar Acids." *J. Am. Chem. Soc.* 126 (2004): 16179-86.

Zhao, J., T. M. Fyles, and T. D. James. "Chiral Binol-Bisboronic Acid as Fluorescence Sensor for Sugar Acids." *Angew. Chem. Int. Ed.* 43 (2004): 3461-64.

Zhong, Zhenlin, and Eric V. Anslyn. "A Colorimetric Sensing Ensemble for Heparin." *J. Am. Chem. Soc.* 124, no. 31 (2002): 9014-15.

Zhou, Huchen, Laura Baldini, Jason Hong, Andrew J. Wilson, and Andrew D. Hamilton. "Pattern Recognition of Proteins Based on an Array of Functionalized Porphyrins." *J. Am. Chem. Soc.* 128, no. 7 (2006): 2421-25.

Zhu, Lei, and Eric V. Anslyn. "Facile Quantification of Enantiomeric Excess and Concentration with Indicator-Displacement Assays: An Example in the Analyses of α-Hydroxyacids." *J. Am. Chem. Soc.* 126, no. 12 (2004): 3676-77.

Zhu, Lei, Shagufta H. Shabbir, and Eric V. Anslyn. "Two Methods for the Determination of Enantiomeric Excess and Concentration of a Chiral Sample with a Single Spectroscopic Measurement." *Chem. Eur. J.* 13, no. 1 (2007): 99-104.

Zhu, Lei, Shagufta H. Shabbir, Mark Gray, Vincent M. Lynch, Steven Sorey, and Eric V. Anslyn. "A Structural Investigation of the N-B Interaction in an O-(*N,N*-Dialkylaminomethyl)Arylboronate System." *J. Am. Chem. Soc.* 128, no. 4 (2006): 1222-32.

Zhu, Lei, Zhenlin Zhong, and Eric V. Anslyn. "Guidelines in Implementing Enantioselective Indicator-Displacement Assays for Alpha -Hydroxycarboxylates and Diols." *J. Am. Chem. Soc.* 127, no. 12 (2005): 4260-69.

Vita

Shagufta H. Shabbir was born in Karachi, Pakistan on April 04, 1976, the daughter of Mushtaq Ali and Fatima Mushtaq Ali. After graduating from University of Karachi in Karachi, Pakistan in 1999, she entered Texas State University in San Marcos, Texas. There she was awarded a Masters of Science Degree in Chemistry in May 2004. In August of that year she entered the Graduate School of The University of Texas at Austin.

Permanent address: 3059 Hill Street, Round Rock, TX, 78664

This dissertation was typed by the author.